AD-A061 255 AEROSPACE CORP EL SEGUNDO CALIF F/G 4/1
DEVELOPMENT OF CLOUD WATER CONTENT METER, EWER.(U)
MAR 78 D A DURRAN, D H ROSS, W J SWARTWOOD F04701-77-C-0078
UNCLASSIFIED TR-0078(3550-38)-1 SAMSO-TR-78-113 NL

1 OF 3
AD A061255

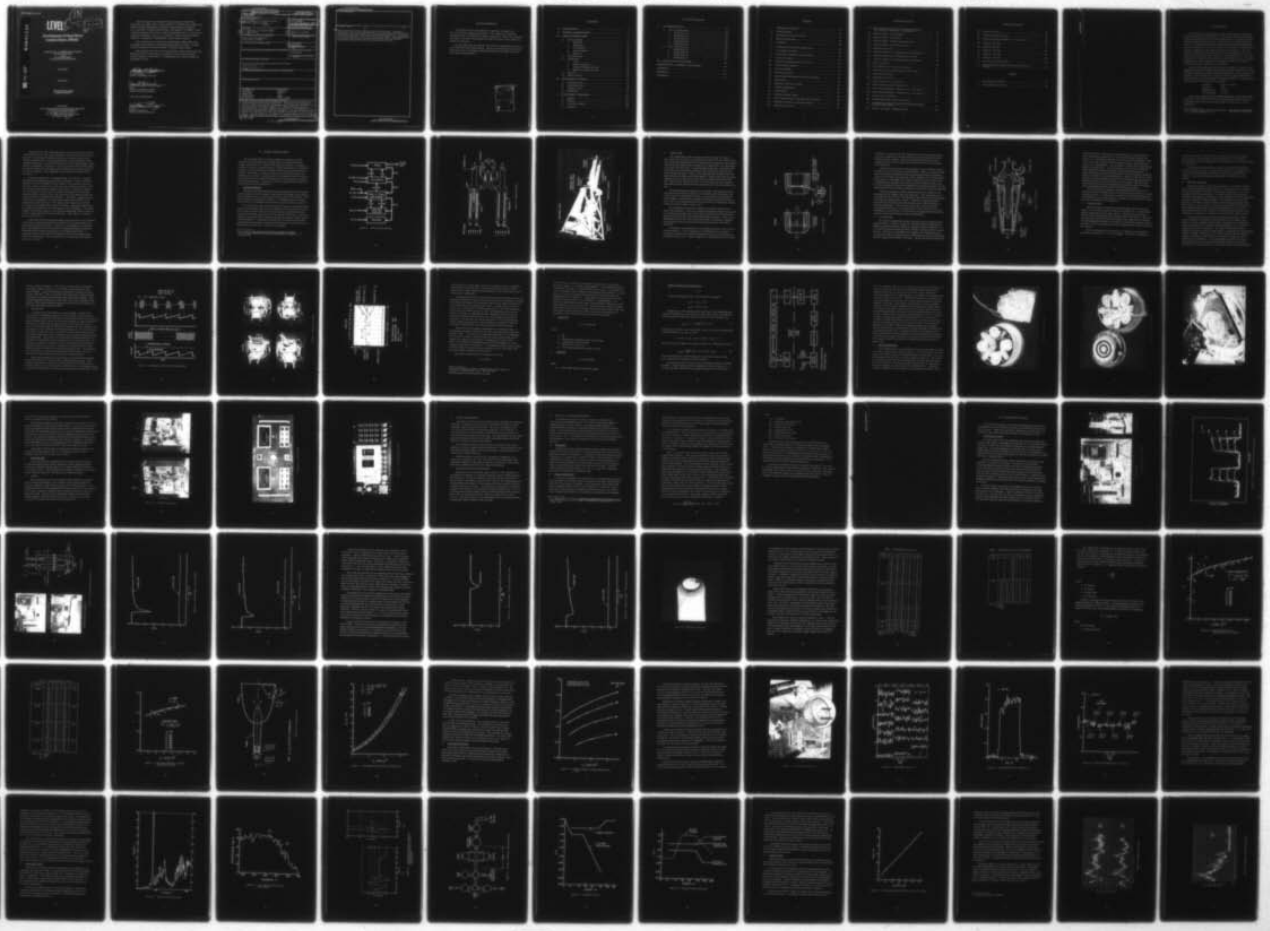

255

REPORT SAMSO-TR-78-113

LEVEL II

13

Development of Cloud Water Content Meter, EWER

Prepared by D. A. DURRAN and D. H. ROSS
Laboratory Operations
and
W. J. SWARTWOOD
Government Support Operations

March 1978

Final Report

APPROVED FOR PUBLIC RELEASE;
DISTRIBUTION UNLIMITED

Prepared for

SPACE AND MISSILE SYSTEMS ORGANIZATION
AIR FORCE SYSTEMS COMMAND
Los Angeles Air Force Station
P.O. Box 92960, Worldway Postal Center
Los Angeles, Calif. 90009

This final report was submitted by The Aerospace Corporation, El Segundo, CA 90245, under Contract F04701-77-C-0078 with the Space and Missile Systems Organization, Deputy for Advanced Space Programs, P.O. Box 92960, Worldway Postal Center, Los Angeles, CA 90009. It was reviewed and approved for The Aerospace Corporation by W. R. Warren, Jr., Laboratory Operations, and W. R. Grabowsky, Reentry Systems Division. Captain F. Kreighbaum, SAMSO/RSSE, was the project engineer.

This report has been reviewed by the Information Office (OI) and is releasable to the National Technical Information Service (NTIS). At NTIS, it will be available to the general public, including foreign nations.

This technical report has been reviewed and is approved for publication. Publication of this report does not constitute Air Force approval of the report's findings or conclusions. It is published only for the exchange and stimulation of ideas.

F. Kreighbaum, Capt, USAF
Project Engineer
Reentry Technology Division

J. M. McCormack, Lt Col, USAF
Chief
Reentry Technology Division
Deputy for Reentry Systems

FOR THE COMMANDER

William Goldberg, Lt Col, USAF
Director
Systems Technology
Deputy for Reentry Systems

UNCLASSIFIED

SECURITY CLASSIFICATION OF THIS PAGE *(When Data Entered)*

REPORT DOCUMENTATION PAGE

READ INSTRUCTIONS BEFORE COMPLETING FORM

1. REPORT NUMBER: SAMSO-TR-78-113
2. GOVT ACCESSION NO.:
3. RECIPIENT'S CATALOG NUMBER:

4. TITLE *(and Subtitle)*: DEVELOPMENT OF CLOUD WATER CONTENT METER, EWER

5. TYPE OF REPORT & PERIOD COVERED: Final Report, Jan 1975 through Dec 1977

6. PERFORMING ORG. REPORT NUMBER: TR-0078(3550-38)-1

7. AUTHOR(s): D. A. Durran, D. H. Ross, and W. J. Swartwood

8. CONTRACT OR GRANT NUMBER(s): F04701-77-C-0078

9. PERFORMING ORGANIZATION NAME AND ADDRESS: The Aerospace Corporation, El Segundo, CA 90245

10. PROGRAM ELEMENT, PROJECT, TASK AREA & WORK UNIT NUMBERS:

11. CONTROLLING OFFICE NAME AND ADDRESS:

12. REPORT DATE: March 1978

13. NUMBER OF PAGES: 205

14. MONITORING AGENCY NAME & ADDRESS *(if different from Controlling Office)*:

15. SECURITY CLASS. *(of this report)*: Unclassified

15a. DECLASSIFICATION/DOWNGRADING SCHEDULE:

16. DISTRIBUTION STATEMENT *(of this Report)*

Approved for Public Release; Distribution Unlimited.

203 p.

17. DISTRIBUTION STATEMENT *(of the abstract entered in Block 20, if different from Report)*

18. SUPPLEMENTARY NOTES

19. KEY WORDS *(Continue on reverse side if necessary and identify by block number)*

Cloud physics	Lyman-α
Condensate	Moisture
Evaporator	Rain
Humidiometer	Snow
Ice particles	Water content

20. ABSTRACT *(Continue on reverse side if necessary and identify by block number)*

An instrument for measuring the total water content of condensed phase(s) in clouds at flight levels to 6 km is described. The instrument is designed to evaluate erosive environments for reentry vehicles where the total water content of particles is less than 1 g/m^3 of air. The instrument is part of a system that offers real-time readout of condensate or recordings that can be analyzed by post-flight data reduction procedures. The system has been calibrated in the laboratory and flown in a C130E aircraft under a variety of conditions. Results obtained on one flight are compared with data from a Particle

next page

DD FORM 1473 (FACSIMILE)

UNCLASSIFIED

SECURITY CLASSIFICATION OF THIS PAGE *(When Data Entered)*

009 500

19. KEY WORDS (Continued)

20. ABSTRACT (Continued)

cont'd

Measuring Systems probe, also operational on this flight. Laboratory calibration of the Lyman-α humidiometer used in the instrument showed that the effective absorption coefficient was about half that given for Lyman-α due to the broad spectrum in the output of the hydrogen lamp. Recommendations for certain modifications to the instrument/system and a preliminary design of the improved version of the instrument are given.

ACKNOWLEDGMENTS

The authors wish to acknowledge the significant contribution of M. E. Gerard for mechanical assembly, J. M. Narduzzi for electronic assembly, and R. M. Shima for computer peripherals. These men supported the project, not only in the laboratory but also in the field, often under very trying circumstances.

We also appreciate the support of the Air Force Geophysics Laboratory crew that manned the C130E aircraft. These men worked long hours to make the system work, contributing significantly with their knowledge of the aircraft systems and operation.

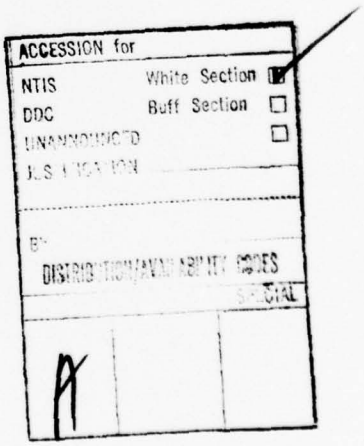

CONTENTS

CONTENTS (Continued)

FIGURES

FIGURES (Continued)

FIGURES (Continued)

TABLES

I. INTRODUCTION

I. INTRODUCTION

The measurement of particulates in the clouds has been a challenge to instrument designers for many years. A wide variety of devices have been used to measure the liquid water content (LWC) and are reviewed by Ruskin.[1] With the advent of high performance reentry systems on USAF missile programs, the definition of the weather environment and especially the particulates in the clouds becomes a critical issue. Not only LWC is of importance, the water content in the solid state also needs to be measured. Since the weather of significance for reentry systems is at high altitude in the cirrus level, the amount of condensed moisture is very small; therefore, any water content meter to operate in this regime must have a high degree of sensitivity. In addition, the number of particles containing the bulk of the moisture is small so that a large sampling area is required.

It was for this application that the Advanced Ballistic Reentry Systems (ABRES) Directorate of SAMSO requested the Aerophysics Laboratory of The Aerospace Corporation to undertake the development of a water content meter. The unit was to be mounted in a weather research aircraft (C130E-40571) operated by the Air Force Geophysics Laboratory (AFGL). The specifications which were given for the device are as follows:

Sensitivity	0.05 - 1.0 g/m^3
Accuracy	20%
Sampling area	10 cm^2
Time response	0.1 sec

The project was given the title EWER (evaporator of water that erodes on reentry). Since the 10 cm^2 inlet was larger than any of the LWC meters extant at the time, the name was also reminiscent of the ewer, a wide-mouthed jar.

---

[1] R. E. Ruskin, "Liquid Water Content Devices," Atmospheric Technology, no. 8, pp. 38-42 (Spring 1976).

II. GENERAL CONSIDERATIONS

II. GENERAL CONSIDERATIONS

The work of Ruskin[2] and Kyle[3], in which small probes containing a Lyman-α humidiometer were used to measure LWC in thunderstorms, was selected as the basis for the EWER design. The high sensitivity and fast response of the Lyman-α humidiometer[4] would be well suited to the EWER requirements. However, the need to measure very small amounts of condensate in a saturated background indicated that a differential rather than an absolute measurement would be necessary. After consultation with Ruskin and Kyle (both of whom were contemplating modification of their probes to make differential measurements) a scheme was devised to make measurements with a single detector in two samples. One sample would contain moist air from which all particles larger than approximately 50 μm radius had been centrifugally separated and would be representative of the background water vapor. (Particles smaller than 50 μm were considered nonerosive as far as the reentry system was concerned.) The other sample would contain moist air containing all particles, which would be heated to melt and vaporize all condensed phases. A detector placed in each sample in rapid succession would give outputs, the difference being the amount of water carried in condensed phases. In this way, the small variations in the detector output due to extraneous absorbers could be cancelled out, since both samples would be subject to the same error. The special features of this measurement system are described in greater detail in Section III. A. 5.

---

[2] R. E. Ruskin, "Measurements of Water-Budget Changes at -5° C in AgI-Seeded Tropical Cumulus," J. Appl. Meteorology, 6, 72-81 (1975).

[3] T. G. Kyle, "The Measurement of Water Content by an Evaporator," J. Appl. Meteorology 14, 327-332 (1975).

[4] D. C. Randall, T. E. Hanley, and O. K. Larisan, "The NRL Lyman-Alpha Humidiometer," Humidity and Moisture, Vol. I: Principles and Methods of Measuring Humidity and Gases, ed. R. E. Ruskin, Reinhold Publishing Corp., N. Y. (1965), Chap. 44.

Another factor in the EWER application which required special design consideration was the wide range of humidity over which the device was to be operated. For an optical extinction-type measurement as utilized in the Lyman-α humidiometer, a strong absorption by a moist background would completely obliterate any signal difference that would be apparent for a small amount of condensate. Therefore, a means is provided in the EWER design to vary the length of the absorbing media to optimize the detector output for any level of humidity. This capability is also discussed in detail in Section III. A. 5.

It has been customary, in sampling probes, to strive for a design in which the flow through the system would be isokinetic. That is, the probe impedance would be negligible and the velocity in the inlet of the device is the same as that of freestream. In this way, the collection efficiency of the probe could be assumed to be 100% for all particles. Isokinetic conditions are very difficult to obtain when one considers the influence of the probe mounting on the aircraft as well as the large change of conditions within the probe as the flow is heated in the evaporator. In addition, ruggedized heater construction to withstand ice particle impact implies that the flow will be impeded by support structures. The design of the evaporator for EWER proceeded in a straightforward manner to achieve a configuration that would be rugged and of high power to accommodate a large throughput. Having this design, the collection efficiency was computed analytically and the result was used as a calibration factor for the instrument. This matter is considered again in Section IV. B.

It was expected that aircraft operations on the ground and at low altitudes could involve environments that would be deleterious to exposed heater elements and ultraviolet (UV) optics. Therefore, an installation was specified that would permit the unit to be sealed in a compartment during storage and backflushed with nitrogen during ground or low altitude operations. A waste gate valve to control the flow through the device and a nitrogen purge to flush the compartment can be activated by the operator after the storage covers are removed.

III. DESIGN CONSIDERATIONS

The operation of the Air Force Geophysics Laboratory weather research aircraft dictated that a EWER system be provided that could perform from takeoff to touchdown with minimum attention. In addition, a readout in real time of condensed water content would permit correlation to be made on a quick-look basis with other instruments operating aboard the aircraft. Therefore, an extensive system was developed to support the sampling device itself. A block diagram of the system is shown in Figure 1. The salient features of each of the components of the system are described in detail in this section. Information concerning operation and maintenance of the system is given in Reference 5.

A. PROBE ASSEMBLY

The probe assembly embodies the actual sampling device and includes various heaters to melt, evaporate, and/or heat the samples and a Lyman-α-type humidiometer to measure the water vapor content in the samples. The probe is shown schematically in Figure 2. A photograph of the unit (with covers off) as it is installed in the left-hand wing pod is shown in Figure 3.

Two samples are taken into the instrument by probes extending forward from the nose fairing on the pod. One sample is used to measure the background vapor content in the freestream by passing a small portion of the incoming air through a separator just inside the lip of the probe. The other sample is passed through an evaporator to melt and vaporize all the water in condensed phases. A small portion of this flow is compared with the flow coming from the separator to determine the difference in water vapor level. This difference is the water contained as condensate.

---

[5] D. A. Durran, Operation and Maintenance Manual for EWER, TOR-0076(6550-19)-1, The Aerospace Corporation, El Segundo, CA (15 May 1976).

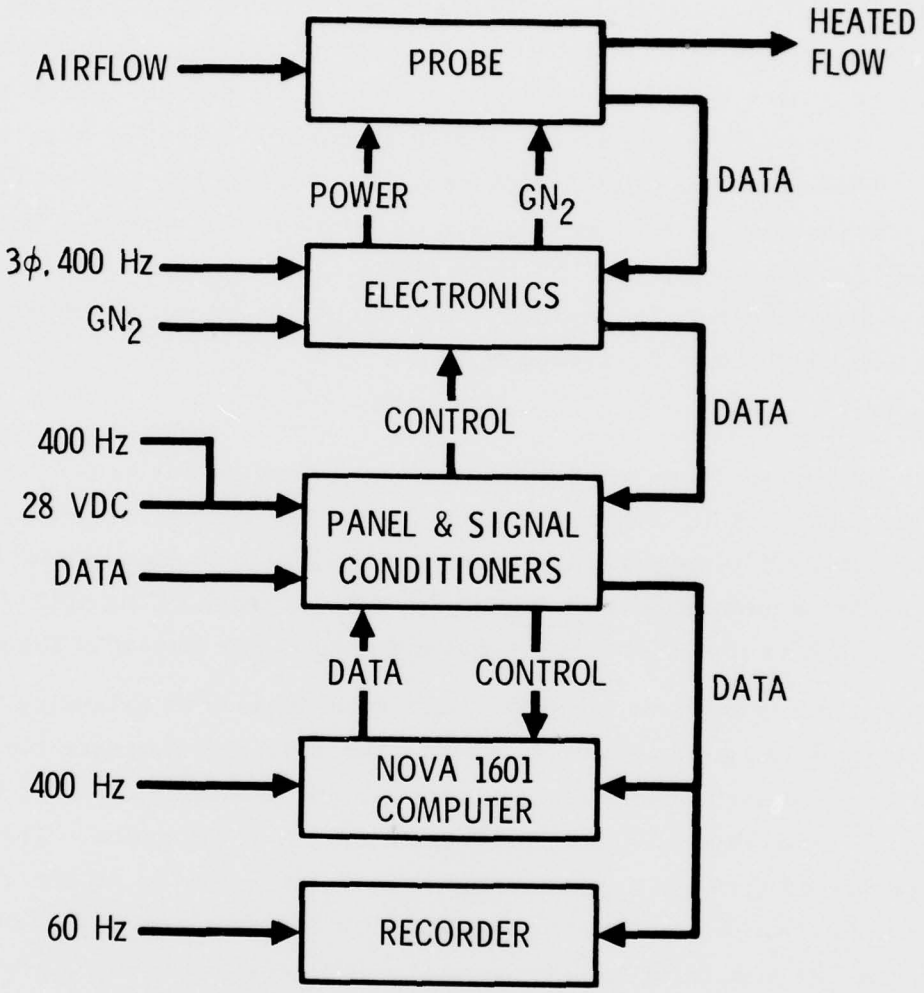

Figure 1. EWER System Diagram

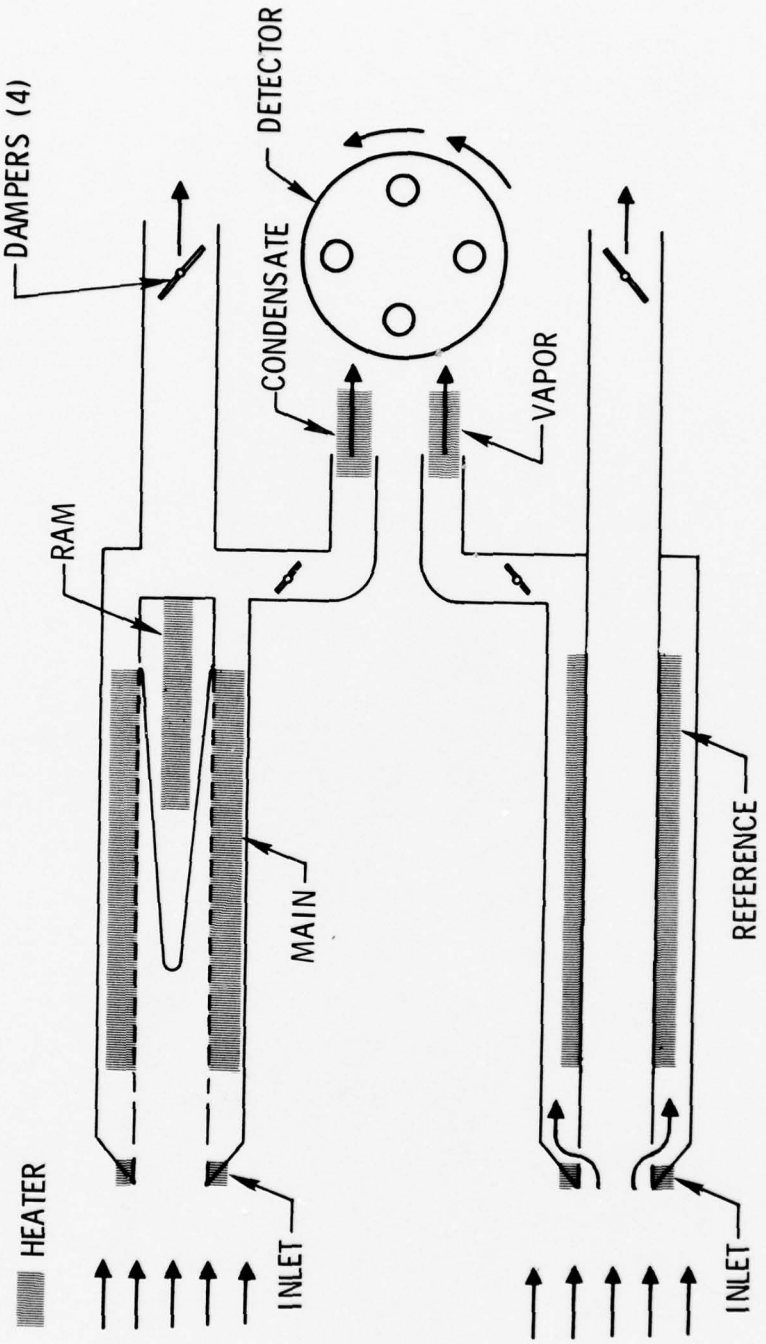

Figure 2. EWER Schematic

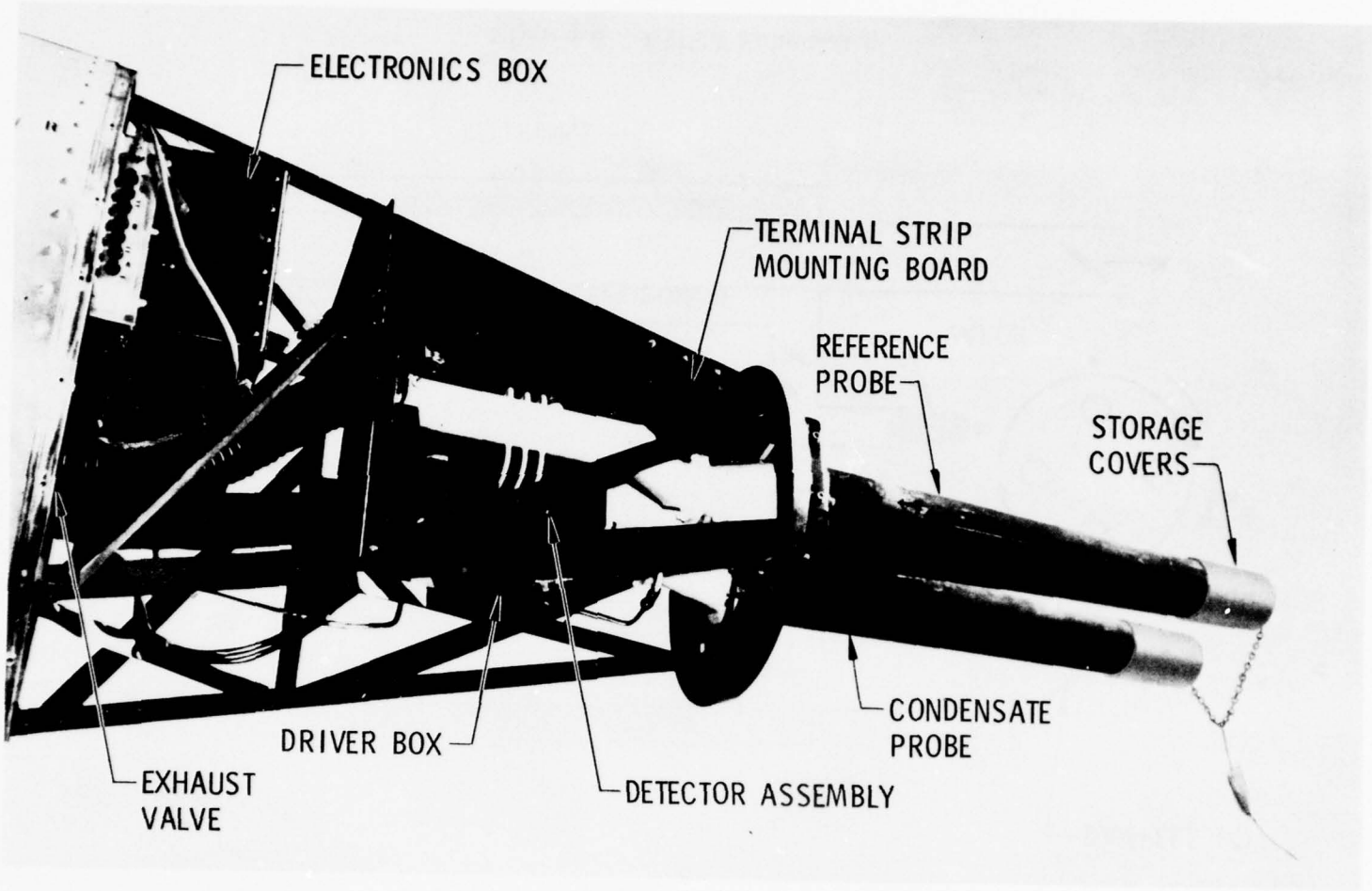

Figure 3. EWER System Probe Assembly

1. SEPARATOR

The configuration of the separator is shown in Figure 4. Small, thin-walled tubes of copper are installed in the wall of the probe duct so that air can pass through the tubes into a chamber that is connected to the detector. This design was evolved from an earlier one in which there were bleed holes in the inner wall of the duct. It was determined that water collecting on the inlet of the probe was running into these holes, giving an erroneous value for the background vapor. Water on the wall and in the boundary layer now passes between the tubes and out the exhaust. The thin wall of the tube offers minimal surface on which local water drops can adhere and pass into the tube. Only one row of tubes is used. If a second row were used, particle separation would be influenced by the turbulence in the base area of the first row.

The flow through the separator is very small. The flow has not been measured directly, but from the power consumed in the small heater used to heat it prior to entering the detector, it is estimated to be less than 2% of the sample. Low flow rates through the separator will facilitate the process, since even small particles will be more likely to drift past the opening in the tubes if the velocity in them is low.

No quantitative measure of the effectiveness of this separator was made in the laboratory. However, during the calibration tests (Section IV. B), it was demonstrated that water on the inlet and wall of the probe duct had no effect on the water vapor level passing through the separator. (There was a significant effect for the earlier bleed hole design.) In addition, atomized water droplets (sizes not measured) sprayed into the probe were totally separated.

Two heaters are incorporated in the separator probe to resist icing on critical surfaces. A 14 cm length of No. 28 Nichrome wire in ceramic insulators is potted in the aluminum fitting that forms the inlet to the probe. It dissipates about 50 W. Another length of No. 28 Nichrome wire in ceramic

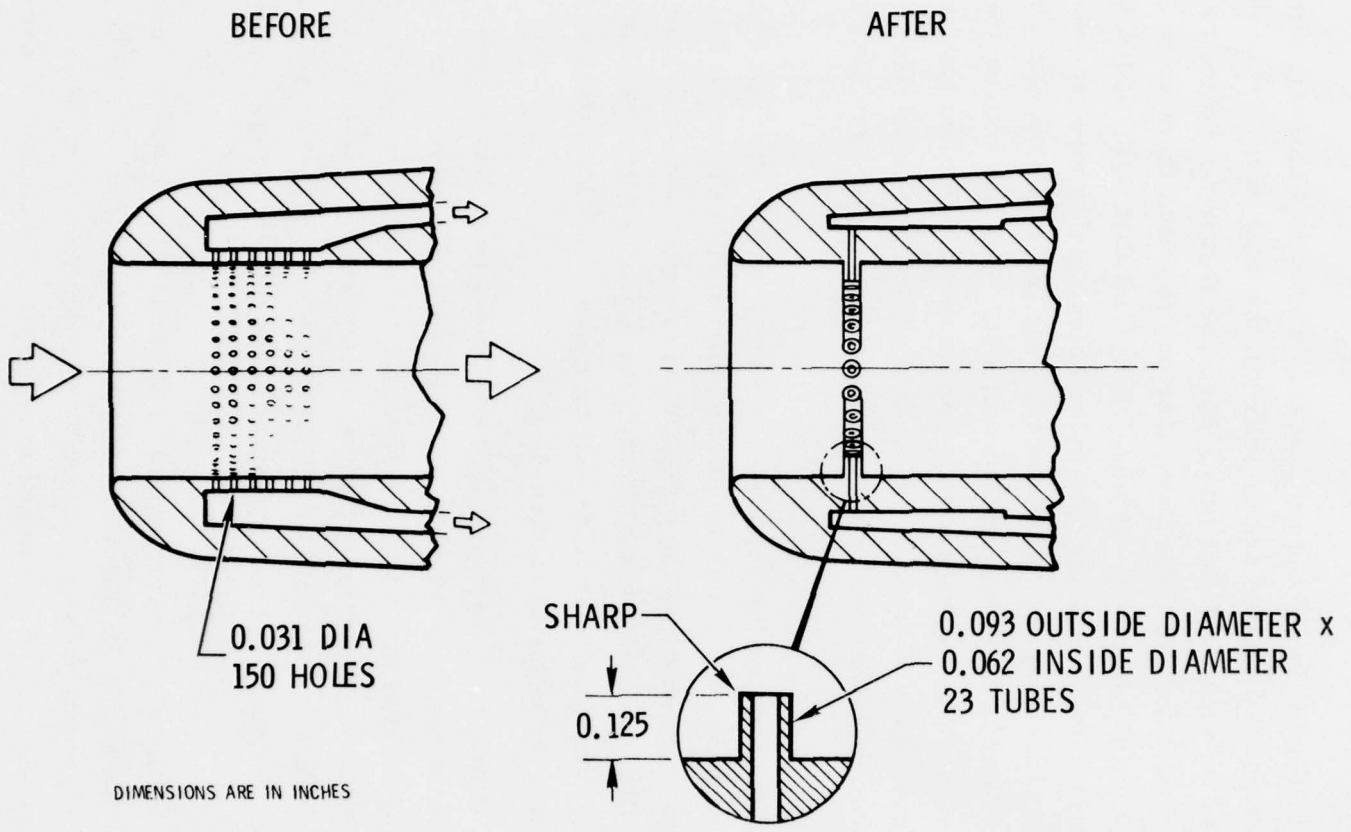

Figure 4. Mechanical Separator

insulators is wrapped around the copper body in which the separator tubes are silver-soldered and along the aluminum tube that conveys the bulk of the flow aft to the exhaust. This heater dissipates about 500 W and is wrapped in such a way that about two-thirds of the power is concentrated at the separator.

Flow from the separator is passed along a narrow (minimum volume) passage to a duct which connects to the detector. There is a damper in this duct to facilitate the adjustment of the flow passing through the separator. (In the current design, the small tubes of the separator act as a flow limiter of the system, so the damper is no longer needed; it can be left full open.) A damper is also installed in the exhaust from the separator probe so its flow can be matched with the flow passing into the evaporator probe, thereby assuring that the same sample is admitted to each probe from the freestream.

The probe housing is a light-weight aluminum cone, flanged at the mounting end and wrapped with epoxy-glass tape. The epoxy glass serves to insulate the cone from the cold slipstream which could cause condensation in the small, separated flow of vapor. The heater wrapped around the aluminum tube inside the probe also heats the inner wall of the probe to prevent condensation. Power leads for the heater, leads for an iron-constantan thermocouple, and a tubulation for a static pressure port, all contained in the probe inlet, are also potted in the epoxy-glass housing and emerge on the outside diameter of the mounting flange.

2. EVAPORATOR

The external configuration of the evaporator probe is identical to the separator probe. However, all the flow is passed through a high powered heater to melt and evaporate all the ice and water particles (Figure 5). It is an 8 kW unit powered from the 120 V, 400 Hz, 3 phase aircraft electrical system. This power is dissipated by 12 lengths of No. 28 Nichrome wire in ceramic insulators wrapped around an aluminum tube which is extensively finned to enhance heat transfer to the flow. The flow entering the evaporator

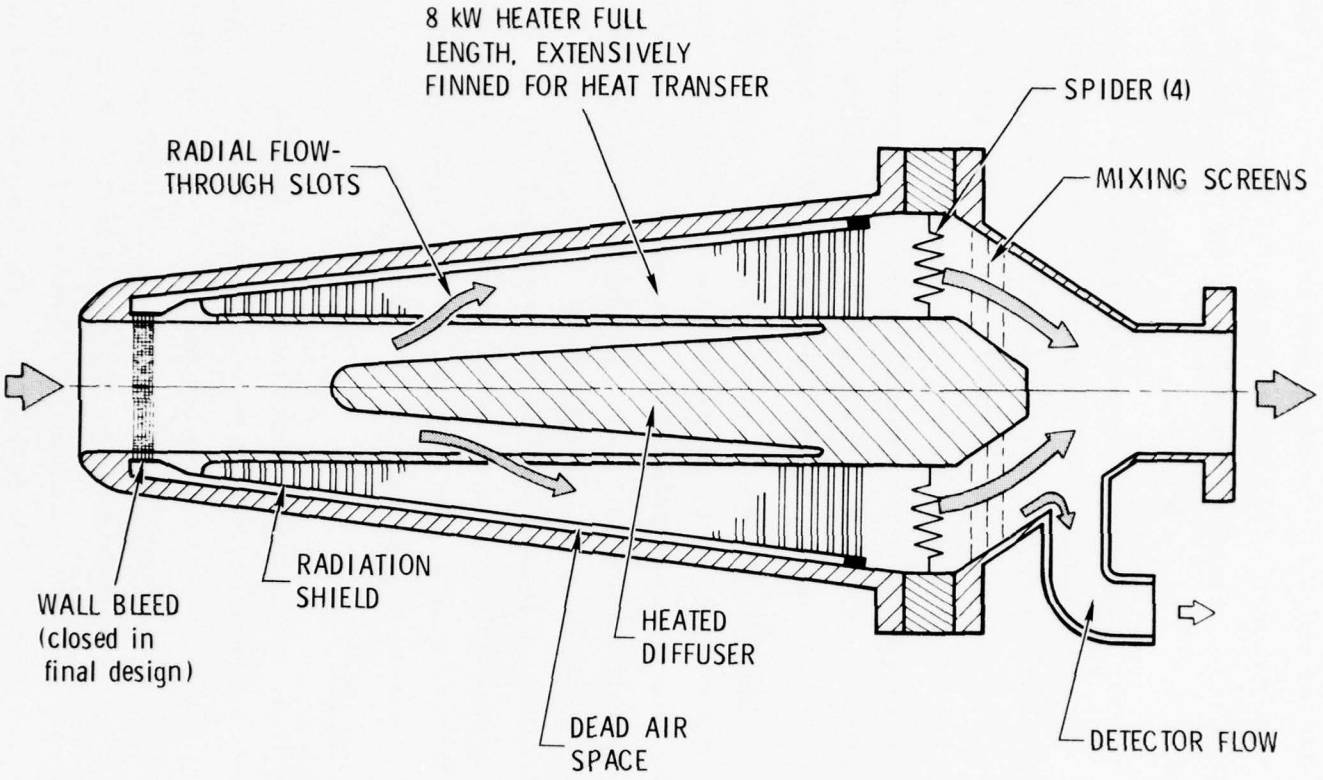

Figure 5. Evaporator

probe is turned by a centerbody to pass through slots in the finned tube. This centerbody is configured to receive the direct impact of particles, shatter ice, and sling the fragments to the inside of the slotted tube. Slots are 0.5 mm wide to impede the larger particles which could damage the heater wires and insulators. The centerbody is heated with a cartridge-type heater to prevent icing. A thin aluminum cone is used to shield the inside of the probe housing from direct contact with the heated flow. A small dead airspace is provided between the cone and housing for insulation. Power is supplied to the heater through four "spiders" at the aft end. Three spiders are connected to the high side of each of the three phases and press on collector bars to which four heater wires are joined. The other ends of the 12 heater wires are terminated on the finned tube which is connected to the fourth spider and the neutral of the three-phase system.

The flow from the evaporator is controlled from 90° C to 100° C as sensed by an iron-constantan thermocouple positioned downstream of a series of mixing screens. A small portion of the flow is diverted at this point into a duct which connects to the detector. A damper is located in the duct so the flow rate to the detector can be adjusted.

3. TRIM HEATERS

Since the Lyman-α humidiometer measures the density of the water vapor, it is of crucial importance that the two samples (i.e., the separator and the evaporator) be at the same density. Equal pressure is assured because of low velocities entering a plenum region in the detector. However, the temperature of the flow from the separator and evaporator are different and vary with flight conditions. Therefore, two small, fast response heaters are used to "trim" the temperature of both samples to 100° C before entering the detector.

Power is dissipated in an array of No. 36 Nichrome wires mounted transverse to the flow in a 1.6×5 cm passage. The wires are soldered to

frames made of copper clad circuit board, which are stacked in a plastic case to form a series-parallel circuit of about 22 ohms. The steps in fabricating the resistor elements and an assembly are shown in Figures 6 and 7, respectively.

The thermal inertia of the trim heater is very small while the heat transfer area is very large. These factors result in a fast response (a few msec) and a small temperature difference between wires and the flow ($\sim 50°C$). Under normal operating conditions the trim heaters are quite reliable.

4. HEATER CONTROLS

The heater elements in the probe assembly are activated by switches on the EWER control panel (Section III. C. 1). The heaters in the separator and both probe inlets are designed to prevent the buildup of ice on critical surfaces in mild icing conditions. A two-step control is provided that is selected by the operator on the basis of icing conditions and/or the temperature measured at the inlet of the evaporator. The first level is powered with half-wave rectification of 120 V, 400 Hz and will dissipate approximately 300 W of power. The second level (boost) uses the full 120 V, 400 Hz power. These heaters should not be used if the inlet temperature is about 20° C. The cartridge heater in the centerbody is turned on when the heater in the evaporator is in operation. It draws 500 W on the 120 V, 400 Hz system.

The three-phase evaporator heater and the trim heaters are each servo controlled to maintain a preset temperature in the outflow of the heater. An iron-constantan thermocouple is positioned a few centimeters downstream of the heater element so a flow through the unit is required if proper control is to be maintained. The output of the thermocouple is amplified to establish a control voltage which is compared to a 30 Hz sawtooth reference voltage. When the control voltage is greater than the reference voltage, an electronic switch (Triac) is switched on to apply full 120 V, 400 Hz power to the heater. As the temperature increases, the control voltage falls below the reference voltage and the 400 Hz is turned off for the remainder of the sawtooth cycle. A diagram of this type of proportional

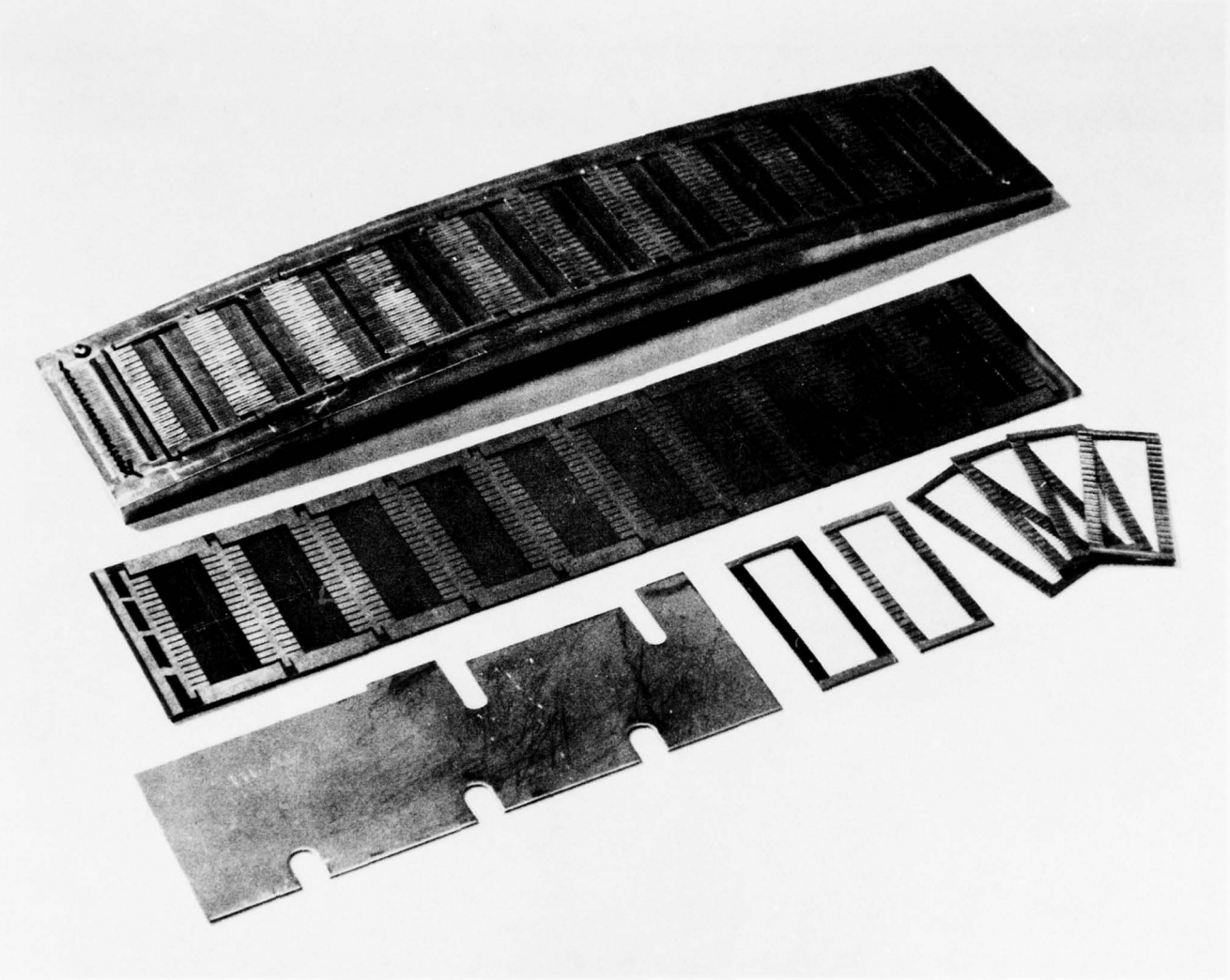

Figure 6. Tooling Used to Fabricate Heater Grids

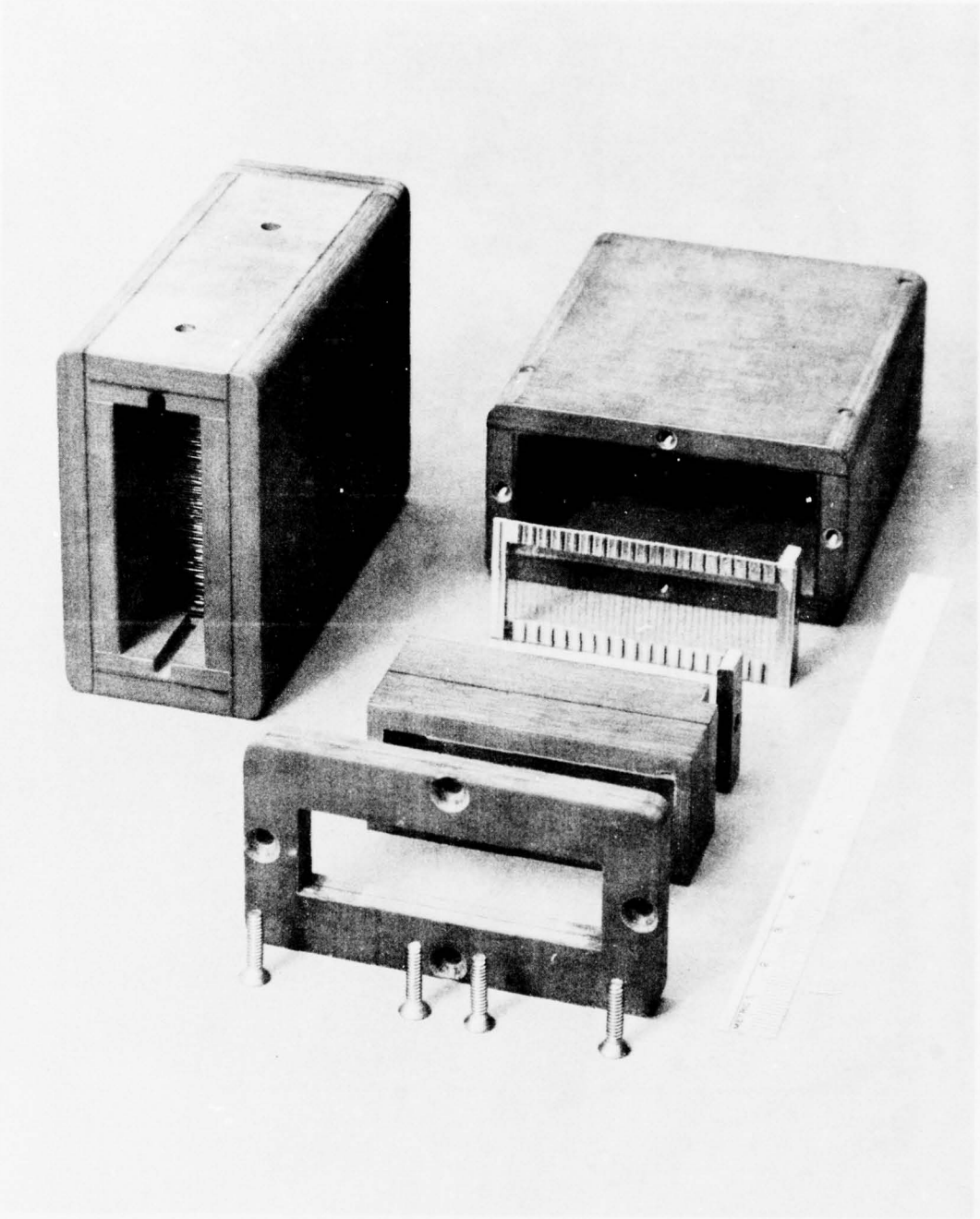

Figure 7. Trim Heater Assembly

control is shown in Figure 8. The Triac is always turned on (off) when the supply voltage crosses zero to minimize electromagnetic interference (EMI). A delay is built into the controller to ramp up the power during a cold start. This is crucial for the trim heaters because of their fast response compared to the thermocouple (inertia and position). Under nominal operating conditions, the duty cycle on the vapor (separator) trim heater is 50%; on the condensate (evaporator) trim heater it is 20%; and on the main (evaporator) heater it is 20%.

5. DETECTOR

A Lyman-α-type humidiometer is used in EWER. Actually, four separate sources (hydrogen lamps) and receivers (nitric oxide detectors) are mounted in rotating housings (Figure 2) so that the airflow to be measured passes between them. Several views of this assembly are shown in Figure 9. With such an arrangement, the optical axis of each source and receiver (sensor) will pass through the vapor and condensate samples in rapid succession, giving a series of pulses as indicated in Figure 10. The first level for each sensor is indicative of the water vapor in the sample coming from the evaporator (referred to as the condensate which is actually background vapor plus condensate). The next level is representive of total absorption and is created by a solid shutter positioned between the two sample streams. The third level is indicative of the water vapor in the sample coming from the separator (referred to as vapor). The three levels from the next sensor follow in sequence as they come into the measuring position. The geometry is such that only one sensor is measuring at a time; the other three are obscured by a shutter placed between the two rotating housings.

Synchronous rotation of the two housings is provided by gearing that drives both sides from a common 120 V, 400 Hz gearhead motor. Each housing is mounted on a single, precision ball bearing so that the optical surfaces of the source (or receiver) are cantilevered into the sampling region. A sharp lip is provided on each housing at this surface to strip the flow coming

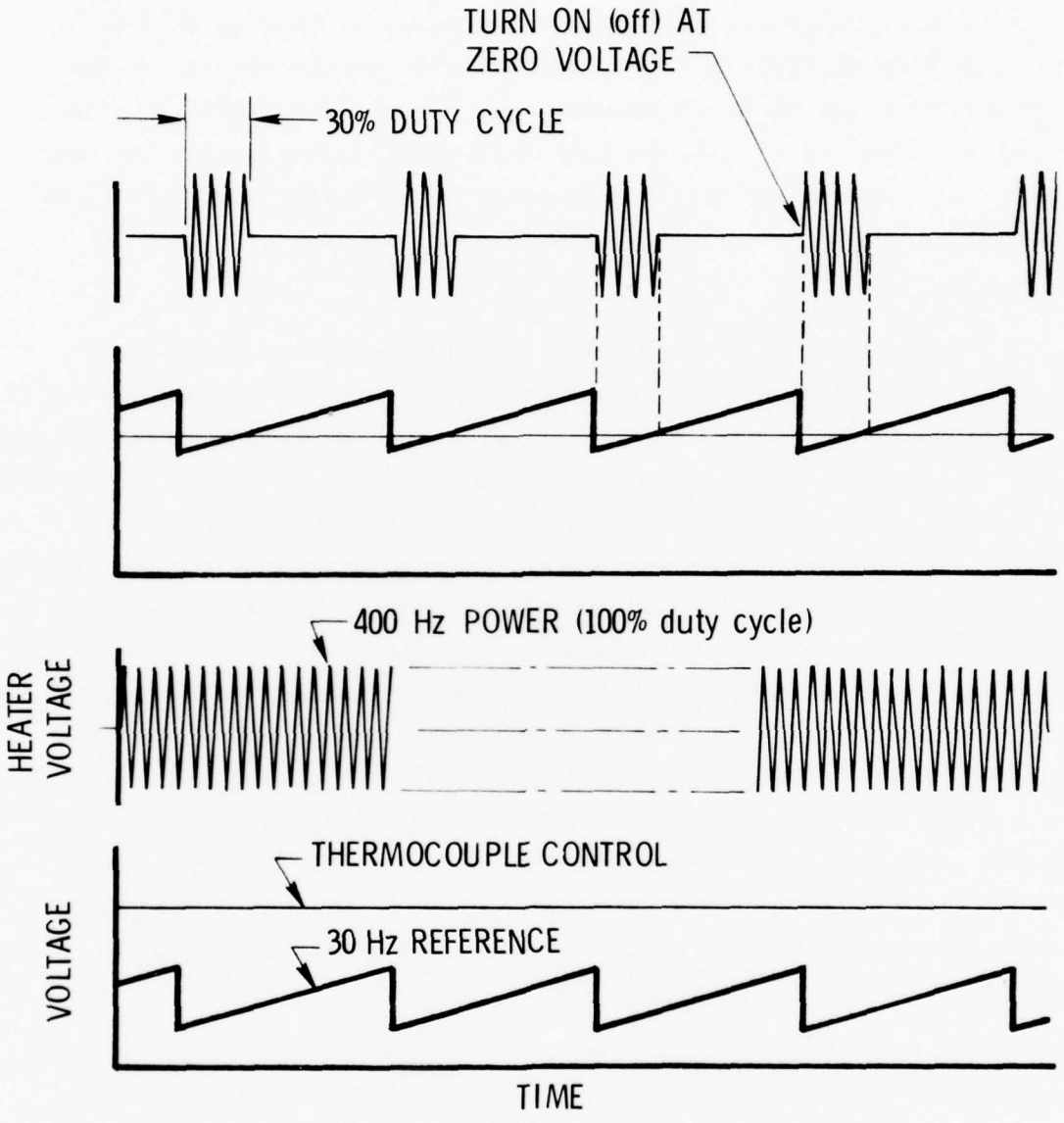

Figure 8. Temperature Controller Characteristics

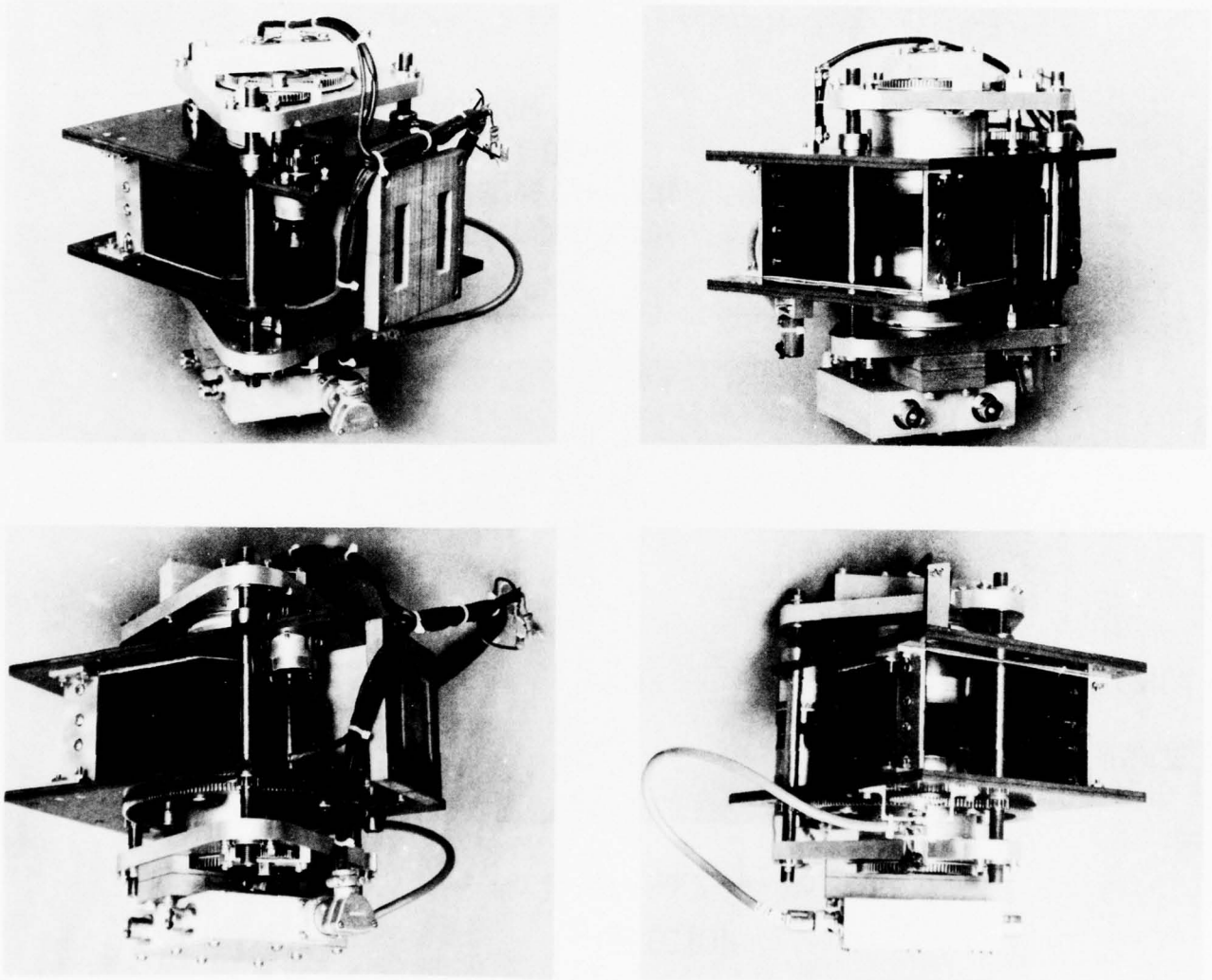

Figure 9. Detector Assembly

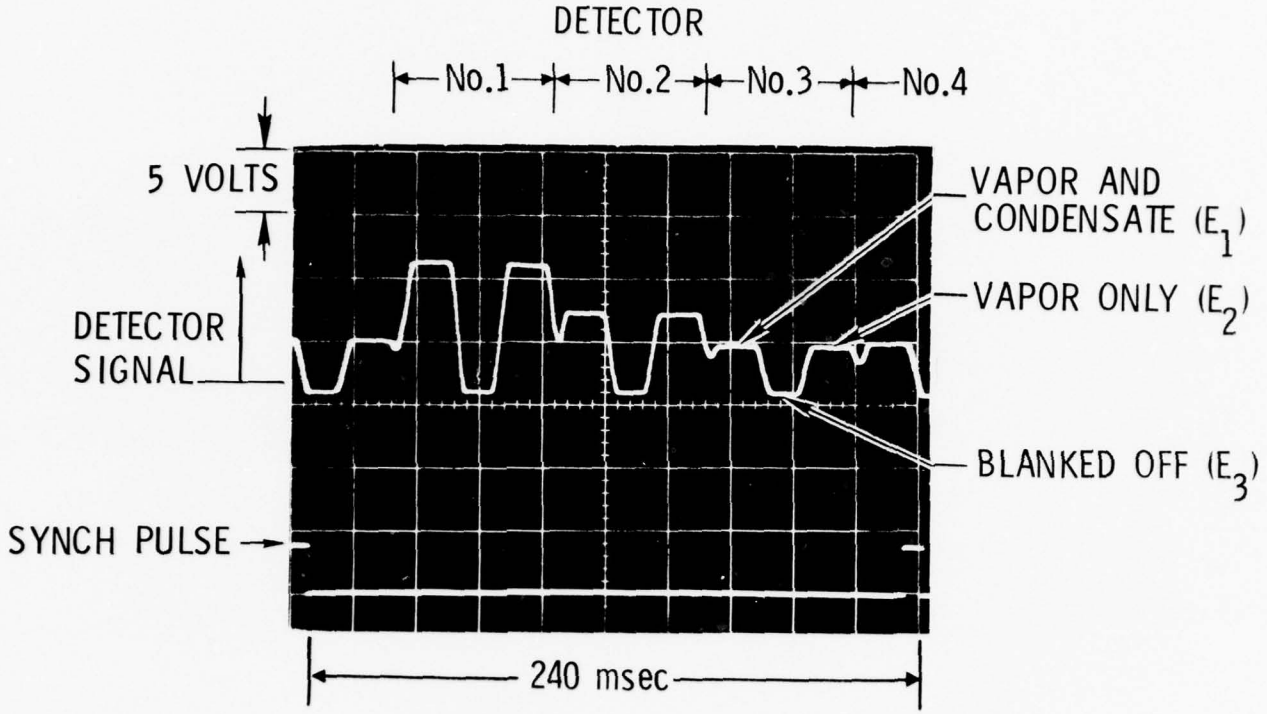

Air temperatures: 68°F
Relative humidity: 50%
Gap: 1.05 cm
No flow

Figure 10. B Detector Assembly Output (5-18-77)

into the detector at right angles to the axis of rotation and give smooth flow across the face of the housing. Sensor optics are flush mounted at this surface with a copper EMI foil providing apertures of 6 and 4.5 mm, source and receiver, respectively.

The bearing mounts for the housings are positioned on three jack screws that permit the distance between source and receiver to be changed. In effect, this changes the length of the absorbing medium so the output of the detector can be optimized for any level of water vapor. All three jack screws are driven by a common 120 V, 400 Hz gearhead motor. The source housing is located on the end of the jack screw with a left-hand thread; the receiver housing is located on a right-hand thread. Depending on the direction of rotation, the distance between source and receiver (gap) is increased or decreased. The operator can vary the gap from 1 to 5 cm while simultaneously making measurements. Microswitches are installed to limit the travel and a potentiometer is provided to indicate the size of the gap.

The source for the Lyman-α humidiometer is a hydrogen lamp. A 19 mm glass envelope is fitted with concentric electrodes and a magnesium fluoride window. The lamp is evacuated and filled with 8 Torr of hydrogen. The receiver is similar, but has a single electrode and the inside of the envelope is coated (as an electrode); it is filled with 16 Torr of nitric oxide. These units are manufactured by Glass Technologists* to a Naval Research Laboratory specification.** The radiation from the source ionizes the nitric oxide in the receiver so that a small current is developed in the tube when voltage is applied on the terminals.

The optical system behaves according to Beer's Law

$$I = I_o \exp(-\alpha x)$$

*Glass Technologists Company, 700 Holly Drive North, Route 10, Annapolis, Maryland 21401, Attn: John Trembly.

**GT 202 M and GT 203 D (except 19 mm OD)

where a source of intensity I_o is attenuated to intensity I, upon passing through a length x, in a medium of absorptivity α. In the EWER system, I_o is the source intensity, I is the intensity at the receiver, x is the gap, and α is the absorptivity of the sample to the hydrogen lamp radiation. It is clear that I_o, I, and α are parameters that depend on many factors that vary independent of water vapor (i.e., lamp output, receiver sensitivity, other absorbers such as oxygen, etc.) Therefore, a small change in α as a result of a small change in water vapor content would be difficult to resolve with an absolute measurement of I/I_o. By measuring two samples with the same detector (over a short interval of time), where the samples differ only in the water content associated with the condensate, these parametric variations can be normalized in the measurements as follows:

a. Evaporator

$$I_1 = I_o \exp(-\rho_1 kx) \tag{1}$$

where

$k = \frac{\alpha}{\rho_o}$

α = absorptivity at standard water vapor density

ρ_o = standard water vapor density
= 805 g/m^3 at 1 atm, 0°C

ρ_1 = water vapor density in evaporator sample

b. Separator

$$I_2 = I_o \exp(-\rho_2 kx) \tag{2}$$

where

ρ_2 = water vapor density in separator sample

c. Shutter Between Source and Receiver

$$I_3 = 0$$

Taking the logarithm of Eqs. (1) and (2) and rearranging

$$\rho_1 k x = \ell n I_o - \ell n I$$

$$\rho_2 k x = \ell n I_o - \ell n I_2$$

Noting that ρ_1 is the density of the water vapor in the background plus condensate and that ρ_2 is the background water vapor density, the difference of these equations is the water vapor density due to the condensate only.

$$\rho_{cond} = \rho_1 - \rho_2 = \frac{1}{kx} (\ell n I_2 - \ell n I_1) \qquad (3)$$

With proper electronics, the output of the receiver can be made proportional to the intensities I_1, I_2, and I_3, that is

$$E_1 = aI_1 + b, \; E_2 = aI_2 + b, \text{ and } E_3 = aI_3 + b = b$$

These are the three signal levels shown in Figure 10. Subsituting in Eq. (3)

$$\rho_{cond} = A\frac{\rho_o}{\alpha x} [\ell n (E_2 - E_3) - \ell n (E_1 - E_3)] \qquad (4)$$

For any measurement, all the parameters in Eq. (4) are known and the water content of the condensate can be calculated.

Electronics for source and receiver are contained within the rotating housings. A block diagram of these components is shown in Figure 11. A current-regulated, 500 VDC power supply furnishes 2 mA to each source

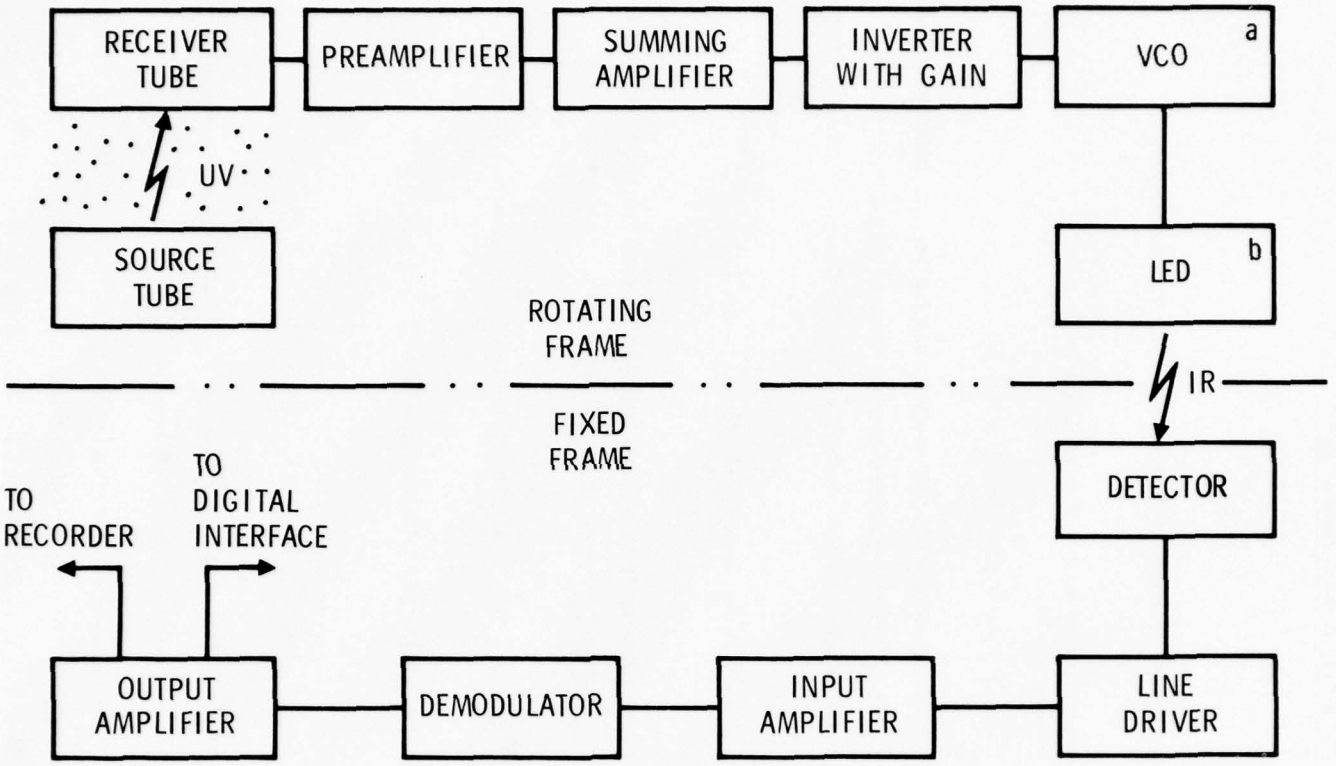

Figure 11. Detector Block Diagram

tube. It is potted in silicone in a recess between the four tubes (Figure 12). The power supply for the receiver is also potted between the tubes and supplies bias for the receivers and ± 15 volts for signal conditioning electronics (Figure 13). A high impedance preamplifier is mounted directly on the pins of the receiver tube. Signals from all tubes are combined in a summing amplifier and then pass, as a single output, through an inverting amplifier of low gain. This output is used to drive a voltage controlled oscillator to give frequency modulation of 60 to 80 kHz on a light-emitting diode (LED). This LED is located on the axis of rotation and looks into a nonrotating photodetector mounted in the brush holder behind the receiver housing. Another LED is mounted in the slipring plate, 2 cm from the axis of rotation. Steady illumination of this LED gives a synch pulse every revolution on another photodetector which locates the rotary position of the housing and identifies the receiver (and source) that is in the measuring position. Power (120 V, 400 Hz) is supplied through copper-graphite alloy brushes which are spring-loaded on copper sliprings on the back side of each housing (Figure 14). A small electronics box is attached to the bottom of the detector assembly (Figure 15) to house additional components required for transmission through the wing to the fuselage of the aircraft. The synch pulse and the gap signal are multiplexed for transmission on a single cable.

B. ELECTRONICS BOX

A box containing the remote controls for the probe assembly is located in the same compartment in the pod (Figure 3). It is also used for the termination of all of the conductors running through the aircraft wing. A view of this component with the cover removed is shown in Figure 16. All circuits are controlled by 28 VDC relays actuated by the operator from the control panel in the aircraft. The flow rate of the nitrogen purge is controlled by a motorized regulator powered by the 120 V, 400 Hz system. (Additional control is afforded by a hand regulator and normally open solenoid valve in

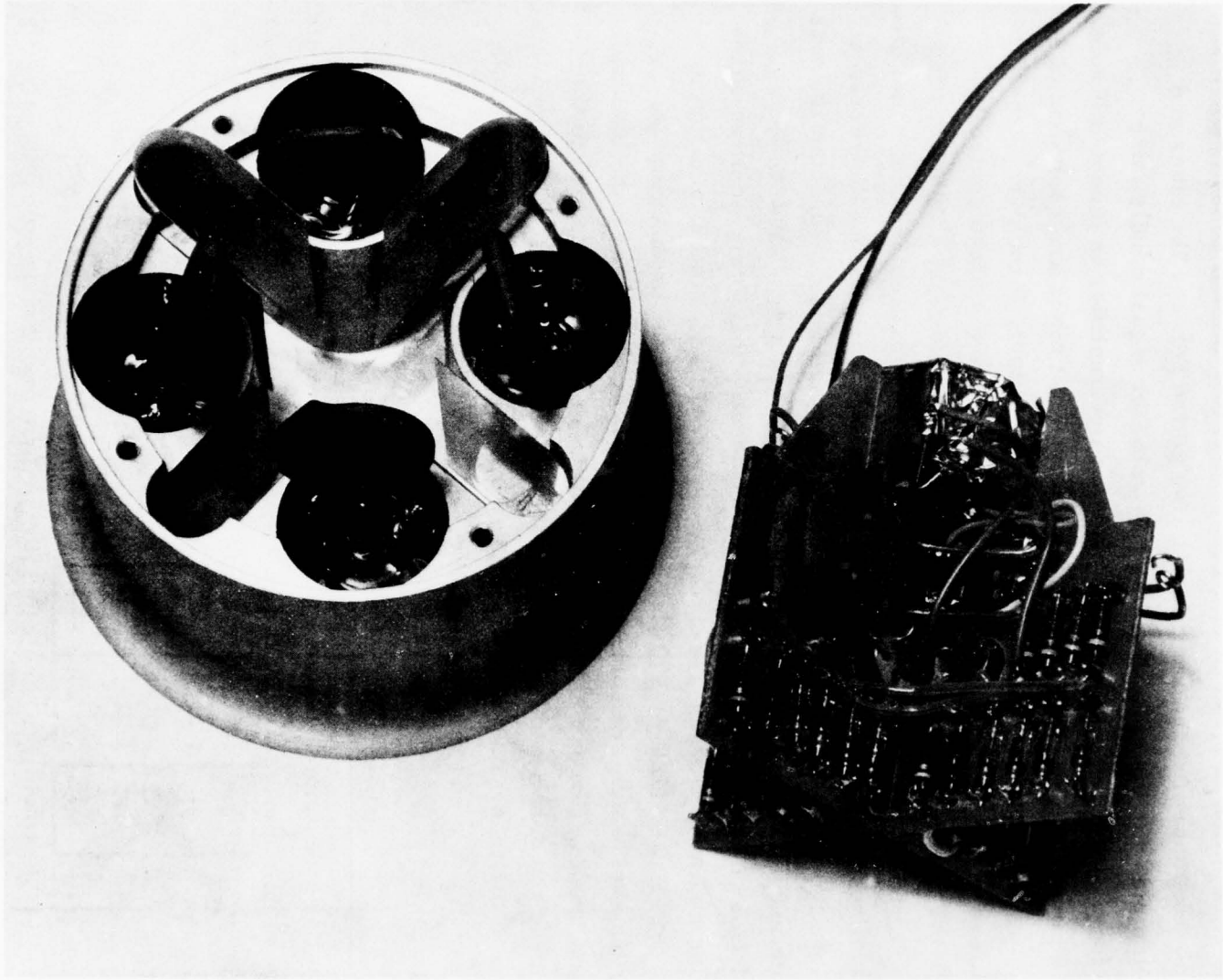

Figure 12. Source Assembly

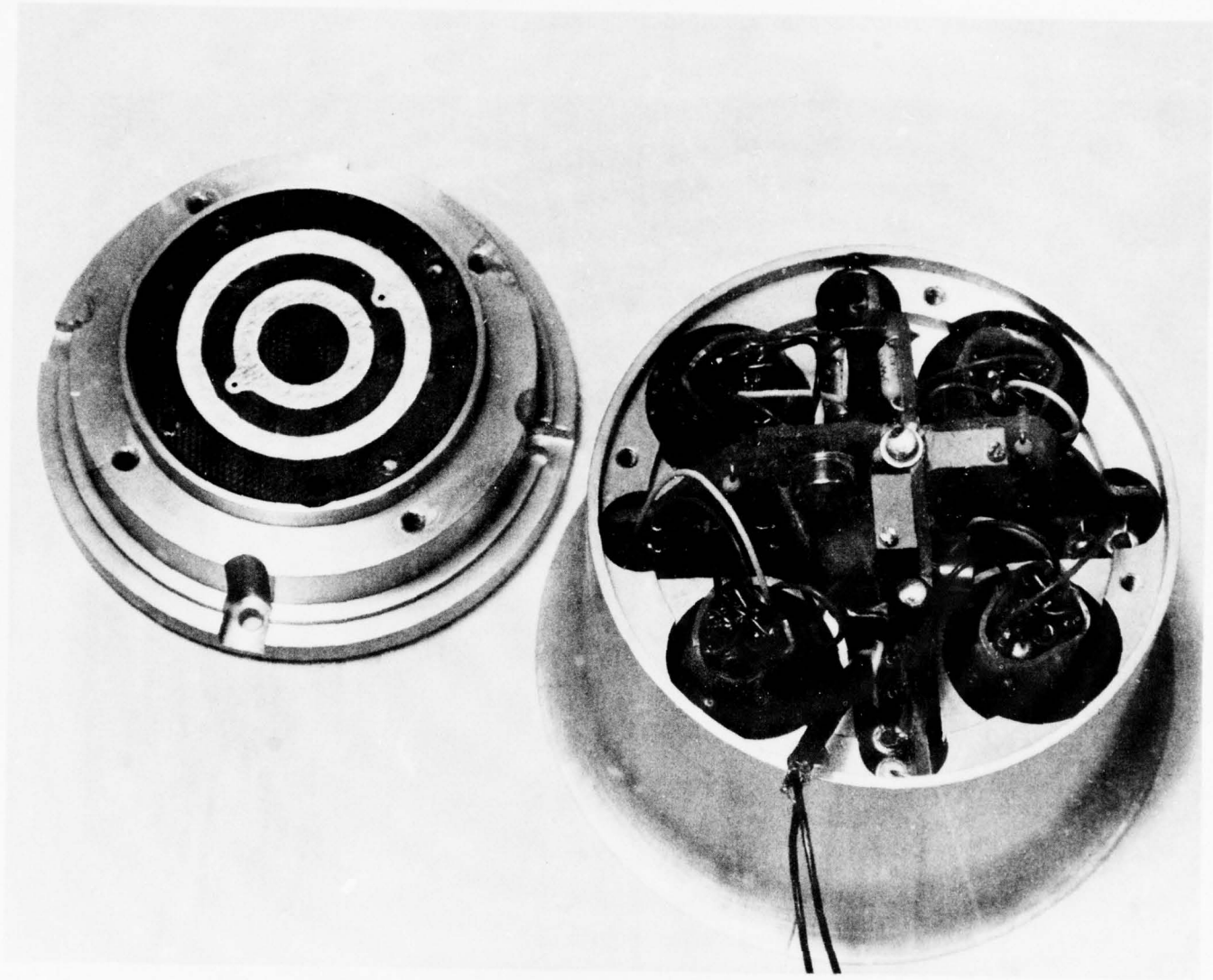

Figure 13. Receiver Assembly

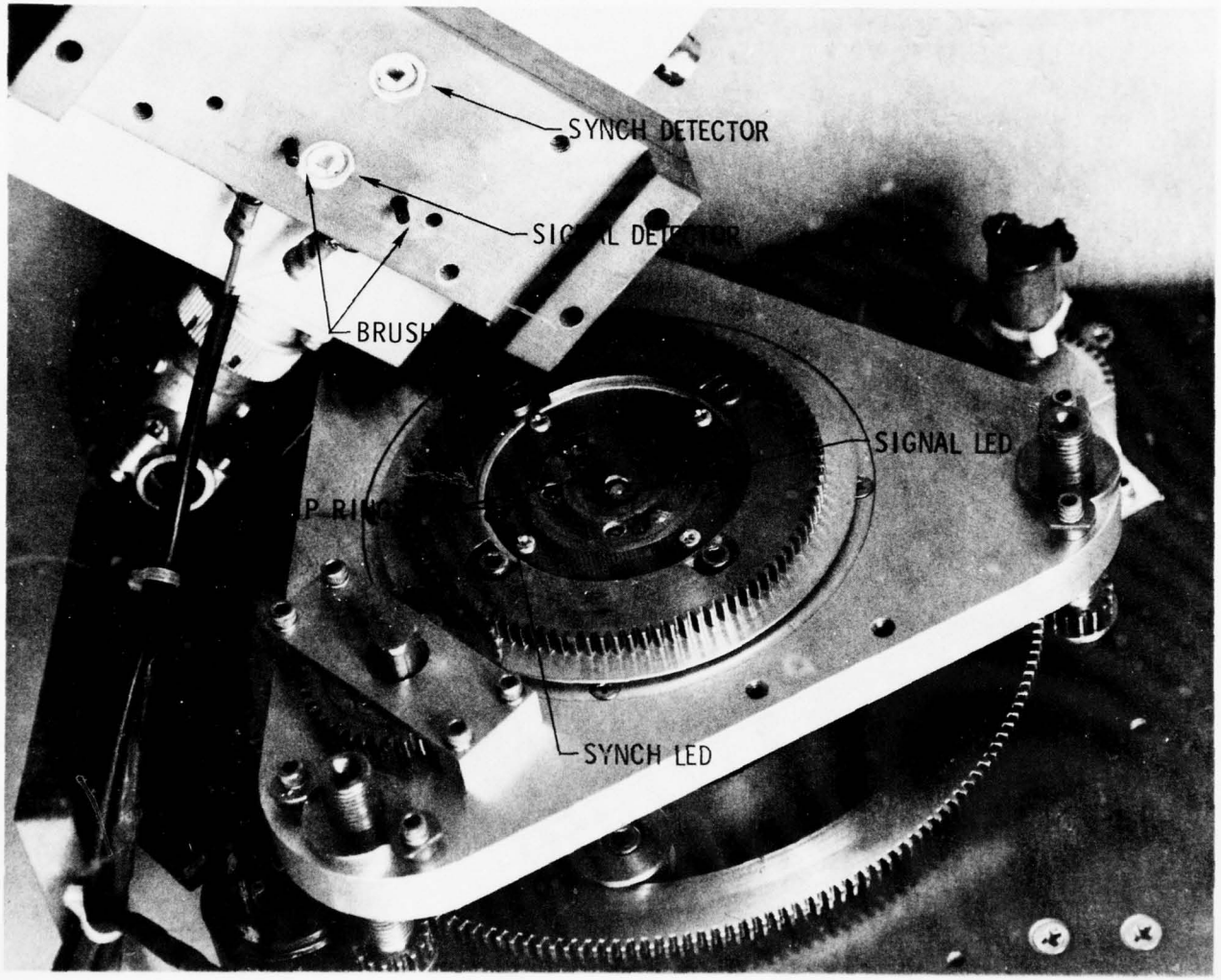

Figure 14. Input-Output Components on Detector Assembly

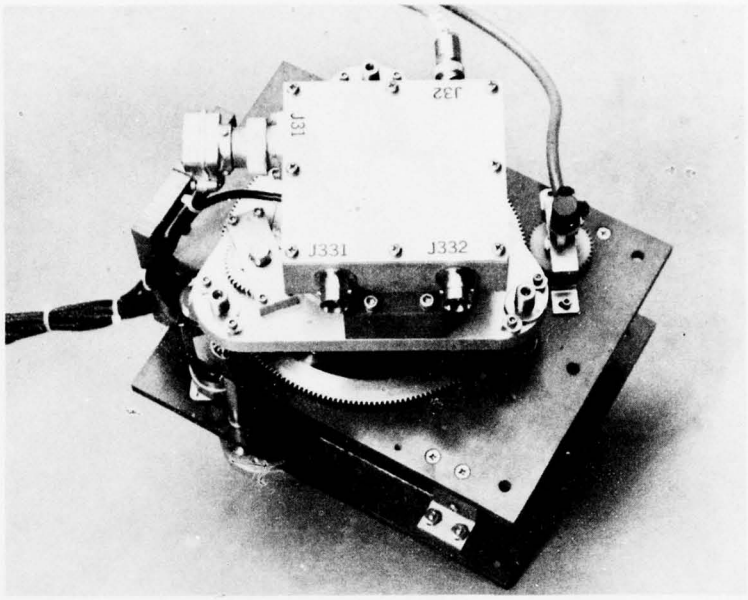

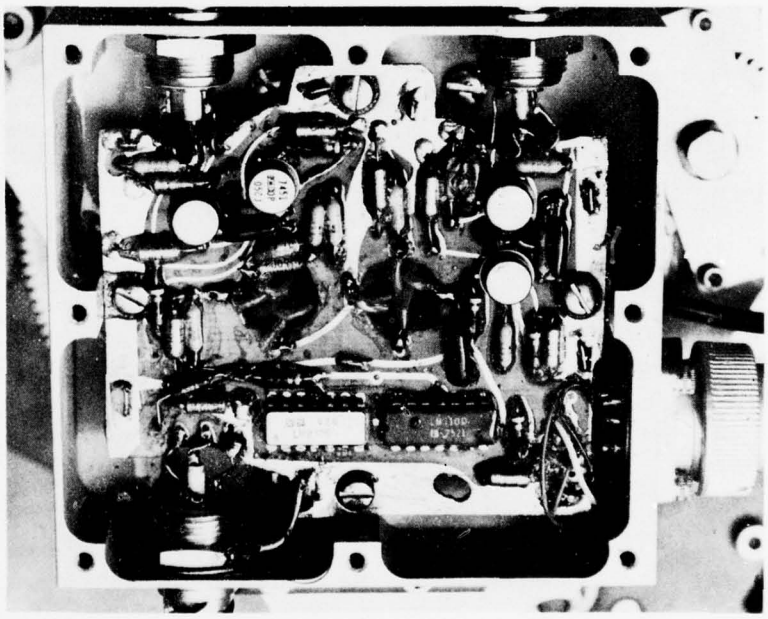

Figure 15. Driver Box

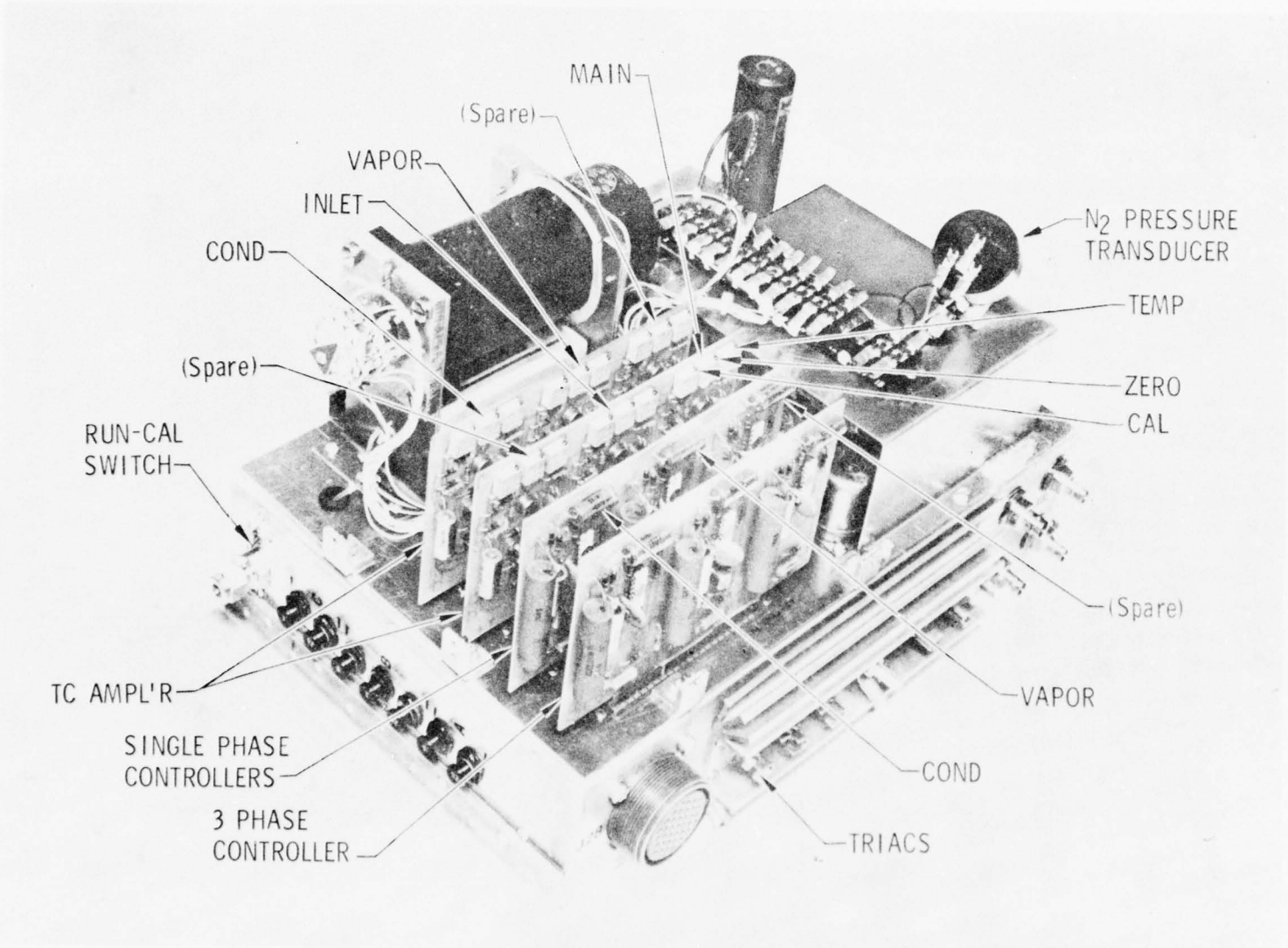

Figure 16. Electronics Box (Covers Off)

the fuselage.) A pressure transducer is located near the outlet of this system to indicate the flow setting.

Thermocouple amplifiers and heater controllers are located on circuit boards that plug into sockets on the main chassis. A servo-driven switch is provided to display various system functions on the operator control panel. Functions such as nitrogen purge pressure, heater or component temperatures, main heater current, and detector gap, are available at the operator's discretion. The electronic switches (Triac) for the main and trim heaters are located on a heat sink on the bottom edge of the main chassis. The studs on these solid-state devices are operating at the 120 V, 400 Hz line potential and so the units are mounted on mica washers and potted in silicone.

All the 120 V, 400 Hz power for the probe assembly ($\sim$ 10 kW) is connected to the bottom panel of the box. Breakers for each circuit are installed on the side and top edge of the chassis.

C. CONTROL BOX

A box is provided for installation in the aircraft which mounts the control panel and contains signal conditioners and the input/output (I/O) devices for a digital computer (Figure 17). On the AFGL C130, this box is mounted in rack 3. All 28 VDC power for EWER is connected to the back of this box along with 120 V, 400 Hz for the components inside.

1. PANEL

The control panel, Figure 18, contains all the switches required to operate the probe assembly. This includes a switch which enables the operator to display certain system functions on the left-hand meter. The right-hand meter is used to display the condensate level (g/m^3) as calculated by the online computer or display certain computer parameters when in a diagnostic mode. Connectors for interfacing with the probe assembly, digital computer, aircraft transducers and/or systems, and an analog recorder are located on the back of the box (Figure 19).

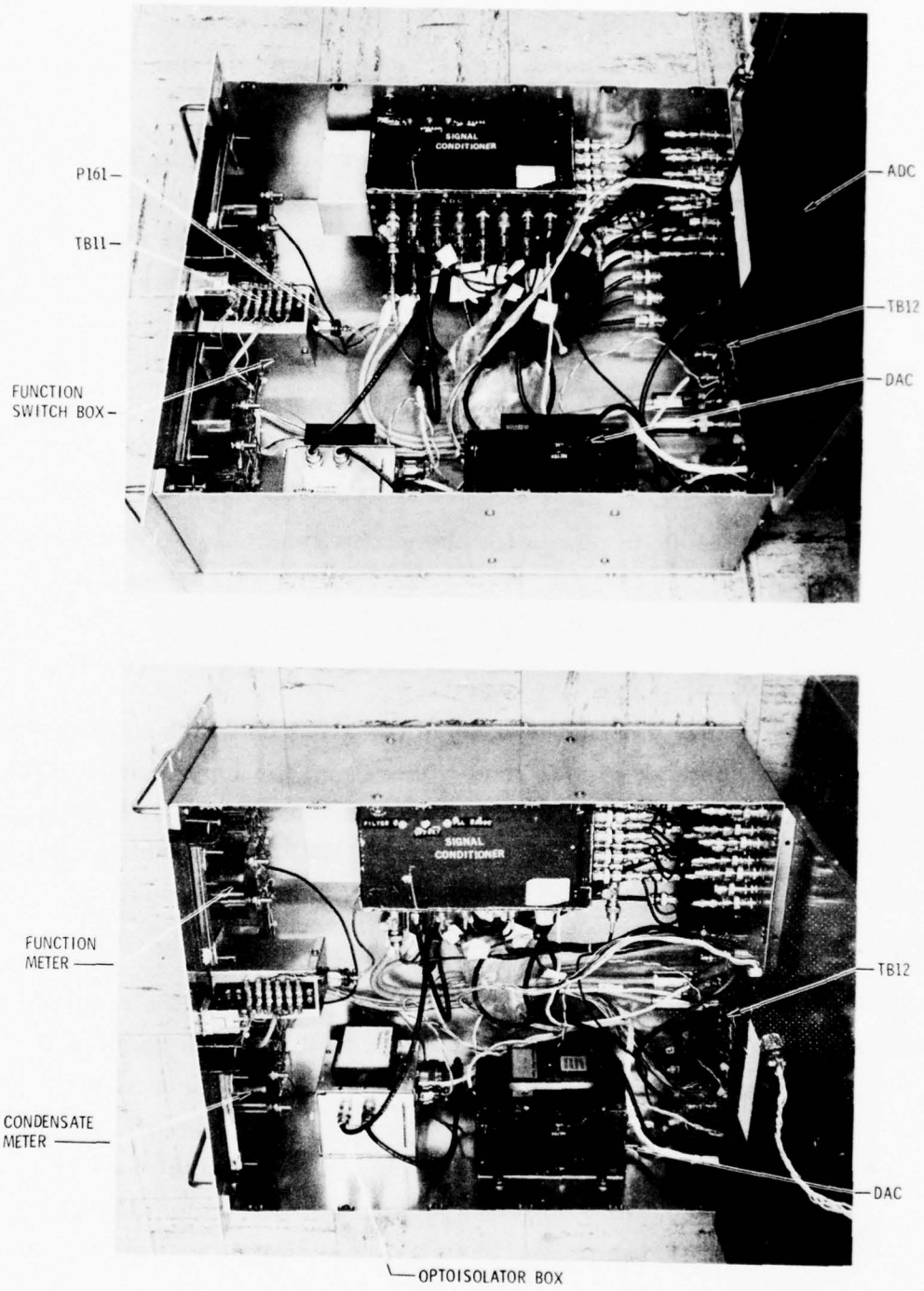

Figure 17. Control Box (Interior)

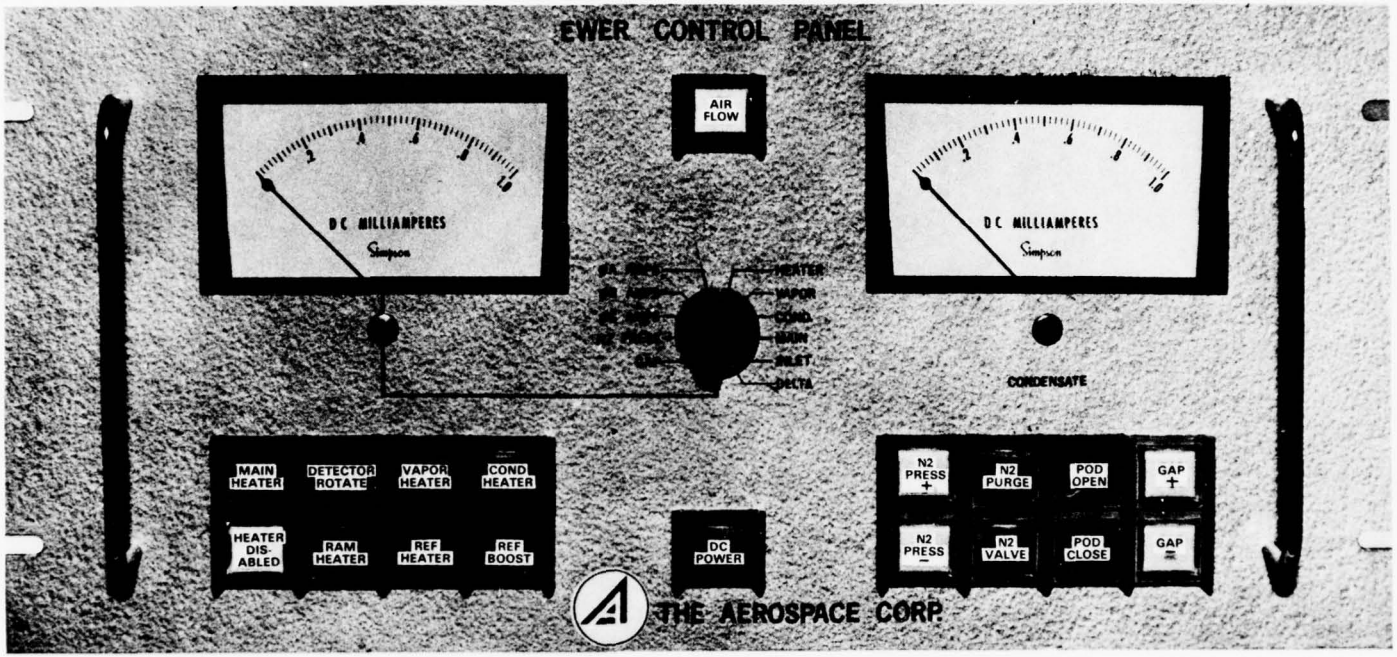

Figure 18. Control Panel

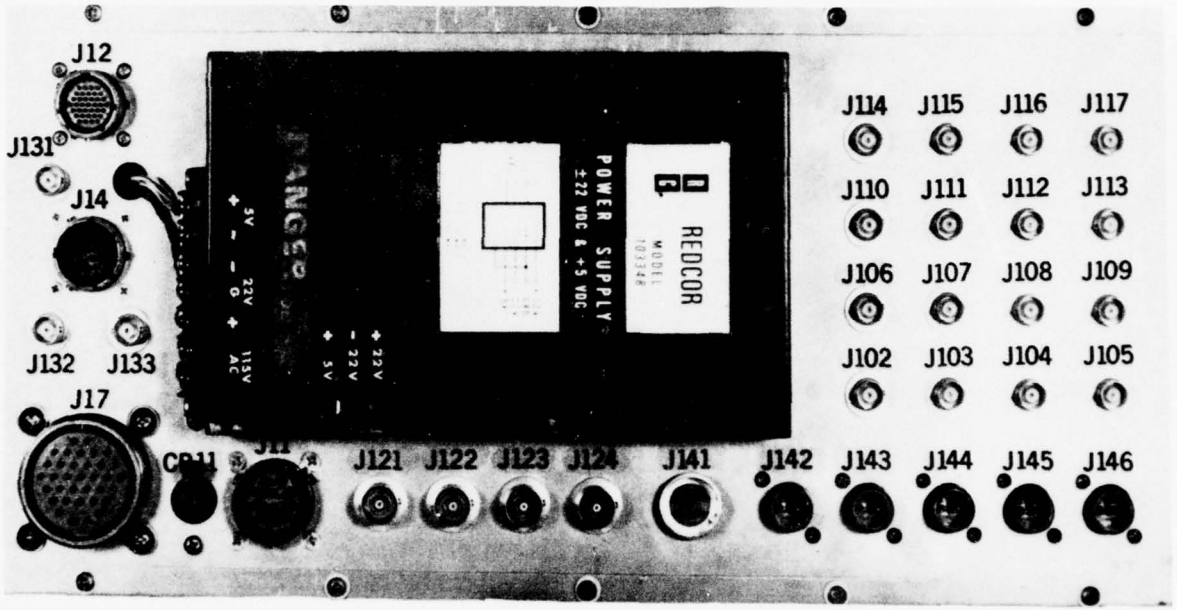

Figure 19. Control Box (Rear Panel)

2. SIGNAL CONDITIONER

The detector signals coming in from the probe assembly are frequency modulated. A phase-lock-loop is used to demodulate the FM and is field adjustable with range and zero controls. The zero is normally set for - 7 V (E_3 in Figure 10) at 57 kHz and the range for + 10 V at 80 kHz. If signal levels are such that the FM exceeds 80 kHz, the gap would be increased to bring the signal back into range. The demodulated signal is high-pass and low-pass filtered to reduce 400 Hz (field adjustable) and divided/buffered for analog recording and digitizing.

The multiplexed synch and gap signals are separated in the signal conditioner by an AC coupling and a low pass filter. The synch pulse is then shaped by a Schmidt trigger, buffered for analog recording and interrupt control for the digital computer.

Flight parameters needed for the calculation of condensate (i.e., temperature, pressure, etc.) are each connected to isolated input, high impedance amplifiers in the signal conditioner. A gain of two is provided with outputs available for analog recording and digitizing.

3. ANALOG-TO DIGITAL CONVERTER

Parameters to be used by the online computer in the calculation of condensate are digitized by an analog-to-digital converter (ADC) located in the control box. The power supply for this unit is located on the back of the box (Figure 19) and is powered by 120 V, 400 Hz. The digitizing process is controlled by the software in the computer and will be detailed in the discussion of the online computer. All digital lines (including the synch pulse) running to the computer are electrically isolated by optoisolators. This is necessary because of the voltage difference between ground in the front and back of the aircraft which affect the transistor-transistor logic (TTL) circuits. Circuit parameters on the optoisolators had to be adjusted also to accommodate cable resistance in the aircraft.

4. DIGITAL-TO ANALOG CONVERTER

The digital output from the online computer is returned to the control box (via optoisolators) where it is converted to analog output by a digital-to-analog converter (DAC). The output condensate (g/m^3), is divided/buffered for analog recording and display on the right-hand panel meter. A series of pulses are superimposed on the output every 30 sec to indicate which sensor in the detector is being digitized (one pulse for No. 1, two for No. 2, etc.). The pulse(s) will be filtered out by the meter movement, but will appear on the analog recording and will be useful for post-flight analysis.

D. RECORDER

An IRIG (inter-range instrumentation group) 14-channel tape recorder operated at 30 in/sec is provided to record all data that are required for post-flight determination of condensate. A method for reducing these data is given in Reference 6. All data are recorded on an FM carrier except the raw FM output from the detector which is direct recorded. FM data channels are calibrated at the beginning of each reel of tape, using a recorder calibrator which is permanently connected on the input to the recorder. A 10-pole switch actuated by 28 VDC permits -10, -5, 0, +5, and +10 V calibration steps to be recorded prior to taking any data.

E. ONLINE COMPUTER

A real-time presentation of condensate level was considered important to the operation of the EWER system in conjunction with other instruments on board the AFGL aircraft. Originally, a microprocessor was proposed that could be installed with the I/O units in the control box. However, a Rolm NOVA 1601 computer became available as GFP and was put to use because of its immediate availability and versatility for programming and debugging

[6] R. A. Meis and J. M. Penna, EWER Post Flight Data Processing Programs, TOR-0076(6550-19)-2, The Aerospace Corporation, El Segundo, CA (1 July 1976).

of the software. Its size dictated that it be installed in the aft part of the fuselage so long digital lines were required. The differences in the ground potential in the aft and forward parts of the fuselage necessitated that all lines be isolated with optoisolators.

Two complete programs are read into core memory via a teletype and punched paper tape. When the computer is first turned on, a static program is used to verify by a compare routine that the dynamic (working) program has not been "damaged." A calibration routine is also performed to verify that the algorithm is being computed correctly and that the output analog is correct. If these routines are accomplished successfully, the computer can be brought online by switching to digitize the output of a particular sensor in the detector.

If No. 1 is selected, the synch pulse will be read as an interrupt signal by the computer. After a preset interval the ADC will be called to digitize the detector output. Sixty-four data points will be digitized on this portion of the signal (condensate level) and then the computer signals the ADC to stop digitizing. The 64 data points are then averaged. After another preset interval, the ADC is called to digitize again and 64 data points are obtained on this portion of the signal (reference level). After averaging these data and another pause, the ADC is called to digitize the final portion of the signal (vapor level). Since there is now á long interval before the detector output again shows data for sensor No. 1 (about 250 msec), the ADC is called to digitize other parameters that are used in the computation of condensate. These data are stored in memory. When the synch pulse comes again the digitizing of the detector output is repeated as before with the average values for the three levels being added to the previous results. After four cycles of digitizing, the results are divided by four to obtain the 1 sec average for each level. These data, together with the other data stored in memory, are used to compute the condensate as follows:

$$\rho_{cond} = A \frac{T_\infty \times p_\infty}{G(p_\infty + \Delta p)} \left[\ell n\,(E_2 - E_3) - \ell n\,(E_1 - E_3)\right]$$

where

A = a constant
T_∞ = outside air temperature (°K)
p_∞ = static pressure, Torr
G = detector gap, cm
Δp = pod pressure, Torr
E_1 = condensate level, octal
E_2 = vapor level, octal
E_3 = reference level, octal

The result is put out on the digital lines to the DAC where it is converted to an analog output for recording or display on the condensate meter. The particular sensor being digitized is indicated in the output every 30 sec by a series of pulses, one for No. 1, two for No. 2, etc. In the event sensor No. 4 is being digitized, only half the data is processed because the synch pulse occurs during the interval the data is available and the computer cannot respond to the interrupt while processing data. The output in this case is held for approximately 2 sec.

A clear-air calibration routine is provided in the software to account for nonzero performance of the detector under these conditions. The operator can digitize each sensor in turn to develop a 10 sec average for each signal level. Any difference between the condensate and vapor level in clear-air conditions is then used to bias data obtained during sampling.

IV. DEVELOPMENT TESTING

IV. DEVELOPMENT TESTING

Four series of tests were performed to demonstrate that the EWER design would meet the conditions set forth in the ABRES specification for the instrument. These were functional, calibration, environmental, and flight tests; they will be discussed in detail in the following sections.

A. FUNCTIONAL TESTS

The initial tests of the probe assembly were performed using a low pressure high volume centrifugal fan to supply the air. An aluminum fitting was made to connect the 10 cm diameter fan outlet to the probe assembly (Figure 20). Flow was regulated by a butterfly valve in the fan outlet. Liquid nitrogen was injected downstream of this valve to compensate for the heating of the air as it was compressed by the fan and to increase the cooling load on the evaporator heater.

Hot-wire anemometers were used to measure the air velocity at the centerline of the inlet of each probe. The damper on the separator probe was adjusted to make the flow at the inlet of both probes the same. A traverse with the hot-wire anemometer across the flow entering the detector (from the trim heaters) was made to balance these flows and to check the flow uniformity across the 5 cm detector gap. A typical traverse is shown in Figure 21. Subsequent adjustments of the various dampers has probably changed the relative flow rates, but the flow uniformity is probably not affected.

There was some concern that the low signal levels in the Lyman-α detector system would be adversely affected by the operation of the high power heater in the evaporator. Figure 22 shows the results of an electrical noise test. For this case, the detector housings were not rotating and a sensor was positioned in the flow coming from the evaporator probe. The base line output was indicated as all systems "off" and had relatively

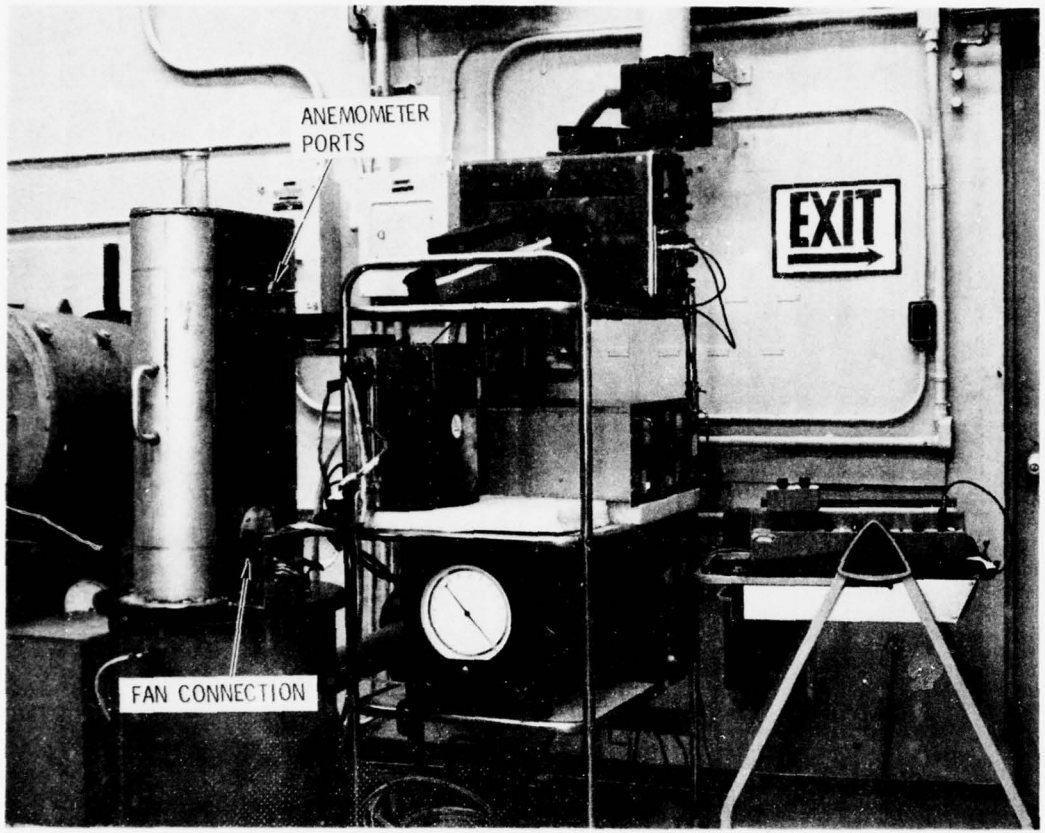

(a) In Test Rig

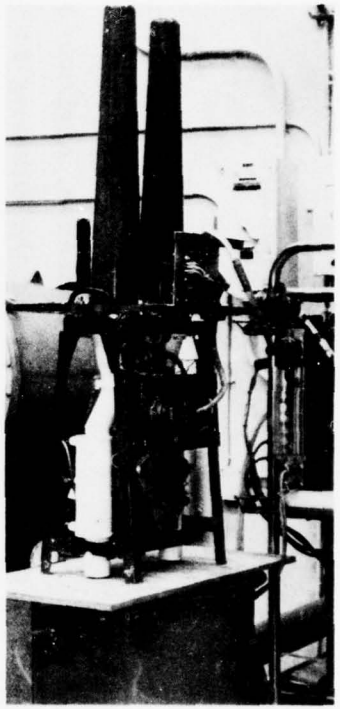

(b) On Test Rig

Figure 20. Probe Assembly

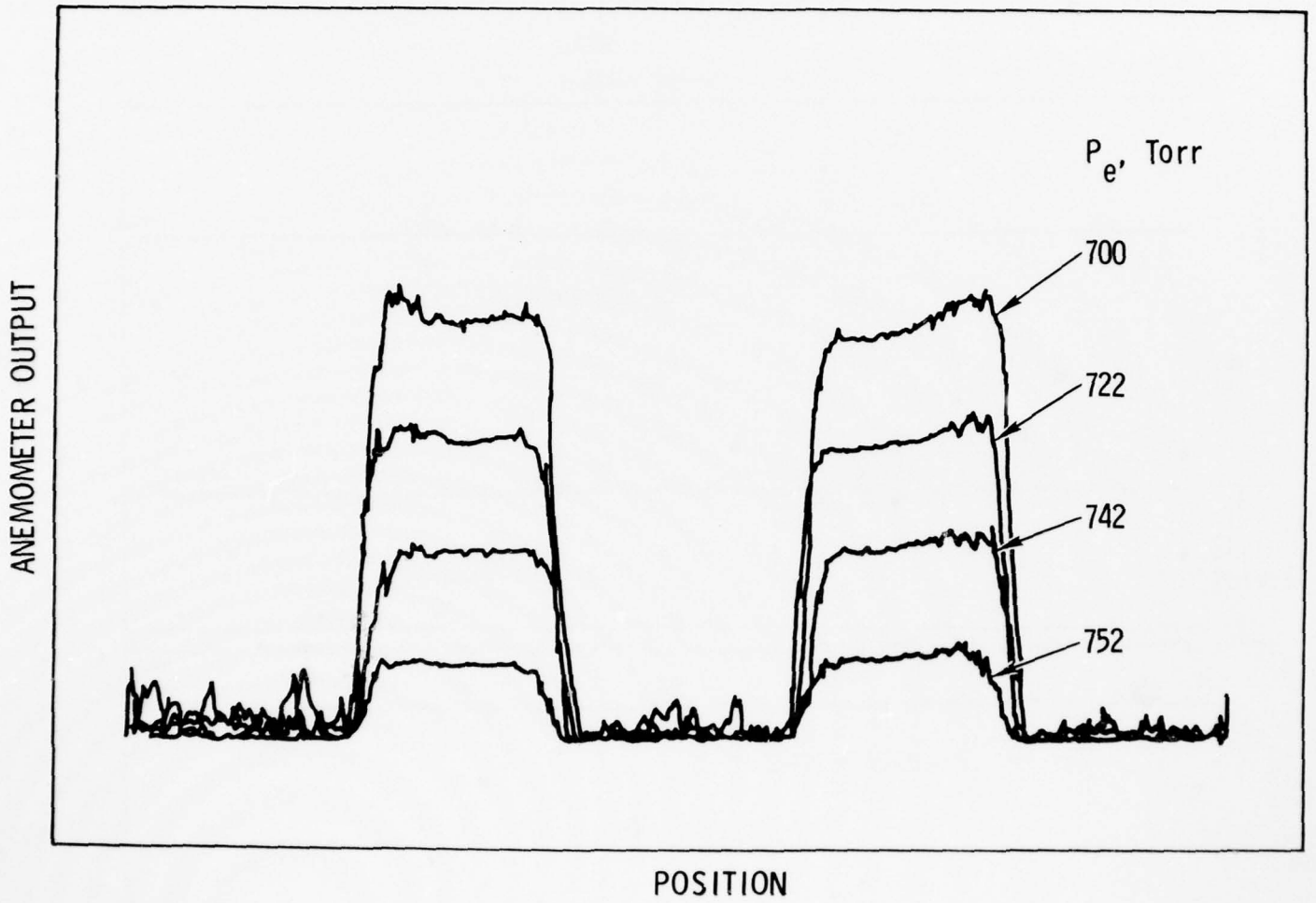

Figure 21. Anemometer Traverse at Detector Entrance

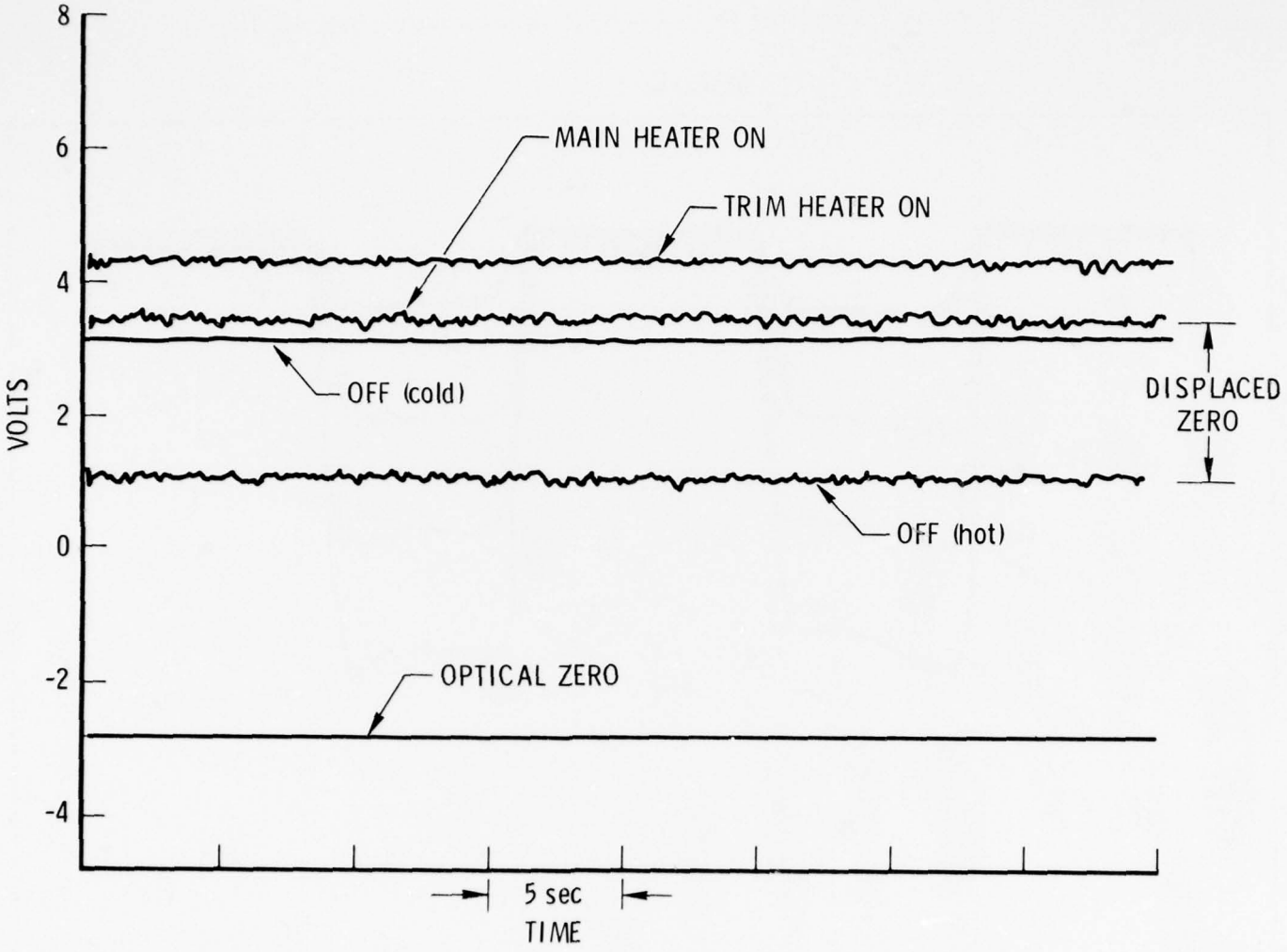

Figure 22. Detector Noise Level

low noise. The main heater was turned on and the signal was increased due to the lowering of the density of water vapor in the detector gap. The noise also increased. The trim heater increased the signal further; the noise remained essentially the same. The heaters were then turned off. The signal decreased quickly as the trim heater cooled and it remained at the level for the main heater because of the thermal inertia in this large heater design. (Note that the zero has been displaced to avoid confusing the two traces.) It is significant that the noise level on the detector signal is not reduced when the heater power is turned off. The fluctuation of the detector signal is not due to electrical noise, but is believed to be representative of the thermal turbulence level in the system. Therefore, instantaneous measurements with EWER would be subject to considerable error, and the averaging of data would be required.

A test of the time response of EWER was arranged by installing the probe assembly in a facility that could be exhausted by a large vacuum system. The arrangement is shown schematically in Figure 23. Altitude is simulated by adjusting the throttle valve to obtain the desired pressure on the detector. Flight velocity is simulated by flow-through orifices located in the aluminum fitting used previously with the fan.

Figure 24 shows the signal from the nonrotating detector, with the sensor positioned in the flow coming from the evaporator. A small particle of water ($\sim$3 mm in diameter) was dropped through the flow orifice on the evaporator. It will be noted that the signal dips sharply as the particle is added to the background water vapor in the flow as it passes through the evaporator. More important is the rapid cleanup as the excess water vapor is swept through the system, indicating a time constant of a fraction of a second. Simulated flight conditions for this case were 150 knots at 20,000 ft. An ice particle was also dropped into the inlet and gave similar results (Figure 25). The smaller dip in signal may be due to the smaller amount of water in the ice (not measured) or to incomplete melting/evaporating of the solid particle.

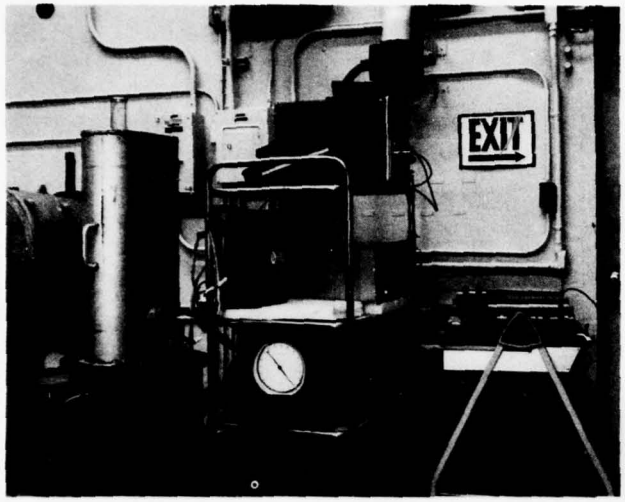

(a) Vertical Arrangement

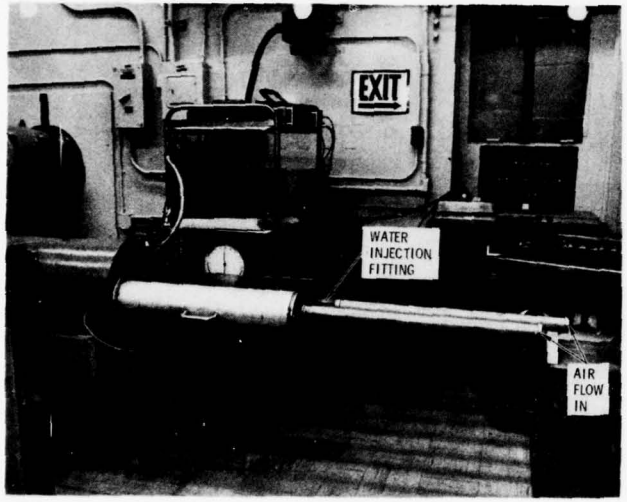

(b) Horizontal Arrangement

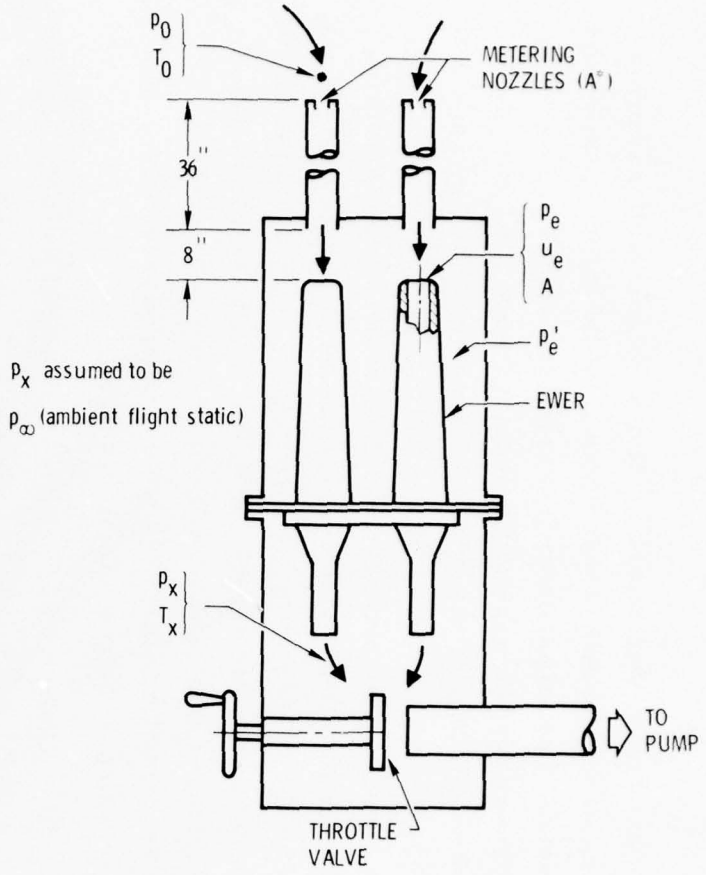

(c) Schematic

Figure 23. Flow Calibration Facility

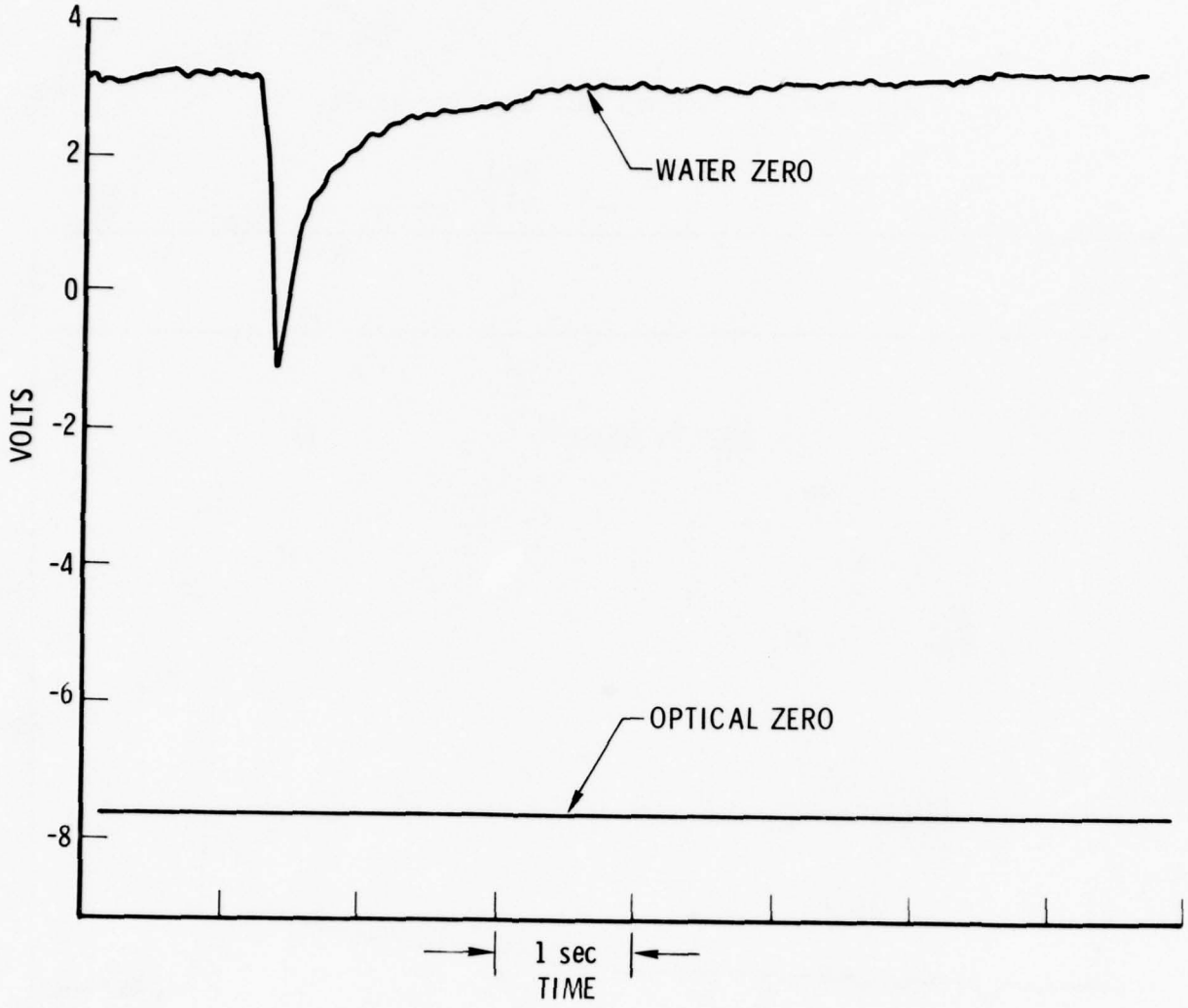

Figure 24. Detector Output - Water Droplet

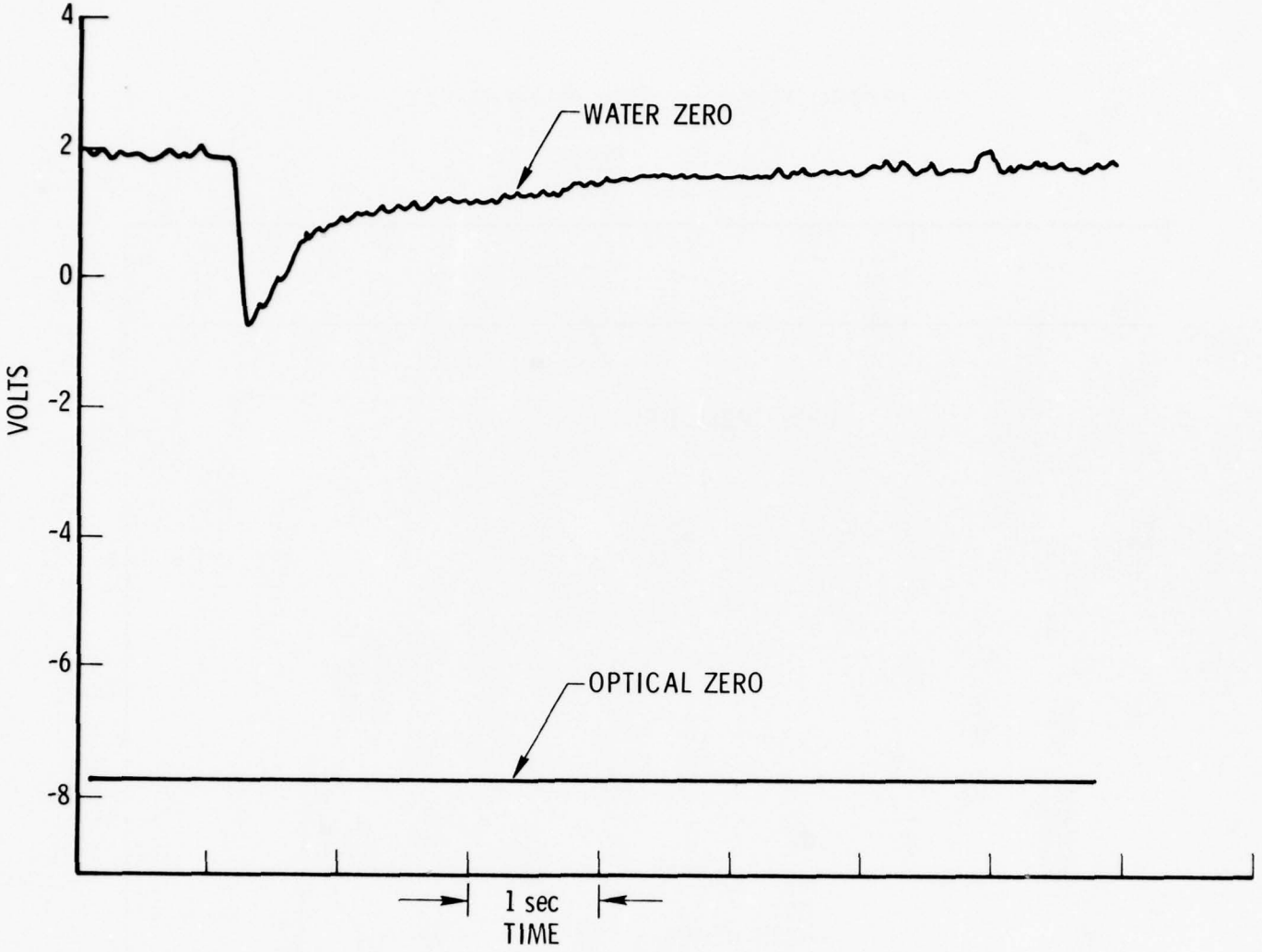

Figure 25. Detector Output - Ice Particle

Liquid water dropped into the separator inlet should have had no effect on the detector signal when the sensor was in the flow from the separator. Figure 26 shows that this is not the case. It was concluded that the passing of the particle through the sonic flow orifice caused the surface water to flash into vapor. Therefore, the aluminum fitting was removed so that the vacuum pump would draw the ambient air directly into the probe (i.e., no metering orifice). When a water particle was then dropped into the flow, no indication was observed on the detector signal.

Water was also sprayed into the separator probe so that some collected on the mouth of the inlet. In this case, there was a noticeable reading on the detector that persisted for some time (Figure 27). It was concluded that the bleed holes in the wall of the probe, just inside the inlet, were being filled with the vapor from the water collecting on the surface at the inlet. Water or vapor flows along the wall in the boundary layer and into the holes, completely masking the true reading of background vapor.

The problem was corrected by changing the bleed holes to thin-walled cylinders that protrude through the boundary layer on the wall of the probe (Figure 28; see also schematic, Figure 4). Spray tests on this separator configuration showed that even large amounts of water adhering to the inlet or injected axially did not give any indication on the detector. Spray directed at approximately 10° to the axis of the probe did show some indication. However, since the flow at the inlet of the probe under these test conditions is two-dimensional (i.e., suction through a sharp-edged orifice) the results are at best qualitative for separator efficiency when sampling at high angles of attack.

A series of tests was performed to evaluate the impedance to flow within EWER. Data from these tests would show how nonisokinetic the flow is and how much air is being bypassed during sampling. The flow facility of Figure 23 was used. It is possible to relate the flow in this facility to that which would obtain in flight by the use of one-dimensional flow equations as discussed in Appendix A. It will be noted that the fixture

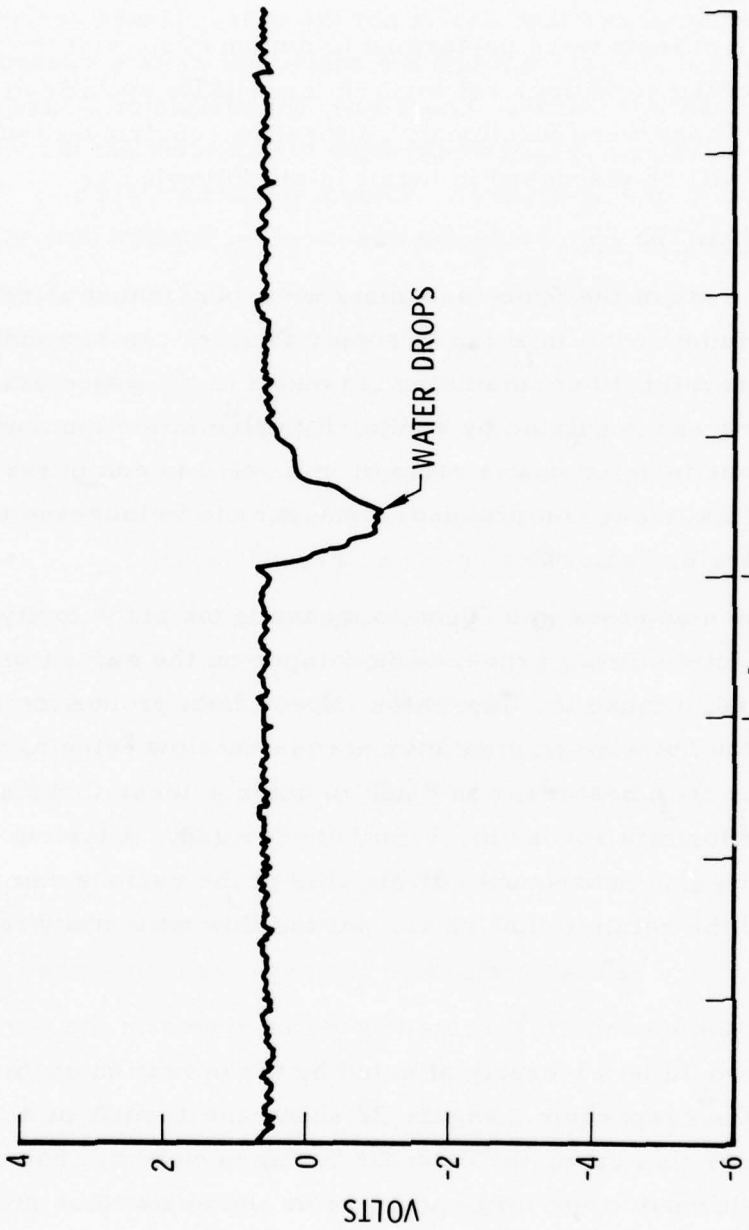

Figure 26. Detector Output - Droplet in Separator Inlet

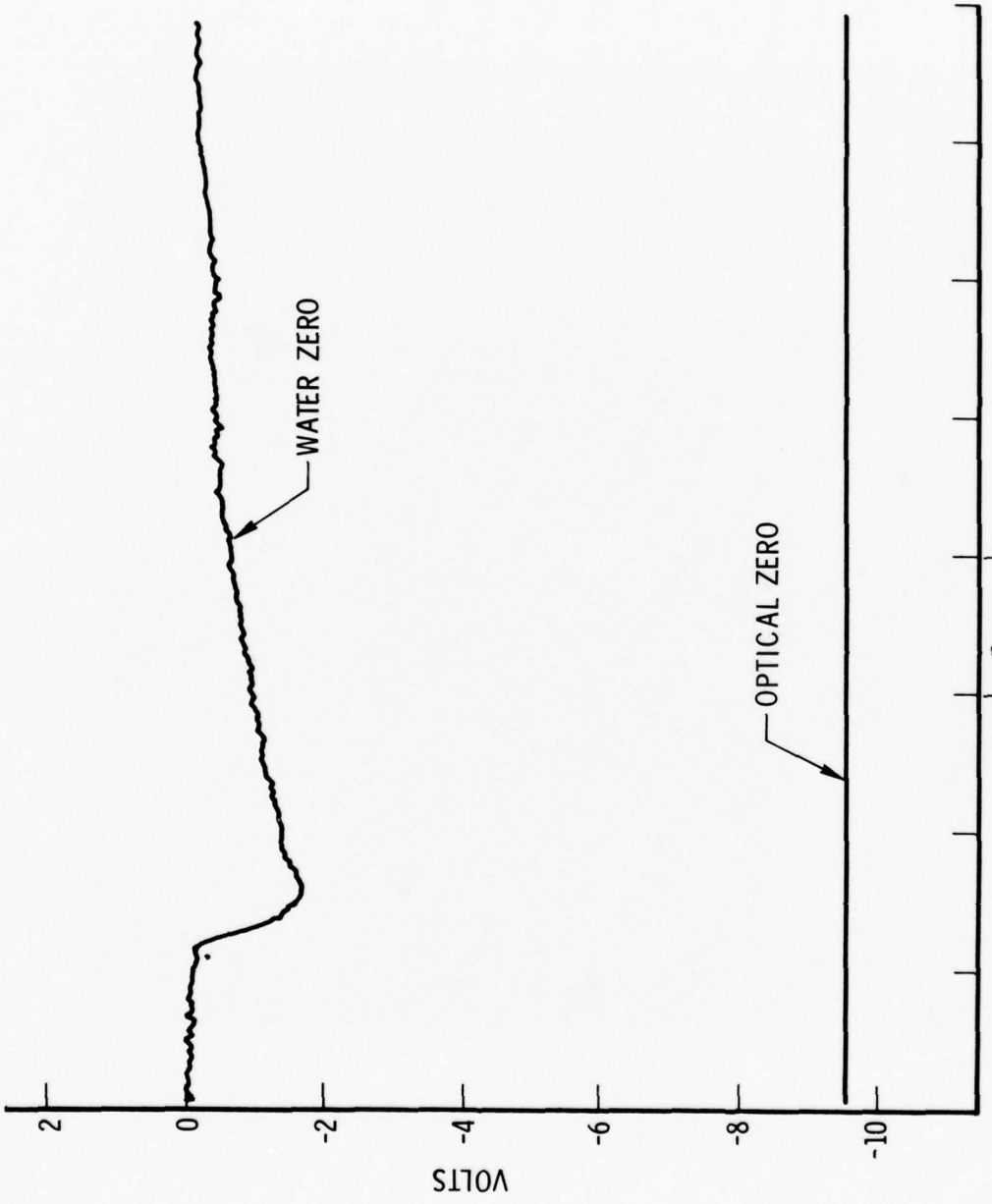

Figure 27. Detector Output - Water Spray on Inlet

Figure 28. Separator Probe Inlet

is arranged so that all the gas entering through the metering orifices passes through the unit. If a critical pressure ratio is maintained across these orifices, the flow will be choked (sonic throat) and the mass flow will be a function of the ambient conditions in the laboratory only. Mass flow can be converted to volume flow if the velocity at the inlet is known.

Although hot-wire anemometers were installed in the facility to indicate the air velocity on the centerline at the inlet of each probe, no quantitative data were derived from these measurements because of difficulties in absolute calibration of the anemometers when used over a wide range of pressure. In addition, knowing the velocity on the centerline is of limited value in converting mass flow to volume flow unless the velocity profile is known. However, anemometer data were useful for comparing the flow rates in the two probes and the relative changes that occur as conditions vary within the unit.

Volume flow for any set of operating conditions can be calculated using the one-dimensional flow equations if the pressure inside the inlet is known. A static pressure measurement was made just inside each probe through a port in the wall about 1 cm from the inlet. Since the flow is directed into each probe by a duct which is approximately the same diameter as the inlet, the flow is essentially one-dimensional and the wall measurement is representative of the static pressure at this position. This was verified by noting that the pressure in the upper chamber (p_e' in Figure 23) was always within a couple of Torr of p_e so no effects were apparent in the vicinity of the inlet that could affect the wall measurement.

Data obtained in a series of test are tabulated in Table 1. Most of the data were taken for cold-flow conditions (i.e., no heat on the evaporator). However, for two cases of flow rate, the evaporator heater was turned on to determine what effect this would have on the flow characteristics of the unit. It will be noted that the change in hot-wire anemometer reading at the inlet to the evaporator shows only a slight change from cold to hot running.

Table 1. Cold Flow Test (7-8-76)

Diameter	p_e	p_e'	p_x	u_{evap}	u_{Sep}
0.504	760	760	760	0	0
	472	475	450	52	57
	447	451	425	51	56
	423	427	400	50	55
	400	404	375	49	54
	376	380	350	48	53
	355	360	325	47	52
	331	336	300	45	50
	309	315	275	43	47
	287	293	250	43	45
	266	273	225	41	43
	246	253	200	39	42
	377	381	350	48[a]	50[a]
0.647	500	510	450	83	95
	481	491	425	83	95
	460	471	400	83	95
	438	450	375	81	93
	417	430	350	80	91
	396	409	325	78	90
	378	391	300	76	87
	360	274	275	76	85
	340	355	250	75	83
	324	340	225	74	82
	310	326	200	74	79
	415	438	350	86[a]	85[a]
0.770	542	559	450	132	118
	508	526	400	135	120
	475	496	350	135	120
	442	466	300	132	118
	415	441	250	129	113
	393	422	200	128	115
0.504	330	335	300	46	47
	336[b]	340[b]	300[b]	45[b]	48[b]
0.647	376	390	300	88	85
	386[b]	398[b]	300[b]	87[b]	87[b]

[a] Anemometers reversed.

[b] Heated.

Units: Dia - inches
p - Torr
u - arbitrary

Table 1. Cold Flow Test (7-8-76) (Continued)

Diameter	p_e	p_e'	p_x	u_{evap}	u_{Sep}
0.288	456		450	12	16
			425		
	405		400	12	16
			375		
	354		350	11	14
			325		
	305		300	10	13
			275		
	255		250	9	11
			225		
	205		200	8	9
0.408	459	461	450	30	33
	435	437	425	30	33
	411	414	400	30	33
	386	387	375	29	33
	362	364	350	28	30
	336	339	325	28	30
	313	315	300	26	30
	286	288	275	26	28
	263	265	250	24	26
	245	248	225	23	26
	223	226	200	22	25

Units: Dia - inches
p - Torr
u - arbitrary

The results of the cold-flow tests can be presented in terms of equivalent flight conditions (see Appendix A). The data are plotted in Figure 29 as collection efficiency versus airspeed for different pressures (viz altitudes). That is, the resistance to flow through the unit at any pressure and velocity causes some of the airflow to be diverted around the device. The ratio of the mass fraction of air actually sampled to that which would be sampled if there were no resistance (i.e., isokinetic flow) is defined as the collection efficiency

$$\eta = \frac{u_e \rho_e}{u_\infty \rho_\infty}$$

where

u = air velocity

ρ = air density

e = at probe inlet

∞ = in freestream

It will be noted that the collection efficiency is about 0.45 and is only slightly influenced by flight conditions. The points plotted in Figure 29 are from data tabulated in Table 1. If one assumes that EWER behaves as a classic flow restriction, these data should be correlated by the expression

$$D^n = k\sqrt{p_\infty (p_e - p_\infty)}$$

where

D = dia of orifice

k = empirical constant

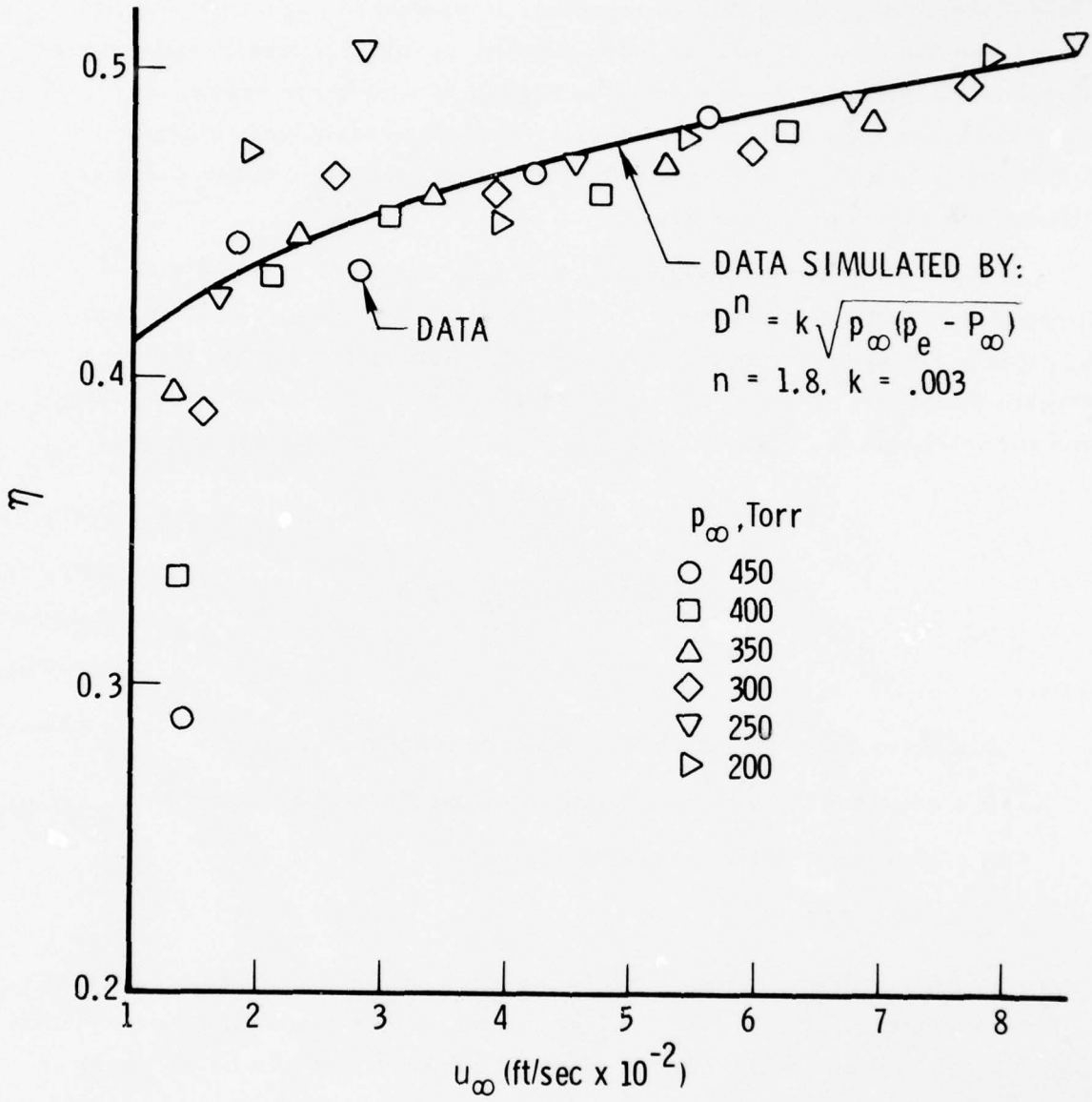

Figure 29. Collection Efficiency vs Flight Parameters (Unheated)

For n = 1.8 and k = 0.0030535, the relation predicts p_e for each measured value of p_∞ with a variance of 0.8 $Torr^2$. The collection efficiency, calculated using this expression, is plotted in Figure 29 and fits the bulk of the data. It will be noted that the result is virtually independent of pressure (altitude) as is evident in Figure 30 where the results are plotted with an expanded scale. Similar data were taken with all heaters operating (Table 2). The results for collection efficiency under these conditions are shown in Figure 31.

Figure 32 shows, schematically, EWER installed in a pod where there is additional resistance to flow created by the exhaust system. In this case, the pressure in the exhaust of the flow facility is not the freestream pressure but some pressure intermediate between the freestream and the inlet values. The exhaust system can be characteristized by the relation

$$\dot{m} = BA_x p_x \sqrt{p_\infty (p_x - p_\infty)}$$

where

$\dot{m}$ = mass flow through EWER (proportional to $u_e A_e p_e$)

B = constant of portionality (includes discharge coefficient)

A_x = equivalent orifice area of exhaust

p_x = pod pressure

if one is willing to neglect the effect of heating between the inlet of EWER and the exhaust port (i.e., $T_e = T_x$ so $\rho \propto p$). For a 6 cm diameter exhaust and B = 0.5, the pressure drop in the exhaust system would be as shown in Figure 33. Note that the parameter here is pod pressure. These results are similar to those measured during flights of C130E-571 where a pressure differential of 8 Torr was typical for 150 knots at 20,000 ft (350 Torr).

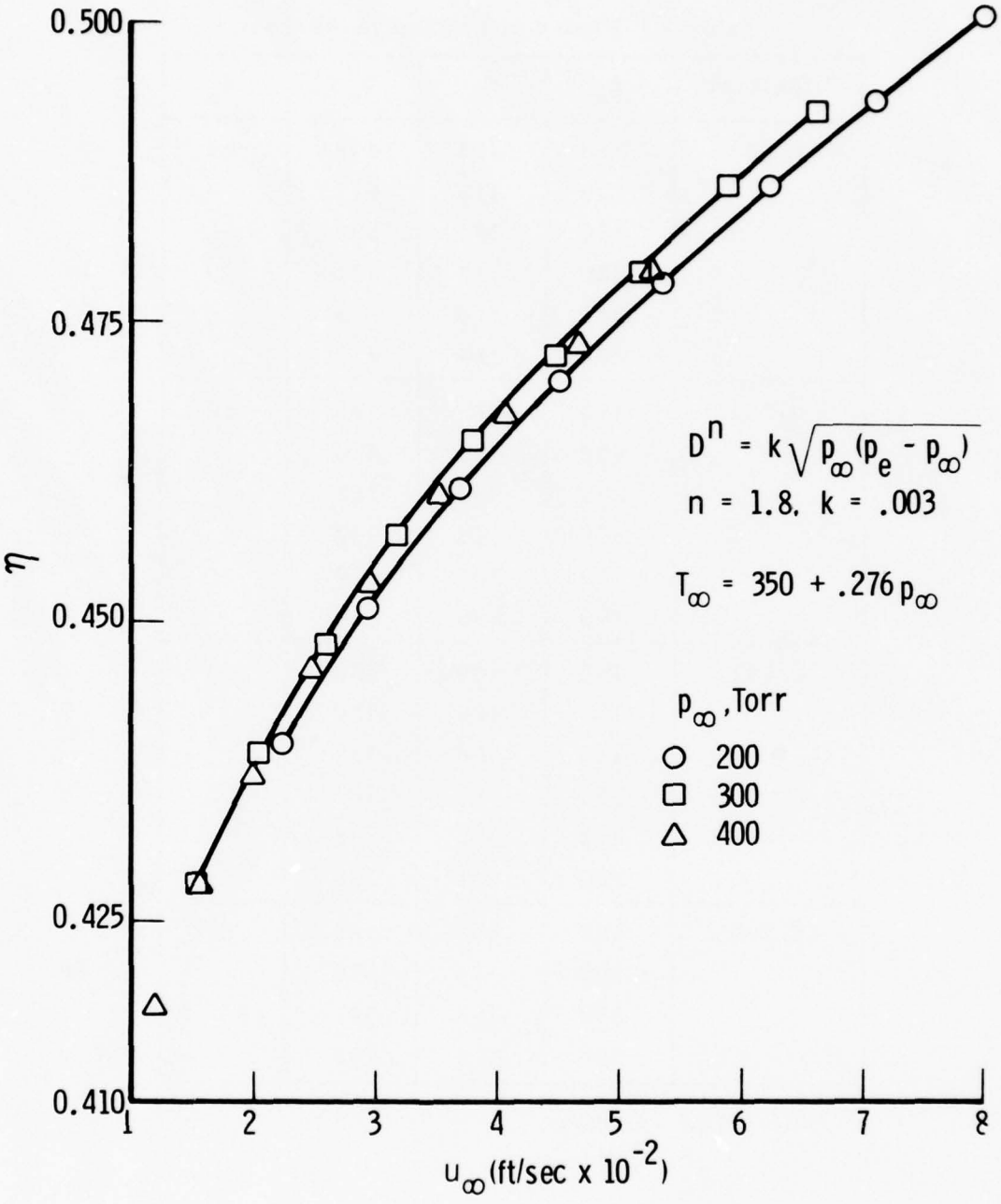

Figure 30. Collection Efficiency (No Backpressure in Pod)

Table 2. Flow Calibration (6-30-76)

Diameter	p_x	p_e	p'_e	T_x
0.408	450	463	468	83
	400	413	417	
	350	365	369	
	300	317	321	
	250	270	275	
	200	224	230	
0.504	450	475	430	86
	400	428	433	
	350	383	388	
	300	346	342	
	250	293	300	
	200	256	263	
0.647	450	509	520	83
	400	468	480	
	350	428	439	
	300	388	402	
	250	352	368	
	200	321	338	
0.770	450	552	469	81
	400	519	538	
	350	488	507	
	300	460	481	

Units: Dia - inches
p - Torr
T_x - °C

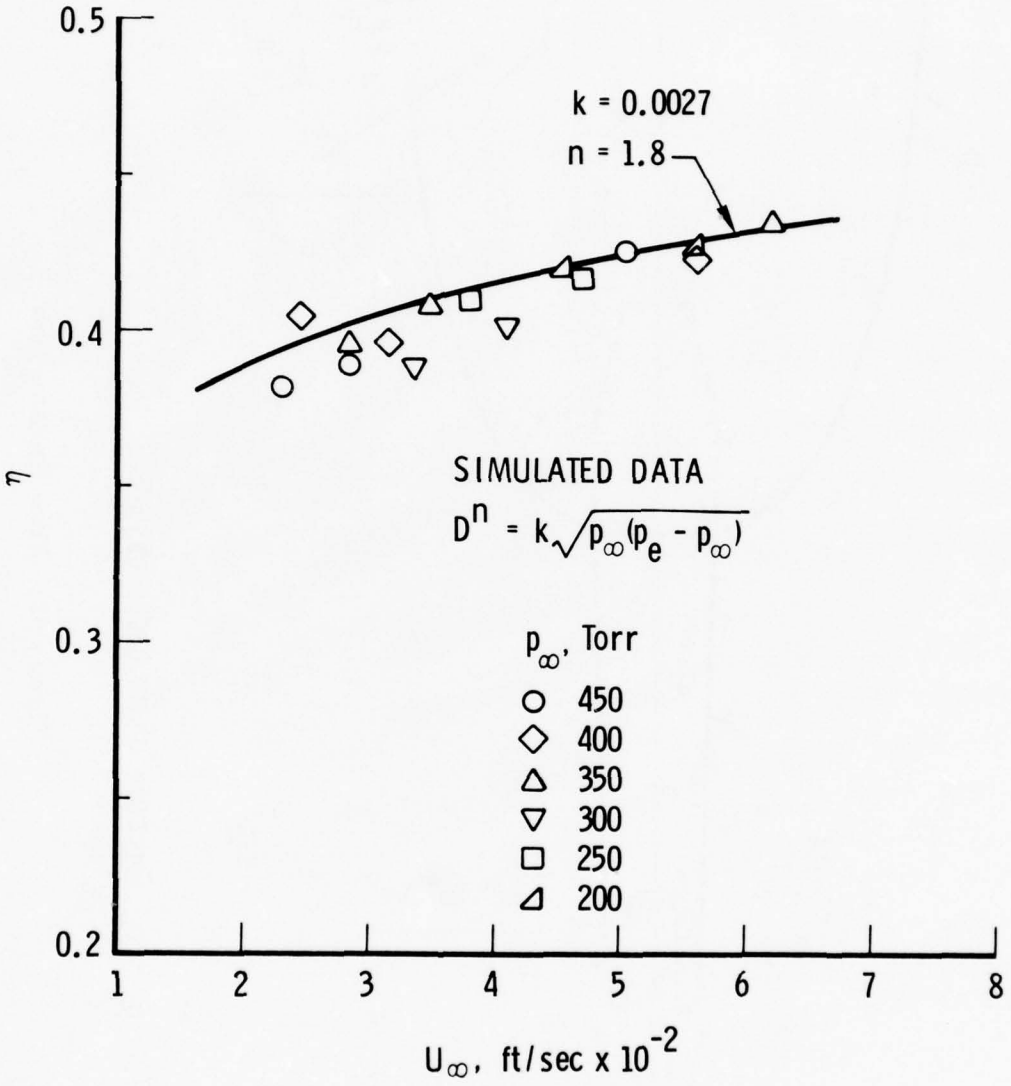

Figure 31. Collection Efficiency vs Flight Parameters (Heated)

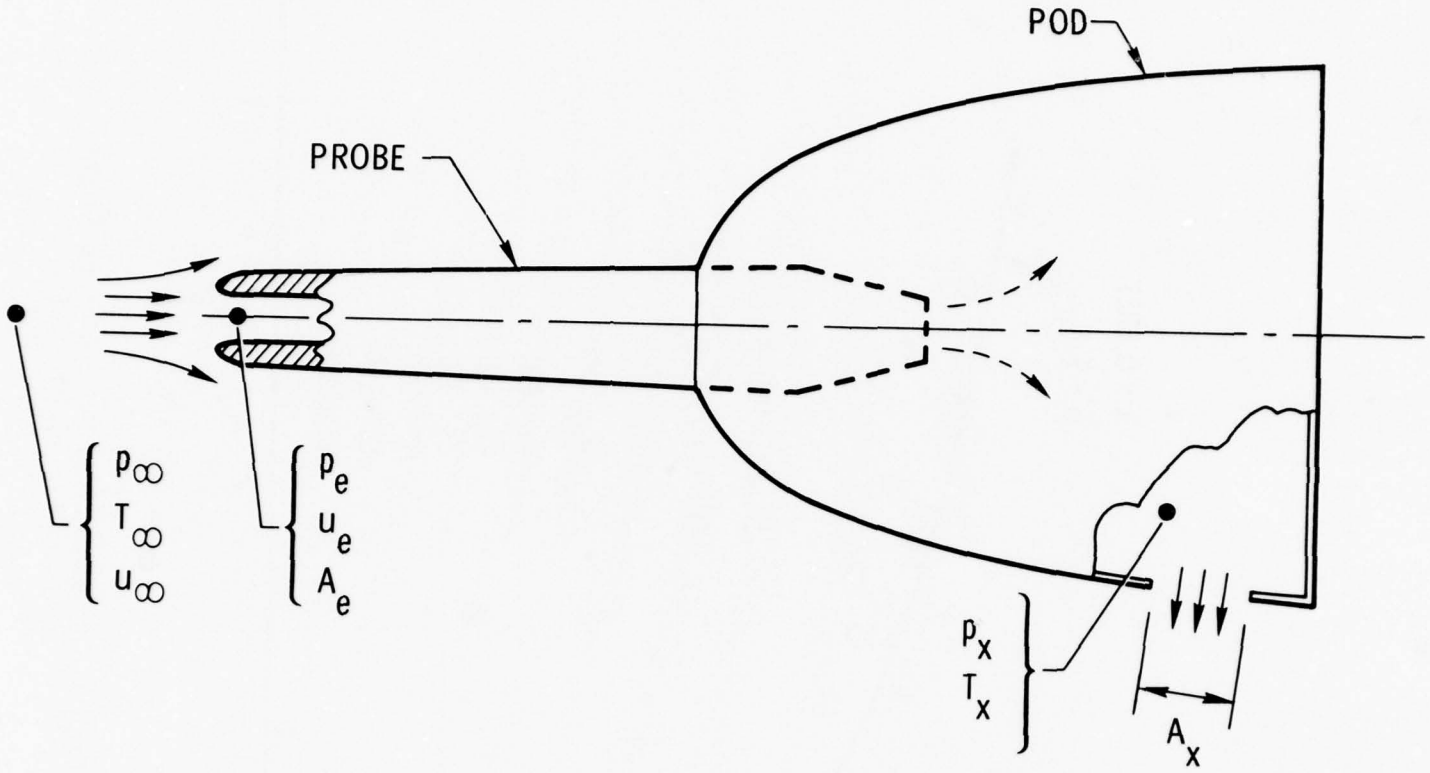

NOTE: $p_x = p_\infty$ For case of no backpressure

Figure 32. Flow Parameters

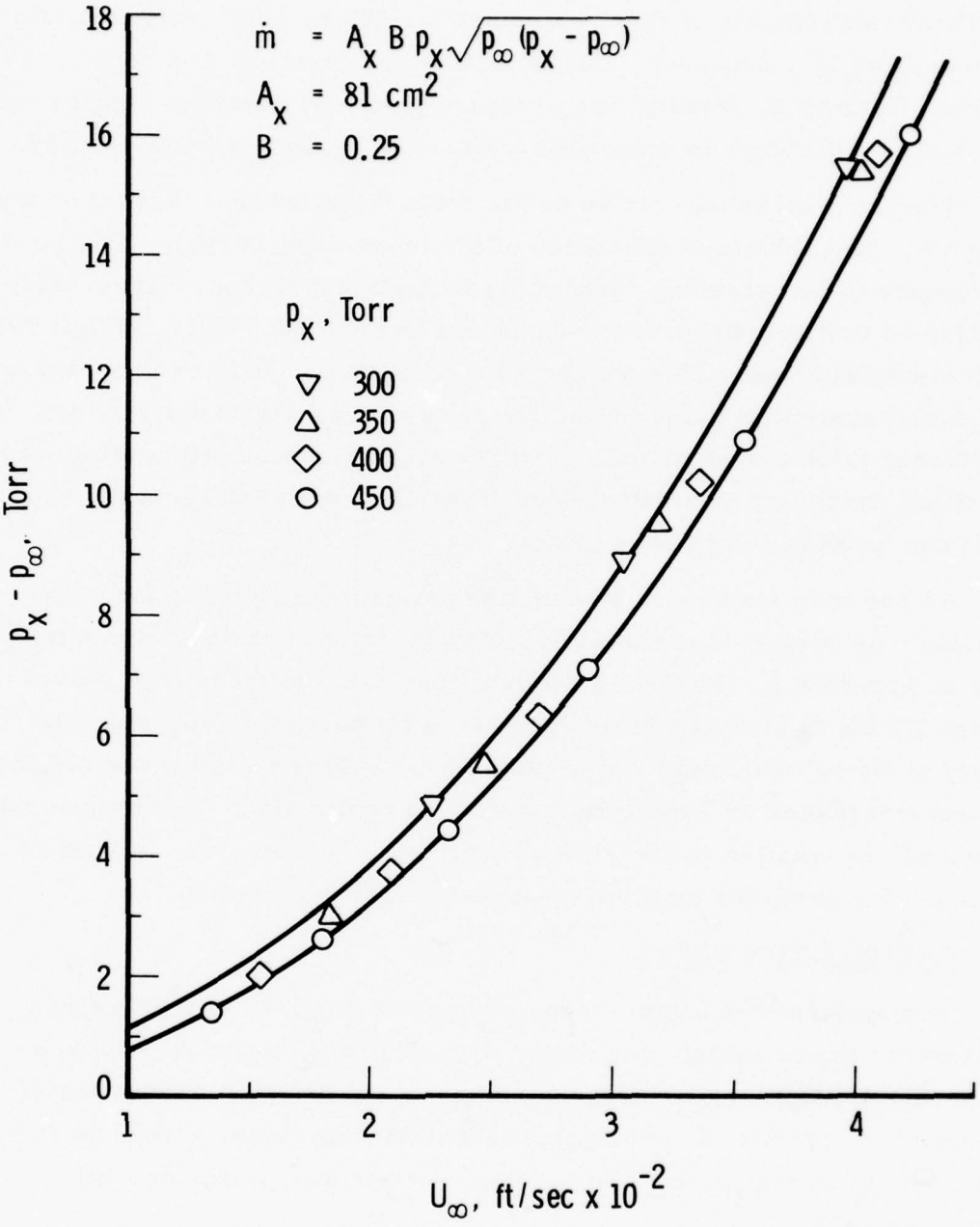

Figure 33. Pod Exhaust Valve Pressure Differential

Combining these estimates for the flow resistance in the exhaust valve with the measurements of flow resistance in EWER, an overall collection efficiency can be calculated. These results are shown in Figure 34. It is apparent that now the results are pressure (altitude) sensitive and the value of collection efficiency is somewhat lower with backpressure in the pod.

Several conclusions can be drawn from the results of these flow tests of EWER. The collection efficiency of the instrument is reasonably good and appears to be relatively insensitive to flight conditions. However, when installed so that backpressure is on the instrument, the collection efficiency is adversely affected. This suggests that a suction should be provided on the exhaust system to maintain the pod pressure as near as possible to the freestream value during sampling. The variation of collection efficiency with flight conditions is small enough (especially with low backpressure) that it can be assumed to be constant.

As has been mentioned before, the collection efficiency for water particles was evaluated analytically. A description of this analysis is given in Appendix B. Suffice to say here that the airflow is free enough through EWER to facilitate the collection of all particles (spheres with density of water) with radii larger than 50 μm. This satisfies the original requirement placed on EWER for the ABRES application. For other applications where smaller particles are of primary concern, the collection efficiency for particles might need experimental verification.

B. CALIBRATION TESTS

Two types of calibration tests were performed. The first series involved the entire system run on the flow facility (Figure 23) in which water was injected into the evaporator probe and detector output was (a) recorded on magnetic tape and (b) processed by the online computer to give water content in real time. This series of tests was performed on 13 October 1976.

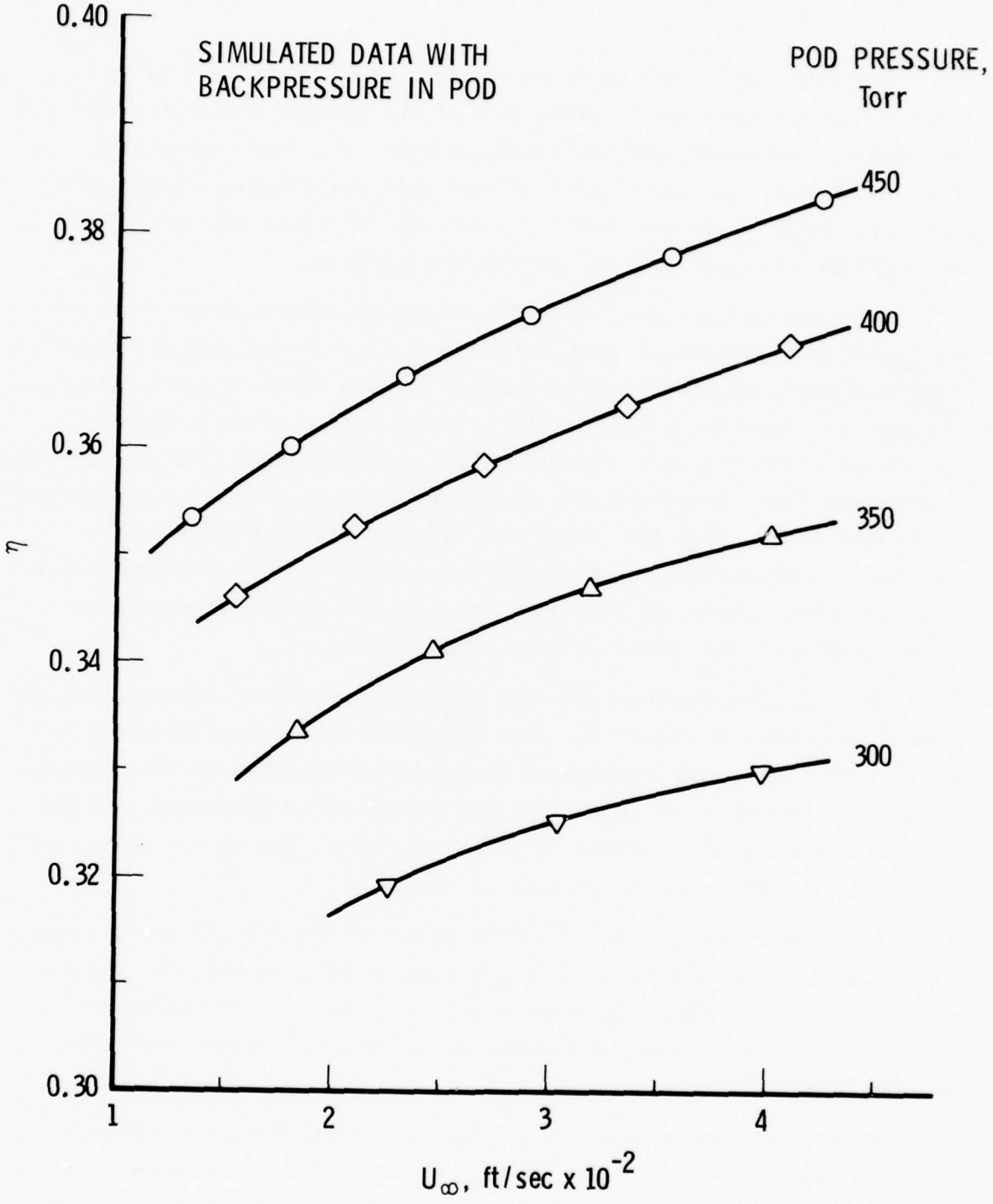

Figure 34. Collection Efficiency (With Backpressure in Pod)

The injection system is shown in Figure 35. Since the flow rates were extremely small a concentric flow of dry nitrogen was injected around the water jet to maintain steady atomized flow. The water tube had a 0.25 mm inside diameter (ID) × 0.15 mm wall; the nitrogen annulus was 0.8 mm outsides diameter (OD) × 0.5 mm ID. The flow rate of nitrogen was negligible compared to the airflow into the probe.

Output from the digital computer during periods when the water rate was constant is shown in Figure 36. This is a composite record in which data from three sensors is shown for several flow rates of water. All data has been averaged for 1 sec. It will be noted that all sensors show a fluctuation of ± 0.05 g/m^3. Since the input was constant over those intervals, it is assumed the variation in the output is the result of thermal turbulence in the system (see page 51). However, it is possible that some of the fluctuation could be attributed to nonsteady evaporation of the liquid water. One way to test this would be to inject dry steam, but the experimental difficulty of doing this precluded making the check.

Another time-constant test was performed with this configuration; the results are shown in Figure 37. The water flow was turned on with a fast-acting valve. Since the hypodermic tube injector throttles the flow through the system, the feed line to the tube was always filled with water and the starting transient can be expected to be negligible. The time-constant for the output is of the order of several seconds.

A test was made to determine the effect of detector gap on the output. With a constant water input and the computer reading one sensor, the gap was varied from a minimum value to 2.8 cm. The result is shown in Figure 38 and confirms that the output is essentially invariant with the detector gap.

Water was then injected for a range of simulated flight conditions giving an input of up to 1.5 g/m^3 based on volume flow at the inlet. The real-time output as a function of input for three sensors in the "A" detector

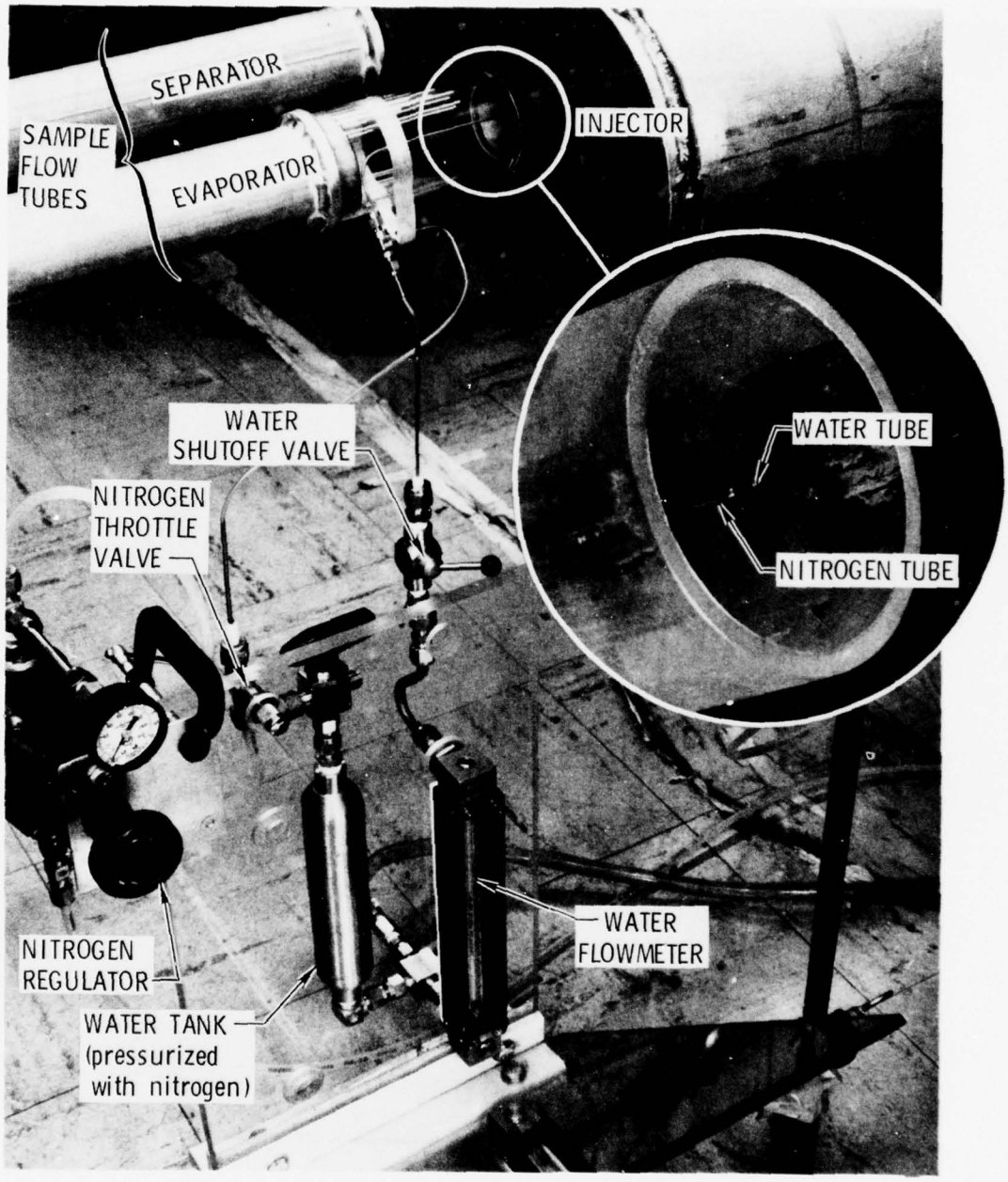

Figure 35. Water Injection System

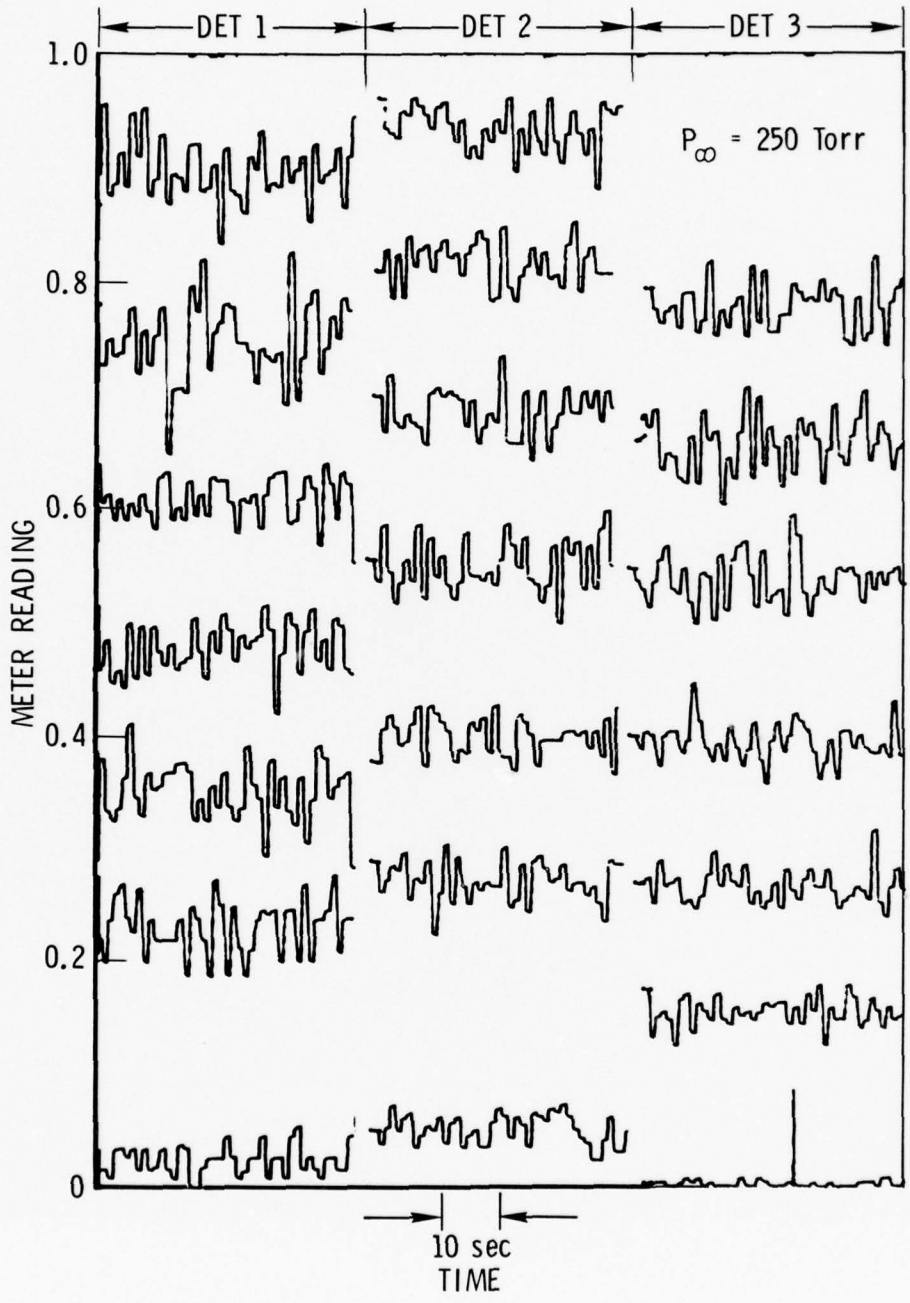

Figure 36. Calibration, Detector A

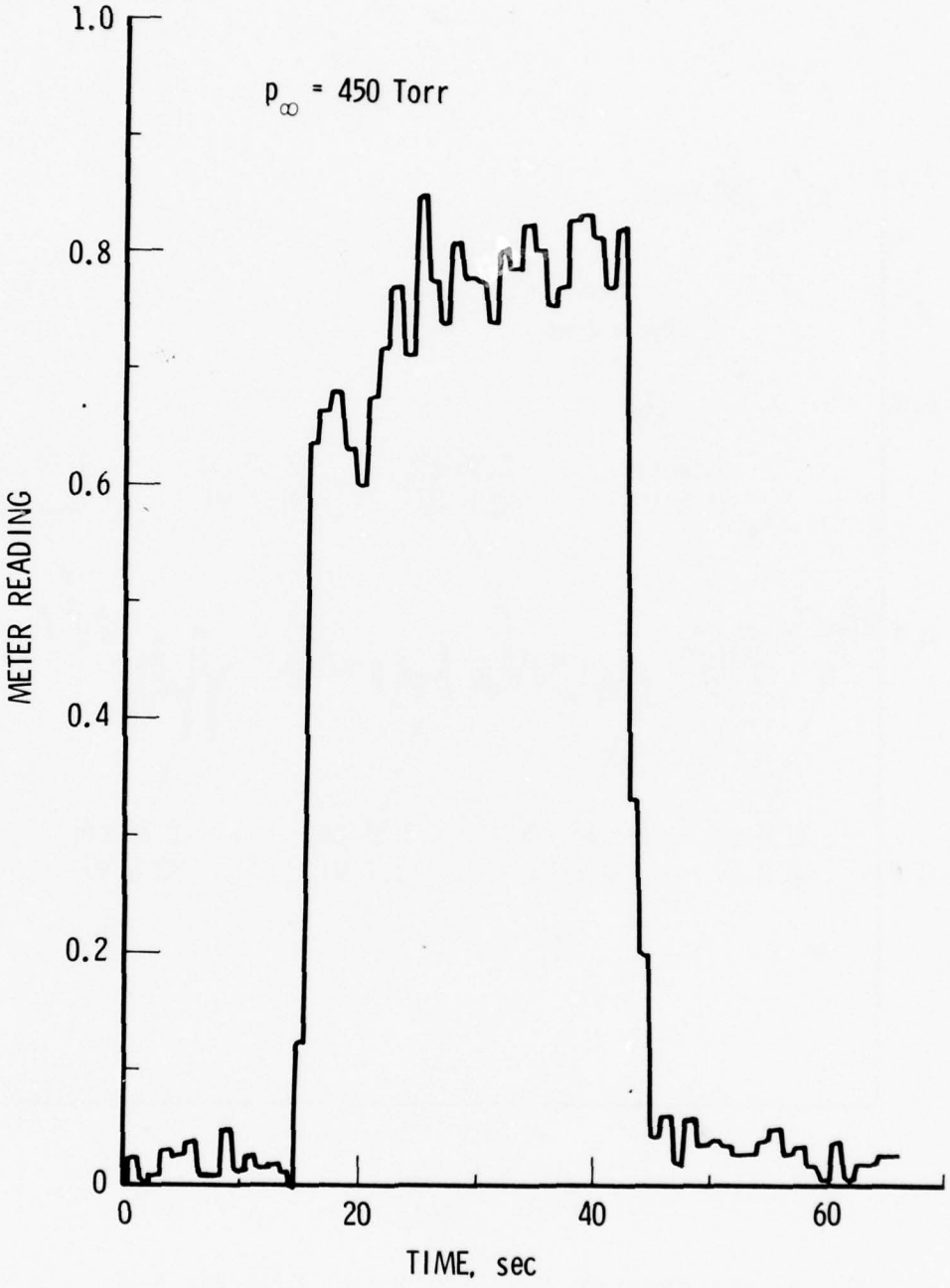

Figure 37. Time Response Test, Detector A-1

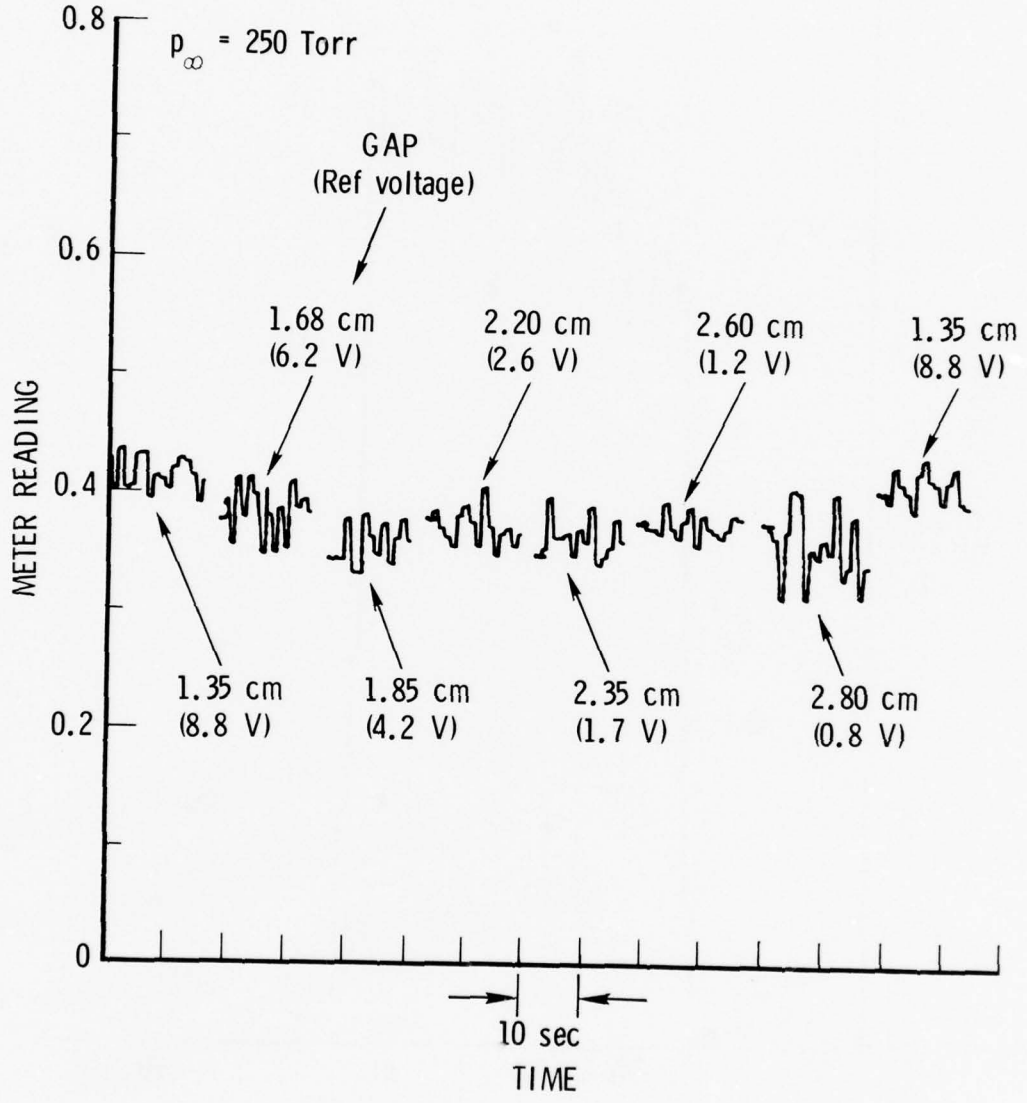

Figure 38. Detector Gap Sensitivity, Detector A-2

assembly is given in Figure 39. Results are linear and independent of detector pressure (altitude). However, there is a significant offset for zero. This is due to the fact that the online computer software does not allow negative numbers and all such data is equated to zero. Hence, a positive value will result when the data are averaged. An extrapolation of the non-zero data to zero input, however, does not pass through zero output. This is due to the fact that the A detector assembly was adjusted at this time with a negative bias, i.e., the signal obtained in the evaporator flow is larger than that of the separator flow. Furthermore, the bias is different for each sensor. Although this condition can be minimized by proper adjustment of two rotating housings with respect to each other, a clear-air calibration feature has been incorporated into the software to cancel out this effect.

For these tests the meter output was scaled to 1 g/m^3 full scale. Then the slope of these data would indicate that the effective absorption coefficient for the detector is 160 cm^{-1} (not 387 cm^{-1} for Lyman-α). Because of this discrepancy, an attempt was made to measure the absorption coefficient for the detector independently from the system. The results will be given later in the discussion of the detector calibration.

Tape recordings made during these tests were reduced in accordance with the postflight data reduction techniques (Ref. 6). An absorption coefficient of 157 cm^{-1} and a clear-air calibration correction were used to obtain the results shown in Figure 40. Again, the output is linear with input and insensitive to pressure. However, the offset still exists at zero. In this case negative values were averaged and the clear-air calibration should have removed the detector bias. An explanation for this effect has not been given at this point in time.

As noted above, the absorption coefficient for the detector was found to be considerably less than 387 cm^{-1} advertized for water absorption of the Lyman-α line. Since the output of the source includes significant

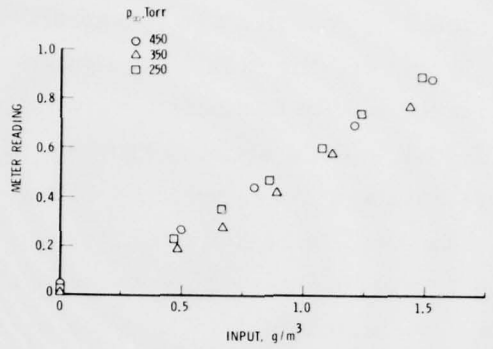

A-1

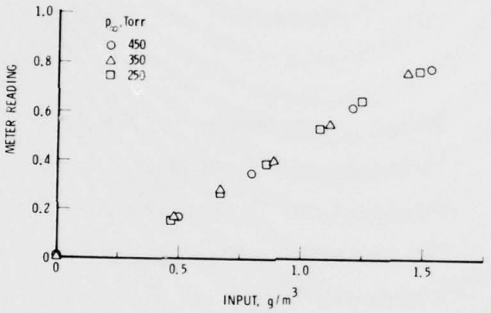

A-2

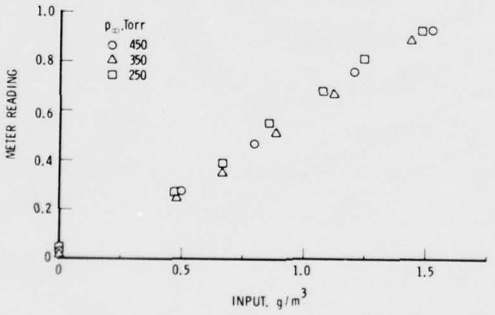

A-3

Figure 39. Real-Time Computation - Detectors A-1, A-2, and A-3

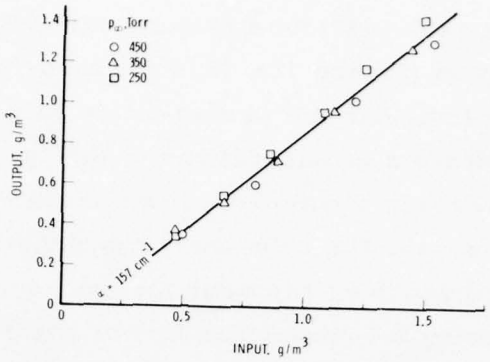

A-1

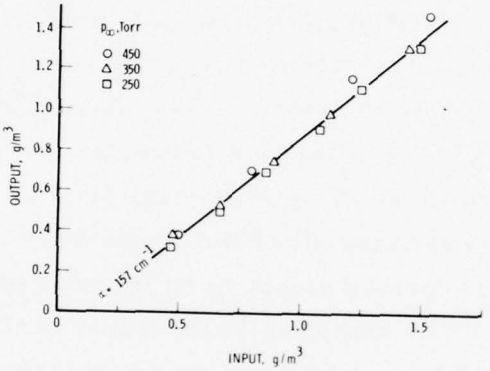

A-2

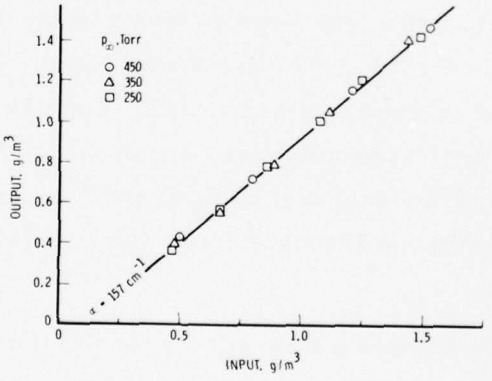

A-3

Figure 40. Post-Test Data Analysis - Detectors A-1, A-2, and A-3

radiation in the range of 1250Å to 1350Å (Figure 41) and the receiver is responsive to this radiation (Figure 42), it is not surprising that the overall absorption coefficient is less than the Lyman-α line value. An evaluation of the absorption coefficient from considerations of the spectral characteristics of the source and receiver was attempted. If we assume that the magnesium fluoride windows on the sensor limit the short wavelengths to 1200 Å, integrating source output and receiver response for the wavelengths between 1200 Å and 1350 Å and using the absorption data of Figure 43, an absorption coefficient of 161 cm^{-1} is inferred. The value here compares favorably with the 157 cm^{-1} obtained in the system calibration.

The second series of calibration tests involved a laboratory calibration of the sensor only and was accomplished with the setup shown schematically in Figure 44. It was possible to determine the absorption coefficient of approximately 225 cm^{-1}. The difference between this value and the one obtained in the system calibration could be explained to two ways: (a) The evaporator may not be vaporizing all of the liquid water. This, too, could have been checked if superheated steam were injected into the evaporator probe (see page 72). (b) The sampling at the outlet of the evaporator is done in such a manner that the detector does not measure all the water content.

C. VIBRATION TESTS

Two series of vibration tests were performed on the equipment to be mounted in the pod of the C130E. The first was based on criteria developed from MIL STD 810C and is shown in Figure 45. Details of the testing are given in Appendix C. After approximately 3 min of random excitation, the heater systems failed and several mechanical defects were observed. It was decided that the conditions imposed were far too severe and the test series was discontinued.

The unit was repaired and a new series was planned. Data for the vibration environment on a C130A were finally obtained and a new set of criteria was developed as shown in Figure 46. All systems performed satisfactorily throughout this test.

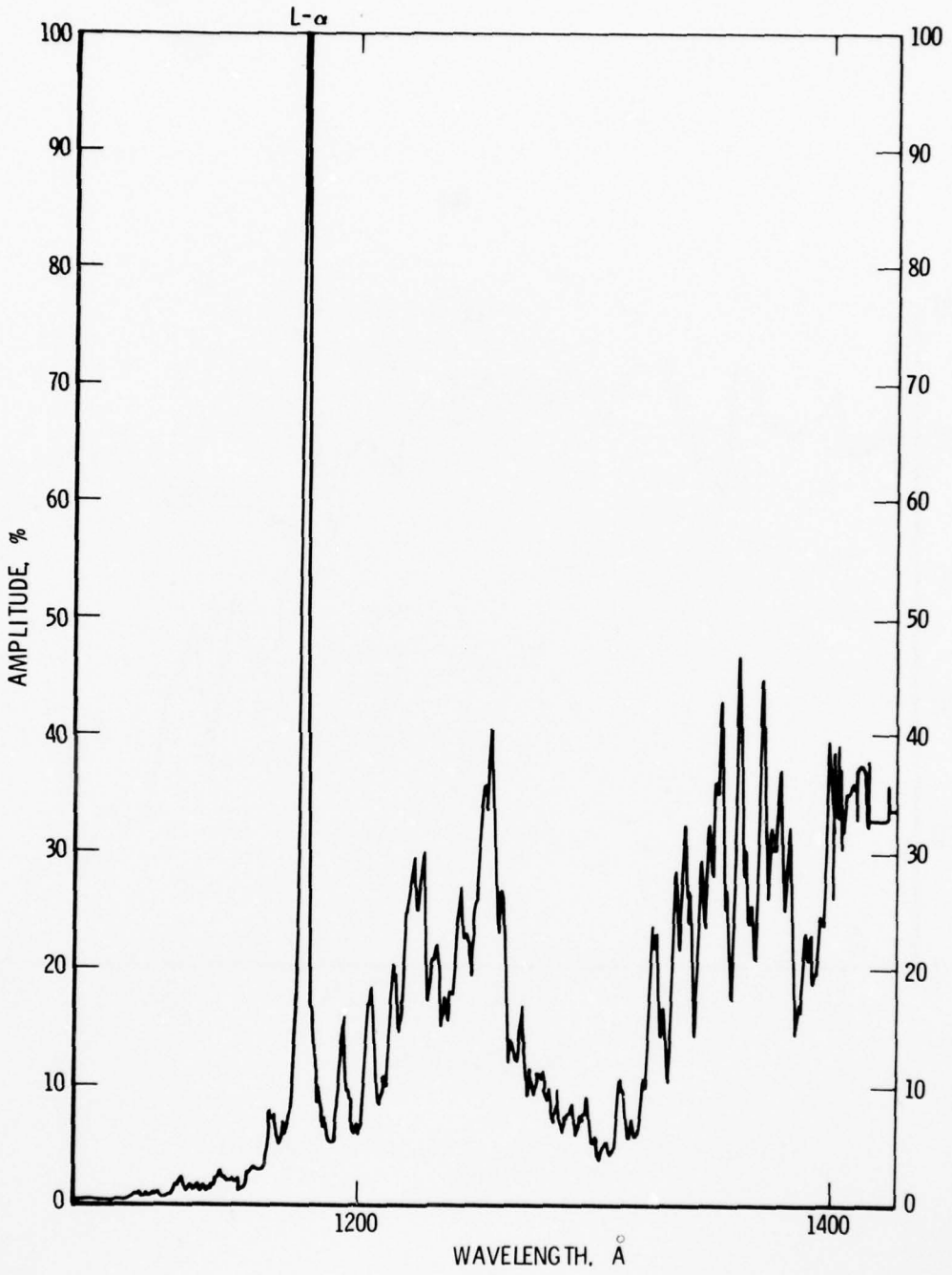

Figure 41. Lyman-α Source Spectrum

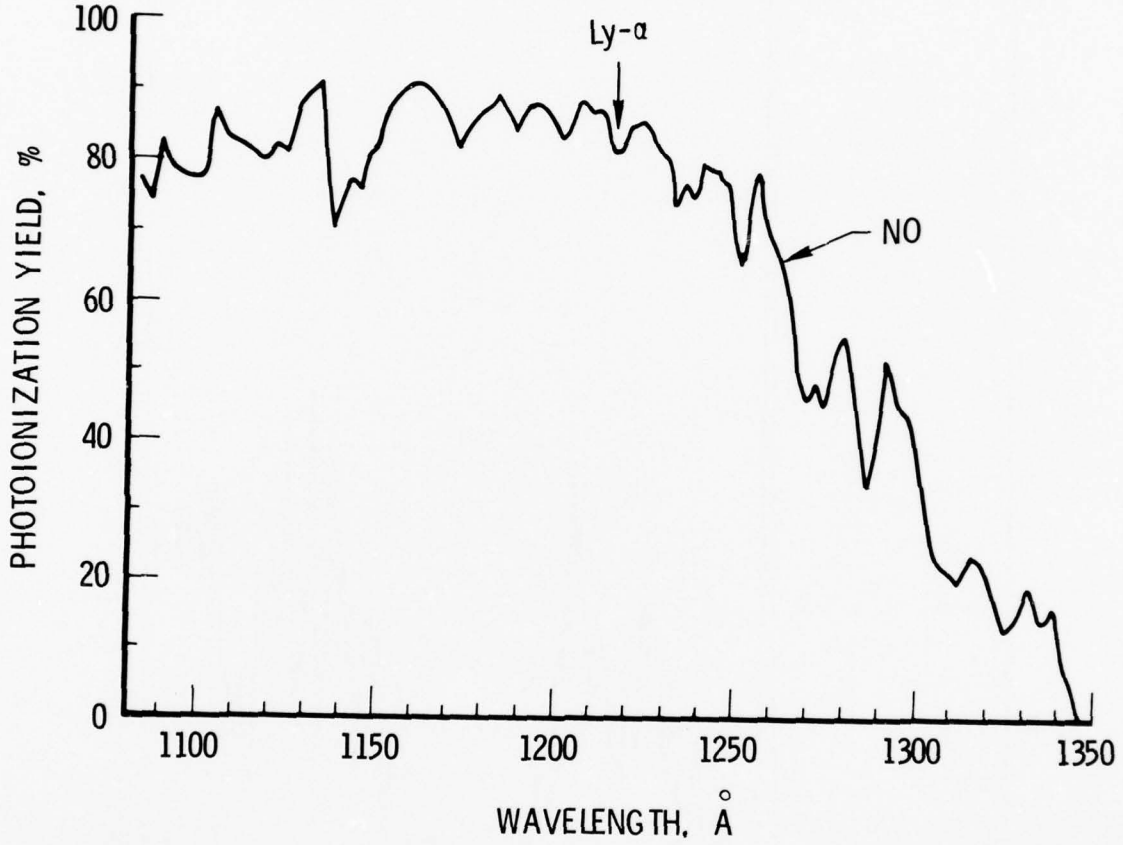

Figure 42. The Photoionization Yield of Nitric Oxide

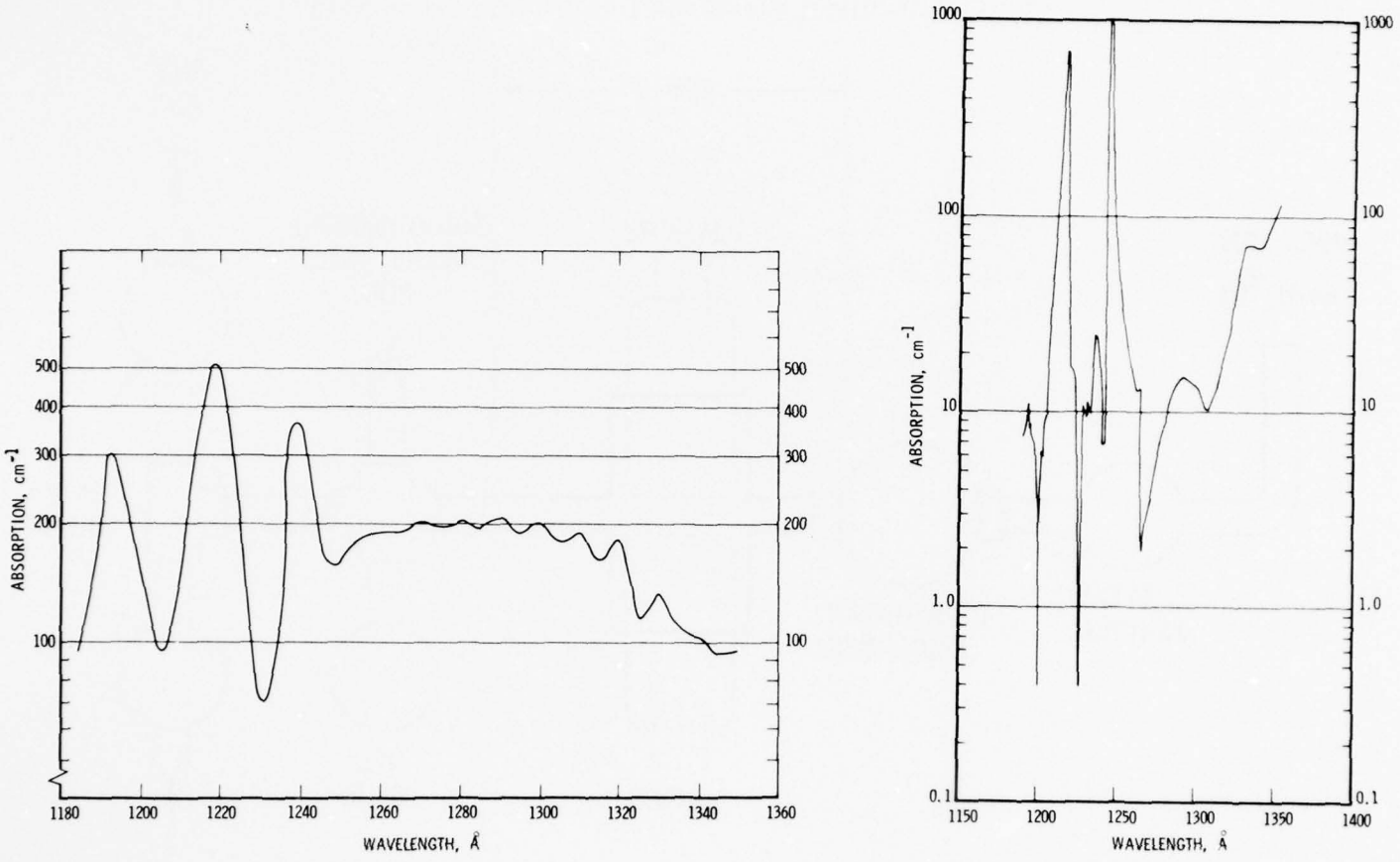

Figure 43. Absorption by (a) Water Vapor and (b) Molecular Oxygen in the UV (1200-1400 Å)

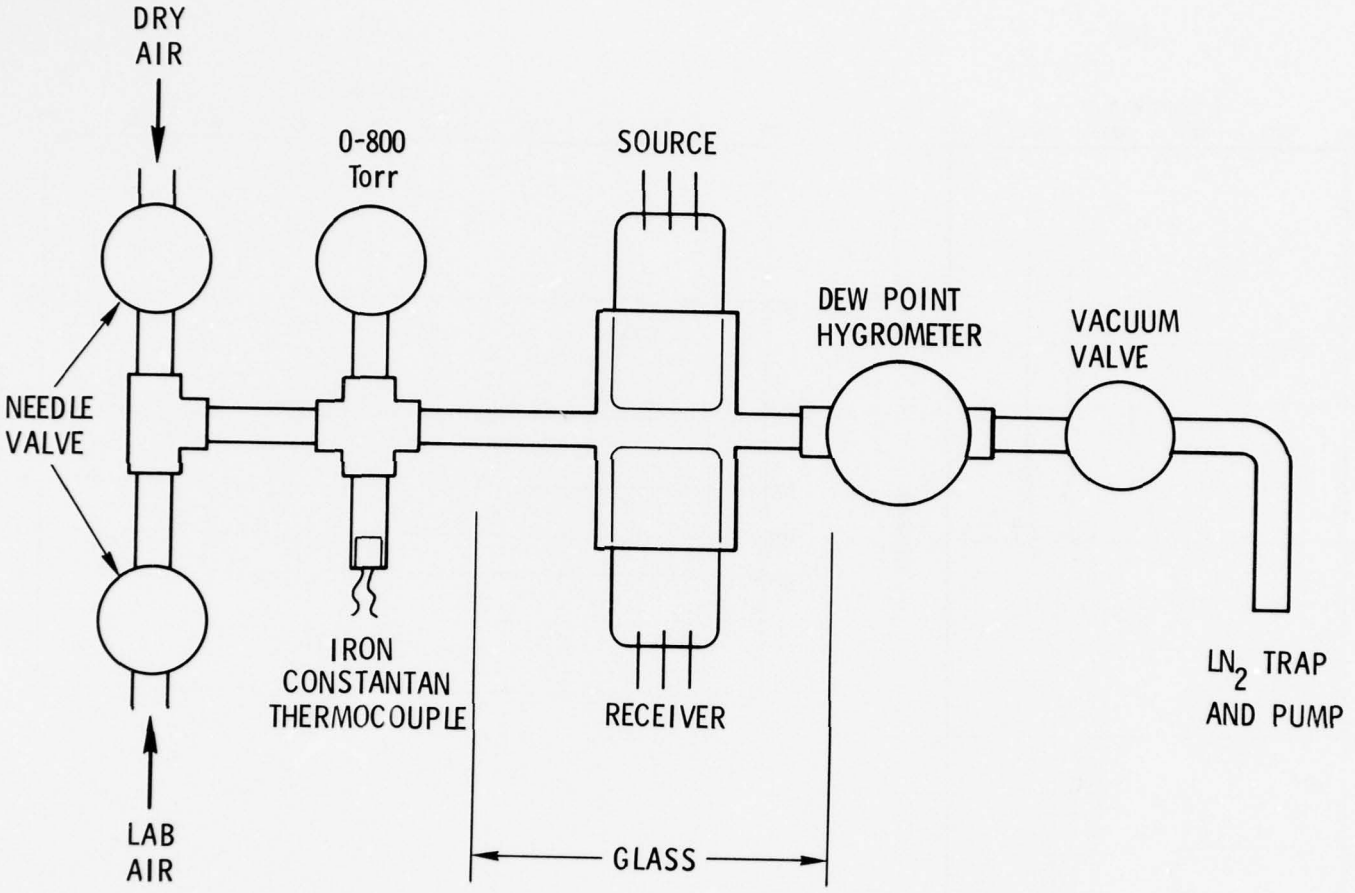

Figure 44. Lyman-α Laboratory Calibration Setup

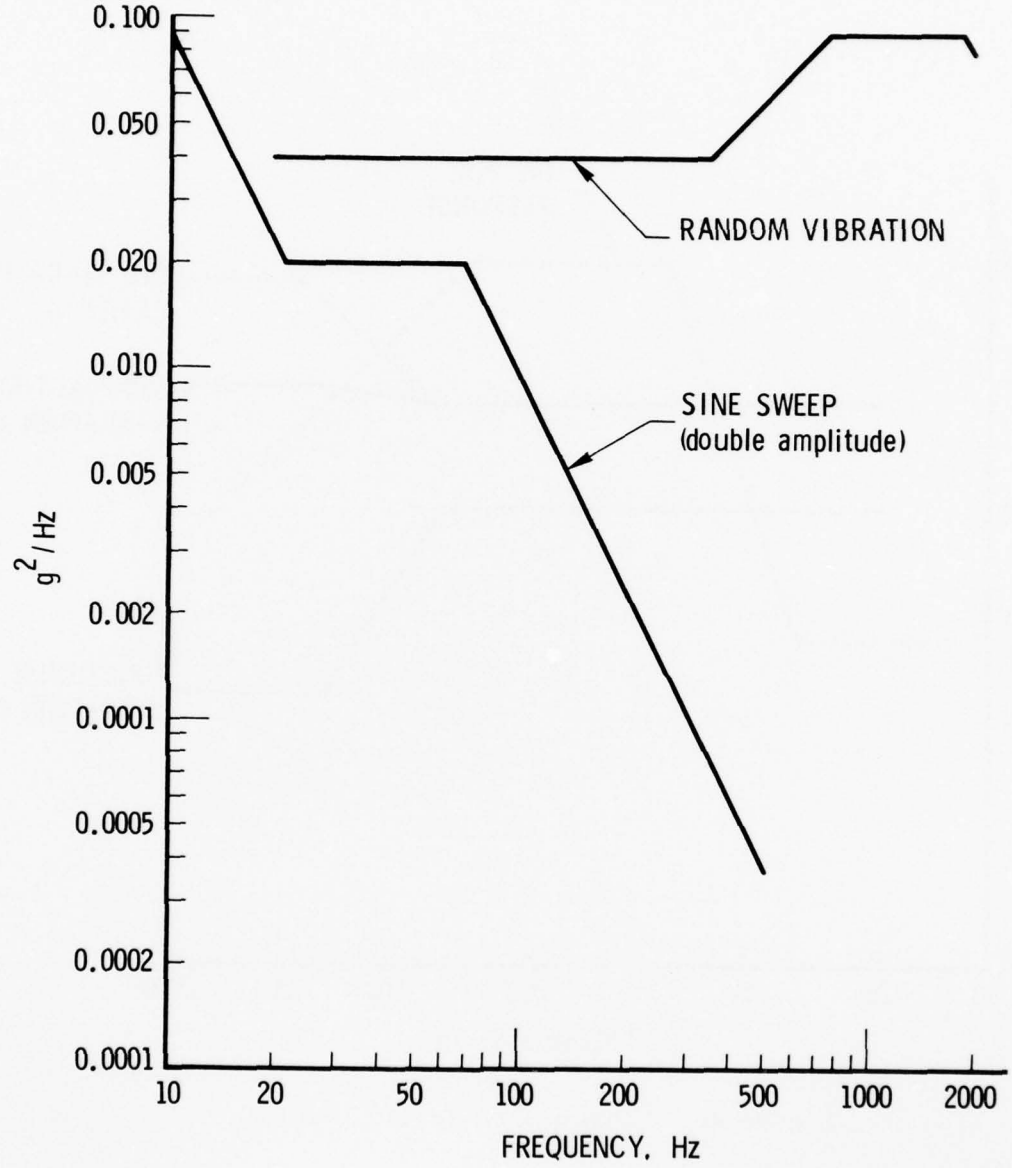

Figure 45. Vibration Criteria

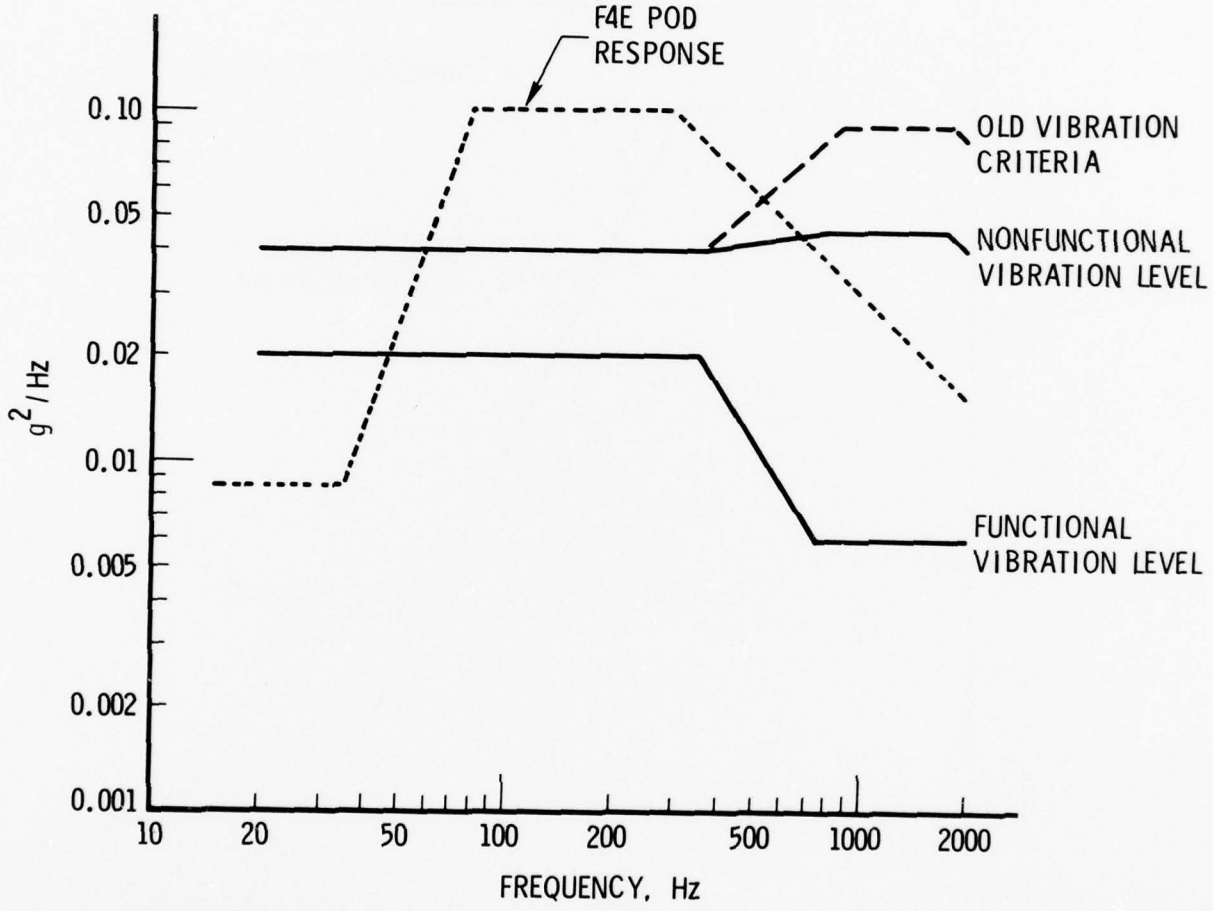

Figure 46. Vibration Criteria (Revised)

It is interesting to note that, during the preparations for this test, a situation developed where the operation of the servo-controlled heaters "ran away." It was found that the 3 phase, 400 Hz power source being used for the test had large, recurring transients on the sine waveform. This caused the solid-state switches (Triacs) to self-trigger and apply full power to the heater. The effect was first observed on the main heater when smoke issued from the evaporator probe inlet; no airflow was on at the time. All heater wires were destroyed and the heater element (AL-2908-2) was shortened by approximately 0.33 cm due to thermal expansion while under end constraint. Wires were replaced and a ring was fabricated to fill the gap at the front end of the heater element.

A solenoid-operated mechanical switch was installed in each heater circuit to "disable" the Triac control. The operator would be able to control a runaway condition by disabling the heaters should this occur in the operation aboard the aircraft.

D. FLIGHT TESTS

Several flight tests were performed to check out the EWER systems while operating in the aircraft and to compare EWER results with data from other systems on board the aircraft.

It was evident from the beginning that the nitrogen purge to protect critical components from exposure to contaminated air was marginal. The pod was not designed to provide a completely pressure-tight compartment. Therefore, large amounts of nitrogen are required and it is questionable if even this is adequate. Figure 47 shows the pressurization of the pod by nitrogen when both probes are sealed. Maximum pressure obtained on this occasion was about 23 Torr. The dynamic pressure at 150 knots (sea level) would be 28 Torr, indicating that the purge would not be adequate.

Attempts were made to "spook" the system by an arbitrary switching of the various functions. For example, with all heaters operating, the

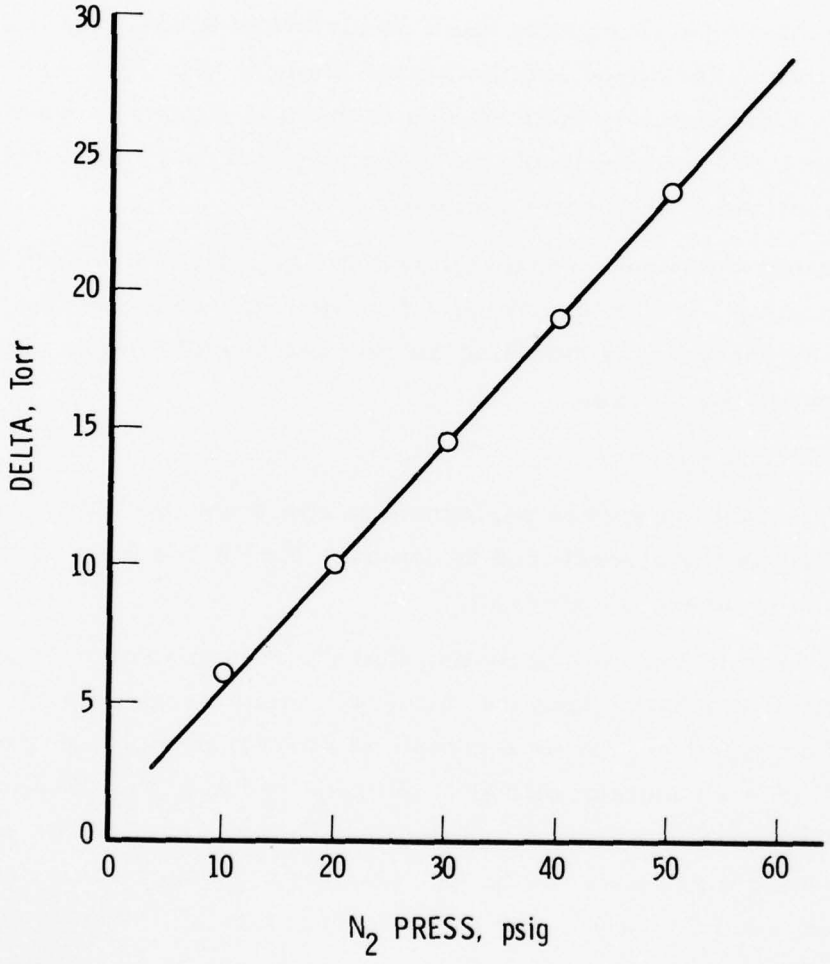

Figure 47. Pod Pressurization (C130E No. 571 on 1-29-76)

waste gate valve was closed, stopping airflow through the system. All heaters that were interlocked with airflow shut down properly and came back online when the valve was opened.

The primary objective of the flight tests was to obtain comparative data on water content measured by EWER and other instrumentation on board C130E-571. In particular, water content inferred from particle measurements by the Particle Measuring Systems* (PMS) instrumentation, especially in cases where the condensate was in liquid form, would give a good flight calibration on EWER. Many flights were attempted where weather conditions were not right or all systems were not operating.

Late in 1976, a mission designated MSV-1 (Material Screening Vehicle) was supported at the Wallops Test Range in which extensive data was obtained with all systems operating. Weather conditions for this mission were such that the condensate was solid, so the comparison with PMS data (and radar) depends on a knowledge of crystal habit. Nevertheless, the best estimates gave very good correlations between EWER and PMS for total water content. Comparative data for a portion of the mission is given in Figure 48.

Subsequent flights were made in early 1977. Two of these missions were dedicated flights in search of liquid water conditions. EWER data from these flights are given in Figures 49 and 50. Two other flights in support of MSV were also made where atmospheric conditions would result in solid condensate. The EWER data for those flights is given in Figures 51 and 52. Additional flights at Wallops Test Range and at Kwajalein Missile Range (KMR) have been made, but the data was not reduced.

*A company in Boulder, Colorado.

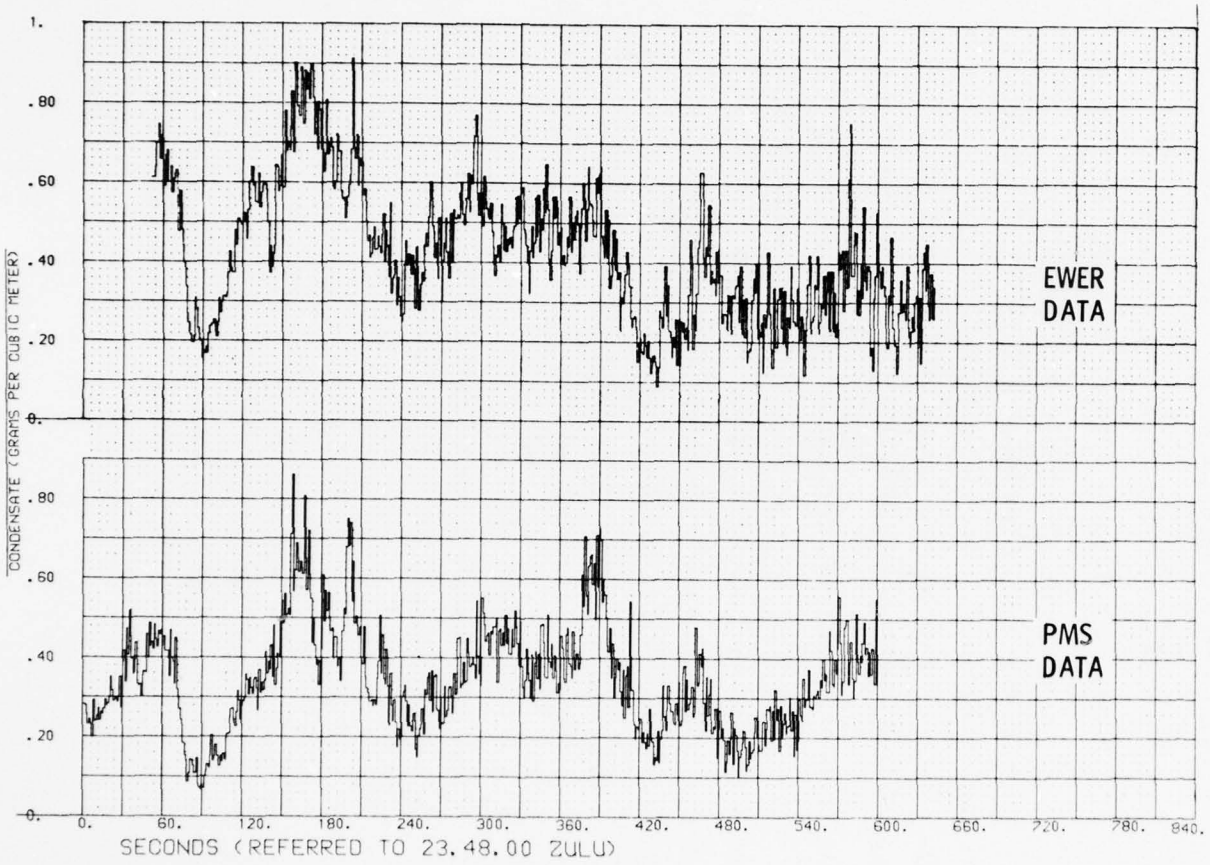

Figure 48. Flight No. E76-040

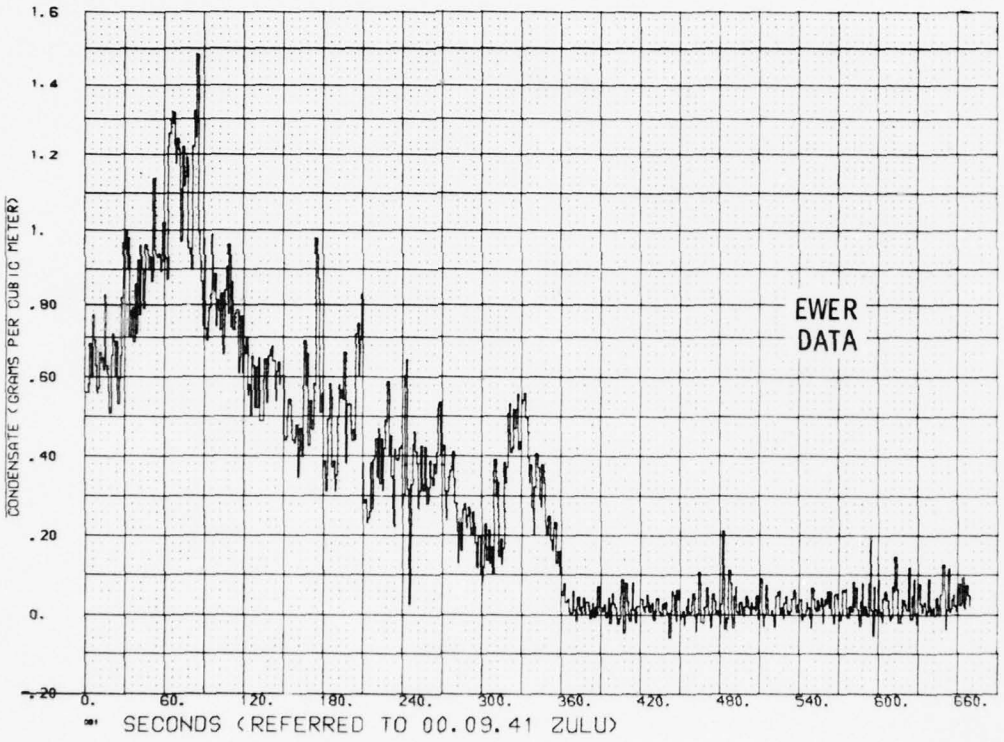

Figure 48. Flight No. E76-040 (Continued)

AD-A061 255 AEROSPACE CORP EL SEGUNDO CALIF F/G 4/1
DEVELOPMENT OF CLOUD WATER CONTENT METER, EWER.(U)
MAR 78 D A DURRAN, D H ROSS, W J SWARTWOOD F04701-77-C-0078
UNCLASSIFIED TR-0078(3550-38)-1 SAMSO-TR-78-113 NL

2 OF 3
AD A061255

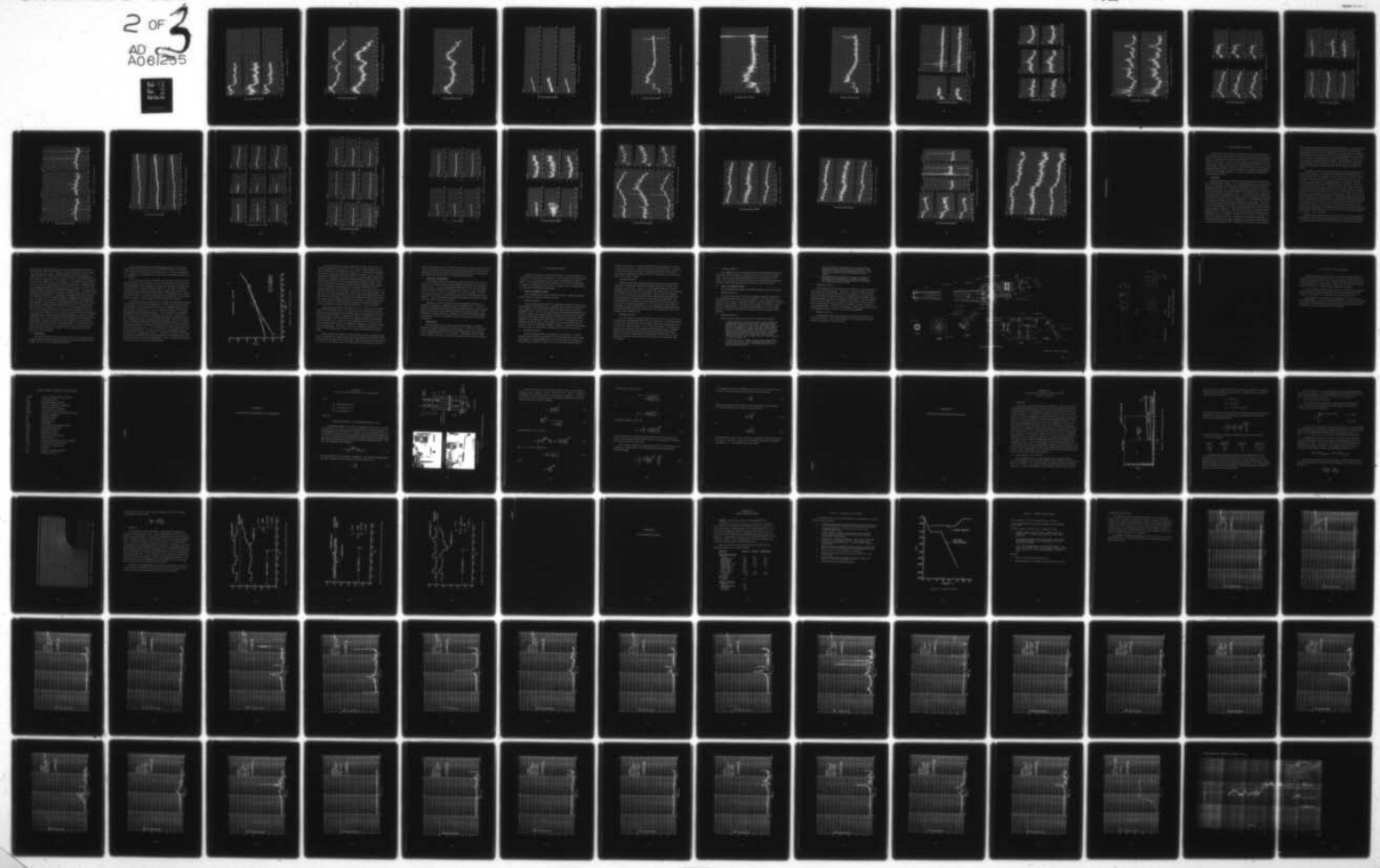


OF
1255

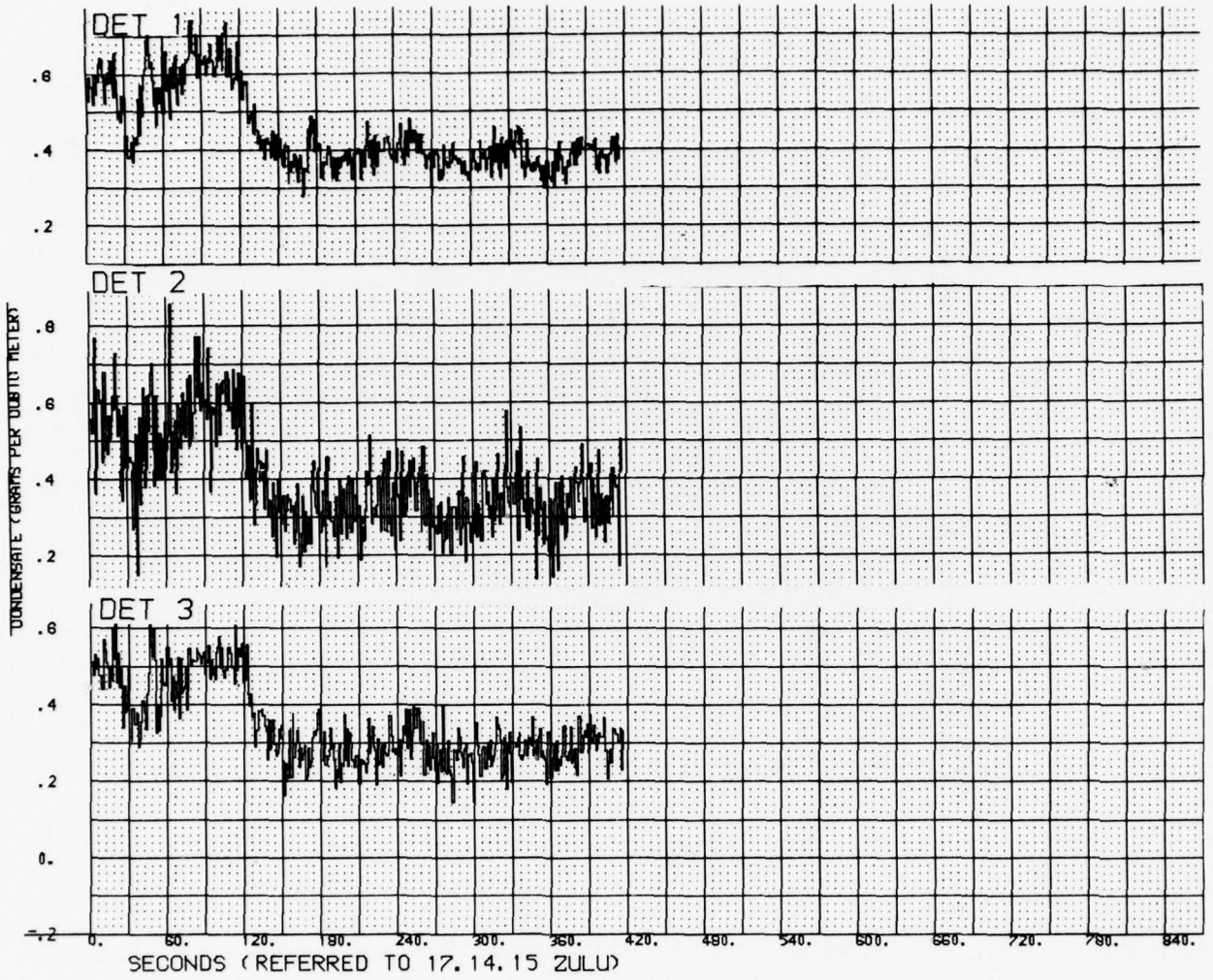

Figure 49. Flight No. E77-007

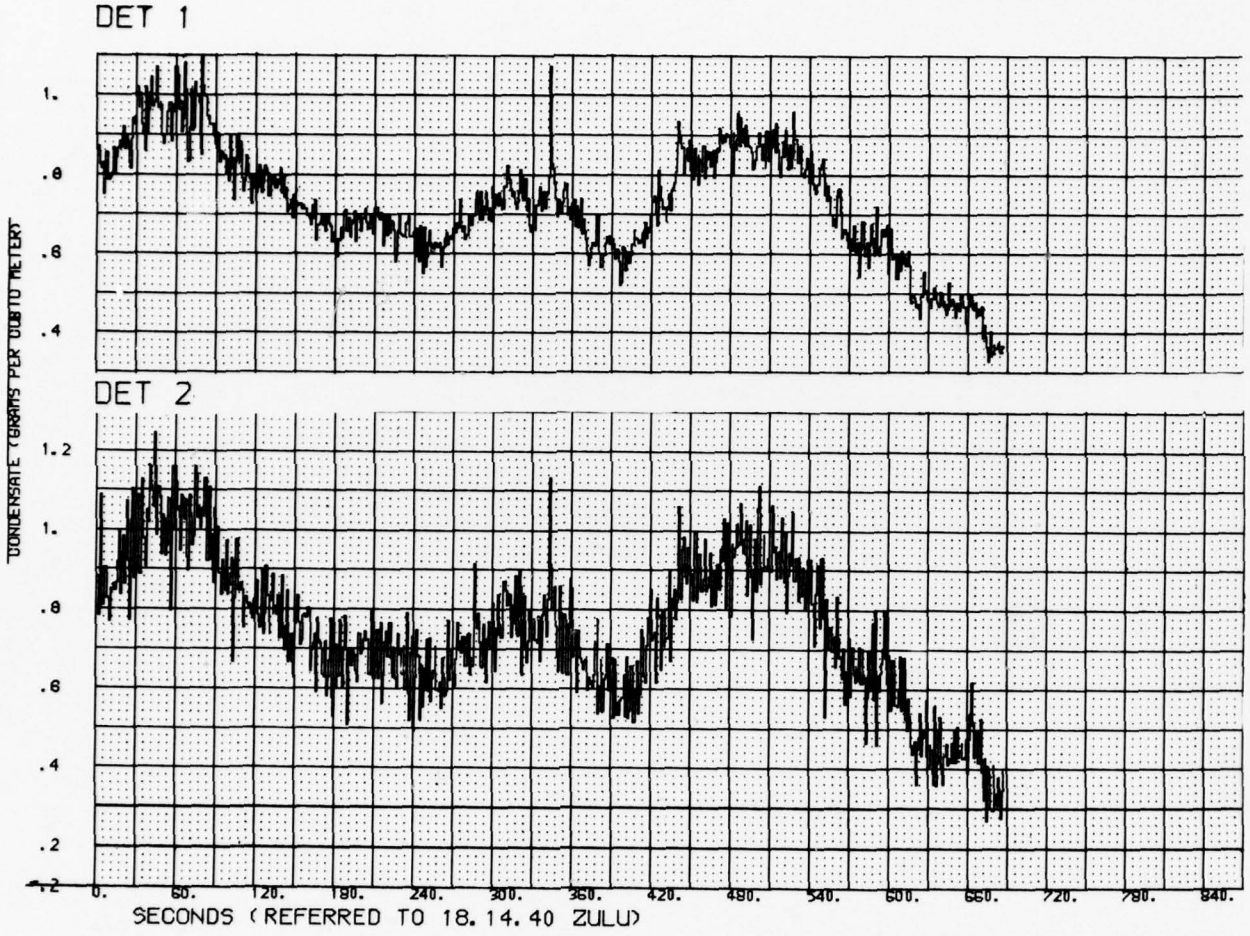

Figure 49. Flight No. E77-007 (Continued)

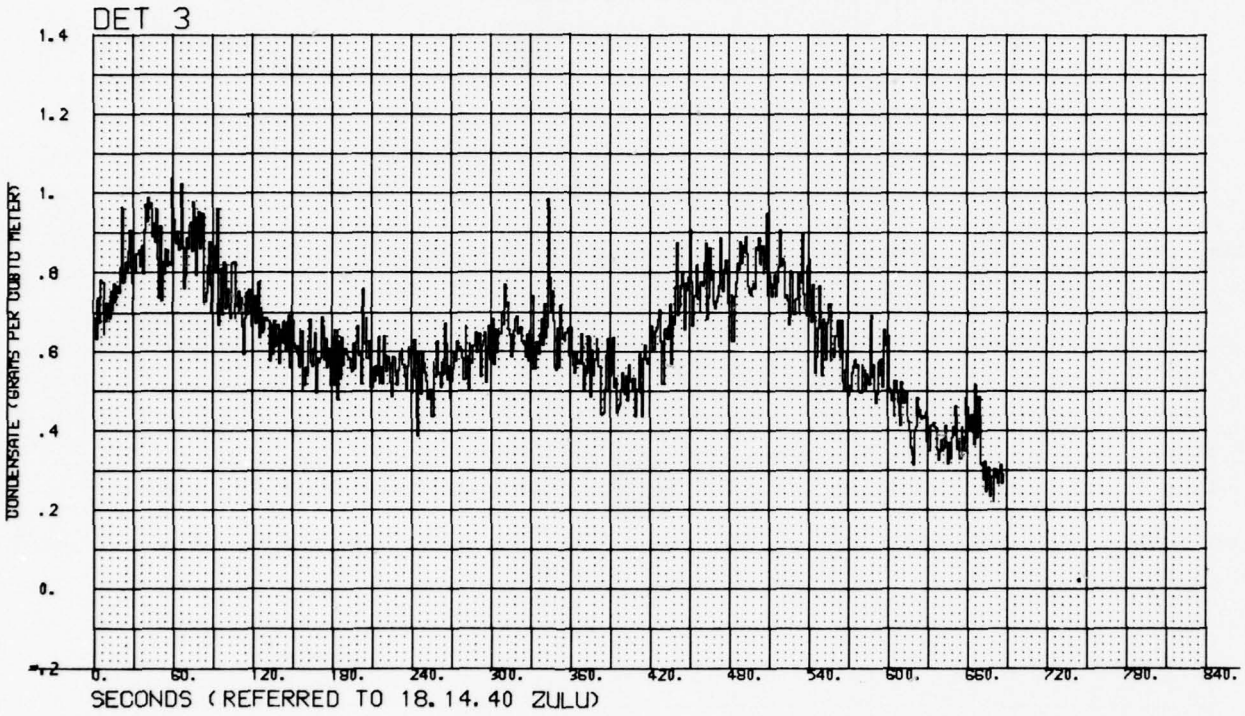

Figure 49. Flight No. E77-007 (Continued)

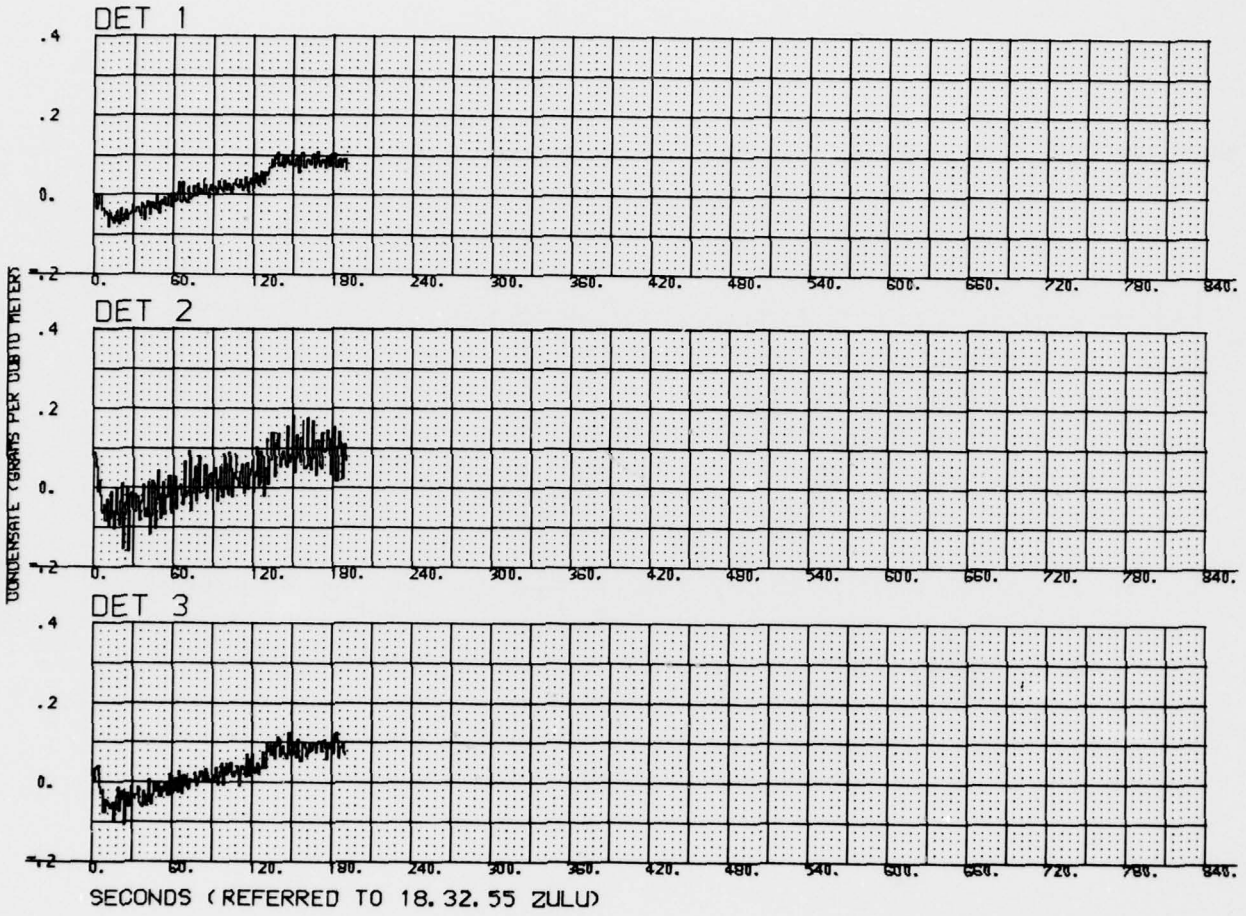

Figure 49. Flight No. E77-007 (Continued)

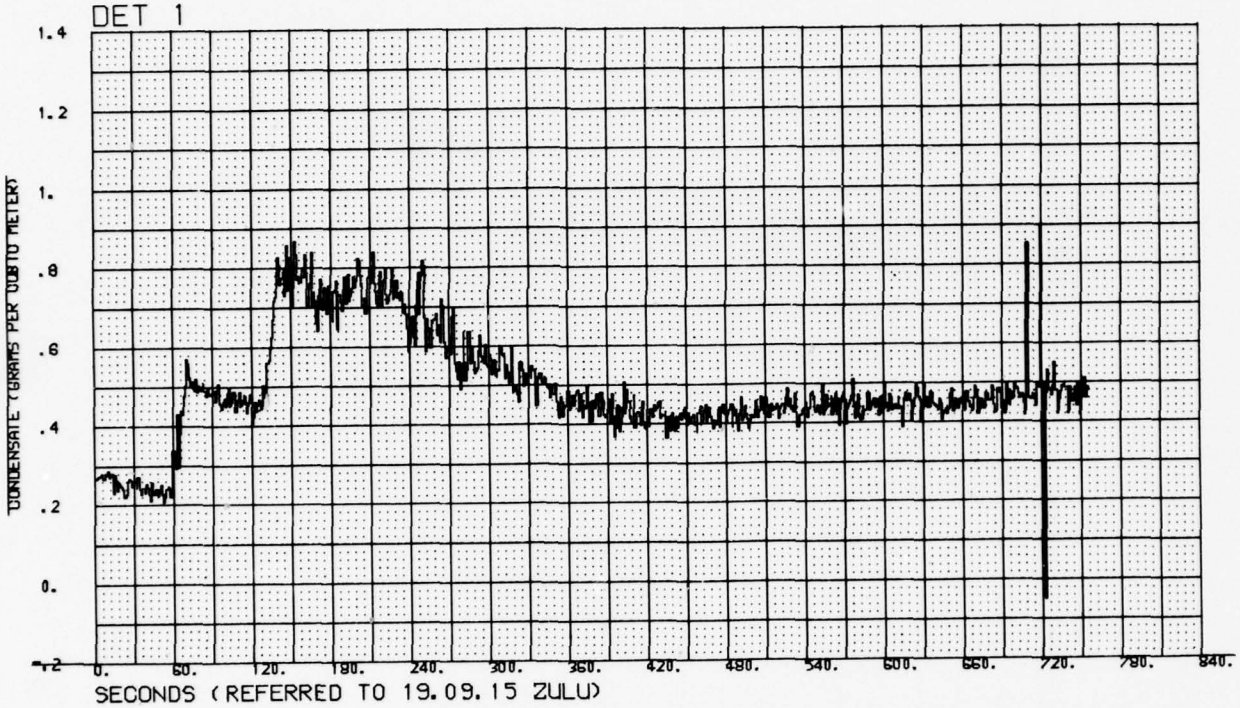

Figure 49. Flight No. E77-007 (Continued)

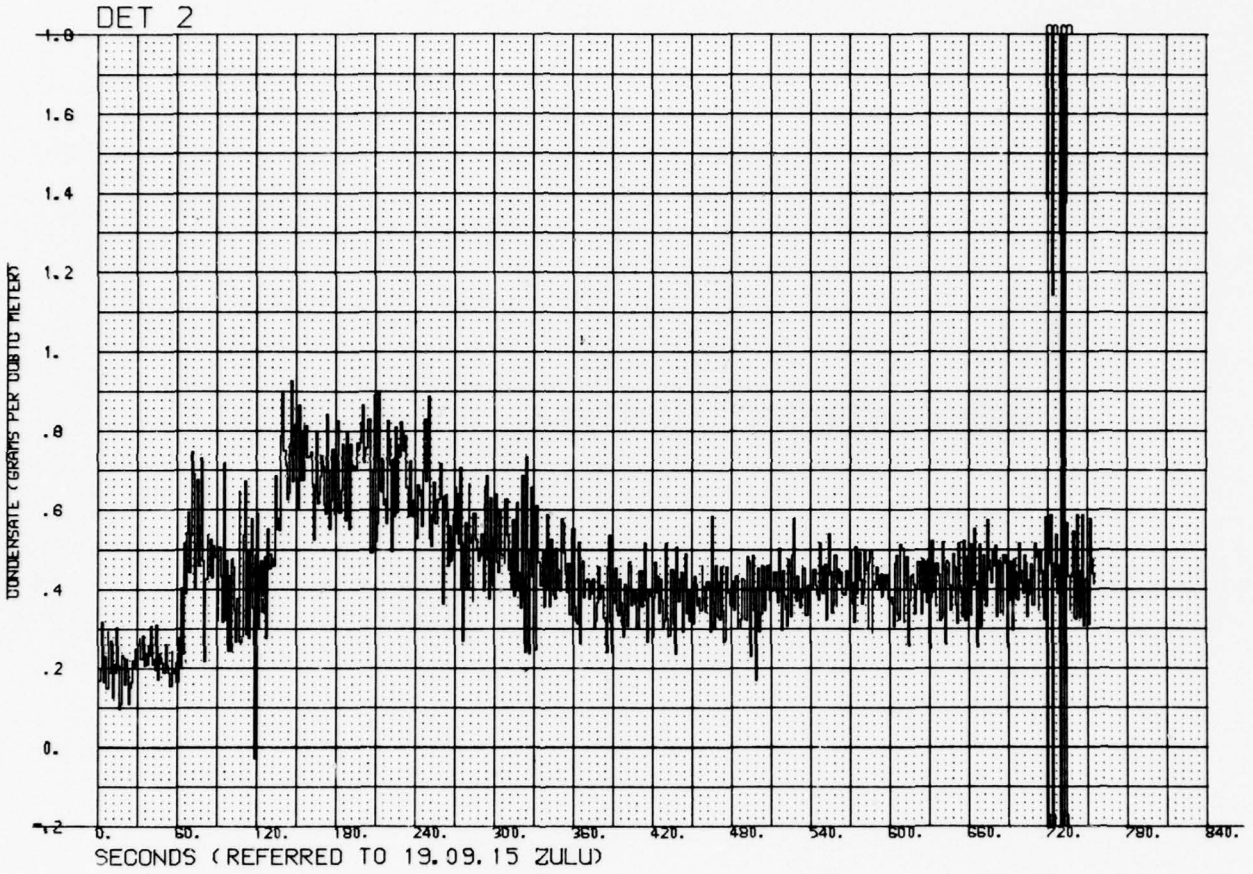

Figure 49. Flight No. E77-007 (Continued)

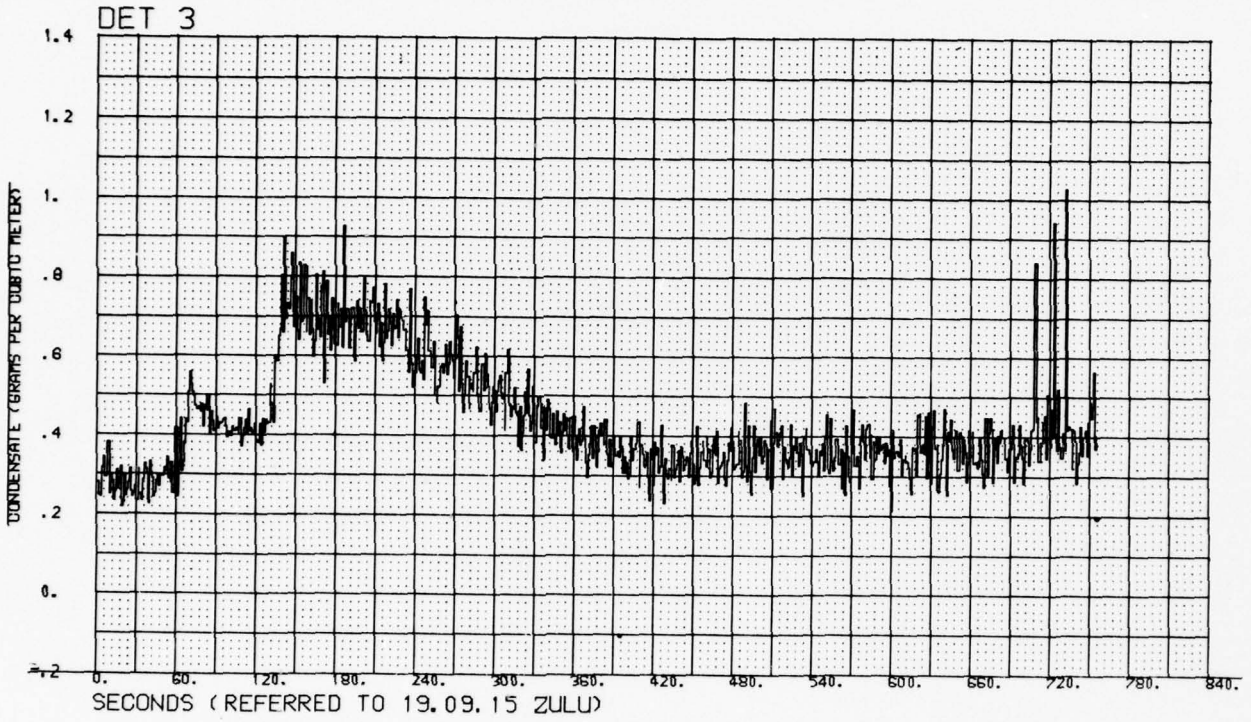

Figure 49. Flight No. E77-007 (Continued)

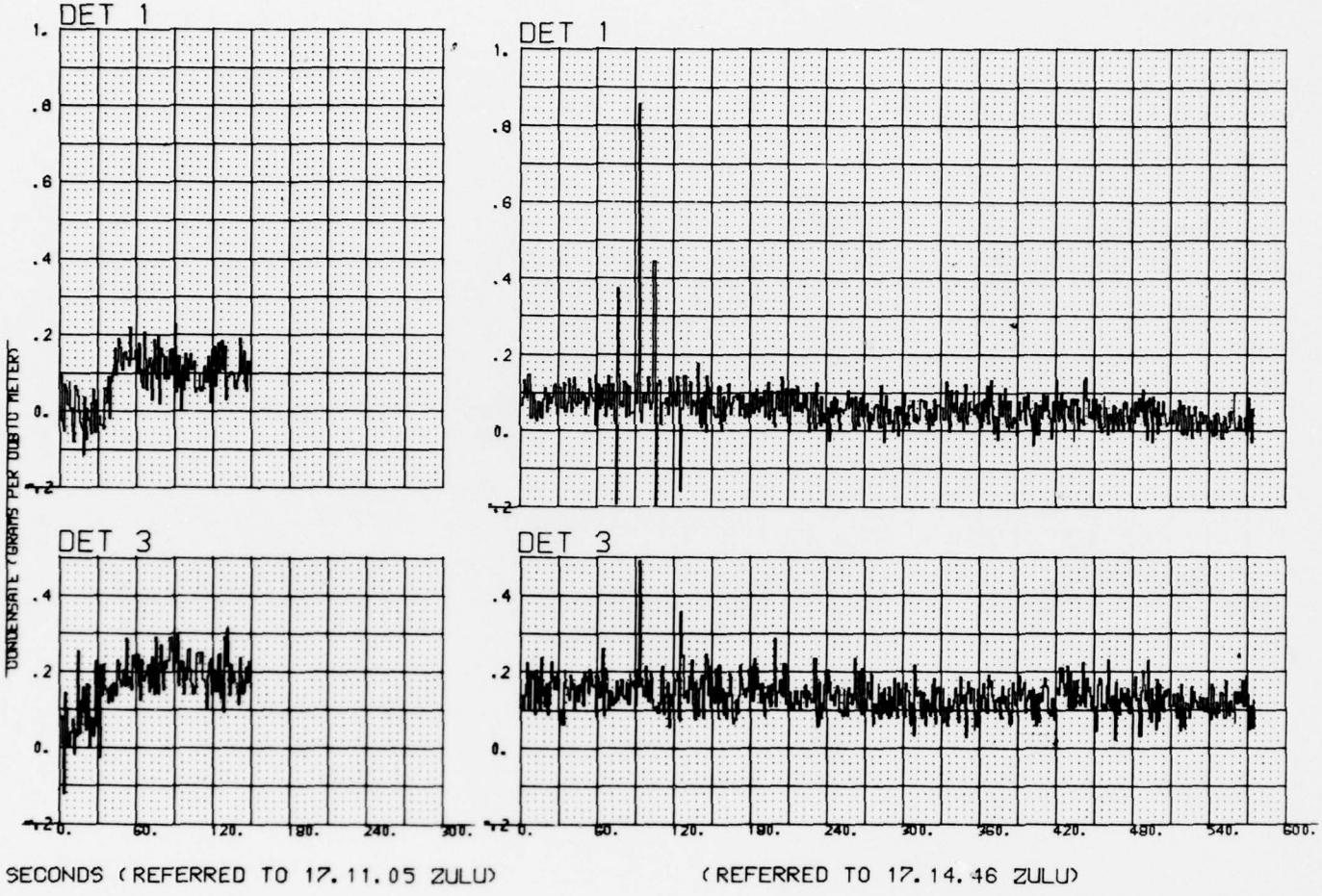

Figure 50. Flight No. E77-014

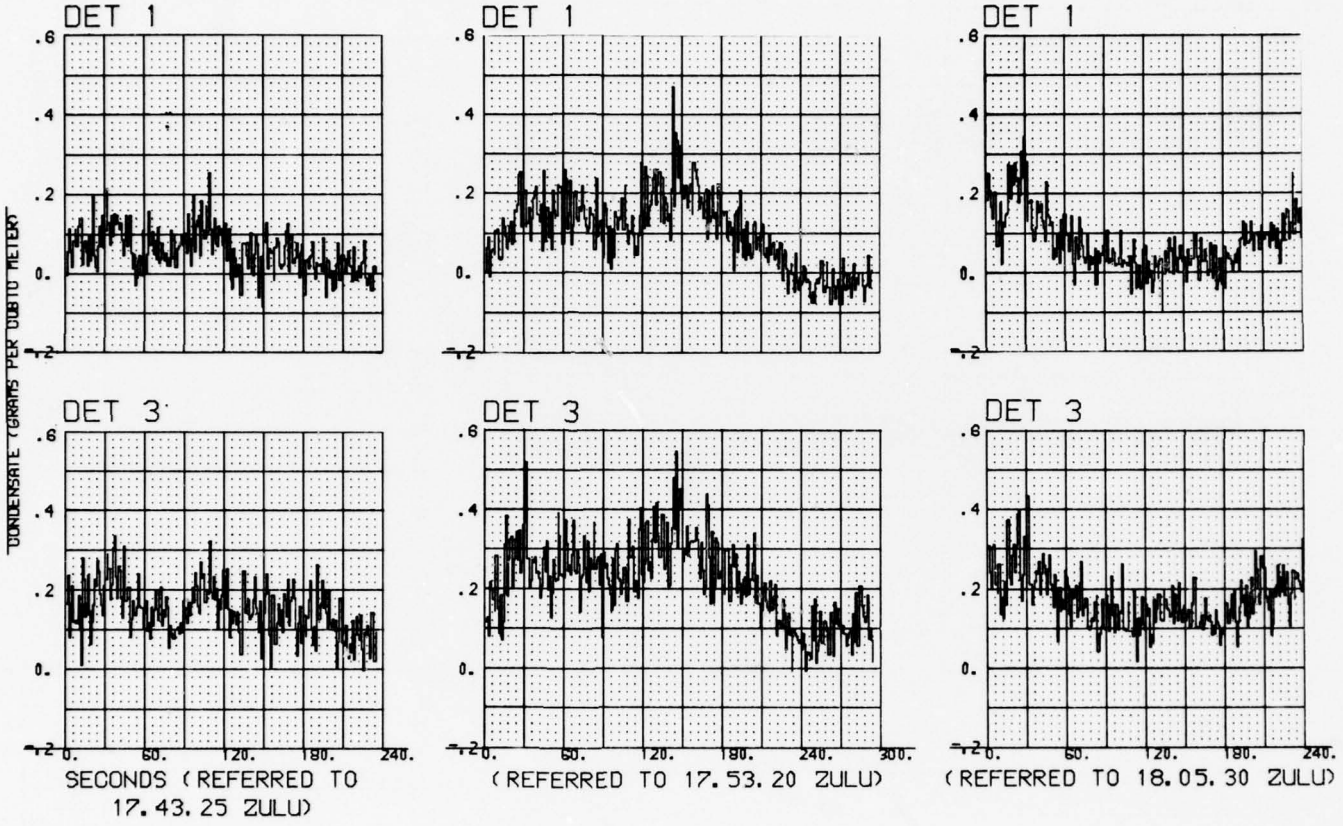

Figure 50. Flight No. E77-014 (Continued)

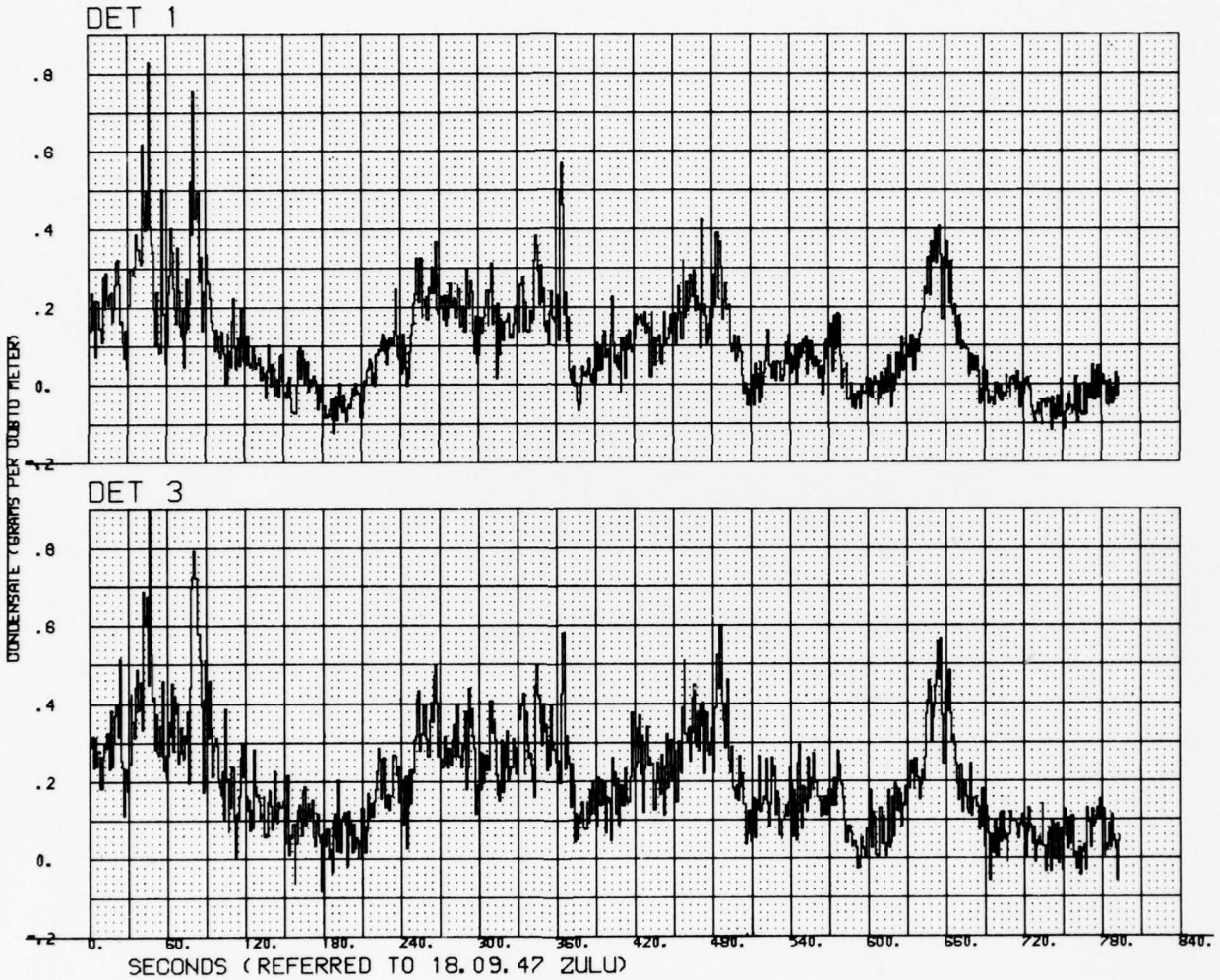

Figure 50. Flight No. E77-014 (Continued)

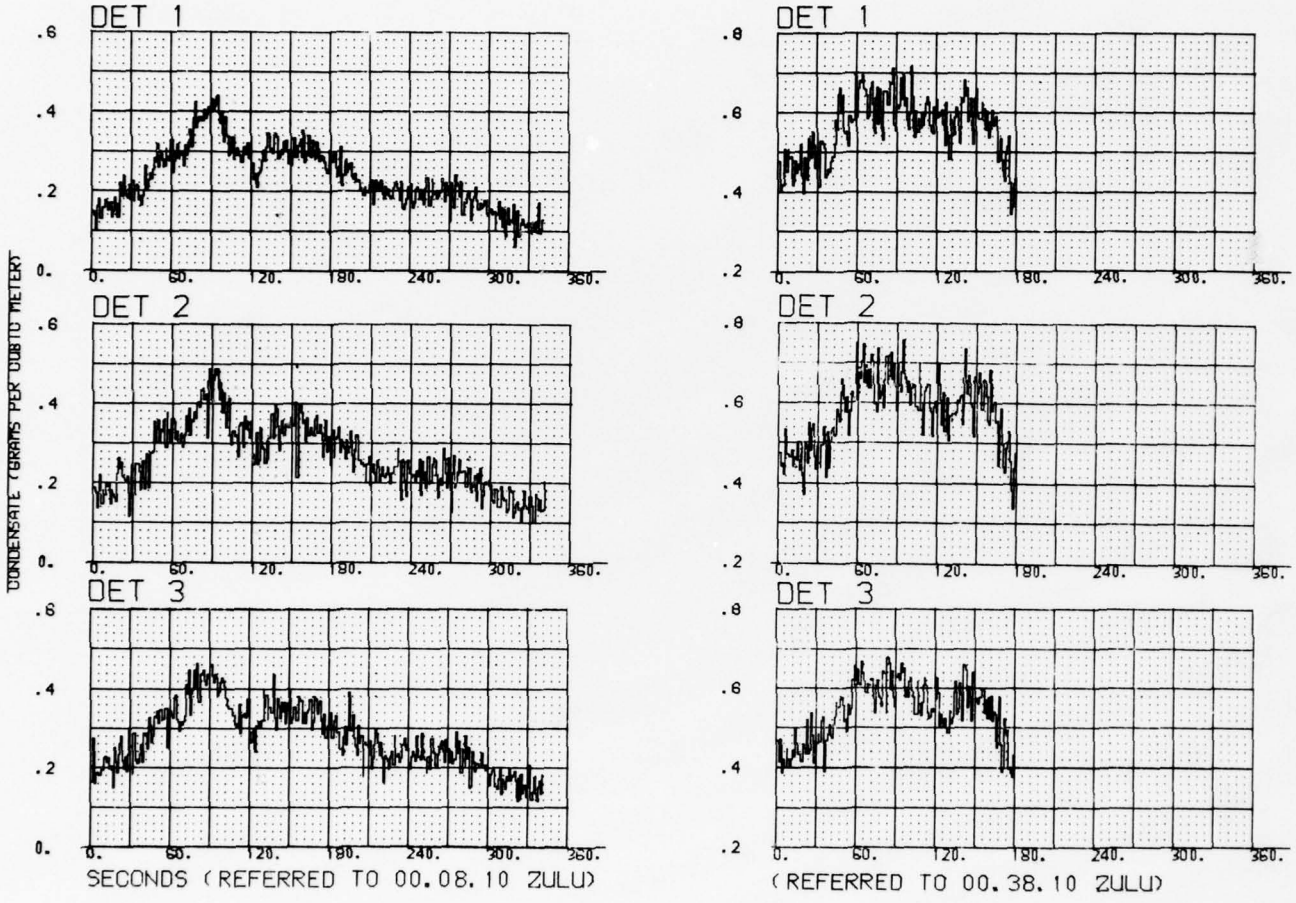

Figure 51. Flight No. E77-002

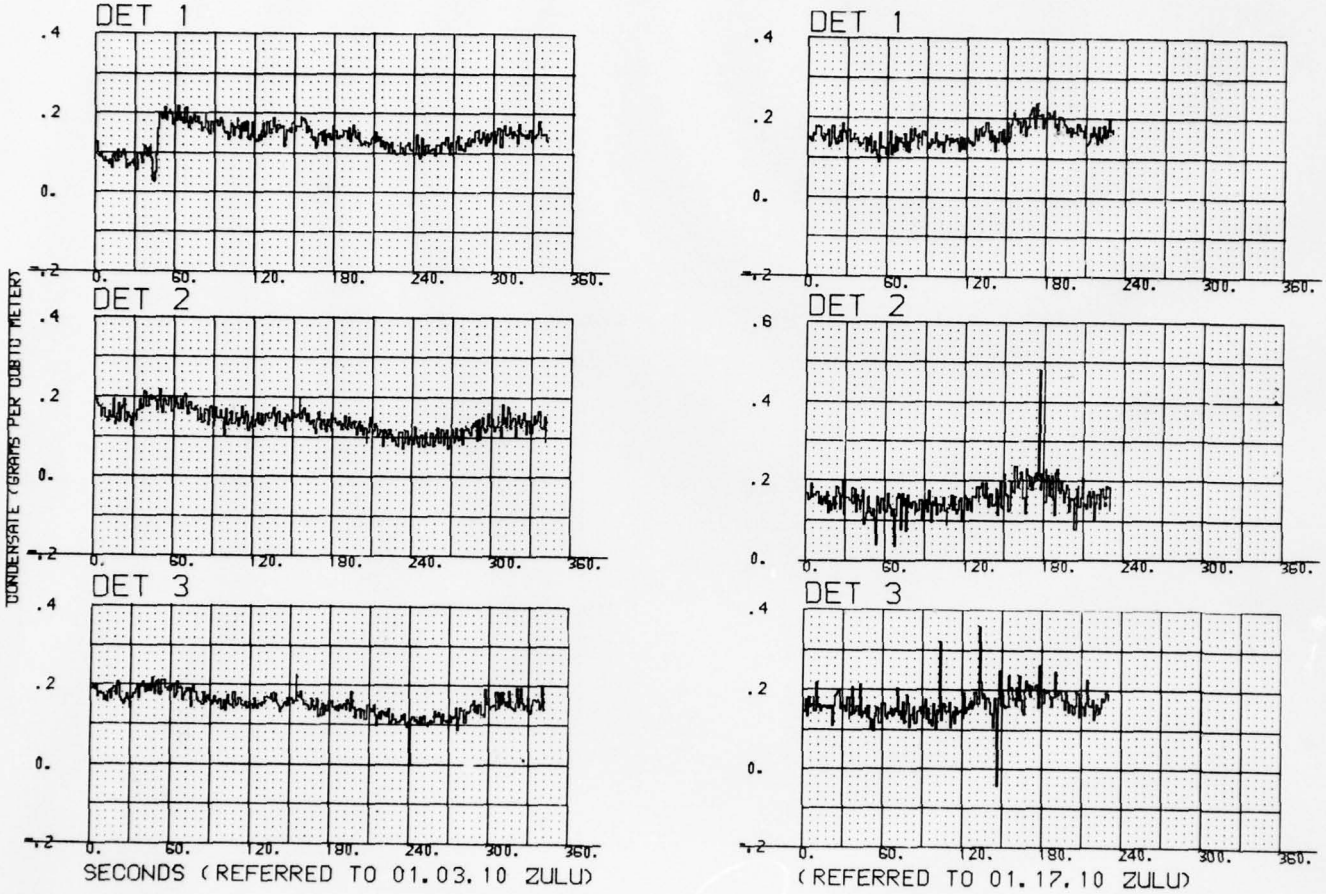

Figure 51. Flight No. E77-002 (Continued)

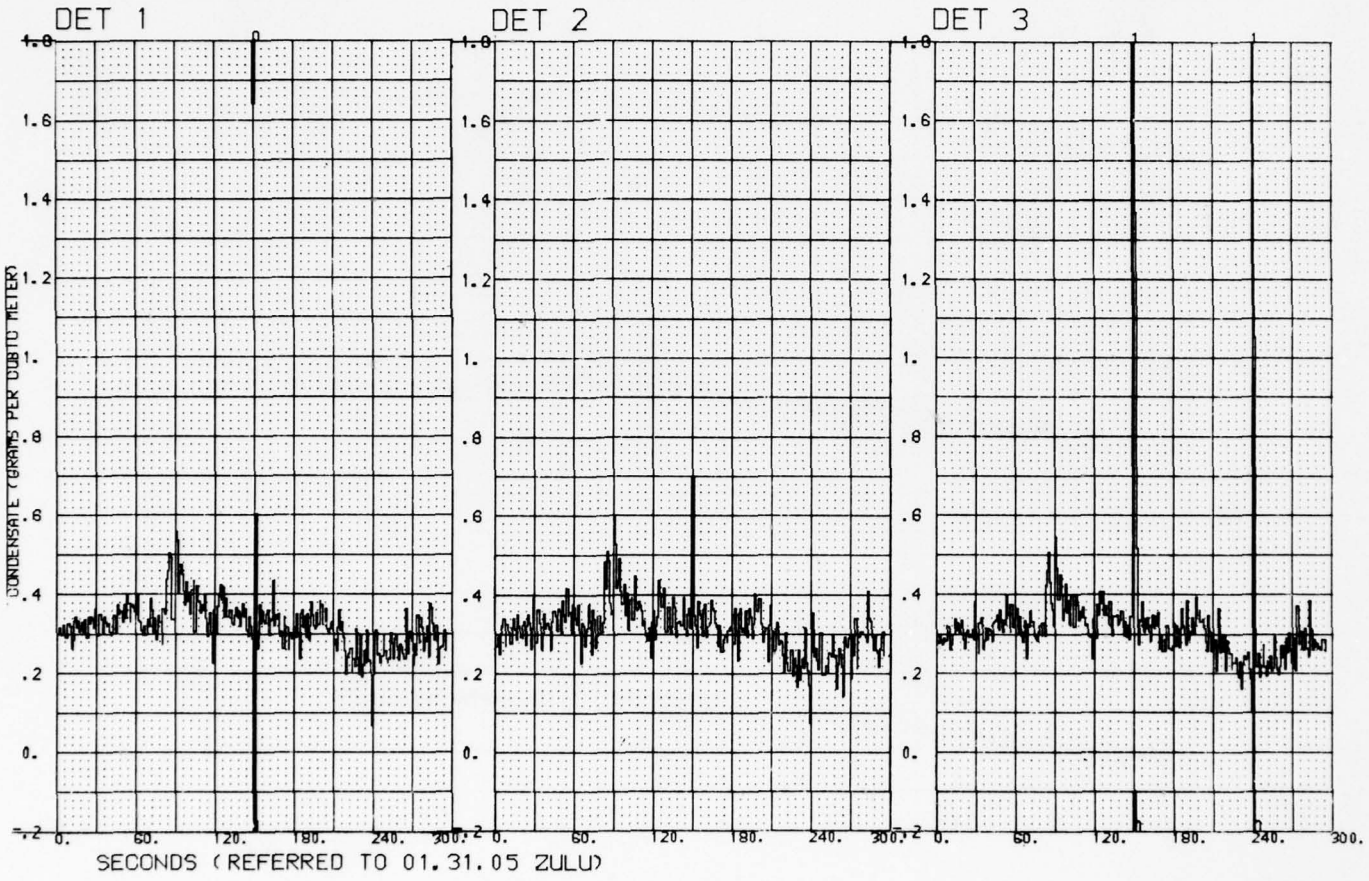

Figure 51. Flight No. E77-002 (Continued)

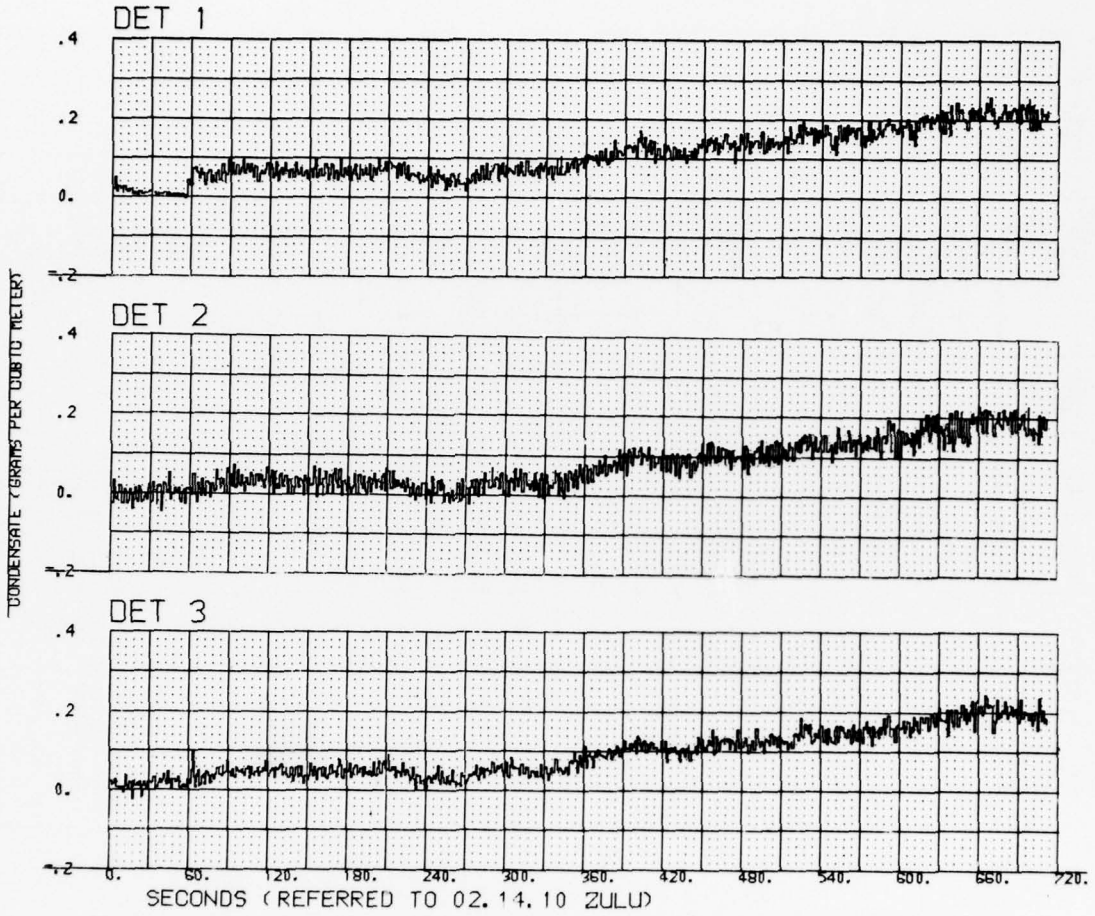

Figure 51. Flight No. E77-002 (Continued)

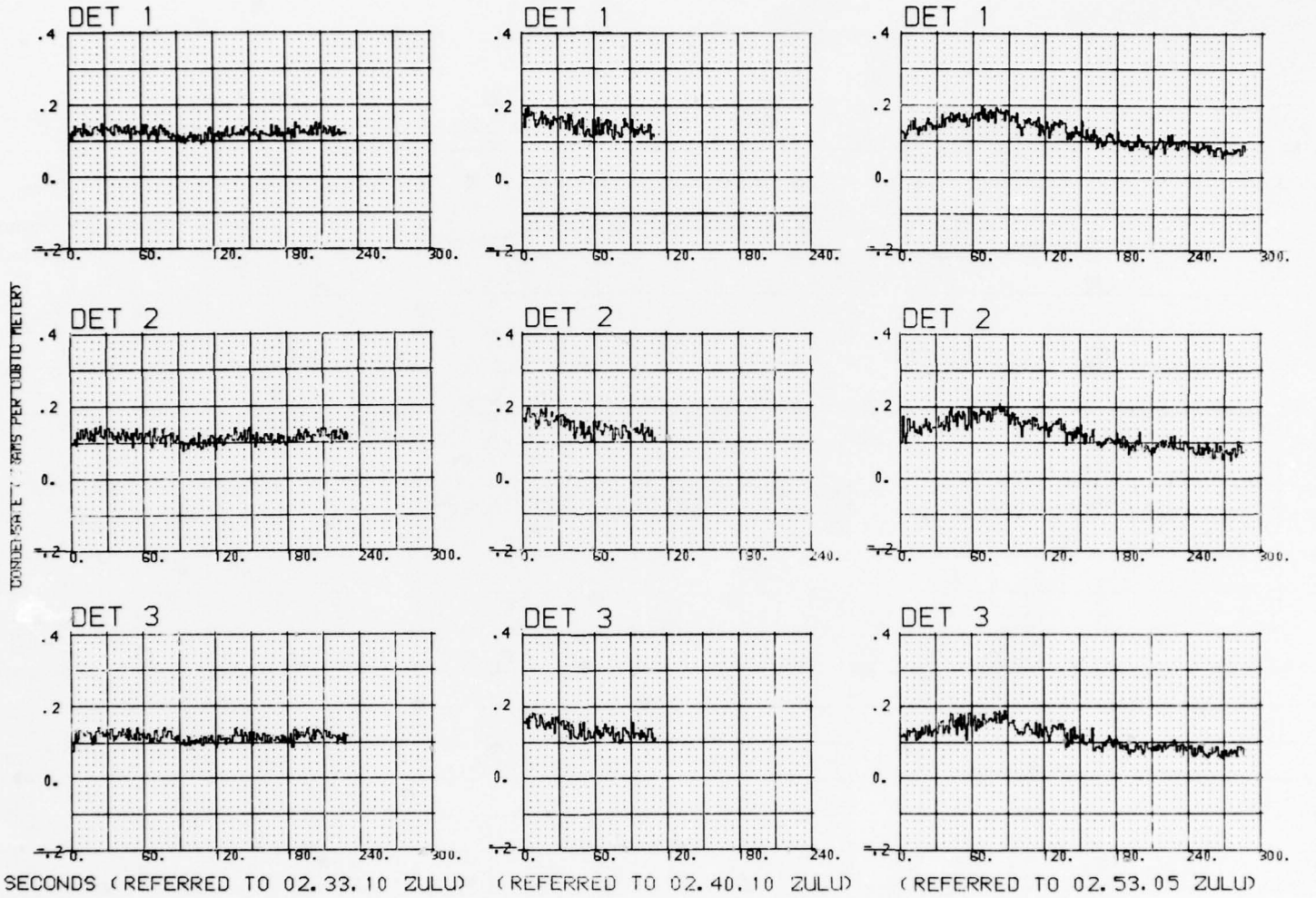

Figure 51. Flight No. E77-002 (Continued)

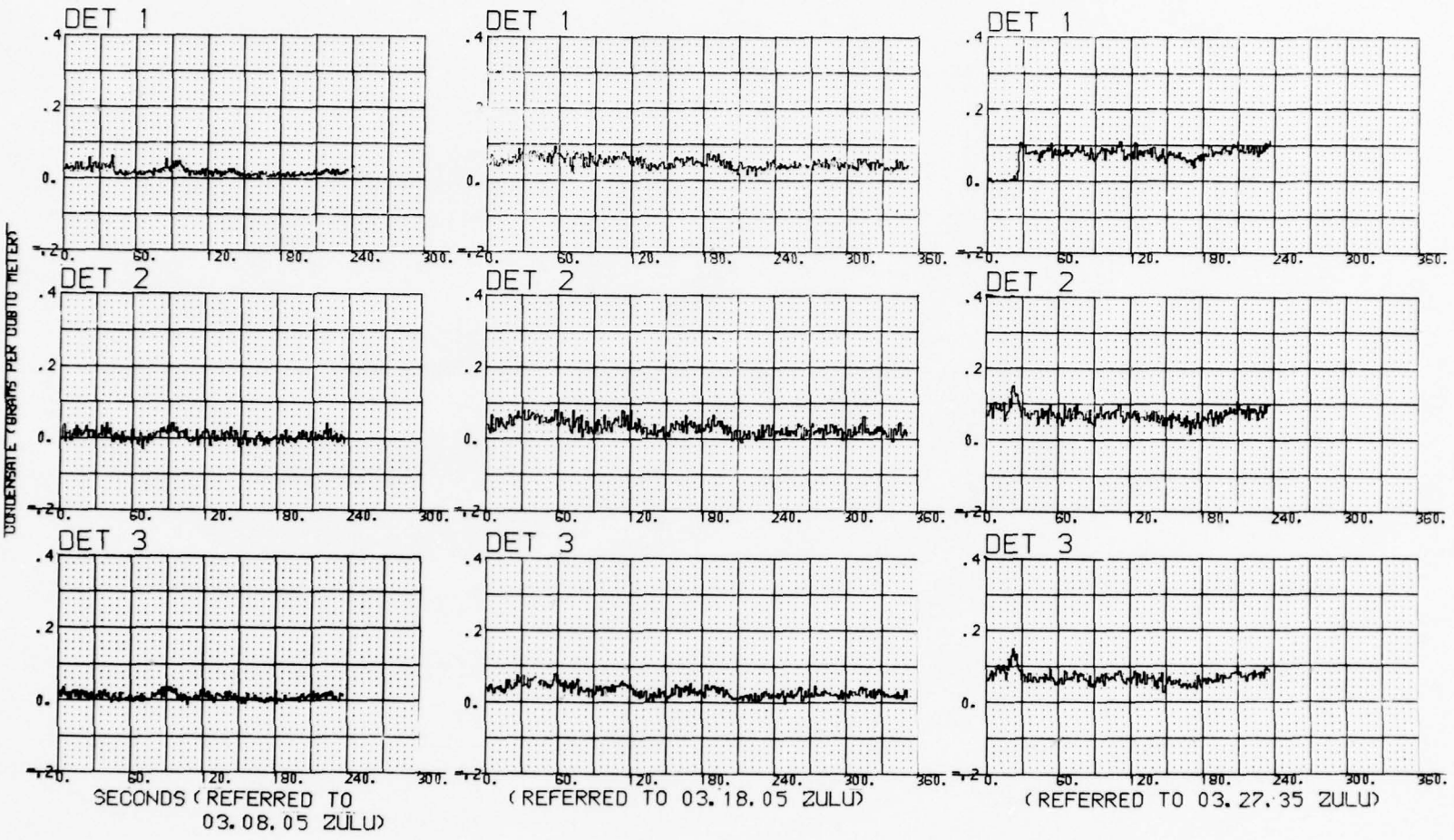

Figure 51. Flight No. E77-002 (Continued)

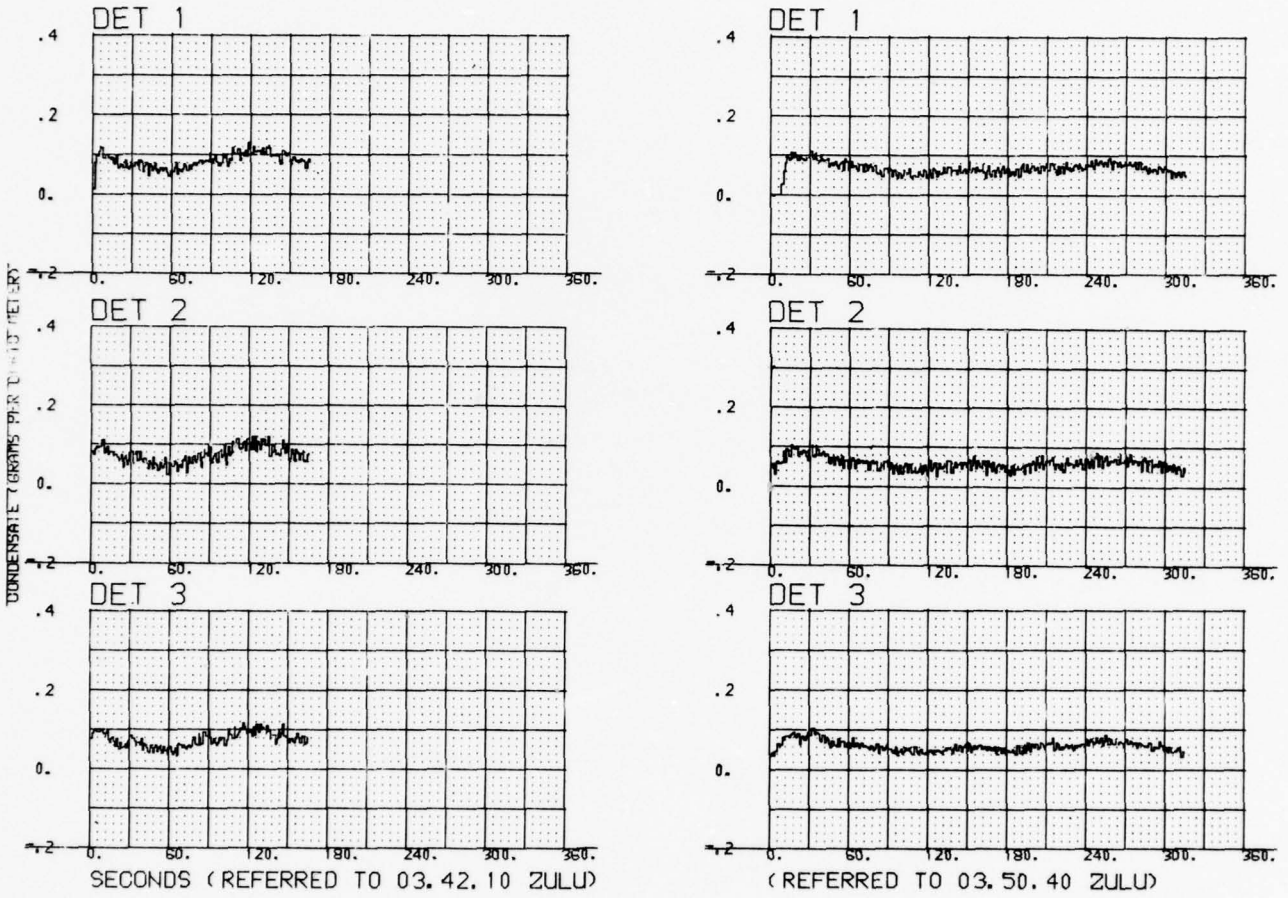

Figure 51. Flight No. E77-002 (Continued)

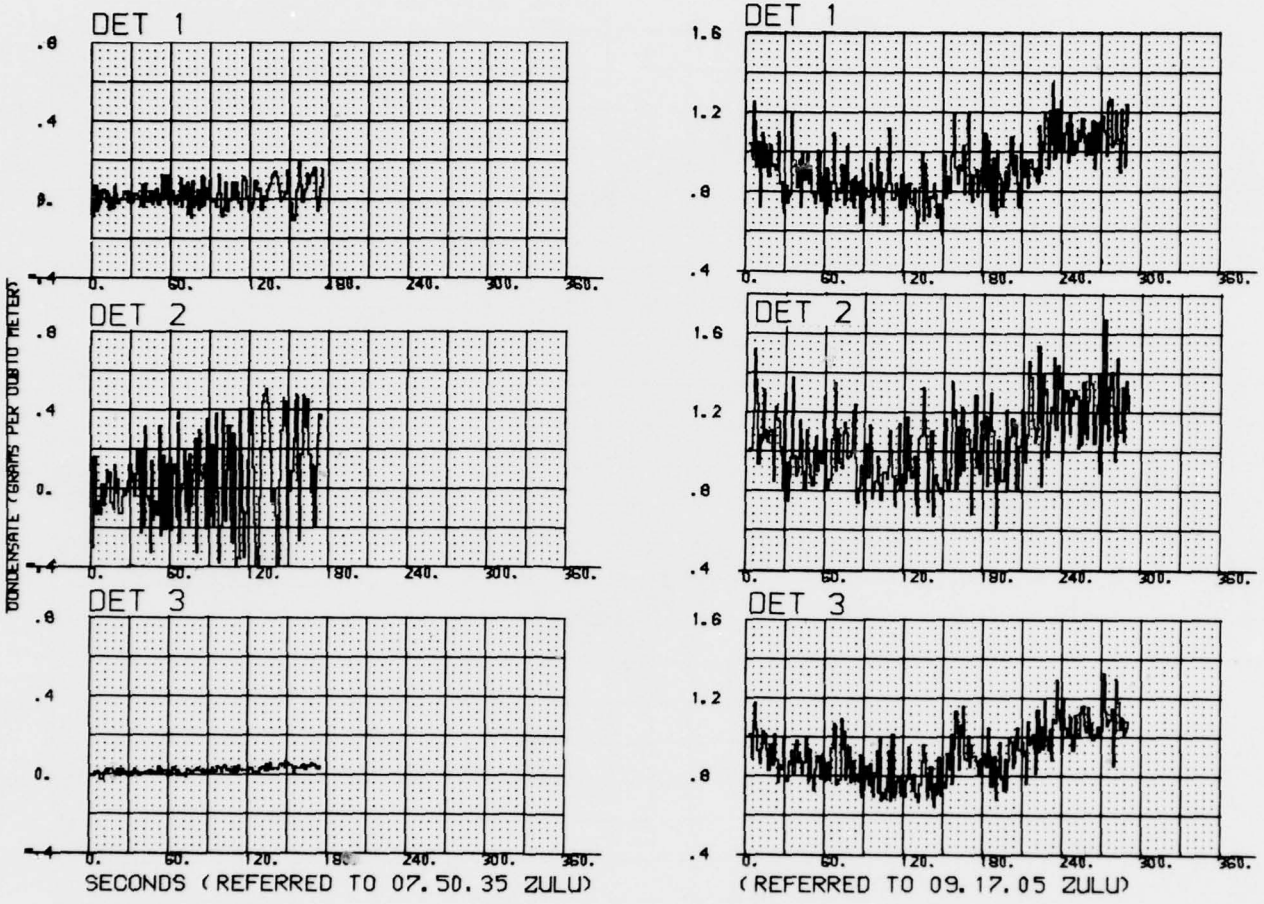

Figure 52. Flight No. E77-022

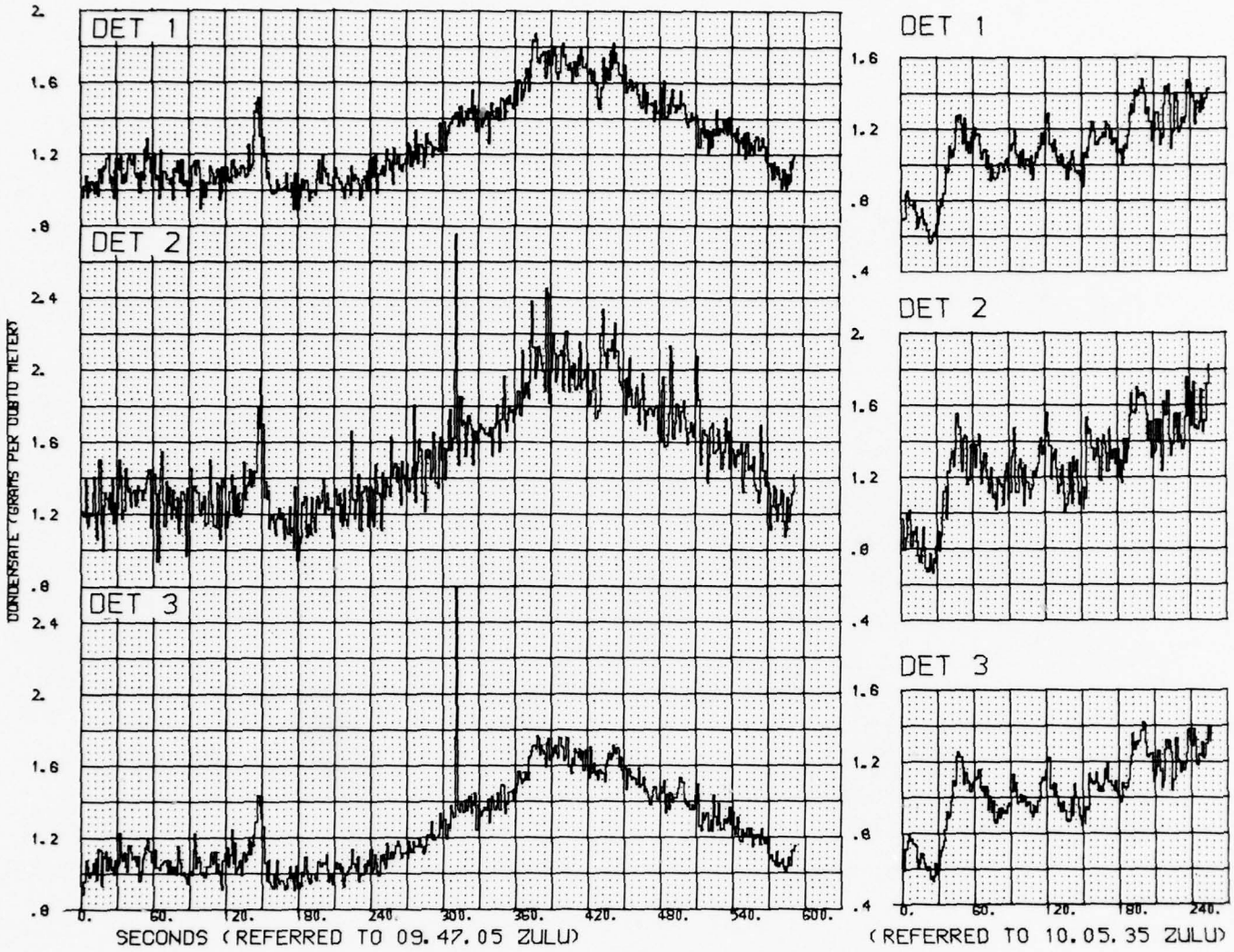

Figure 52. Flight No. E77-022 (Continued)

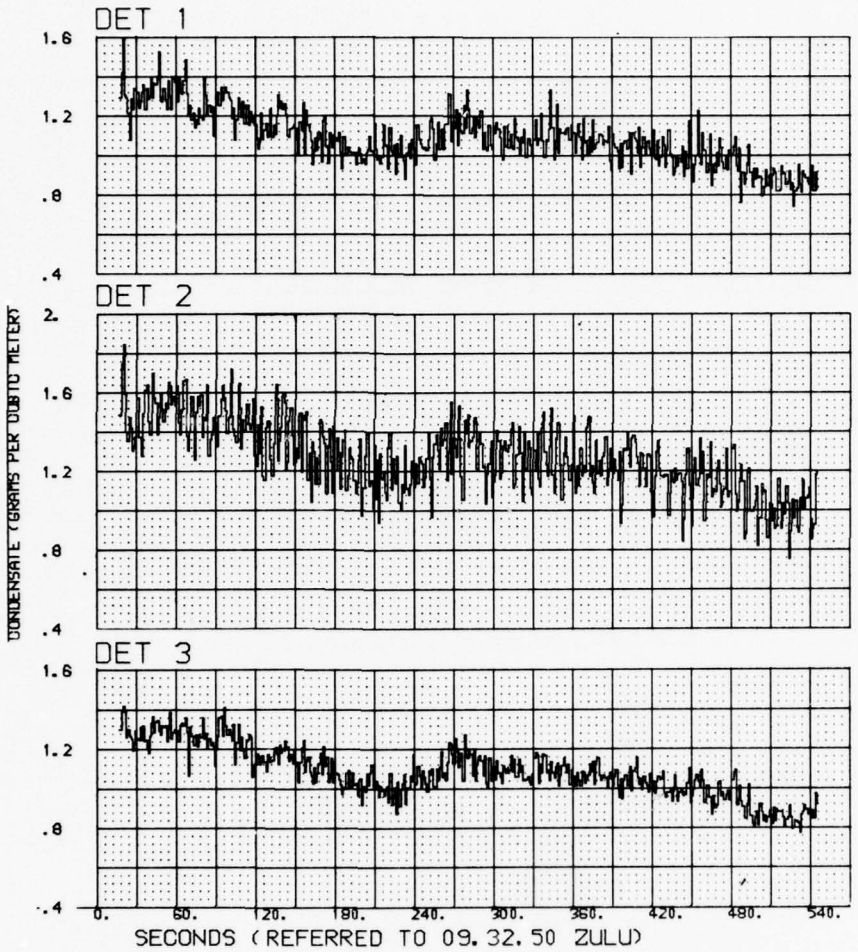

Figure 52. Flight No. E77-022 (Continued)

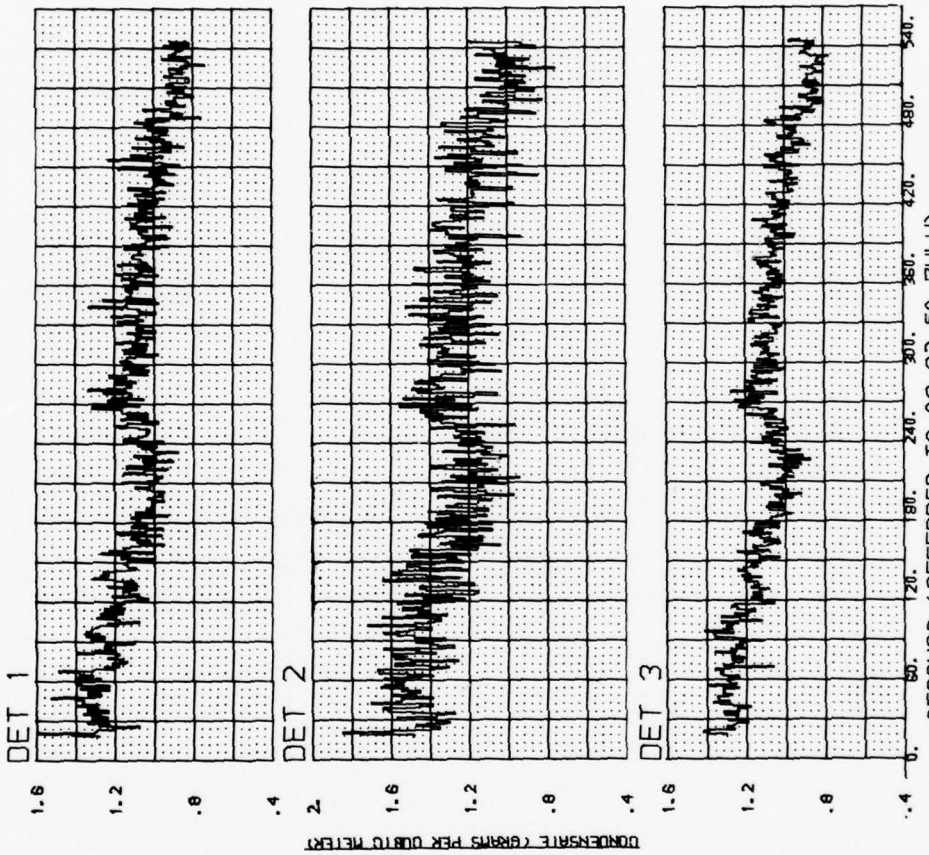

Figure 52. Flight No. E77-022 (Continued)

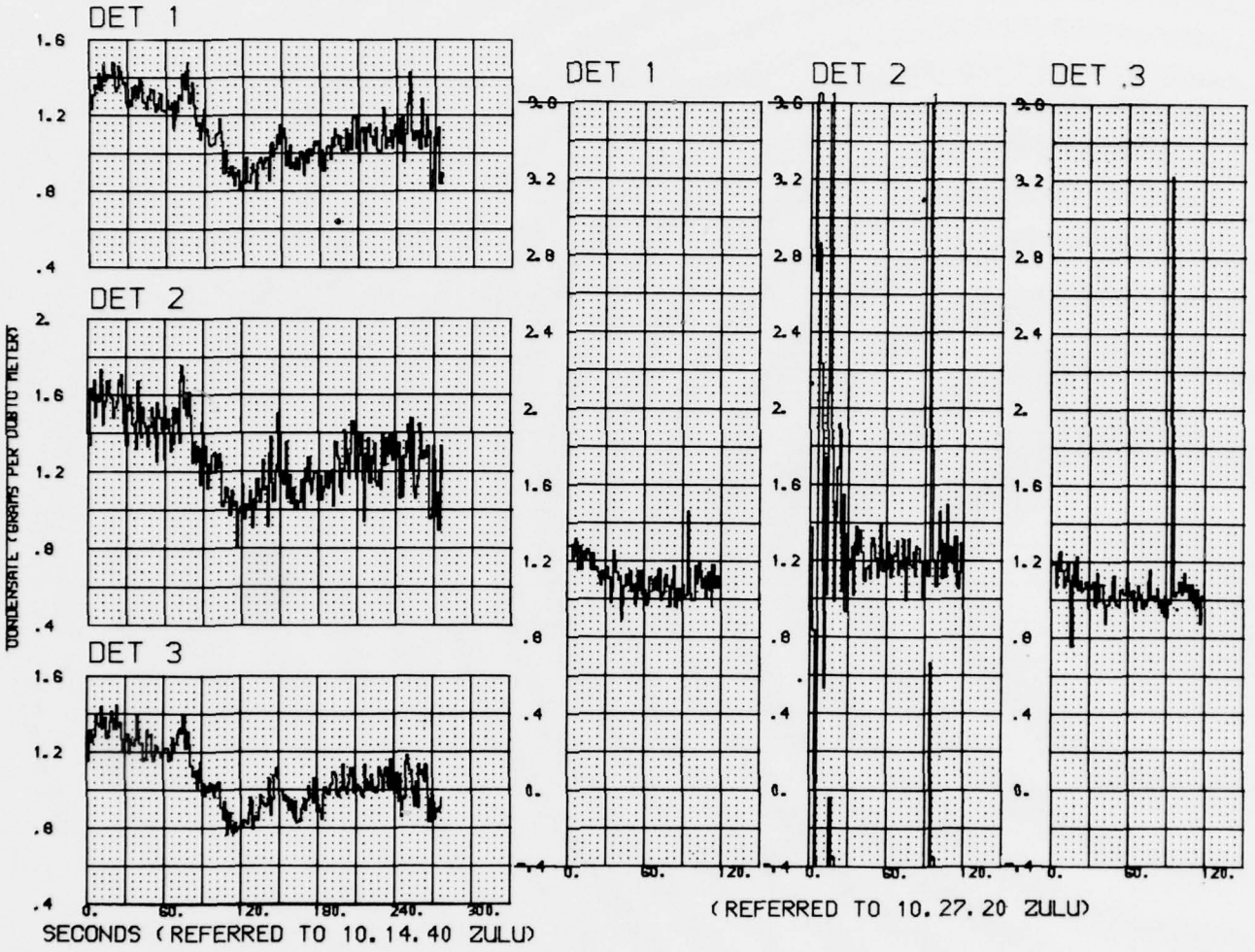

Figure 52. Flight No. E77-022 (Continued)

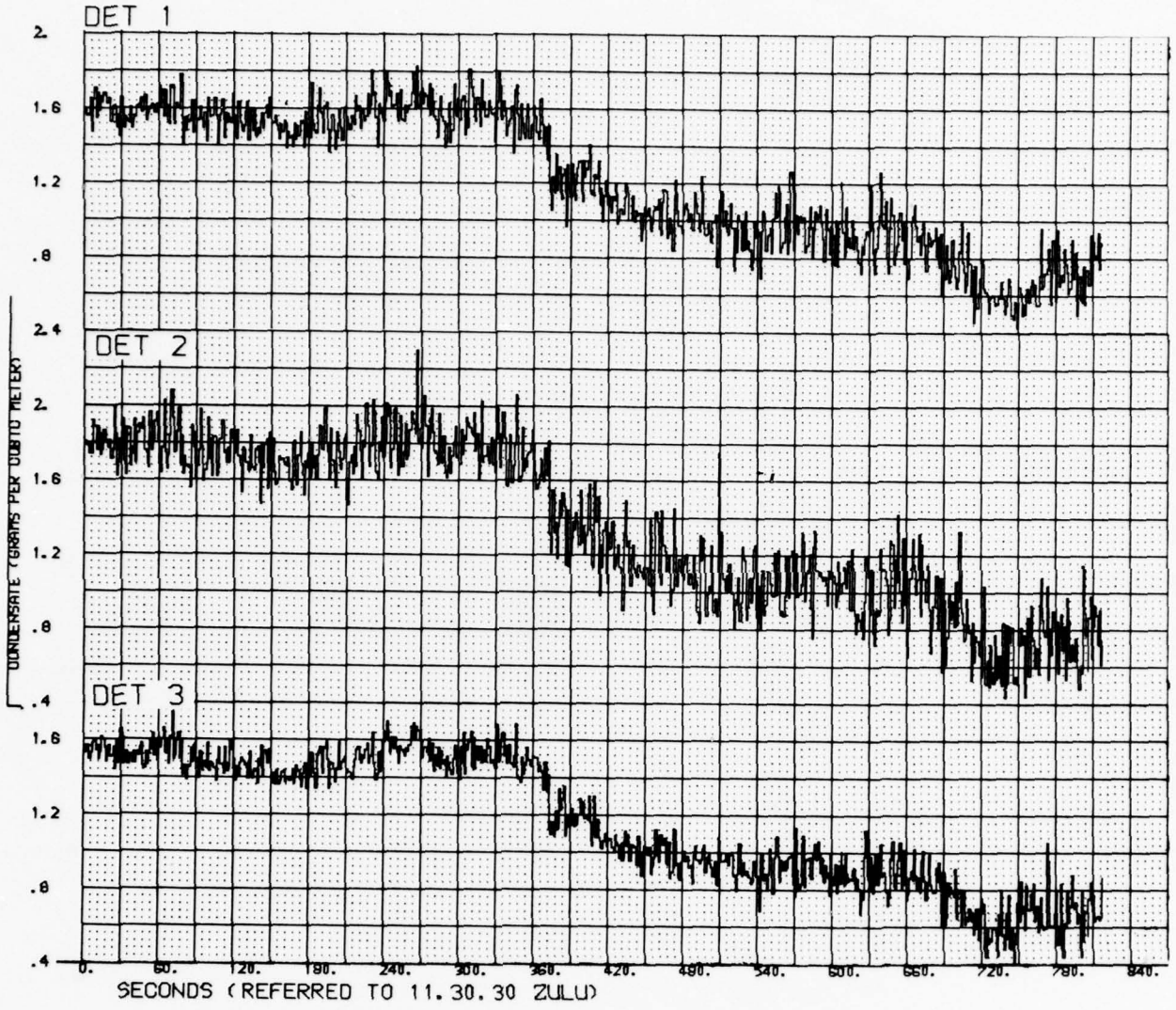

Figure 52. Flight No. E77-022 (Continued)

V. DEVELOPMENT PROBLEMS

V. DEVELOPMENT PROBLEMS

Several parts of the EWER system proved to be especially difficult to develop to the level of performance/reliability necessary for this application. Some of the problems have already been alluded to in the design and testing sections of this report. These and other problems are discussed in greater detail in this section, so that the user of the equipment will know the reasons certain things were done the way they were and where special precautions in handling and operating the system are in order. In addition, any upgrading of the design in building another unit should be considered in light of this development experience.

A. HEATERS

Several problems were encountered in the development of the heaters that required special attention. The original design for the trim heaters had the No. 36 Nichrome wire strung in the opposite direction such that the unsupported span was 5 cm. It was possible with this arrangement to obtain the desired resistance by having all eight wires in parallel on a circuit board and all circuit boards arranged in series. A minimum amount of soldering was required for assembly of the boards. These units operated satisfactorily in all tests up to the first series of vibration tests. At this point they failed, even though the vibration input was along the axes of the wires. Therefore, it was decided that the wires would be oriented to span the short dimension (1.58 cm) and arranged so that they would be staggered from board to board to give maximum separation. This required much more soldering along the long sides of the circuit board, but with special tooling (see Figure 6), the assembly effort was reasonable. In this case, the wires on each board are all in series and the boards are arranged to give the proper resistance. It should be noted that the parallel groupings are arranged to give the highest current in the downstream wires. Since these wires are also operating at a

higher temperature due to the gradient through the heater, it is expected that a control failure (should it occur) would destroy only the last eight boards and the forward units could be salvaged for the next assembly. It should be noted that the trim heater design has proved quite durable under normal operation. However, any deviation from normal (control failure, no flow, etc.,) can easily cause serious damage or failure. When difficulties of this type are encountered in the trim heater(s), the detector optics are coated with a brownish residue that completely absorbes the UV radiation and kills the output.

Two problems have been encountered in the closed-loop controls for the trim and main heaters. The first was mentioned in the discussion of the second vibration test series (page 87) where the AC power unit had a series of spikes on the 400 Hz sine-wave. This caused the solid-state switches (Triacs) to conduct without any triggering signal. Changing to a standard ground power unit (MB-1) and in subsequent aircraft operations, there was no further problem of this type. At this same time, the wiring in the electronic box was conformal coated and some of the coating material flowed into the sockets of the connectors on the controller circuit boards. As a result, the contact was intermittent and caused several heater failures that were not properly diagnosed as control failures. At KMR these sockets were replaced and it was determined that 50% of the contacts had lost their spring action due to the potting. Since the sensor for the controller on each heater is a few centimeters downstream of the heater, airflow is required before proper control can be established. No satisfactory scheme for signaling an imminent heater failure could be devised in view of the very low flow rates through the trim heater in normal operation.

Initially, the main heater was to be made with bare wires insulated by the aluminum oxide coating on the heating element. Tests with wire wrapped around a hard anodized tube showed that adequate insulation was available.

However, the extensively finned heater element prevented the formation of the oxide down in the grooves where the wires would contact it and so separate insulation was required. Mullite (aluminum silicate) sleeving was slipped over the No. 12 Nichrome wire and broken into short lengths so the wire could be wrapped on the heater element. This arrangement worked well for some time until the wires were replaced. A new batch of Mullite tubing was used. Poor life was obtained from this batch and it was attributed to the low mechanical strength of this particular batch. Another set of wires with (better) Mullite was installed and failed in calibration tests. This failure was attributed to the high pressure fluctuations (acoustic noise) in the flow coming from the metering orifices. The Mullite was replaced with alumina (Al_2O_3) in an effort to correct a marginal condition. Reliability has been good and bad. Recently, it has been determined that the insulators (both Mullite and alumina) have not been broken to short lengths with square ends, thus giving rise to kinks and large separation when the heater wire is wrapped on the heater element (23° helix on 3.5 cm dia). A tool was designed to enable the precise and consistent breaking of the insulator when installed on the wire. As a result, the insulated wire now appears as though it has flexible spaghetti insulation with no opening apparent between the alumina insulators along the length of the wire. It is expected that the reliability of this assembly will be much higher. It might be possible to return to Mullite insulation which is cheaper and has better resistance to thermal shock. It is interesting to note that the reference heater which is configured the same as the main heater (except only one wire) has never failed. It is not exposed directly to the airflow and water condensate.

B. DETECTOR

The requirement that all the electronics for the source and receiver be contained in the rotating housings placed some significant constraints on the design. This led to some development problems.

Although all components were thoroughly potted in the housing, the signal and synch LEDs were prone to break at their leads. As a result, quite a number of flight tests came up with no data. Several configurations for mounting these components were tried before a satisfactory compromise was obtained.

Some thermal drift in the VCO output was evident in early assemblies, which caused the output frequency to move out of the range of the phase-lock-loop demodulator. Some changes were made in components and a relatively low thermal drift resulted as shown in Figure 53. Recently, the detector assembly has been instrumented with a thermocouple to determine the temperature excursions of the main bearing frame. Although this part, running from 30°C to 50°C, is not at the temperature of the electronics, it is expected that the variation is representative of that occurring in the housing.

Considerable trouble developed in the bearings that support the rotating housings after 50 to 100 hours of operation. Initially, these bearings were run virtually dry, since the drivemotor torque was relatively small and the viscous drag of lubricant in a 7.5 cm diameter bearing would be large (especially at low startup temperatures). The bearing loads are negligible and speeds are low so heavy lubrication was not required. Furthermore, these bearings are a fractured-race design and of open construction so lubricant would attract and hold contaminants in the bearing. When the insulators in the main heater began to fail, the bearings picked up particles of ceramic and began to get pitted. About the same time, the gearbox in the drivemotor began to show signs of wear. To ease the problem, more lubricant was used in the damaged bearings. The net result was that several flights returned no data because of no detector rotation. A new motor of half the speed (twice the torque) was installed and the bearing assembly was redesigned to provide shields and slingers to prevent contamination. With a few drops of high-grade instrument oil, this system is working reliably.

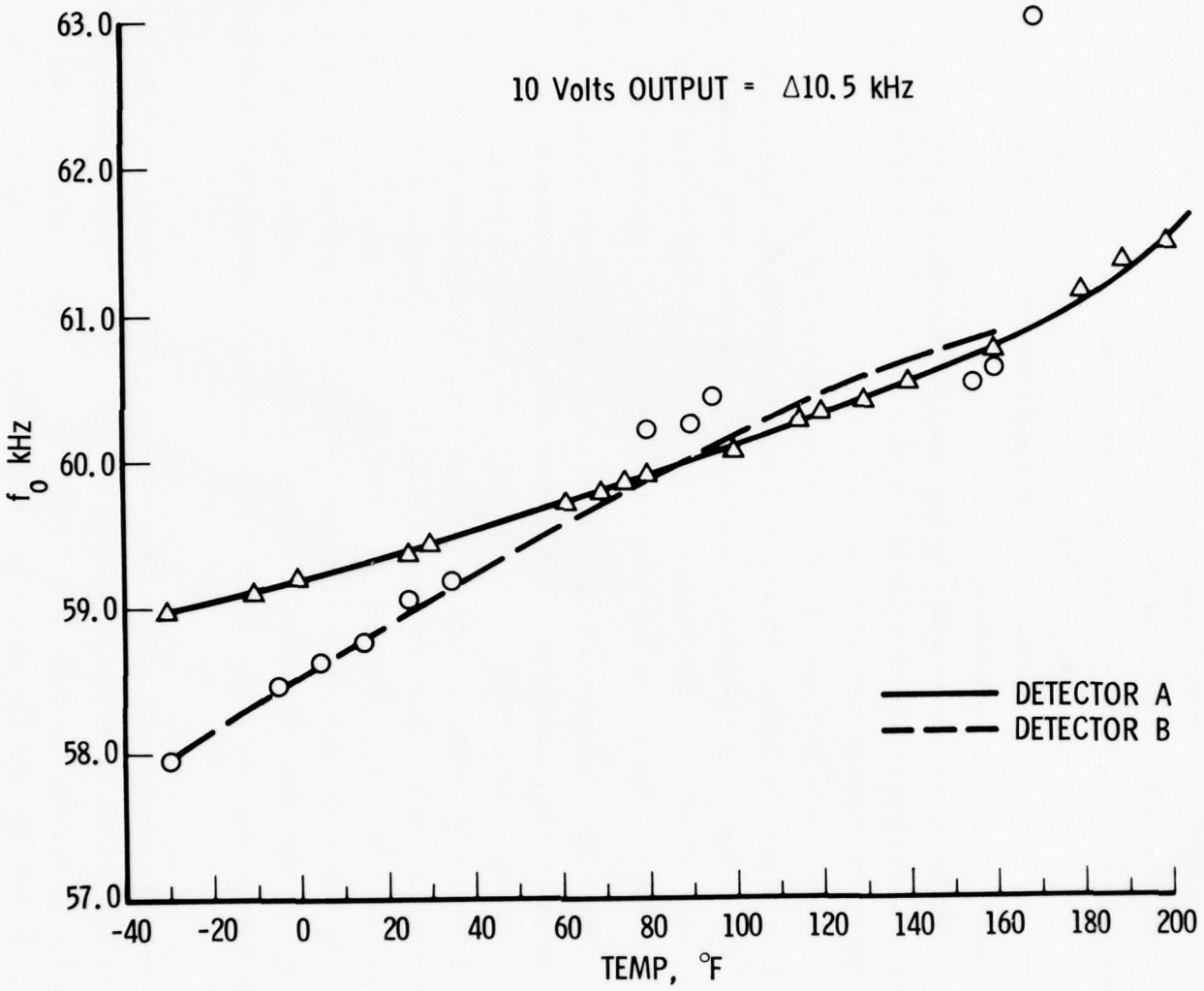

Figure 53. Detector Temperature Offset

Several attempts were made to aperture the source and receiver for optimum signal level and waveform. As a result, several flights came up with no data because the signal level was too low. The gain of the preamplifier in the receiver was increased to obtain more output. At the same time the aperture of both the source and receiver were decreased to improve the waveform. In addition, changing the relative positions of the four sources with respect to the four receivers significantly modified the output. Movements of 90° and/or a few teeth on the drivegears resulted in large changes. Vernier adjustments are possible by the use of the slotted holes in the mounting of the gear on each housing. It was determined that a 6 and 4.5 mm aperture on the source and receiver, respectively, were about optimum. The apertures are made by punching holes in the copper EMI shield placed on the front face of each housing. These holes are located on the theoretical centerline of the Lyman-α components potted in the housings. With these apertures, a 1 cm wide tab on the baffle between the housings is sufficient to blank the source and obtain the output for total absorption (i.e., reference level).

After proper adjustment, the output from each sensor should be within about 50% of the highest value. The lowest source is positioned to coincide with the synch pulse period, since the data rate from that position is one-half that for the other positions. Nevertheless, there is a tendency for the condensate and vapor levels in the output to be slightly unequal for the condition of no condensate (i.e., no flow). Vernier adjustments can be made to minimize this effect, but it has been impossible to eliminate it on all sensors with the same adjustment. Therefore, a clear-air calibration is required to evaluate the offset and determine a bias to be used in calculating the condensate water.

Another problem encountered in the particular Lyman-α components used was the breakdown of the epoxy seal on the silver chloride cement used to bond the magnesium fluoride window on the tubes. When the seal was in the proximity of a conductor, the voltage on the tube would cause current to flow to ground.

This would destroy the seal, compromise the bond, and permit the tube to leak. For the assembly in the aluminum housing (ground potential), a layer of insulating tape was placed across the magnesium fluoride window underneath the EMI shield with a hole in it that is larger than the aperture.

C. AIRCRAFT GROUNDING

Considerable trouble was experienced when the EWER system was installed in the C130E aircraft because of different potentials in various parts of the airframe. This was particularly troublesome in the online computer cabling where low-voltage TTL operations are involved. It was determined that, on occasion, a "zero" of less than 0.7 V was not possible. To avoid this problem, all lines to and from the computer were terminated with opto-isolators. This system, first operated in the laboratory, had to be "retuned" in the aircraft to account for line losses.

Difficulty was also encountered in recording flight parameters (i.e., outside air temperature, indicated airspeed, pressure, etc.). There appeared to be potential differences between the EWER system and the aircraft/project systems that caused spurious signals on most data channels. High impedance, isolated input buffer amplifiers are in all EWER data channels. The problem was never resolved but seemed to come and go and currently may be gone.

D. SEPARATOR

As was mentioned in the section on functional testing, the original mechanical separator design was not satisfactory. At the time this was discovered, the general configuration of the sampling probes was committed, so any modification had to fit this constraint. Although the elected change seems effective, the manner in which it was implemented could be improved.

VI. RECOMMENDATIONS

During the development of the EWER system, certain deficiencies in some of the components were discovered. Many of these were satisfactorily resolved as has been discussed in the section on development problems. Others, of a relatively minor nature (called Level 1), have been identified in separate correspondence with AFGL. Two other levels of modifications are discussed in the following paragraphs.

A. LEVEL 2 MODIFICATIONS

These modifications should be made when there is extensive downtime and the system is removed from the aircraft.

1. MODIFICATION 2A

A servo-operated wafer switch is employed to control the system functions displayed on the panel meter. Although there has been no trouble from this component, it is recommended that it be replaced with an electronic multiplex system. Such a scheme will make all functions immediately available for viewing by the operator without having to wait for the servomotor to drive the switch to the selected position. In addition, all functions will be available for recording on the tape recorder as an aid to diagnosing system problems should they occur. On occasions, the servomotor has been observed to "hunt" at a particular position. Continual movement at the contacts will cause wear and could lead to malfunction of the switch in the future.

2. MODIFICATION 2B

The flow through EWER is exhausted to the slipstream via a flush fitting located aft and on the underside of the pod at about the 4 o'clock position looking aft. During flight tests it was observed that the backpressure in the pod was sometimes as high as 10 Torr and varied with the angle of

attack of the aircraft. As has been mentioned, this backpressure can have a significant effect on the collection efficiency of the instrument. Therefore, it is recommended that a fairing be installed ahead of the exhaust port to develop some aerodynamic suction and reduce the backpressure and its variation with the angle of attack.

3. MODIFICATION 2C

Difficulties have been experienced in the control of the trim heaters, mostly due to conformal coating inadvertently placed in the sockets of the controller circuit boards. However, a severe icing condition occurred in one flight and the trim heaters may not have been turned off in time to prevent their being burned up due to lack of airflow. Also, if the heater disable switch is cycled after the trim heaters have been operating at temperature, it is possible that heater elements may be momentarily overheated. It is recommended that a controller circuit be devised to shut down the heater in the event of an open thermocouple (i.e., thermocouple or contact failure). In addition, it might be possible to move the controlling thermocouple nearer to the heater itself and be better able to sense the temperature of the wires should an airflow failure occur.

4. MODIFICATION 2D

When the separate, heated nitrogen flow to the detector was removed, a controller for a single-phase heater became a spare unit. It would be possible to connect the inlet heaters to this controller and thereby separate their function from the reference heater. Also, it would be possible to dissipate more power in those heaters to give greater protection against icing. In addition, the operator would not be bothered with the manual control of the heater. However, it should be noted that the configuration of these heaters is such that great caution should be exercised so that they are not exposed to full line voltage.

5. MODIFICATION 2E

Some difficulty has been experienced with the small thermocouple wire used in the EWER assembly, especially where it is in a lug on a terminal strip. Upon assembly and disassembly the wires are inclined to break. Larger wire could be used at the connections, or standard thermocouple disconnects could be incorporated where the mounts screw into the unit.

B. LEVEL 3 MODIFICATIONS

These modifications might be considered if another unit is to be built.

1. MODIFICATION 3A

The main heater wires have been susceptible to damage, possibly because of thermal shock to the ceramic insulators. This fact, plus the vulnerability of the wires to corrosion by salty air, could be avoided if a sheathed assembly were available. Although several companies manufacture small diameter sheathed heaters, the standard terminations are much too bulky. However, a special design might be developed with the aid of one of these suppliers.

2. MODIFICATION 3B

Several changes should be considered on the detector assembly.

a. A larger housing for the Lyman-α sensor would facilitate the arrangement of electronic components. Going to a larger diameter and rotating at a lower speed would make room for more sensors and make a center drive (on a splined shaft) feasible. In addition, it might be possible to move only one housing in order to vary the gap. The Lyman-α source tubes seem to be the component that fails most often; it could be located on the shaft in such a way that it could be easily replaced and/or the sensor windows cleaned. These features are shown in Figure 54.

b. An improved, active, constant-current power supply should be used in the source. Better regulation might tend to reduce any spurious oscillation in the lamp discharge, which could result in longer life.

c. The VCO and phase-lock-loop (PLL) center frequencies should be increased from 70 kHz to about 200 kHz. This will allow an improved tradeoff position for the PLL with respect to percent deviation and baseband frequency response.

d. Although the glass envelopes of the Lyman-α sensor are controlled by the manufacturer, it might be possible to bond a socket to the unit that would permit the envelopes to be replaced on a plug-in basis.

3. MODIFICATION 3C

Final adjustments on the system have resulted in a very small amount of air being used in the sample. Therefore, it would be feasible to reconfigure the probe assembly with only one sampling probe. The separator would be located just inside the inlet of the evaporator and the flow would be contained outside the shell surrounding the main heater. Such an arrangement is shown in Figure 54. It is apparent that all the functions of the two-probe configuration are similar in this arrangement, but in a much more streamlined package. The error in removing a small amount of the air from the evaporation sample, say 5%, is believed to be negligible.

4. MODIFICATION 3D

A standard demodulator unit should be used which is matched to the VCO in the detector. This would eliminate a lot of the problems with the custom designed phase-lock-loop circuit.

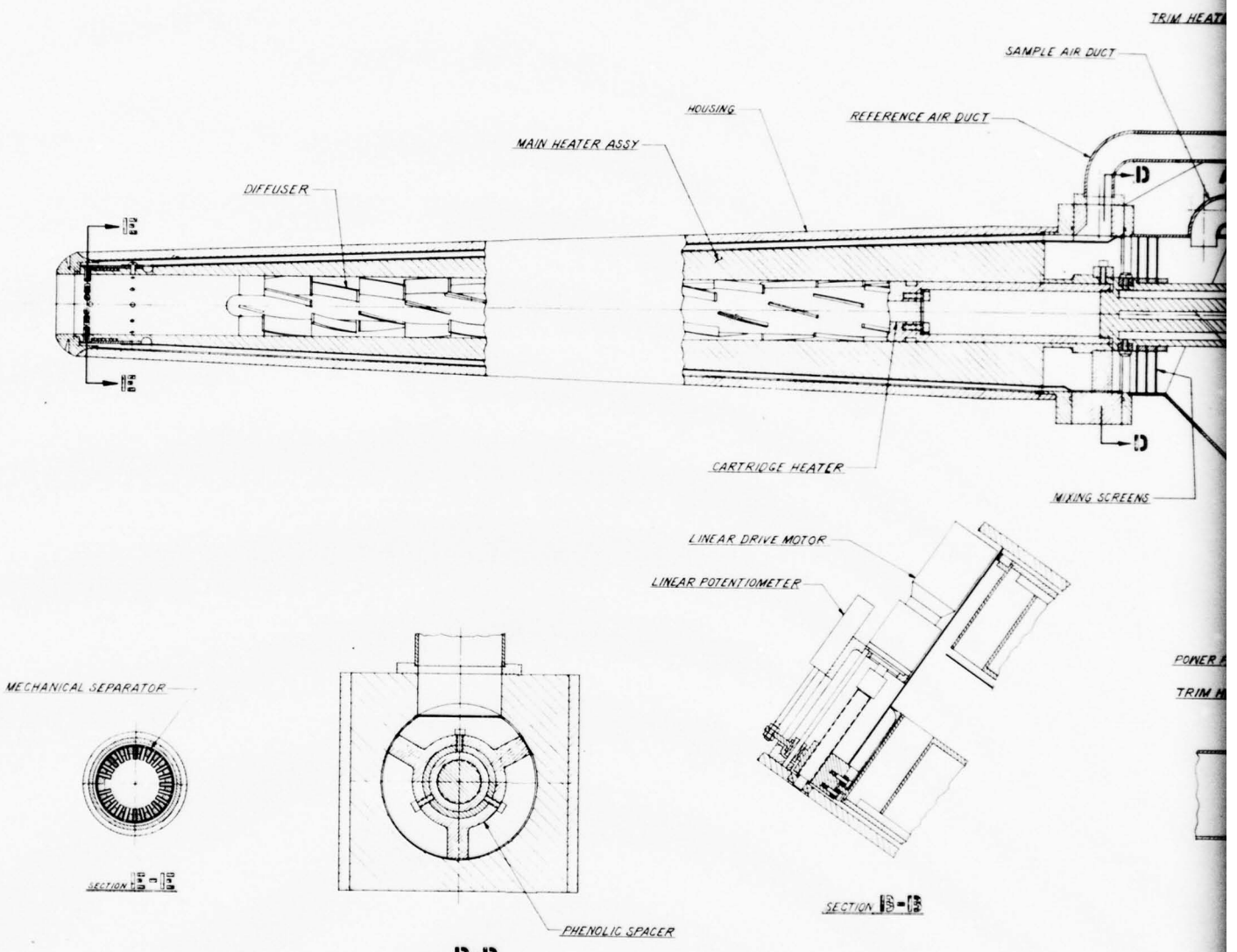
TRIM HEAT
SAMPLE AIR DUCT
HOUSING
REFERENCE AIR DUCT
MAIN HEATER ASSY
DIFFUSER
D
D
CARTRIDGE HEATER
MIXING SCREENS
LINEAR DRIVE MOTOR
LINEAR POTENTIOMETER
POWER
TRIM H
MECHANICAL SEPARATOR
SECTION
SECTION
PHENOLIC SPACER
SECTION D-D
SECTION

(a) Detail D

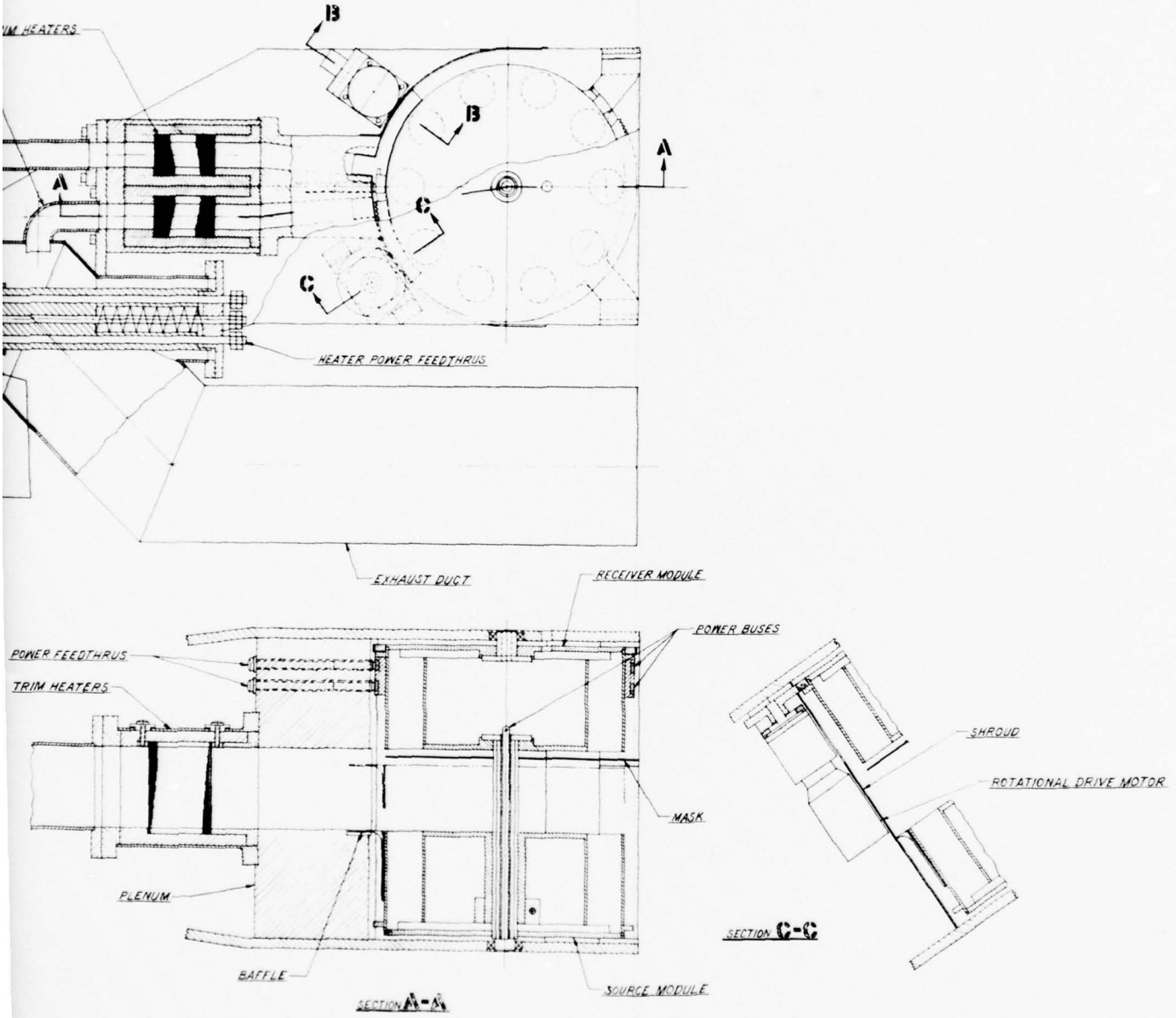

il Drawing

Figure 54. Improved Design

2

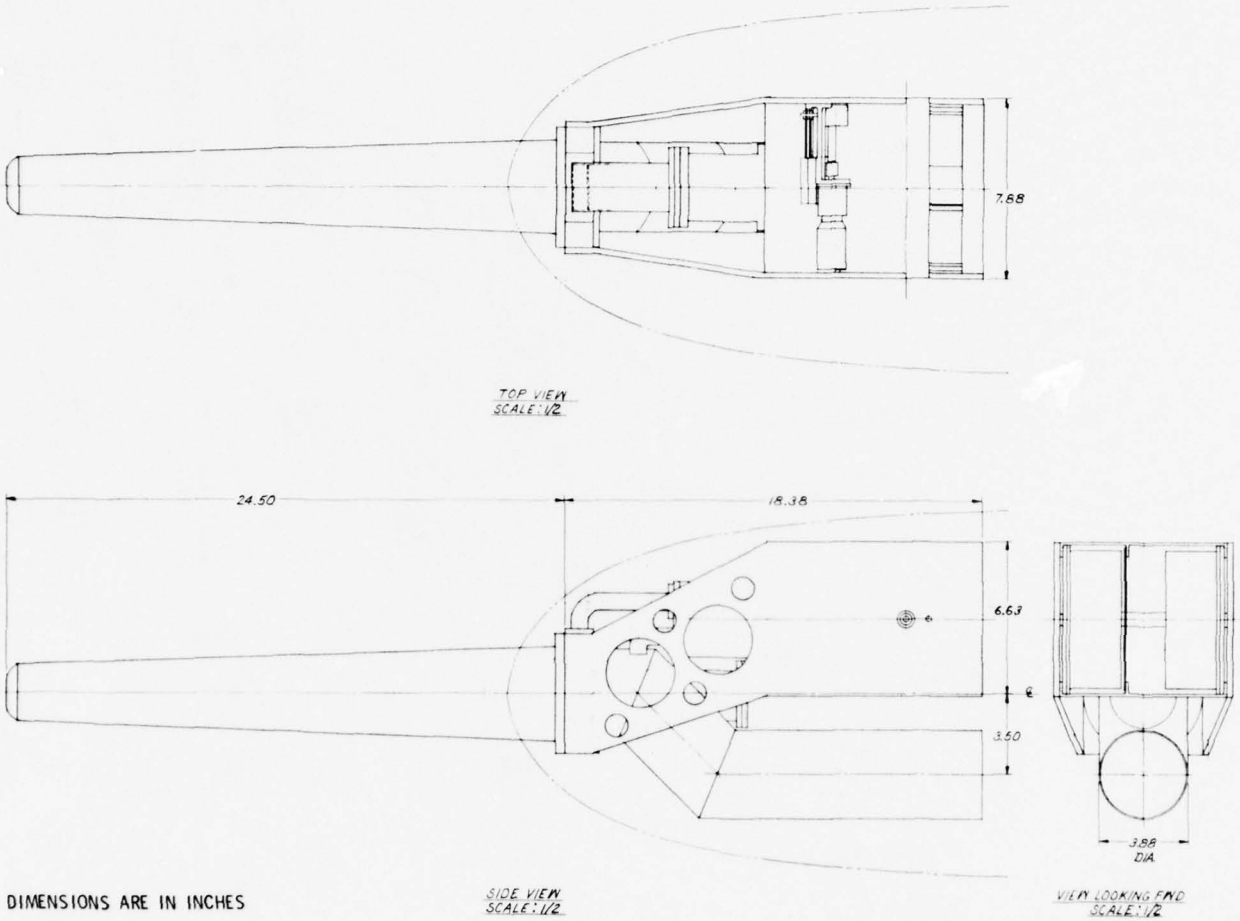

(b) Three-View Drawing

Figure 54. Improved Design (Continued)

VII. SUMMARY AND CONCLUSIONS

VII. SUMMARY AND CONCLUSIONS

An instrument has been developed for in-flight sampling of cloud condensate that has a sensitivity and size to measure water content down to a fraction of a gram per cubic meter. Supporting software/hardware has also been developed for the AFGL weather research aircraft to permit real-time readout of the data or recording and post-flight data reduction.

The results obtained in laboratory tests and a few flight tests indicate that the device can measure both liquid and solid condensate with a time response of the order of a second and an accuracy of perhaps 10%.

Some difficulty was experienced in "hardening" the instrument for aircraft operations, so several modifications would be in order should another unit be built. Additional flight testing is needed to compare EWER results with other data over a wide range of cloud conditions.

ABBREVIATIONS, ACRONYMS, AND SYMBOLS

ABRES	Advanced Ballistic Reentry Systems
AC	alternating current
ADC	analog-to-digital converter
AFGL	Air Force Geophysics Laboratory
DAC	digital-to-analog converter
EMI	electromagnetic interference
EWER	Evaporator of Water that Erodes on Reentry
FM	frequency modulation
IAS	indicated airspeed
ID	inside diameter
I/O	input/output
IRIG	inter-range instrumentation group
KMR	Kwajalein Missile Range
LED	light-emitting diode
LWC	liquid water content
MSV	Material Screening Vehicle
OD	outside diameter
PMS	Particle Measuring Systems (a company)
Triac	a solid-state electronic switch
TTL	transistor-transistor logic
UV	ultraviolet
VCO	voltage-controlled oscillator
VDC	volts direct current

APPENDIX A

APPENDIX A

FLOW EQUATIONS PERTINENT TO CALIBRATION

APPENDIX A
FLOW EQUATIONS PERTINENT TO CALIBRATION

Given

p_e = inlet static pressure

p_∞ = discharge pressure

D = sonic orifice dia

Determine

collection efficiency η versus flight parameters u_∞, p_∞.

In the facility (Figure A-1), all flow through the sonic orifice must pass through EWER so the pressure drop characteristics of the flow passages versus throughput can be determined. In flight, the flow entering the device will be analogous to that in the test rig under the same pressure differential (i.e., p_e to p_∞). It remains to be determined what flight conditions give this throughput and how much of the freestream flow is deflected around the device. The flow rate through the sonic orifice is

$$\dot{m} = \left(\frac{2}{\gamma + 1}\right)^{\frac{\gamma+1}{2(\gamma-1)}} \frac{p_o}{R T_o} a_o A^* \tag{1}$$

where subscript o is for laboratory conditions. Since all the flow must enter the inlet, the velocity at the entrance to the inlet of area A is

$$u_e = \frac{\dot{m}}{\rho_e A} \tag{2}$$

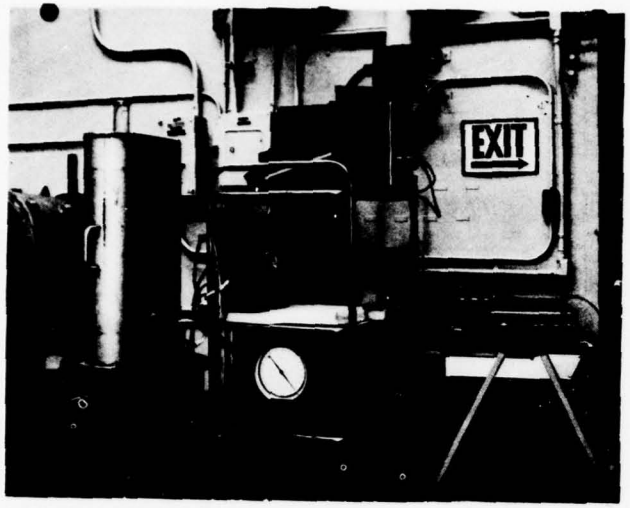

(a) Vertical Arrangement

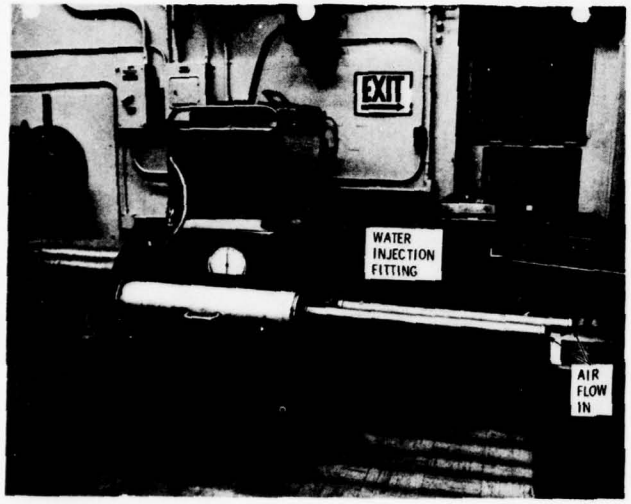

(b) Horizontal Arrangement

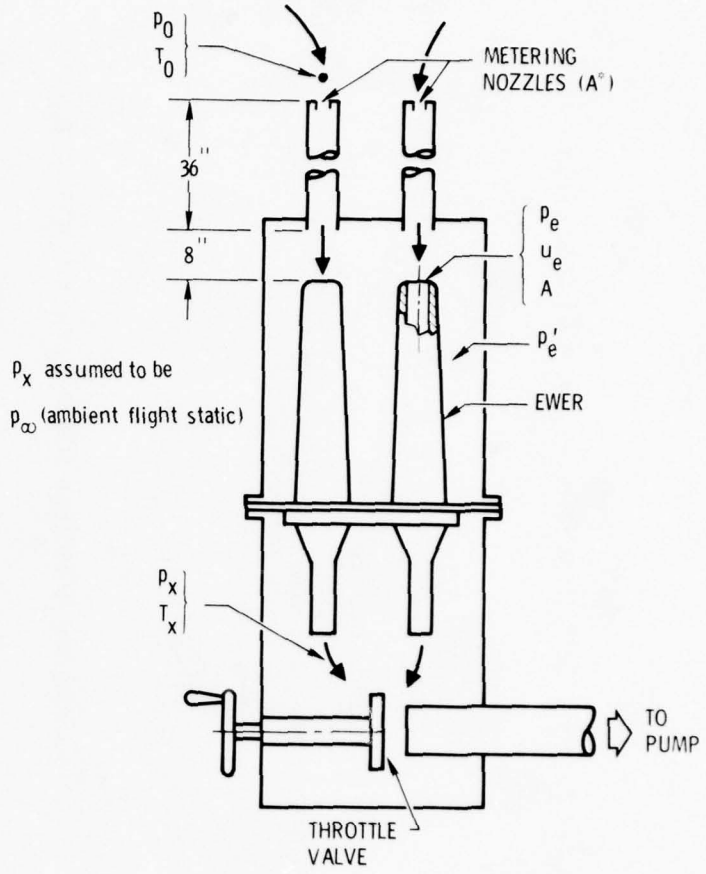

(c) Schematic

Figure A-1. Flow Calibration Facility

Because the flow from orifice to inlet involves shocks, the isentropic relations between stations "o" and "e" cannot be used. However, the process is adiabatic and, therefore, the total temperature is constant T_o. The density in the inlet can be determined from an adjusted stagnation pressure p'_o using the following isentropic relations:

$$\rho_e = \frac{p'_o}{RT_o}\left(\frac{p_e}{p'_o}\right)^{\frac{1}{\gamma}} \tag{3}$$

$$\left(\frac{p'_o}{p_e}\right)^{\frac{\gamma-1}{\gamma}} = \frac{1}{1 - \frac{\gamma - 1}{2}\left(\frac{u_e}{a_o}\right)^2} \tag{4}$$

Combining Eqs. (1), (2), and (3)

$$u_e = \left(\frac{2}{\gamma + 1}\right)^{\frac{\gamma+1}{2(\gamma-1)}} \frac{p_o}{RT_o}\, a_o A^* \Big/ \frac{p_e A}{RT_o}\left(\frac{p'_o}{p_e}\right)^{\frac{\gamma-1}{\gamma}} \tag{5}$$

For $\gamma = 7/5$, Eq. (5) simplifies to

$$u_e = \left(\frac{5}{6}\right)^3 a_o \frac{p_o A^*}{p_e A} \frac{1}{p_r} \tag{6}$$

where

$$p_r = \left(\frac{p'_o}{p_e}\right)^{\frac{\gamma-1}{\gamma}}$$

Substituting Eq. (6) in Eq. (4)

$$p_r = \frac{1}{1 - \frac{1}{5}\left(\frac{5}{6}\right)^6 \left(\frac{p_o A^*}{p_e A}\right)^2 \frac{1}{p_r^2}} \tag{7}$$

or

$$p_r^2 - p_r - \frac{1}{5}\left(\frac{5}{6}\right)^6 \left(\frac{p_e A^*}{p_e A}\right)^2 = 0 \tag{8}$$

Solving the quadratic of Eq. (8)

$$p_r = \frac{1}{2} + \left[\frac{1}{4} + \frac{1}{5}\left(\frac{5}{6}\right)^6 \left(\frac{p_o A^*}{p_e A}\right)^2\right]^{\frac{1}{2}} \tag{9}$$

Since all parameters in the right-hand member of Eq. (9) are known, the value of p_r can be determined and used in Eq. (5) to calculate the velocity of the flow in the entrance to the inlet.

If one assumes that the discharge pressure is the freestream pressure in flight p_∞, a flight velocity can be determined with the compressible Bernoulli equation

$$u_\infty = \left\{u_e^2 + \frac{2a_\infty^2}{\gamma - 1}\left[\left(\frac{p_e}{p_\infty}\right)^{\frac{\gamma - 1}{\gamma}} - 1\right]\right\}^{\frac{1}{2}} \tag{10}$$

The collection efficiency is defined as the ratio of mass flow in the inlet of the device to that through an equivalent area in the freestream.

$$\eta = \frac{\rho_e u_e}{\rho_\infty u_\infty} \tag{11}$$

Since the compression of the flow in front of the probe inlet is isentropic, the density changes can be related with the expression

$$\frac{\rho_e}{\rho_\infty} = \left(\frac{p_e}{p_\infty}\right)^{\frac{1}{\gamma}} \tag{12}$$

or

$$\eta = \left(\frac{p_e}{p_\infty}\right)^{\frac{1}{\gamma}} \frac{u_e}{u_\infty} \tag{13}$$

The parameters of Eq. (13) are measured or calculated during calibration in the test rig. Therefore, a plot or η versus flight conditions in a standard atmosphere (i.e., u_∞, altitude) should be possible.

APPENDIX B

APPENDIX B

COLLECTION EFFICIENCY FOR PARTICLES

APPENDIX B
COLLECTION EFFICIENCY FOR PARTICLES

Walter F. Reddall III

1. SUMMARY

Trajectories of spherical particles of radii 10 μm and 50 μm have been calculated from initial positions well upstream of the proposed LWC meter, in the disturbed flow field produced by the device when moving 300 ft/sec at 20,000 ft altitude. The flow field was obtained using the Lockheed Godunov code for two different conditions of inlet internal backpressure, $p/p_o = 0.998$ and 0.980, which correspond to internal velocities of approximately 56 and 180 ft/sec, respectively (p_o is the freestream stagnation pressure). In the first flow field the particle number-flux at the inlet plane of the device is reduced about 30% below freestream levels for the 10 μm particles and about 4% for the 50 μm particles, while number-density is increased about 15% and 2% for the two sizes. The second flow field, which is less like a stagnating flow, produces a 15% decrease in number-flux and a 5% increase in number-density for the 10 μm particles, while the 50 μm particle flux distortions are less than a percent, which is probably less than the errors involved in the calculation. Thus, it can be concluded that, to the extent the liquid water content in the freestream is predominantly contained in drops of radius 50 μm or larger, the meter readings should not be significantly altered by flow-field effects. These calculations do not account for any aircraft-induced flow-field effects such as those produced by propellers.

2. FLOW-FIELD CALCULATION

The aerodynamic flow was found approximately using the in-house version of Lockheed's time-dependent Godunov code, adapted for axisymmetric flow by J. Murdock. The region of solution and inlet geometry are shown in Figure B-1. Tick marks indicate the cell spacing, which is finest near the

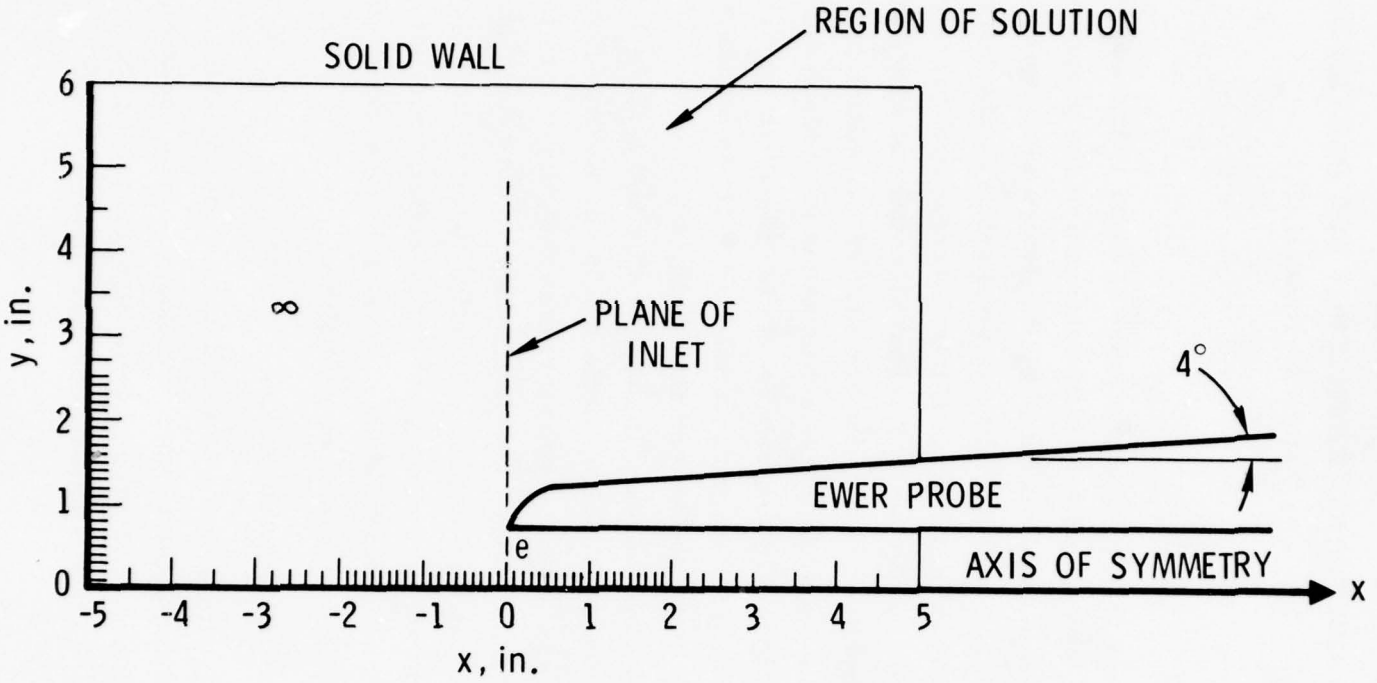

Figure B-1. Flow-Field Setup for Gudunov Code

axis-of-symmetry and near the inlet. The cells that comprise the upstream and downstream boundaries of the region are assigned fixed gas properties: upstream cells were held at

$$u_\infty = 300 \text{ ft/sec}$$

$$p_\infty = 973 \text{ lb}_f/\text{ft}^2$$

$$\rho_\infty = 1.27 \times 10^{-3}, \text{ slug/ft}^3$$

while two pressure levels in the downstream cells inside the inlet were chosen arbitrarily, using the one-dimensional compressible Bernoulli equation to obtain the corresponding velocity

$$u_e = \left\{ \frac{2\gamma}{\gamma - 1} \frac{p_o}{\rho_o} \left[1 - \left(\frac{p_e}{p_o} \right)^{\frac{\gamma-1}{\gamma}} \right] \right\}^{1/2}$$

For the two cases run, the values of backpressure and exit velocity for $\gamma = 7/5$ were as follows:

p_e/p_o	$p_e[\text{lb}_f/\text{ft}^2]$	$u_e[\text{ft/sec}]$	$\rho_e[\text{slug/ft}^3]$
0.998	1030	56	1.32×10^{-3}
0.980	1011	177	1.30×10^{-3}

Properties in the downstream boundary cells outside the body were adjusted from freestream levels to conform to the requirements for conservation of mass, momentum, and energy in the average one-dimensional sense, given the blockage caused by the body and its internal flow. The outer boundary cells correspond to a solid wall parallel to the axis-of-symmetry, and far removed from it relative to the body radius.

All interior cells were set to freestream values and the program was then run to convergence. The resulting velocity vector flow field for the case of the nearly stagnating flow ($p_e/p_o = 0.998$) is shown in Figure B-2.

3. TRAJECTORY CALCULATIONS

The particles were assumed to be solid spheres with the density of water, 1.939 slug/ft^3, and with variable drag coefficient depending on Reynolds number based on diameter

$$C_D = \begin{cases} \frac{24}{Re}\left[1 + 0.15\, Re^{0.687}\right] & Re \leq 1000 \\ 1.0 & Re > 1000 \end{cases}$$

In each of the two flow fields computed, 15 trajectories were constructed for each particle size, starting from initial positions at the upstream boundary of the flow field and displaced from the axis-of-symmetry by $y_o/Y = 0.1, 0.2, \ldots 1.5$, where Y (= 0.719 inch) is the internal radius of the inlet.

A continuum of particles was assumed for number-flux and number-density (N) calculations, and it was assumed that trajectories do not cross upstream of the inlet. Then if ΔA is the area of the resulting particle flux tube between adjacent trajectories, cut by a plane normal to the axis-of-symmetry, conservation of particles at two different stations gives

$$[N(\vec{V} \cdot \vec{n})\Delta A]_{\text{Station 1}} = [N(\vec{V} \cdot \vec{n})\Delta A]_{\text{Station 2}}$$

So the ratio of particle number-flux (number crossing a unit area per unit time) at the plane of the inlet to that far upstream is the ratio of the flux tube areas

$$\frac{(N\,u)_{\text{nose}}}{(N\,u)_\infty} = \frac{\Delta A_\infty}{\Delta A\ \text{nose}}$$

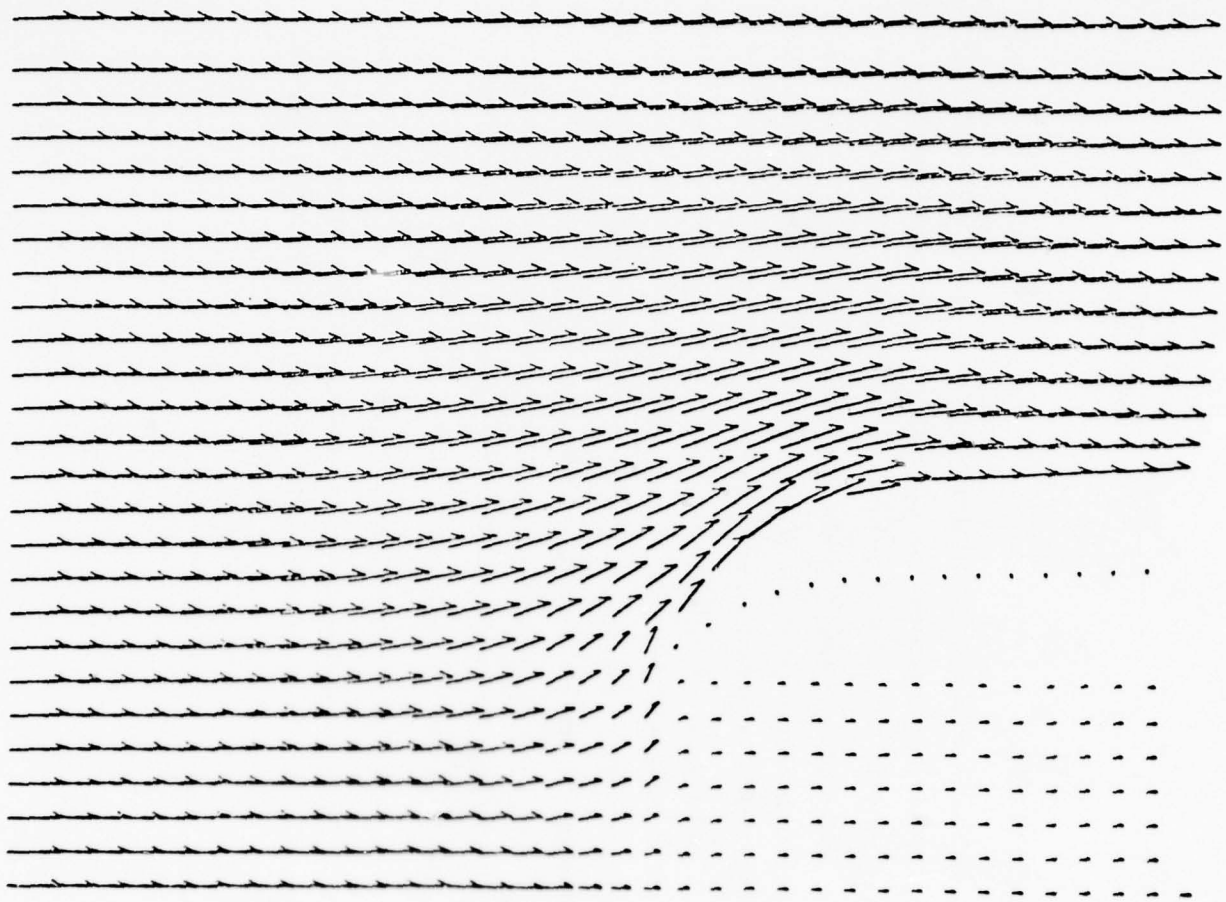

Figure B-2. Blowup of Inlet Region Velocity Vector Plot (p_e/p_o = 0.998)

and the number-density ratio is found by dividing by the ratio of velocity components in the x-direction

$$\frac{N_{nose}}{N_{\infty}} = \frac{(u\Delta A)_{\infty}}{(u\Delta A)_{nose}}$$

4. RESULTS

The number-flux at the inlet plane is reduced because trajectories spread as they approach the nose. However the particles slow down more than they spread laterally, so the number-density increases over freestream levels. Figures B-3 and B-4 show the effect of the more strongly disturbed flow on two different particle sizes, 10 μm and 50 μm. The effect on the 10 μm particles is pronounced, producing an increase of about 15% in number-density, but the effect of the flow on 50 μm particles is negligible (about 2%). The flow field produced with an inlet backpressure of 0.980 is less disturbed, and, consequently, the increase in number-density of 10 μm is only about 5%, as shown in Figure B-5. The trajectories of 50 μm particles are hardly disturbed beyond the estimated error bounds of the integration procedure, and hence distortions are so negligible they are not plotted. Of course, larger drops would be even less affected by the flow field.

It can thus be concluded that, to the extent the liquid water content in the freestream is contained in drops of radius 50 μm or larger, the meter readings should not be significantly altered by flow-field effects.

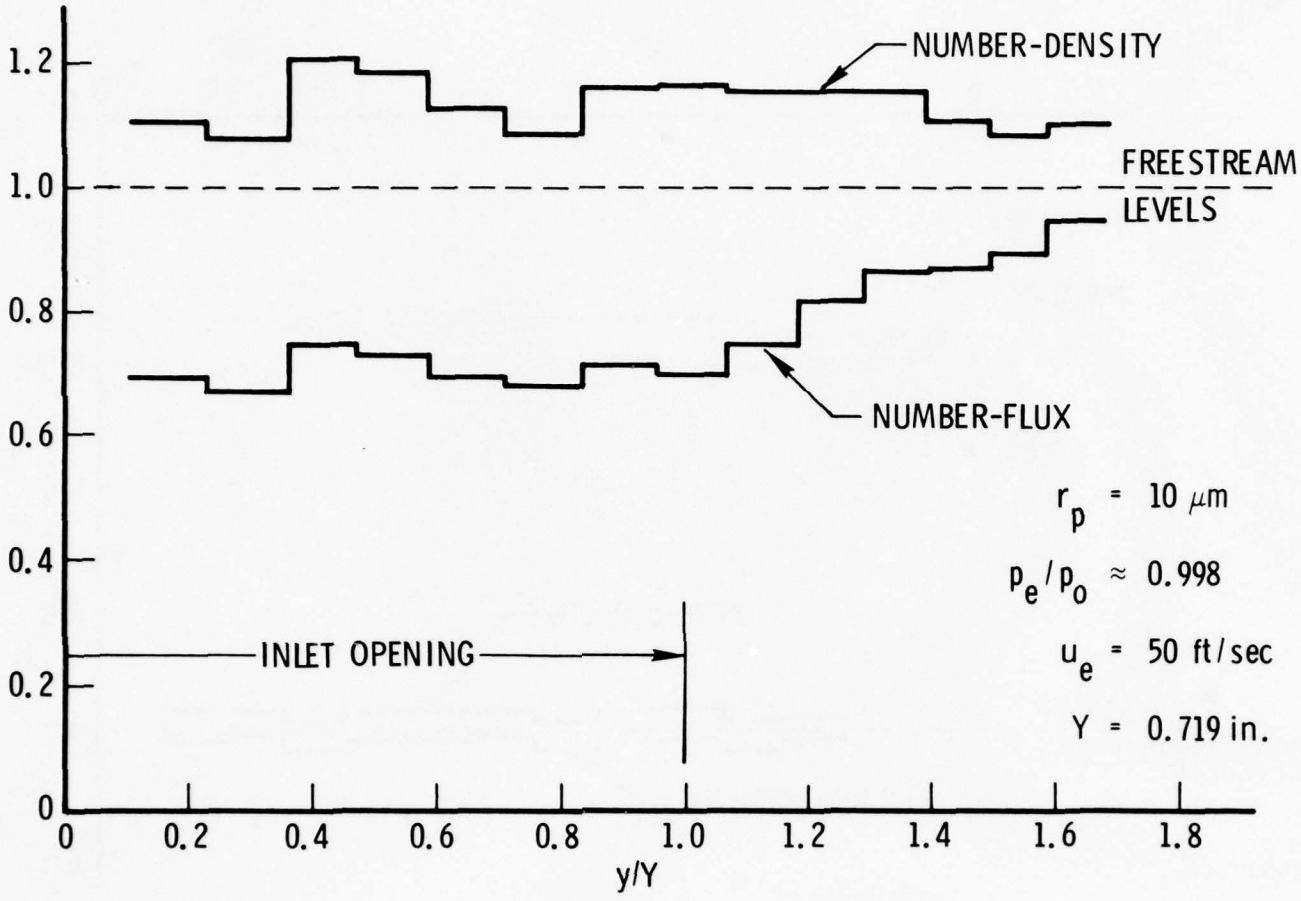

Figure B-3. Particle Number-Density and Flux Distortion at Inlet Plane

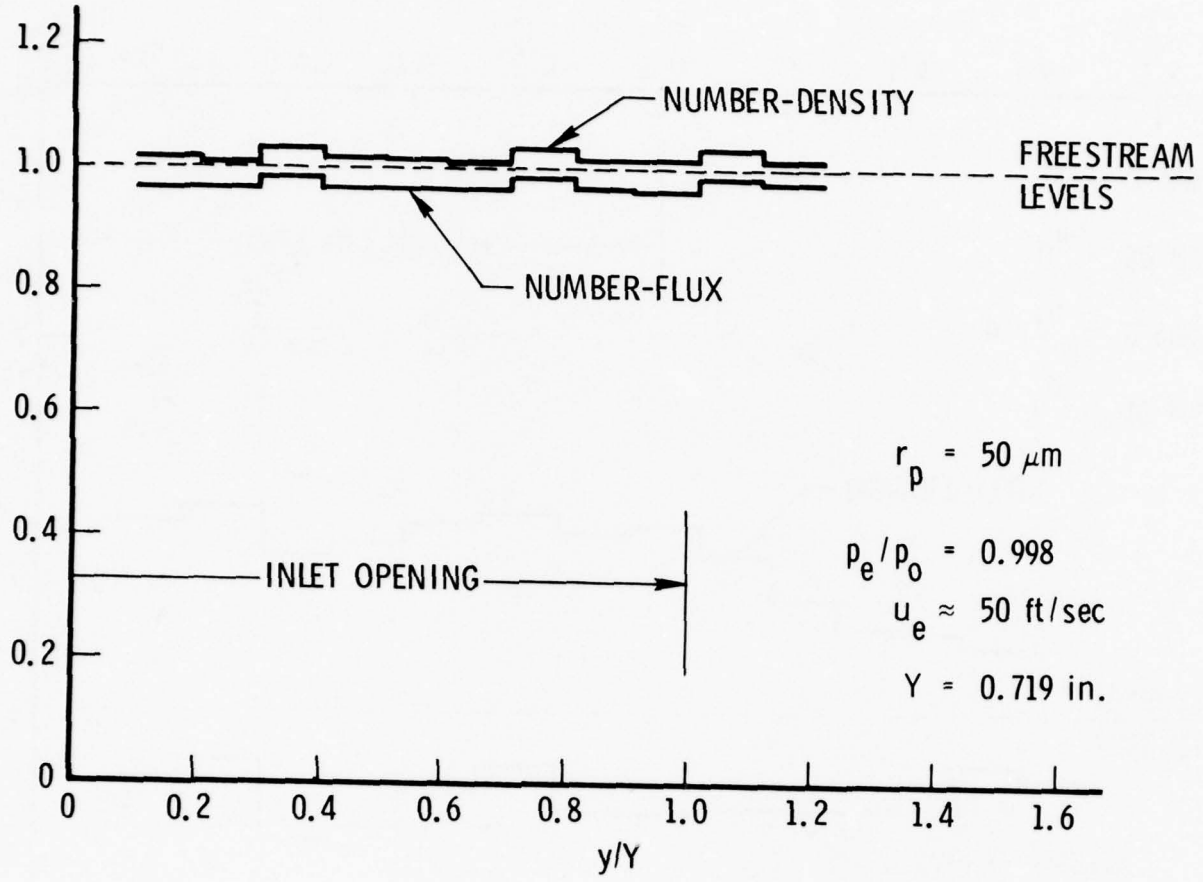

Figure B-4. Particle Number-Density and Flux Distortion at Inlet Plane

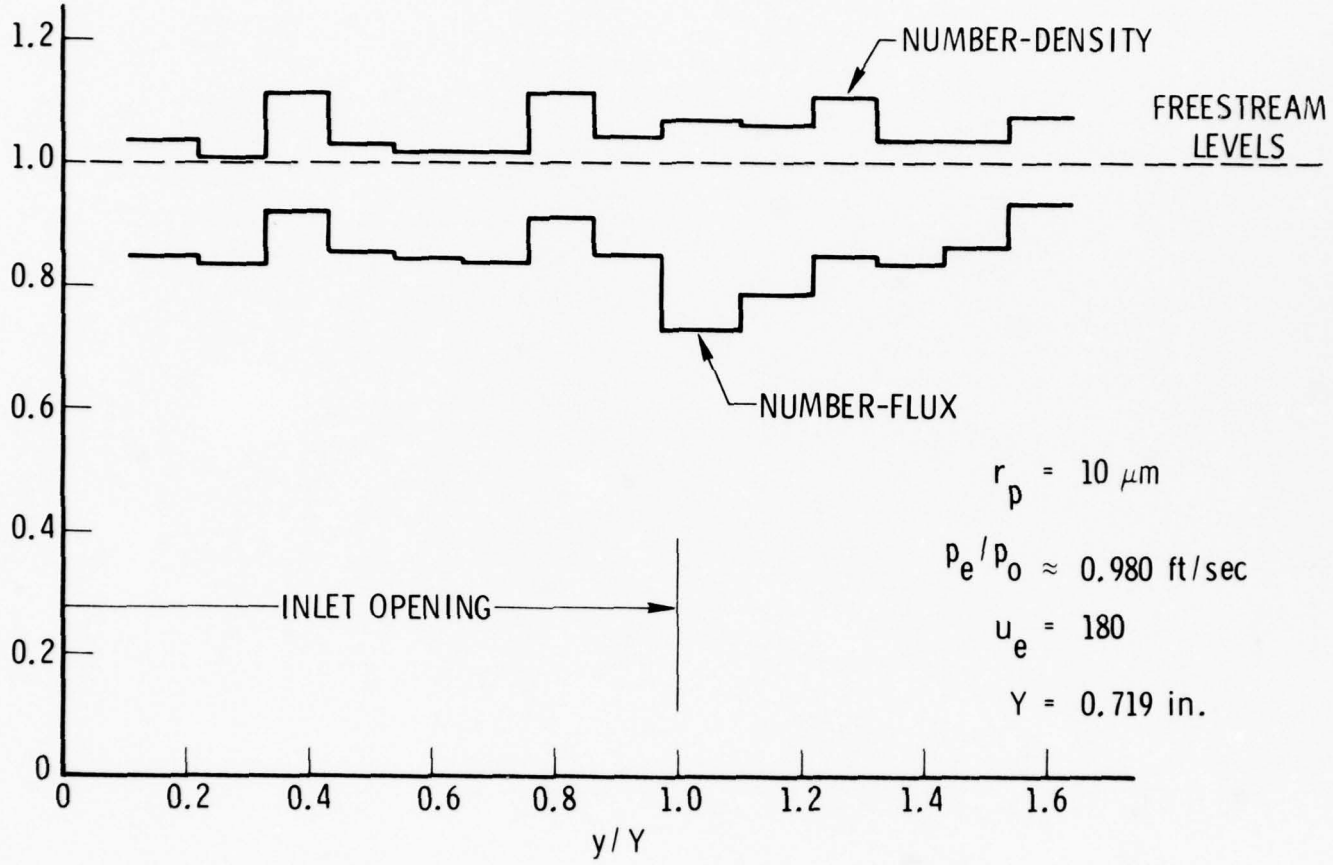

Figure B-5. Particle Number-Density and Flux Distortion at Inlet Plane

APPENDIX C

APPENDIX C

EWER VIBRATION TESTS

APPENDIX C
EWER VIBRATION TESTS

1. PHASE 1 (Aeronutronic-Ford, 24-30 September 1975)

The EWER systems to be mounted in the LH pod of C130E #571 were vibrated in accordance with the schedule shown as Table C-1. During the random excitation phase of the schedule (input on the vertical axis) it was apparent that the environment was much too severe. The test was terminated with many EWER functions not working, (see Table C-2). An attempt was made to revive these functions for a more mild test. However, it was only possible in the time available to perform the resonance search in the other two axes.

Data for all of these tests are shown in the attached figures. The figure numbers are coded as follows:

Input axis	Vertical	Lateral	Longitudinal
Resonance searches			
Control	1-1	2-1	3-1
Front fixture	1-2	2-2	3-2
Rear fixture	1-3	2-3	3-3
Side fixture	1-4	2-4	3-4
Condensate tube	1-5	2-5	3-5
Vapor tube	1-6	2-6	3-6
Circuit board	1-7	-	-
Driver box, x	1-8	-	-
Driver box, y	1-9	-	-
Driver box, z	1-10	2-8	3-8
N_2 heater	1-11	2-11	3-11
Sine sweep			
Control	4-1		
Random excitation			
Control	5-1		
Condensate tube	5-5		
Driver box	5-8		
N_2 heater	5-11		

Table C-1. Vibration Test of EWER

The EWER system is to be vibrated while it is operating in accordance with the following criteria:

1. Position probe assembly on shaker so that unit center of gravity is on-axis and mount is rigid in vertical direction of vibration.
2. Install electronics box on mount above or below probe assembly (within 4 ft).
3. Locate vibration response sensors on inlet of evaporator probe, detector assembly, and electronic box to measure acceleration at these points.
4. Connect 115 V, 400 Hz, 5 kW power, and 5 g/sec at 100 psig N_2 sources to mounting face of box. Also connect cable (10 ft) from control panel to box. Supply 28 VDC, 5 amp to control panel.
5. Blow air into probe assembly (2 inlets) at a rate of 200 to 300 standard cubic ft/min (backpressure approximately 40 Torr).
6. Make sine-scan at 0.5 g to look for resonances.
7. Vibrate with sinusoidal input according to Figure C-1 with 60 sec sweep.
8. Vibrate with random noise input, according to Figure C-1, ±3 dB (-1.5 dB, 20 to 500 Hz) for 1 hr.
9. Repeat for lateral and longitudinal axes.

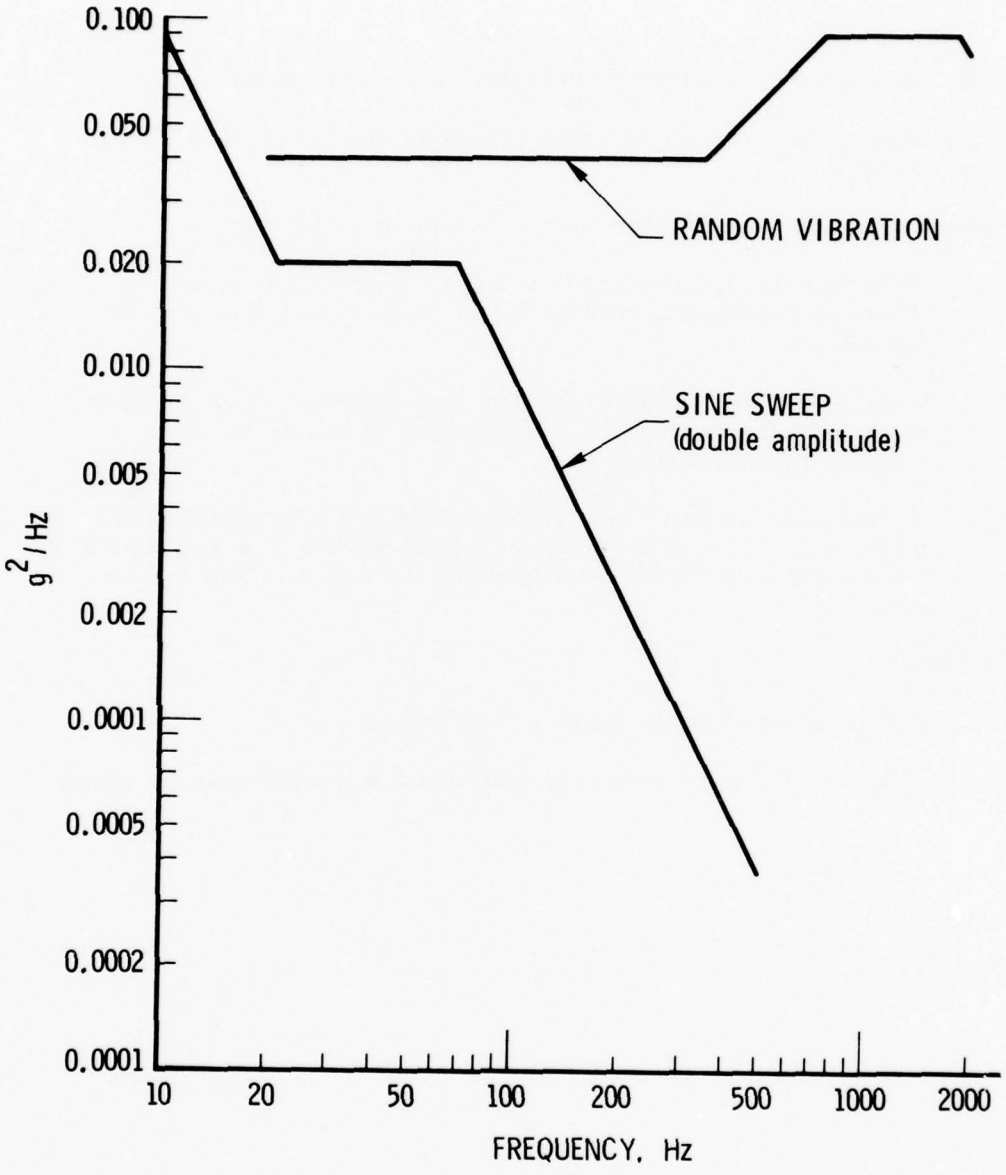

Figure C-1. Vibration Criteria

Table C-2. EWER Vibration Results

O.K. through 0.5 g sine sweep (total time, ~10 min).

O.K. through the Air Force Special Weapons Center (AFSWC) sine sweep.

Failed in random excitation mode - stopped in 17 min.

1. Detector dead, no signal on LED. Appears that unit is drawing excess current (voltage down to ~40 V). Synch LED O.K.

2. Only vapor and A phase heater operational. Both trigger boards badly damaged - TC boards appear to be O.K. Inlet heaters shorted.

3. Two 5 amp circuit breakers open (B and C phases). Set screws on all shafts loose. Limit-switches on gap inactive, wide. Broken wire, microswitch damaged. Gap pot no good.

Pending:

1. Relay on condensate heater may be out.

2. Pulse transformer on B phase of main heater may be open.

SUMMARY/CONCLUSION

The EWER probe assembly and electronics box were vibrated to determine the resonances in certain components. The unit was operated during a sine sweep (vertical) through a vibration environment suggested by AFSWC as "typical" for the C130. All systems were operating after this 3 minute test. In a subsequent endurance test with random excitation at levels estimated from MIL STD 810C, the unit was inoperative after a few minutes. Significant damage was sustained.

The EWER is probably adequate for the C130 environment, but with small safety factor. It should be treated as a scientific instrument, not as an aircraft accessory.

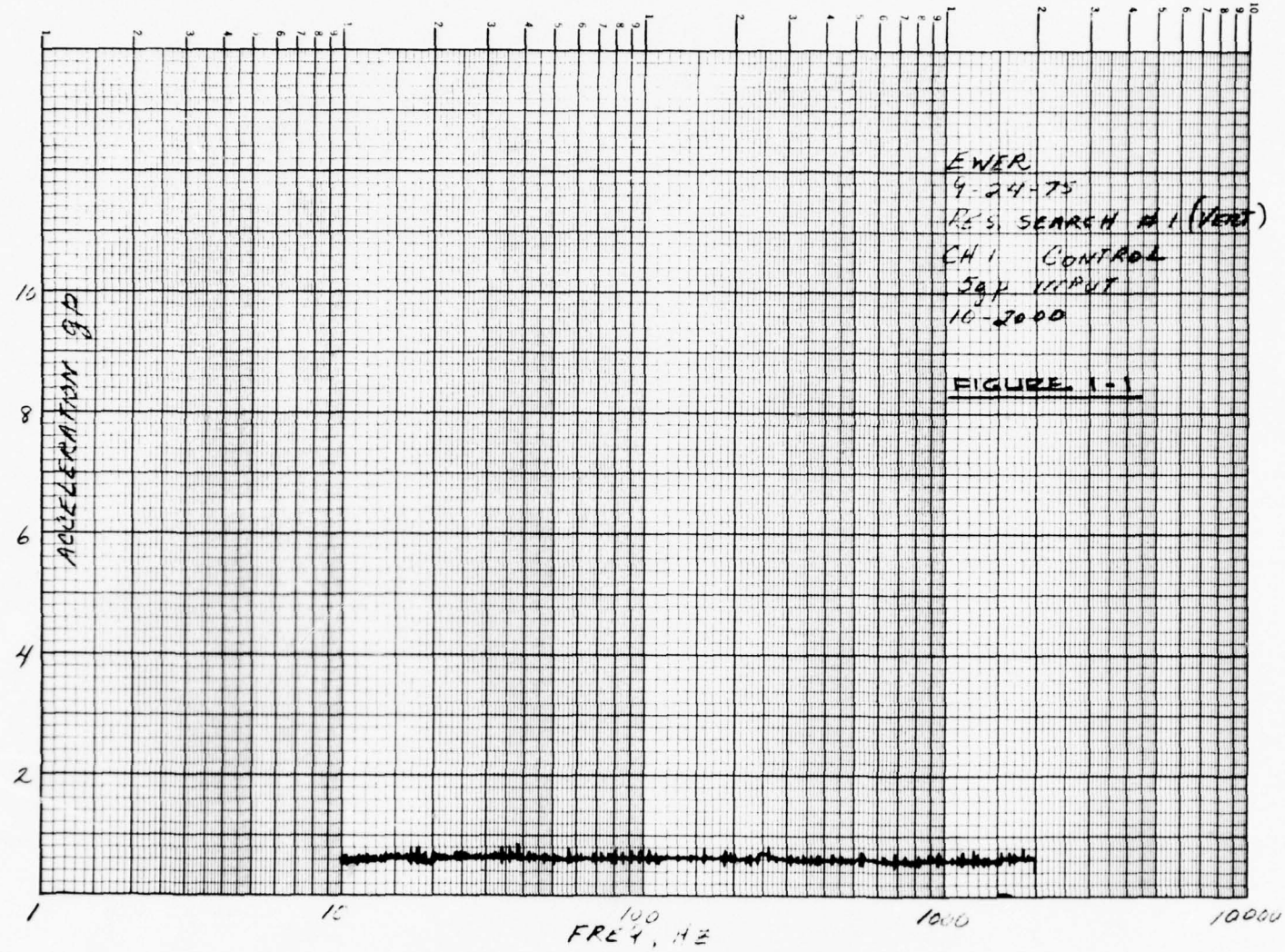
EWER
4-24-75
R.S. SEARCH #1 (VERT)
CH 1 CONTROL
5g p INPUT
16-2000
FIGURE 1-1
ACCELERATION g'D
10
8
6
4
2
1
10
100
1000
10000
FREQ, HZ

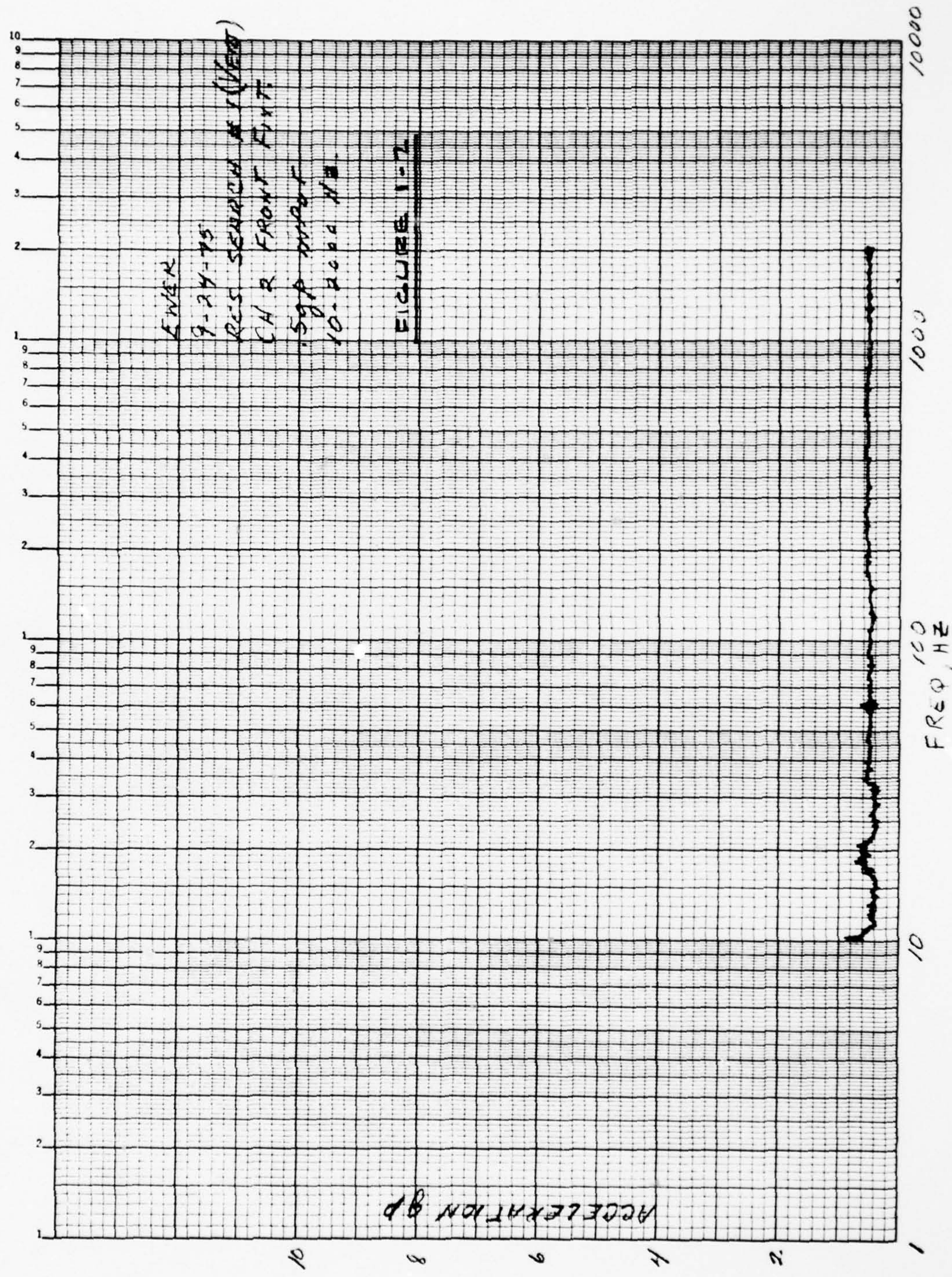
EWER
9-24-75
RES SEARCH #1 (VERT)
CH 2 FRONT FIXT.
FIGURE 1-2
FREQ, HZ
ACCELERATION g

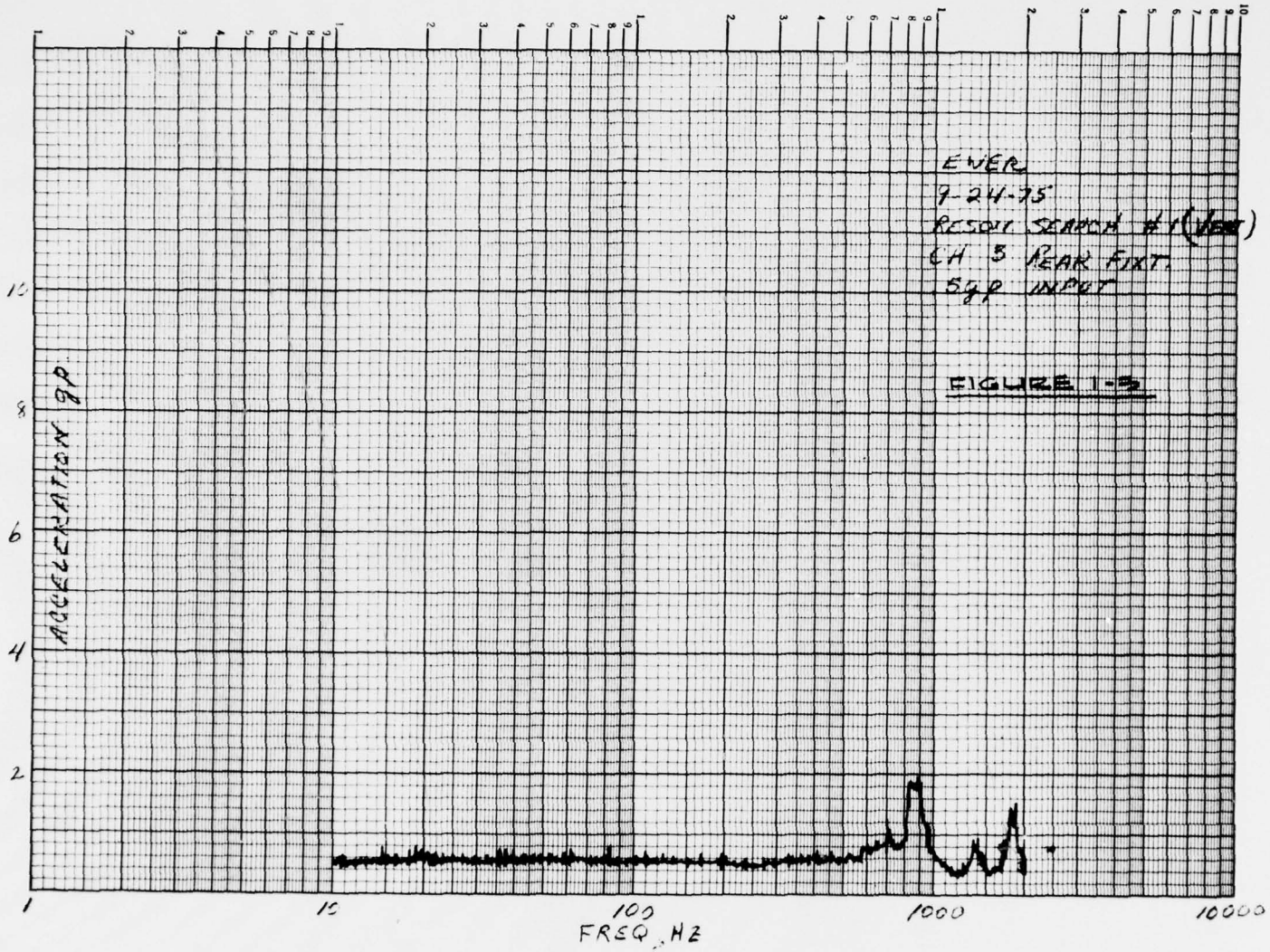
EVER
7-24-75
RESON SEARCH #1 (VERT)
CH 3 PEAK FIXT.
SYP INPUT
ACCELERATION GP
10
8
6
4
2
1
10
100
1000
10000
FREQ. HZ

FIGURE 1-3

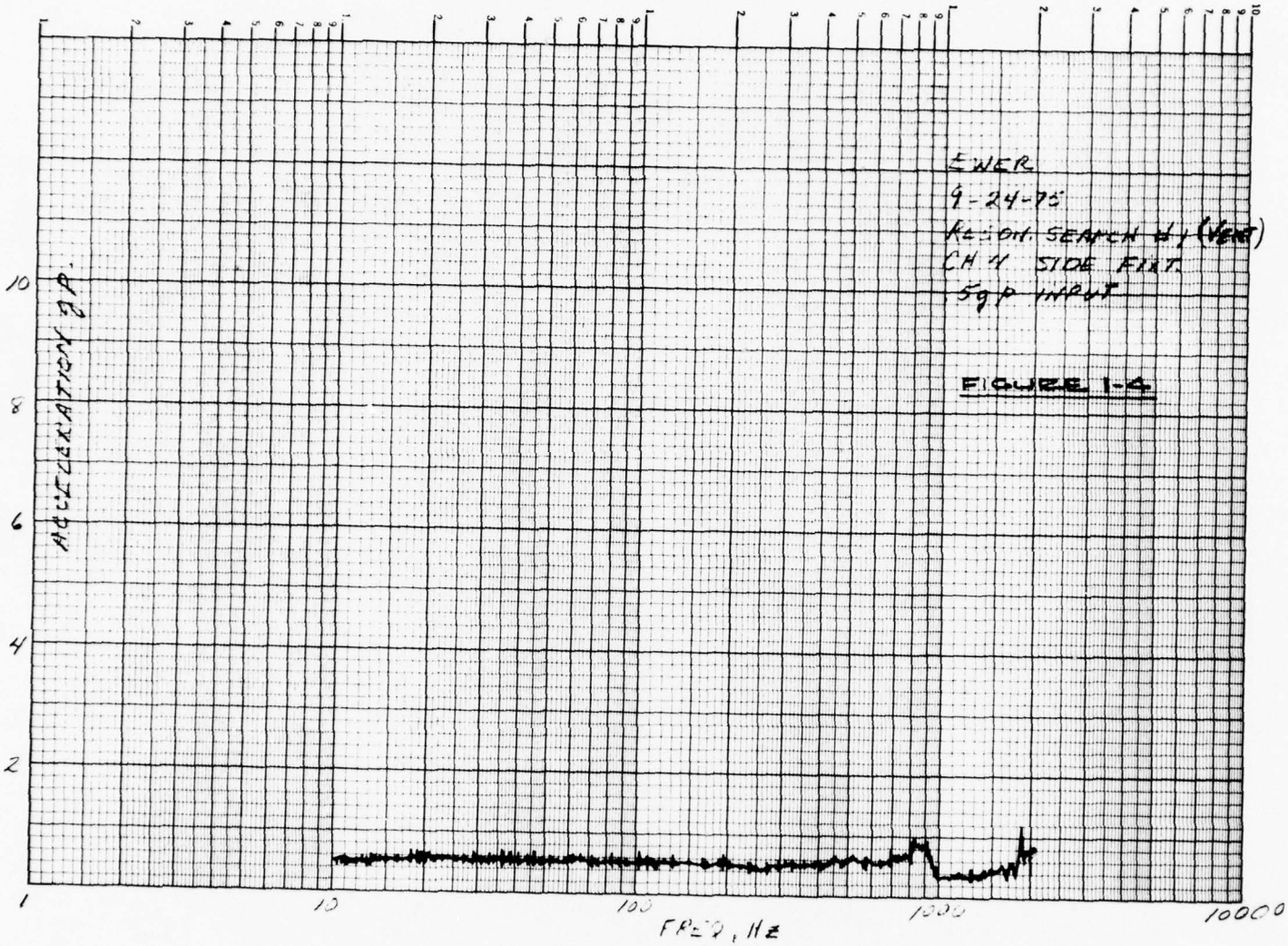
EWER
9-24-75
Random SEARCH dy (VERT)
CH 4 SIDE FIXT.
.5g p INPUT
FIGURE 1-4
ACCELERATION g p.
10
8
6
4
2
1
10
100
1000
10000
FREQ, Hz

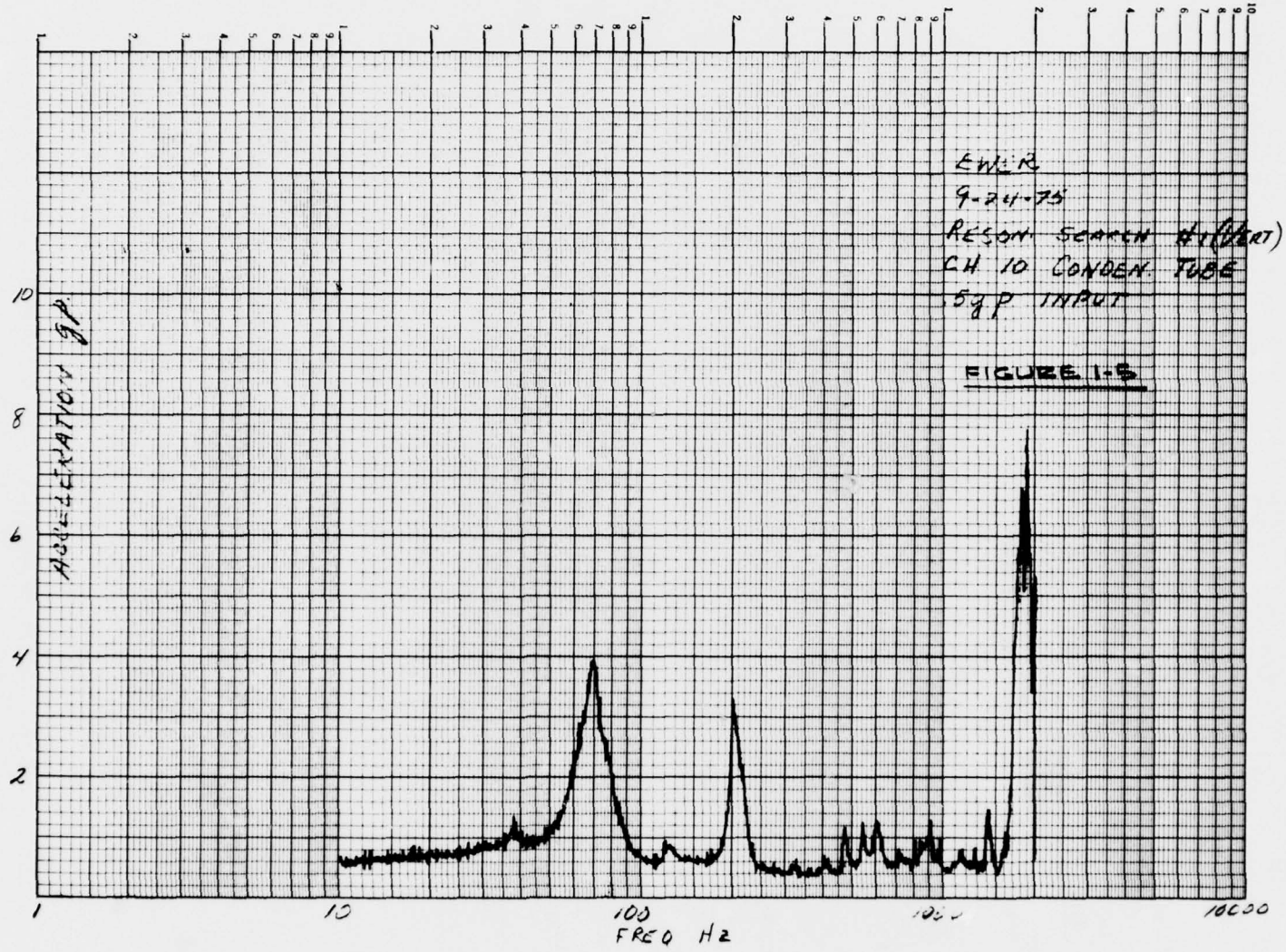
ENIR
9-24-75
RESON. SEARCH #1(CURT)
CH 10 CONDEN. TUBE
.5g P INPUT
FIGURE I-5
ACCELERATION g's
10
8
6
4
2
1
10
100
FREQ Hz
10000

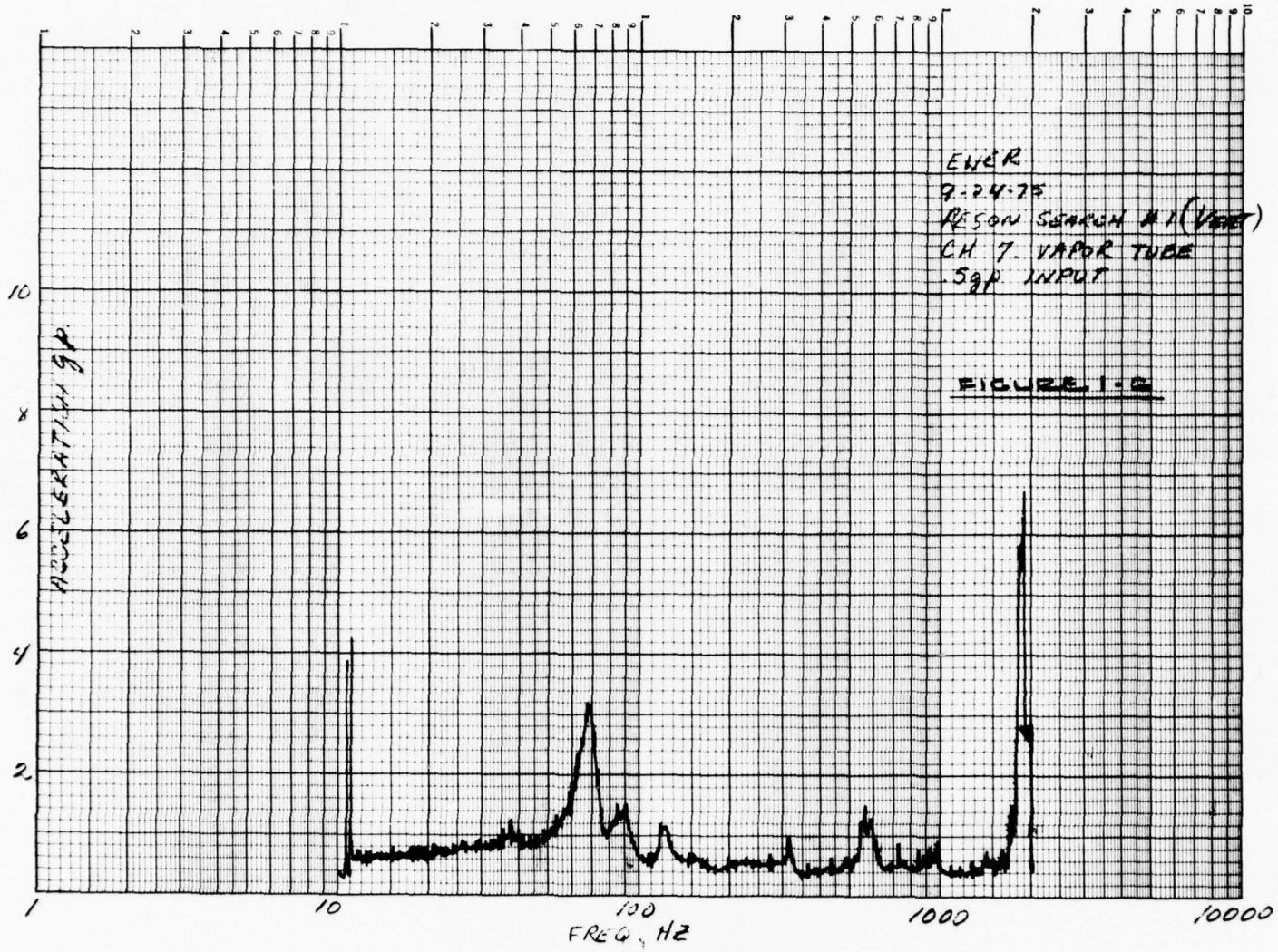
EWER
9-24-75
RESON SEARCH #1 (VERT)
CH 7. VAPOR TUBE
.5gp INPUT
FIGURE I-C
ACCELERATION gp
10
8
6
4
2
1
10
100
1000
10000
FREQ., HZ

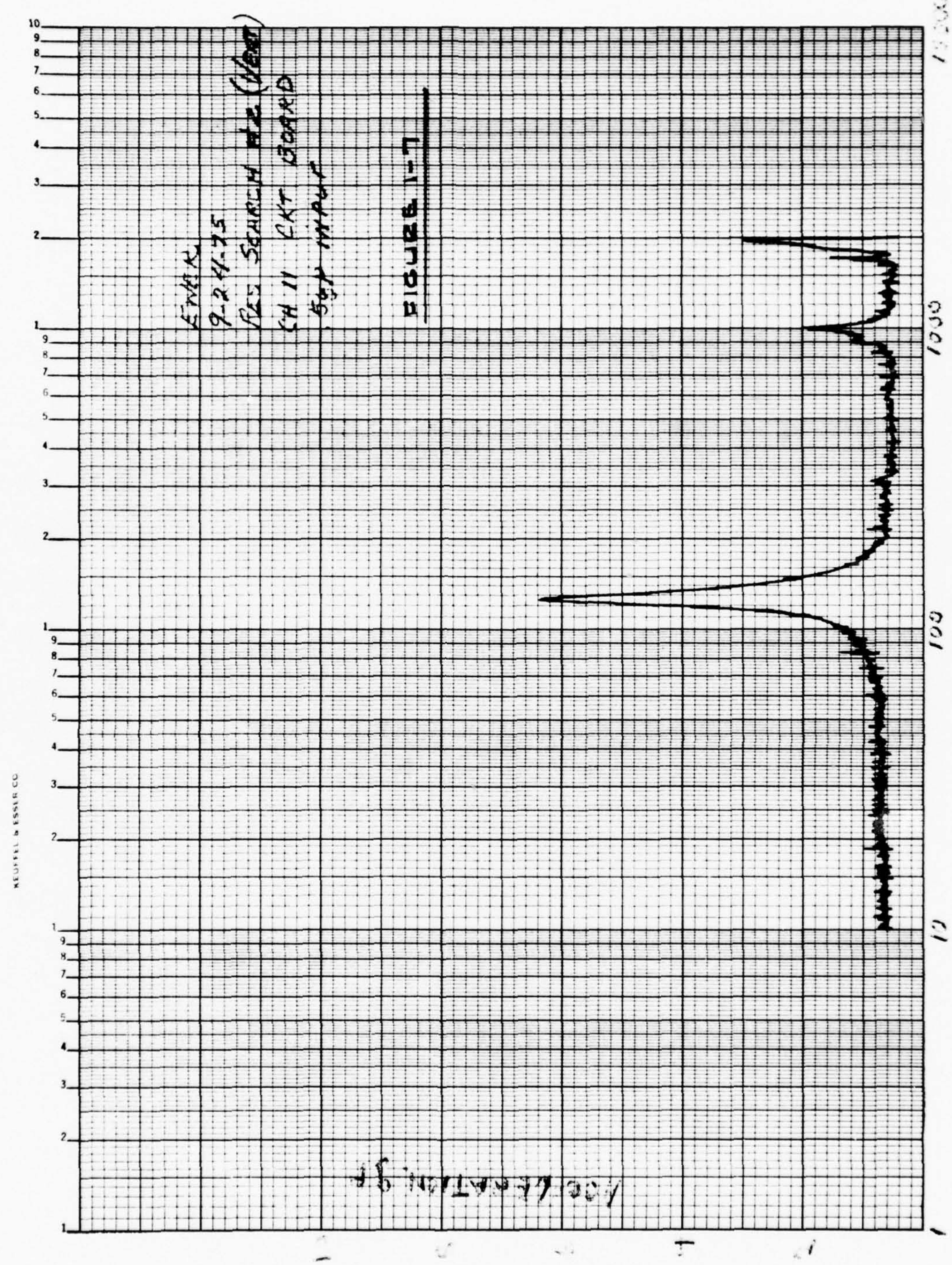
FIGURE 1-7
CH 11 CKT BOARD
1000
100
10

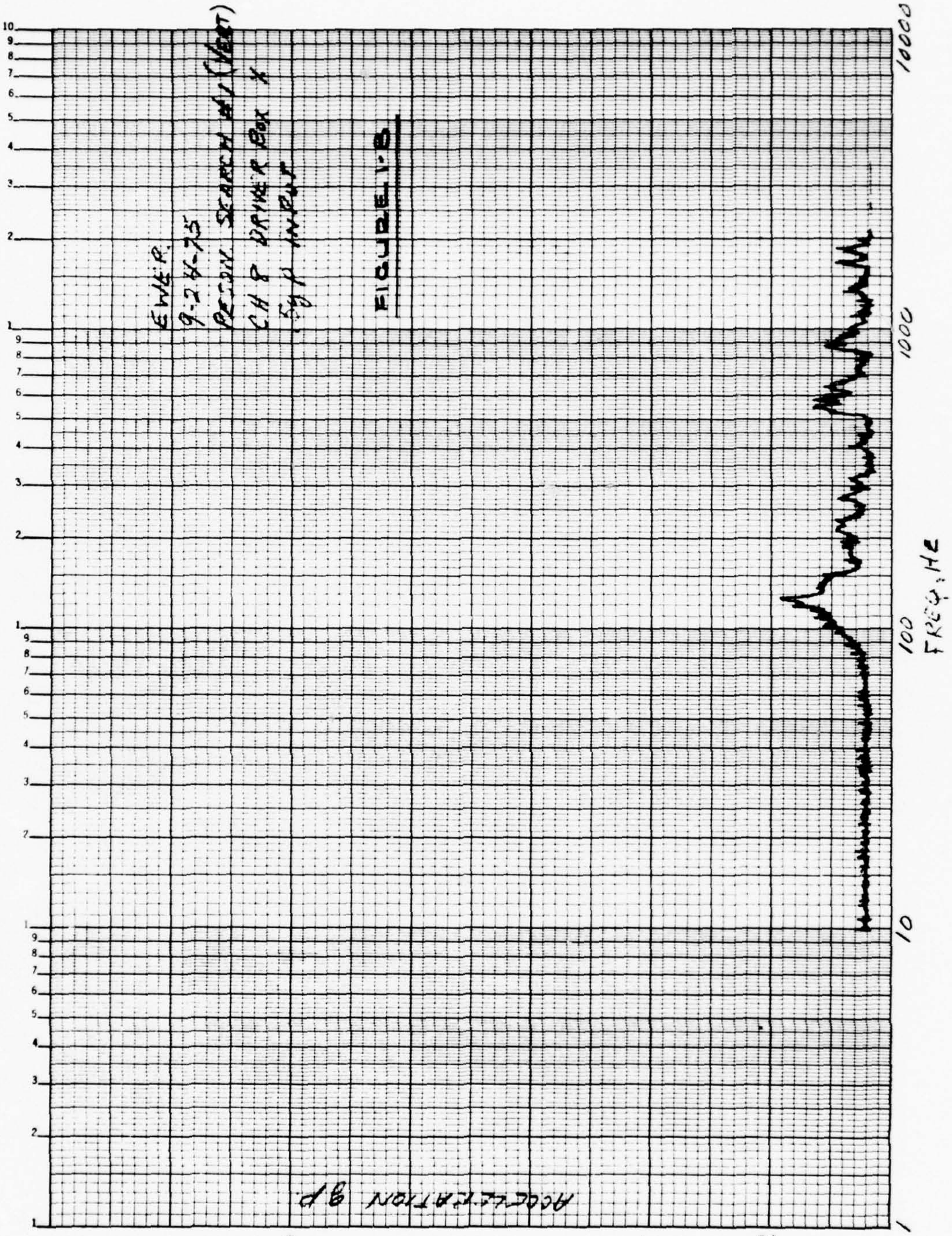
FIGURE 1-8
FREQ, HZ
1
10
100
1000
10000
2
4
6
8
10

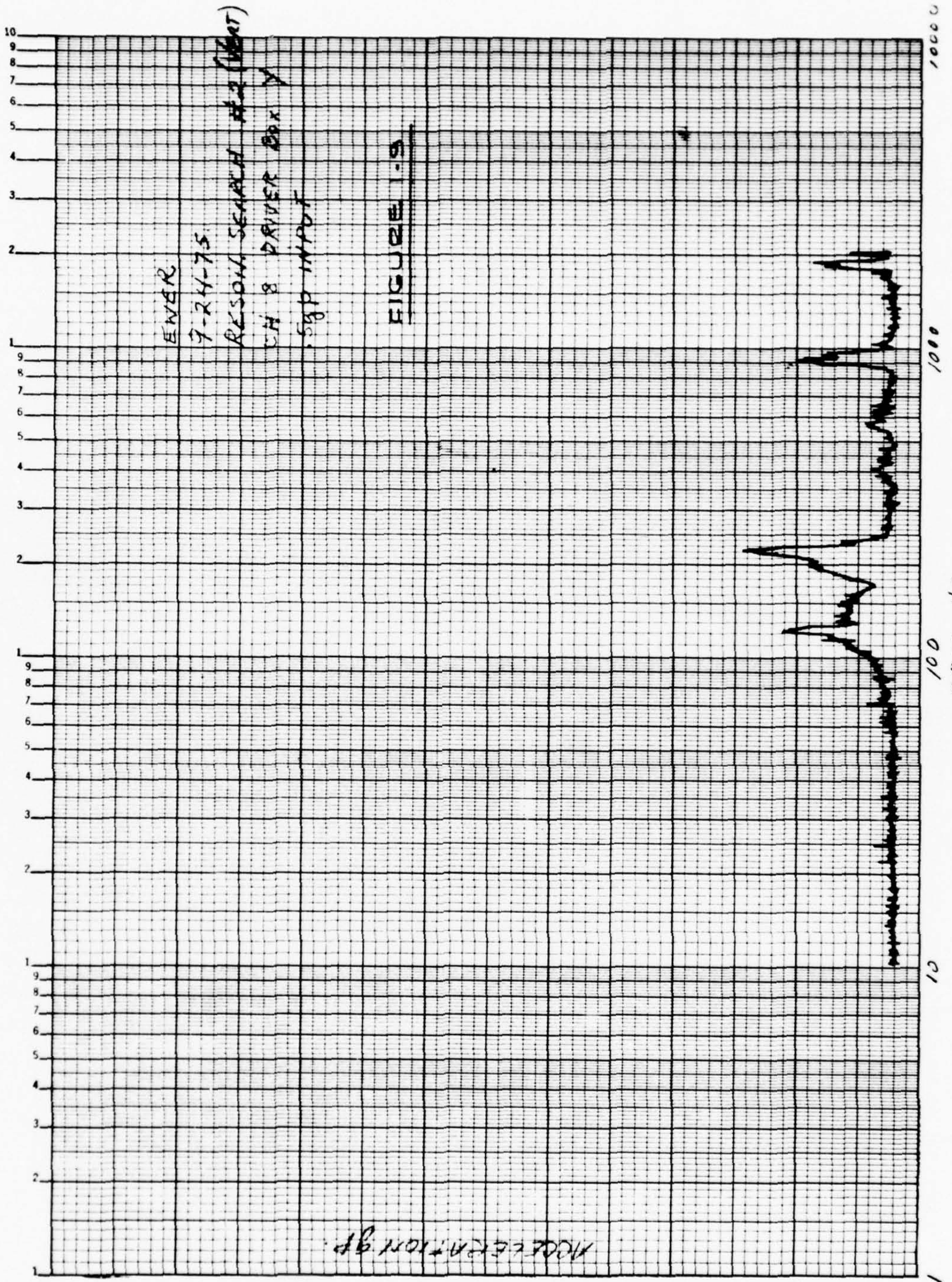
EWER
7-24-75
RESON. SEARCH #2 (VERT)
CH 8 DRIVER BOX Y
.5gP INPUT
FIGURE I-9
FREQ., Hz
ACCELERATION, gP

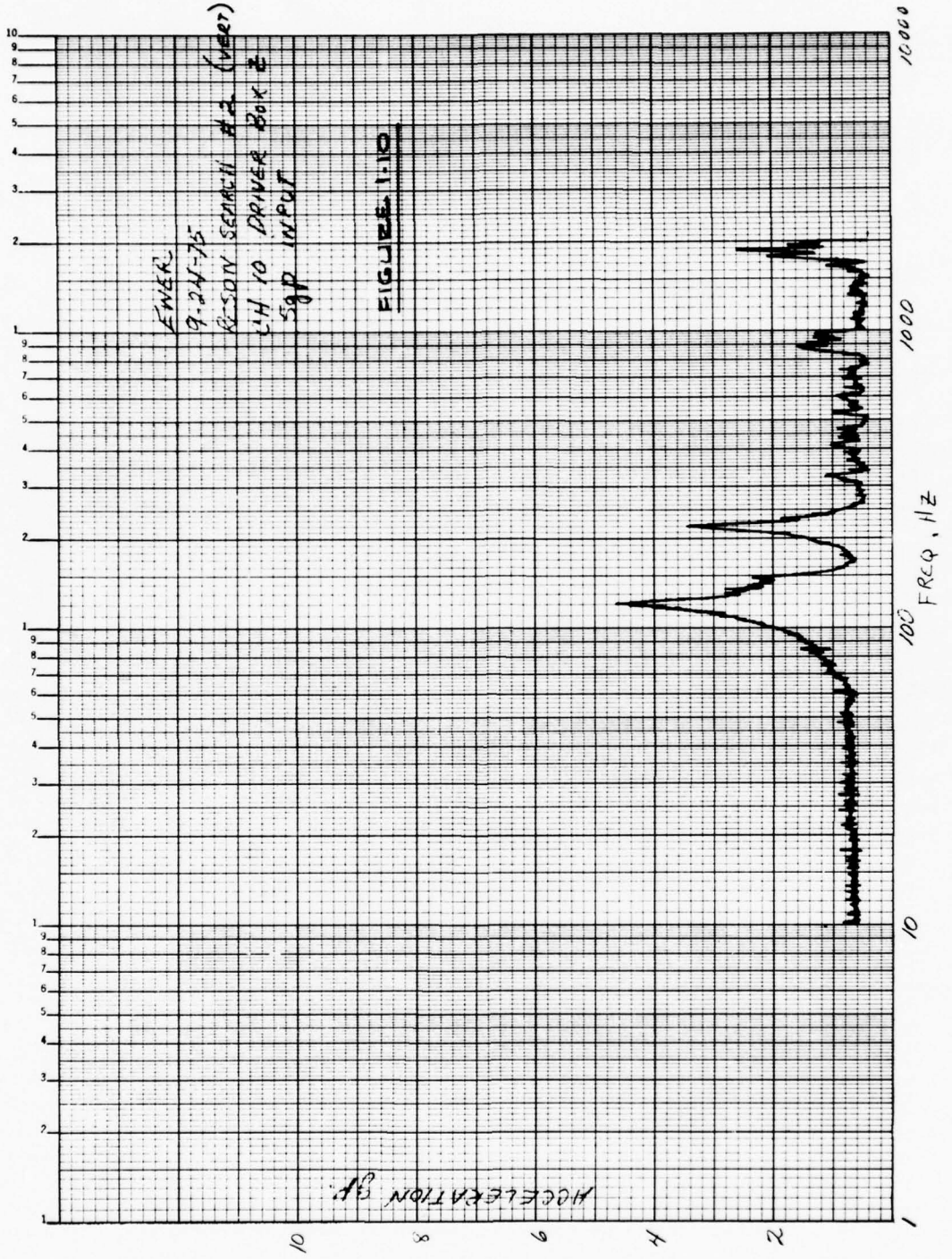
FIGURE 1-10
LEWER
9-24-75
KISSON SEARCH #2 (water)
LH 10 DRIVER BOX 2
5gp INPUT
ACCELERATION g's
FREQ, Hz
10
8
6
4
2
1
10
100
1000
10000

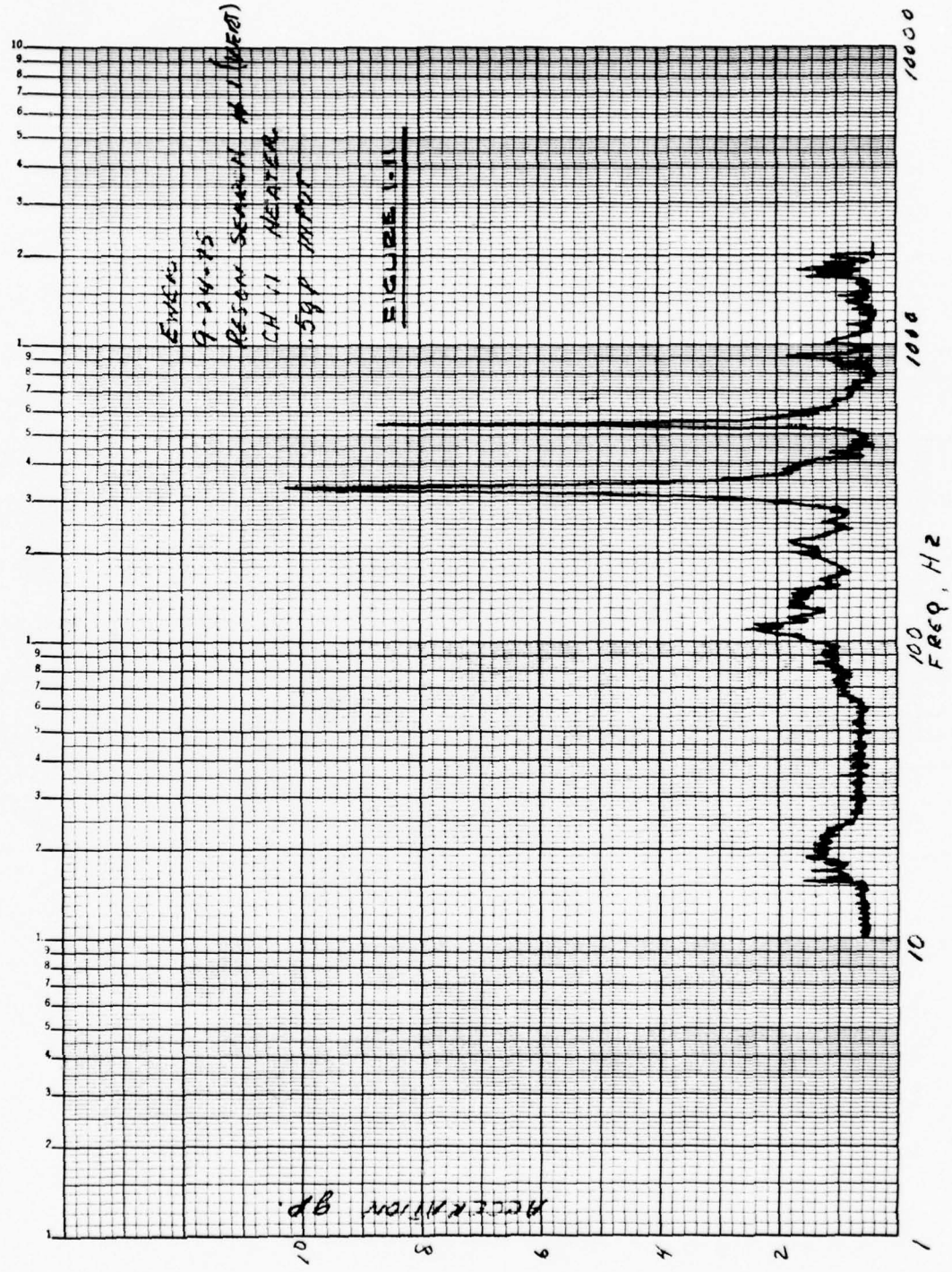
ACCELERATION gP.
FREQ, Hz
10
100
1000
10000
FIGURE 1.11
.5gP input
CH 11 HEATER
RESONANT FREQUENCY
9-24-85
ENVELOPE

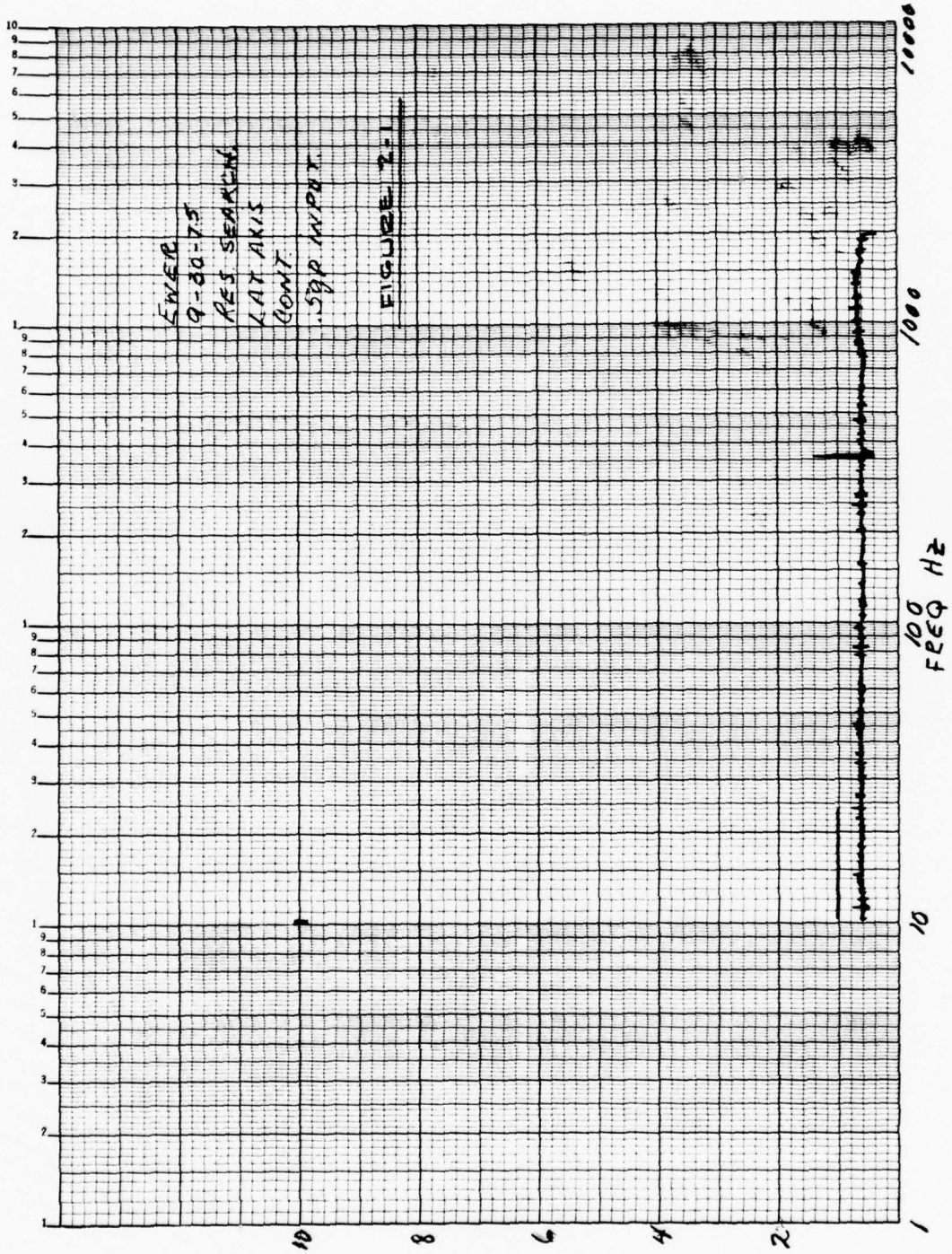
ENERG
Q-30-75
RES SEARCH
LAT AXIS
CONT
.5gp INPUT
FIGURE 2-1
10000
1000
100
10
1
FREQ Hz
10
8
6
4
2

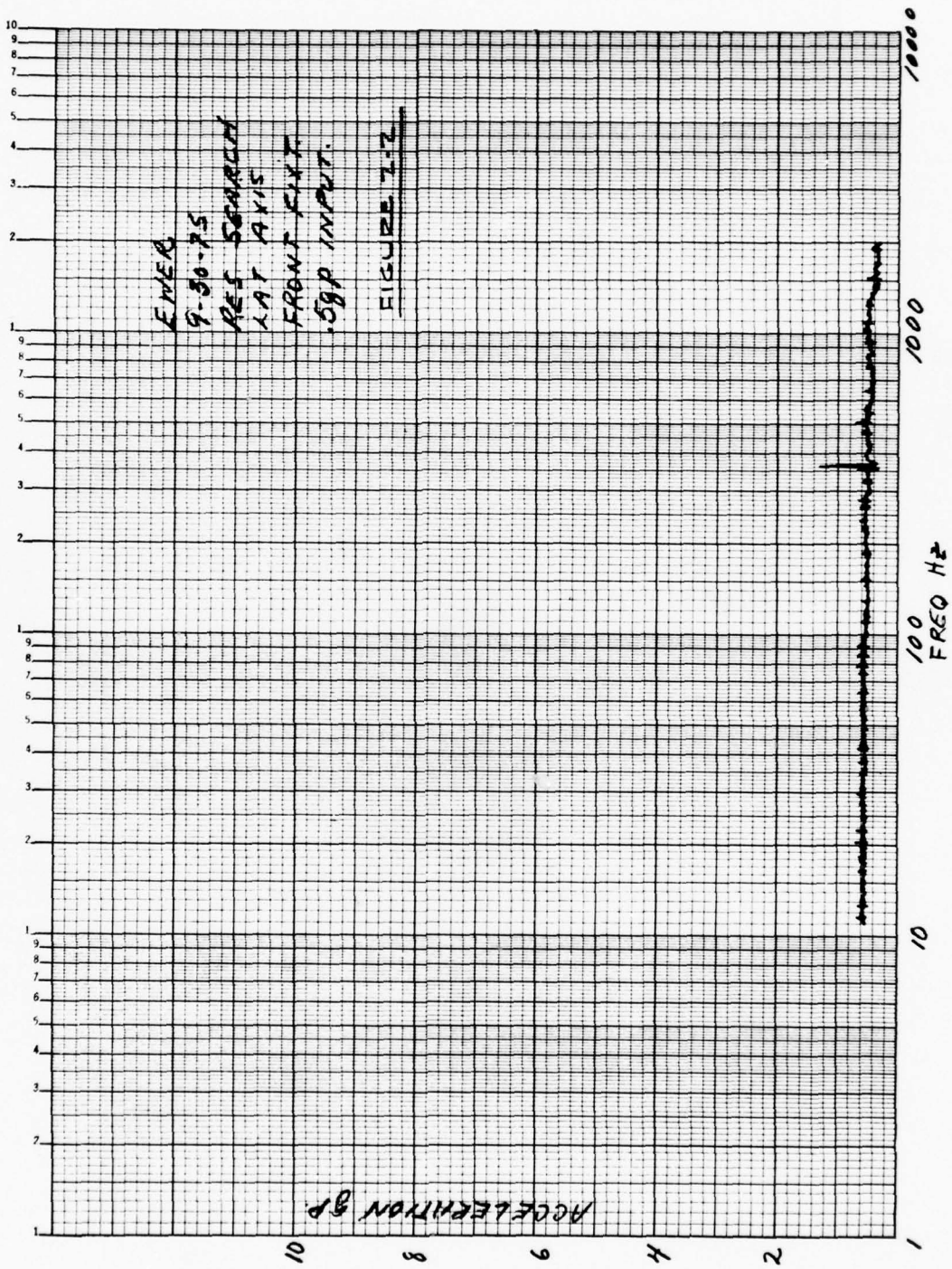
EMER
9-30-75
RES SQUARED
X9T AXIS
FRONT EXIT
.5gp INPUT.
FIGURE 7-7
ACCELERATION gp
FREQ Hz
10000
1000
100
10
1
10
8
6
4
2

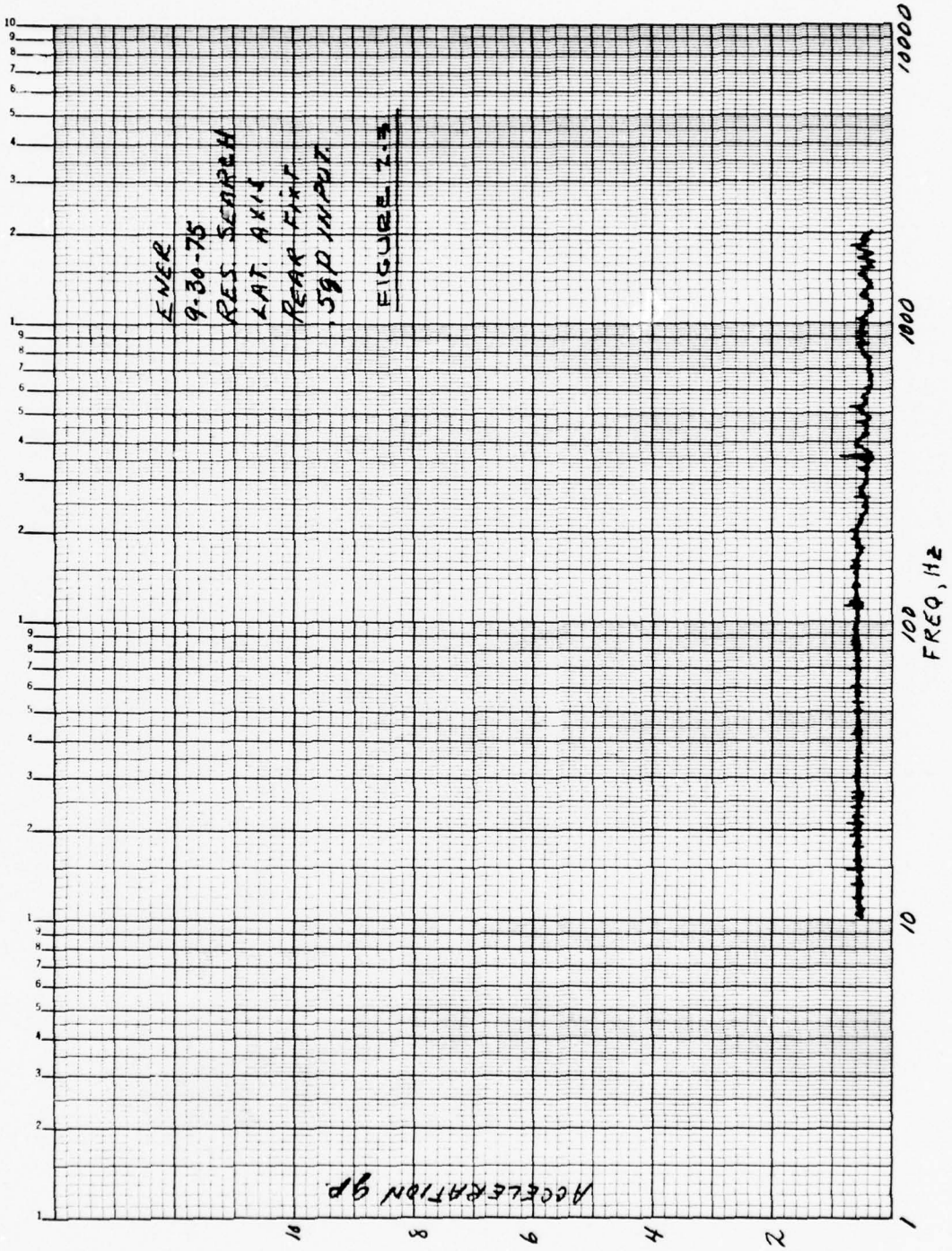
ENER
9-30-75
RES. SCAN 4
LAT. AXIS
REAR FWF
SQD INPUT
FIGURE 2.3
ACCELERATION g's
FREQ, Hz
10000
1000
100
10
1
10
8
6
4
2

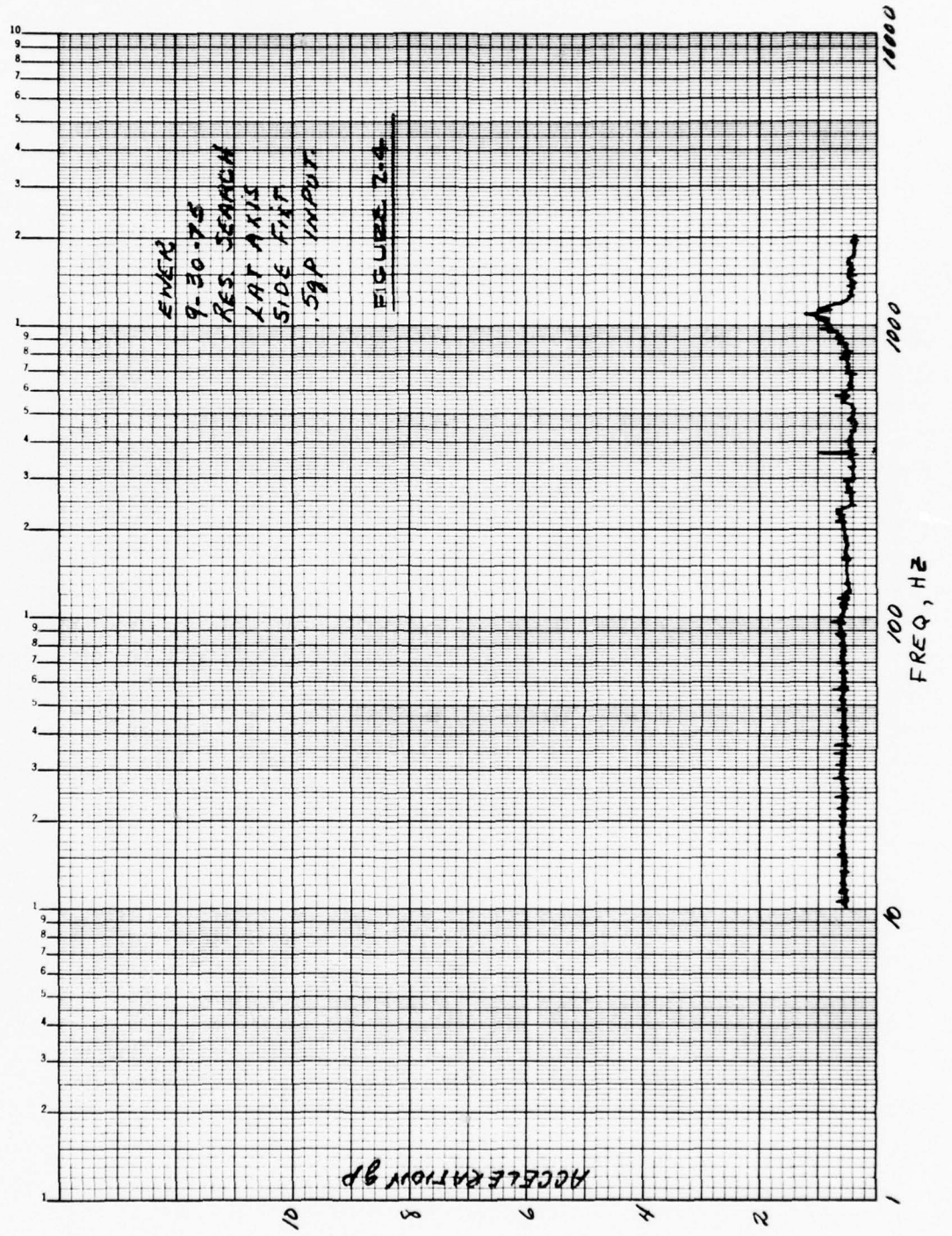
ENERT
9-30-75
RES. SEARCH
LAT AXIS
SIDE FLT
.5gp INPUT
FIGURE 2.4
ACCELERATION gp
FREQ, HZ
10
8
6
4
2
1
10
100
1000
10000

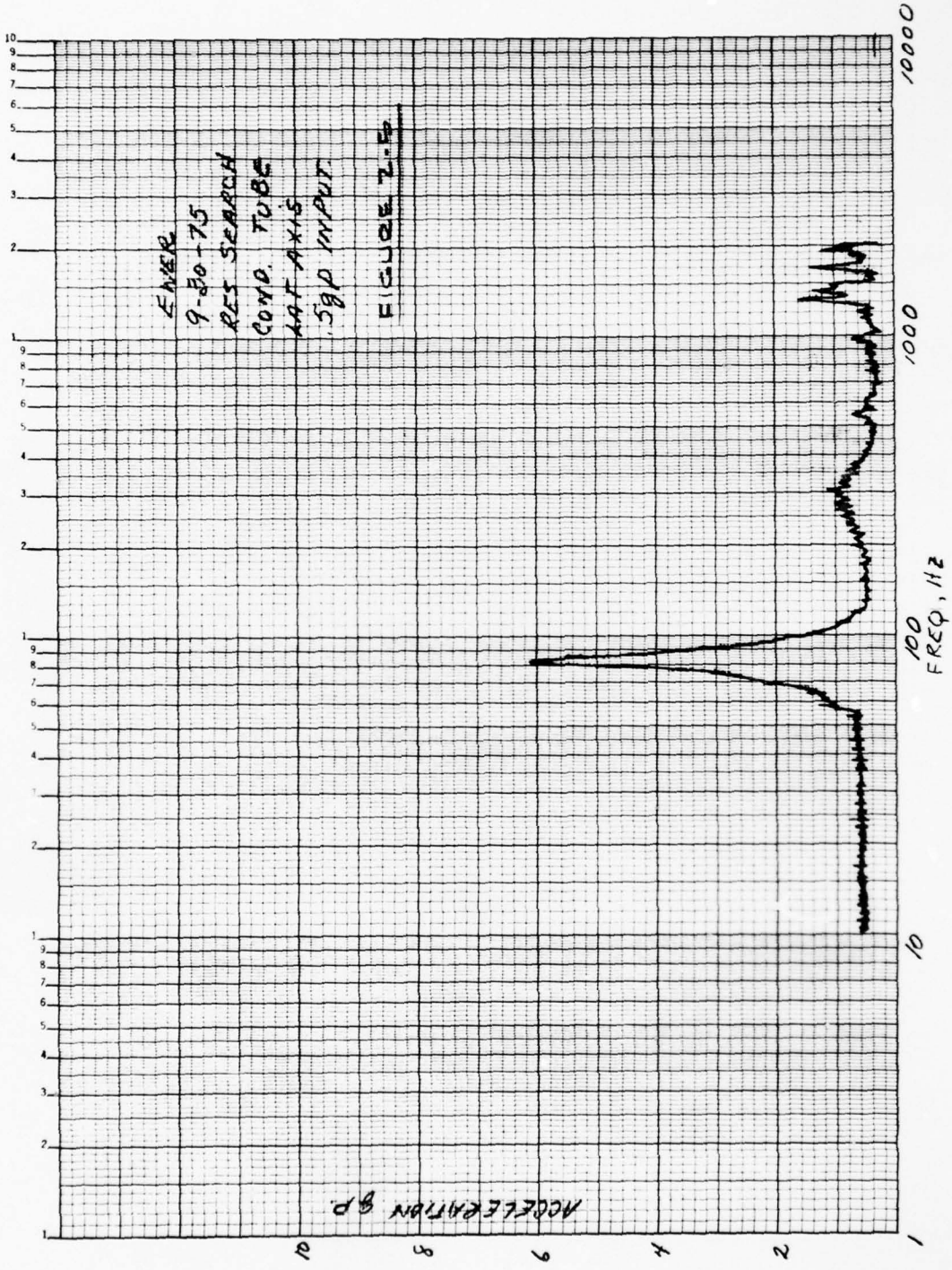
ENDEVCO
9-80-75
RES SEARCH
COMO. TUBE
HOT AXIS
SGD INPUT
FIGURE 2.5
ACCELERATION g's
FREQ, Hz
10000
1000
100
10
1
10
8
6
4
2

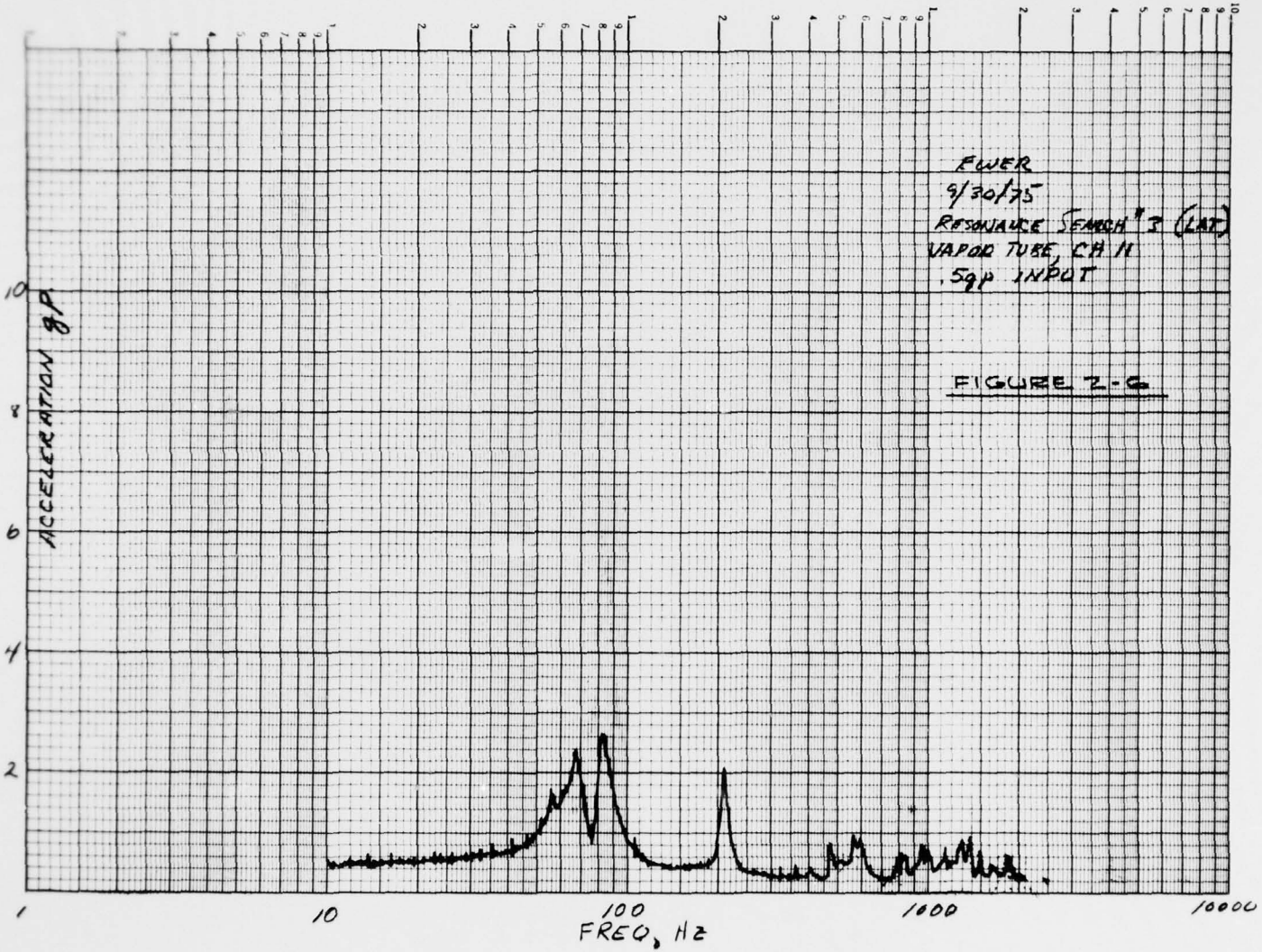
FLWER
9/30/75
RESONANCE SEARCH #3 (LAT)
VAPOR TUBE, CH 11
.5gp INPUT
ACCELERATION gp
10
8
6
4
2
1
10
100
1000
10000
FREQ, Hz

FIGURE 2-6

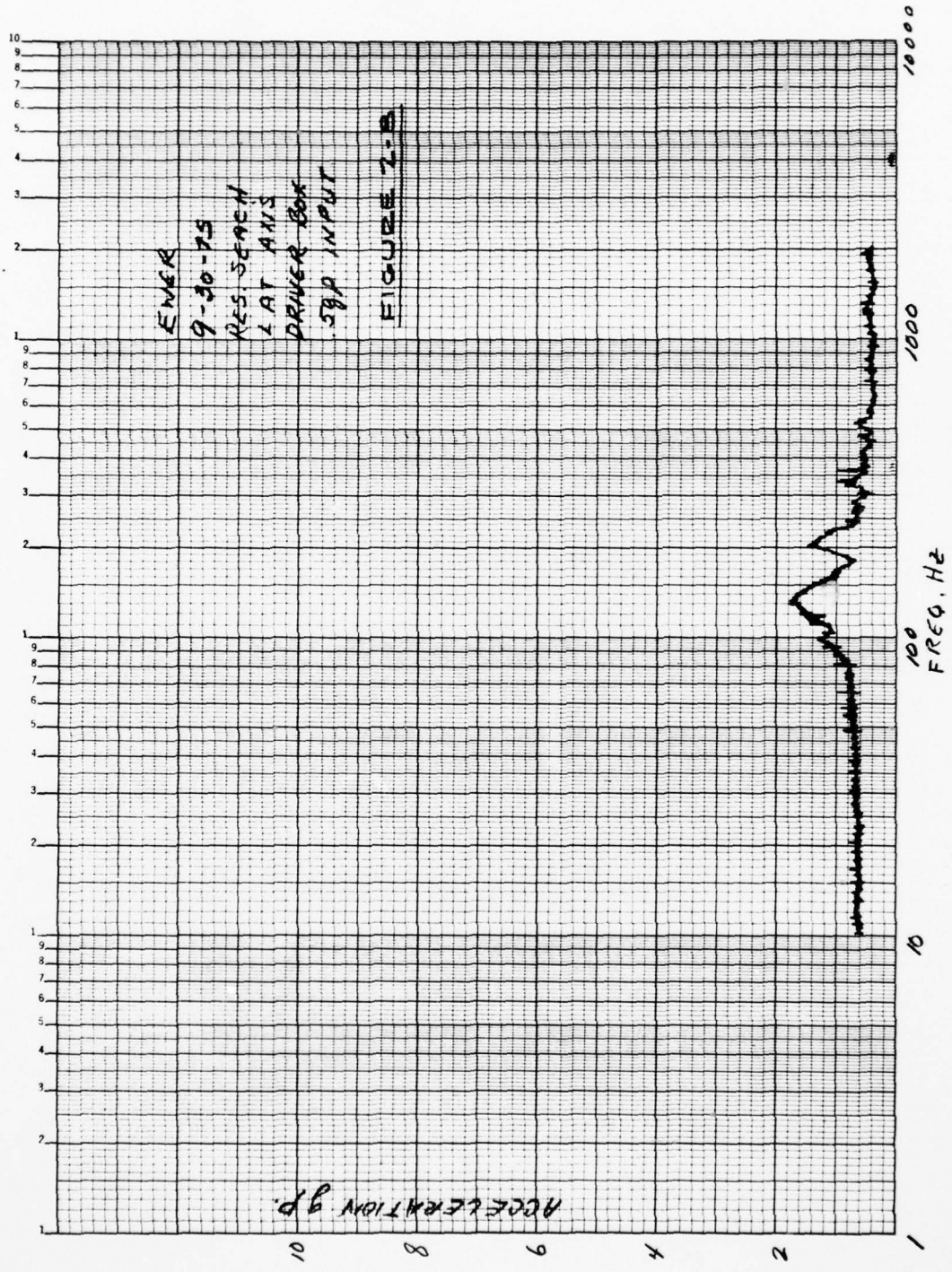
ENER
9-30-75
RES. SCAN
LAT AXIS
DRIVER BOX
SYD INPUT
FIGURE 2-B
ACCELERATION g's
FREQ. Hz
10000
1000
100
10
1
10
8
6
4
2

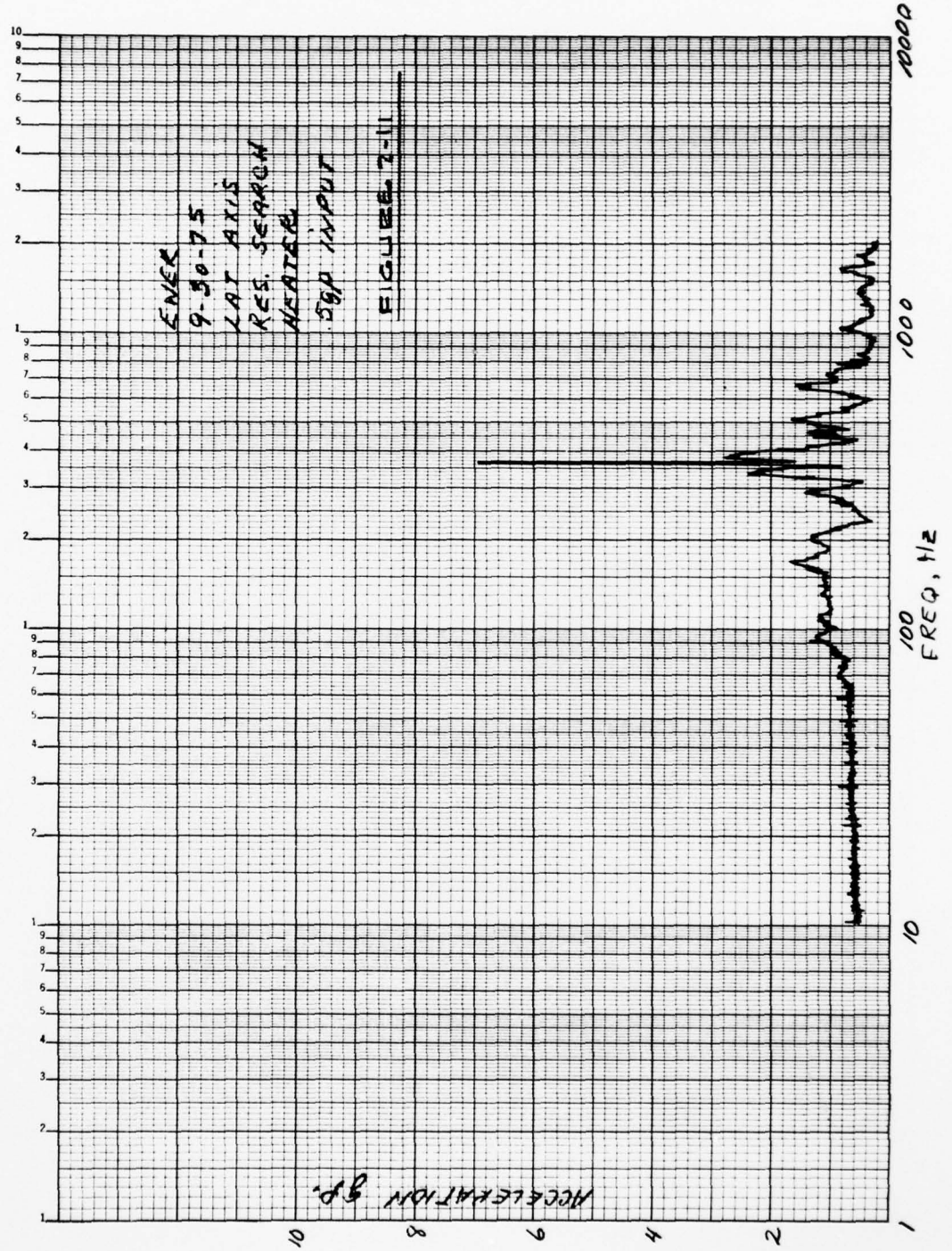
ENEK
9-30-75
LAT AXIS
RES. SEARCH
HEATER
SGD INPUT
FIGURE 2-11
ACCELERATION g's
FREQ, Hz
10000
1000
100
10
1

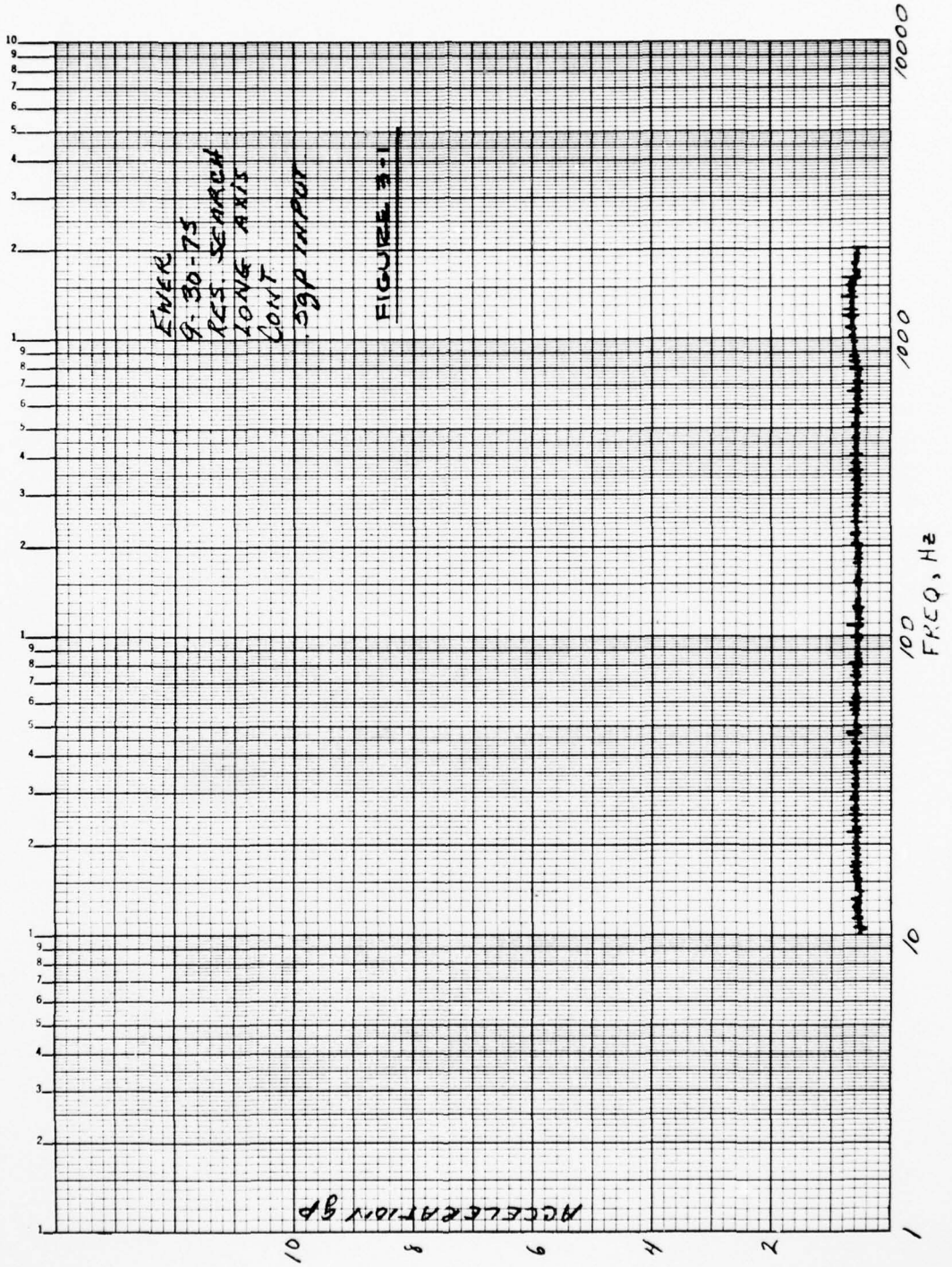
ENER
9.30-75
RCS SEARCH
LONG AXIS
CONT
.5gp INPUT
FIGURE B-1
ACCELERATION gp
FREQ, Hz
10
8
6
4
2
1
10
100
1000
10000

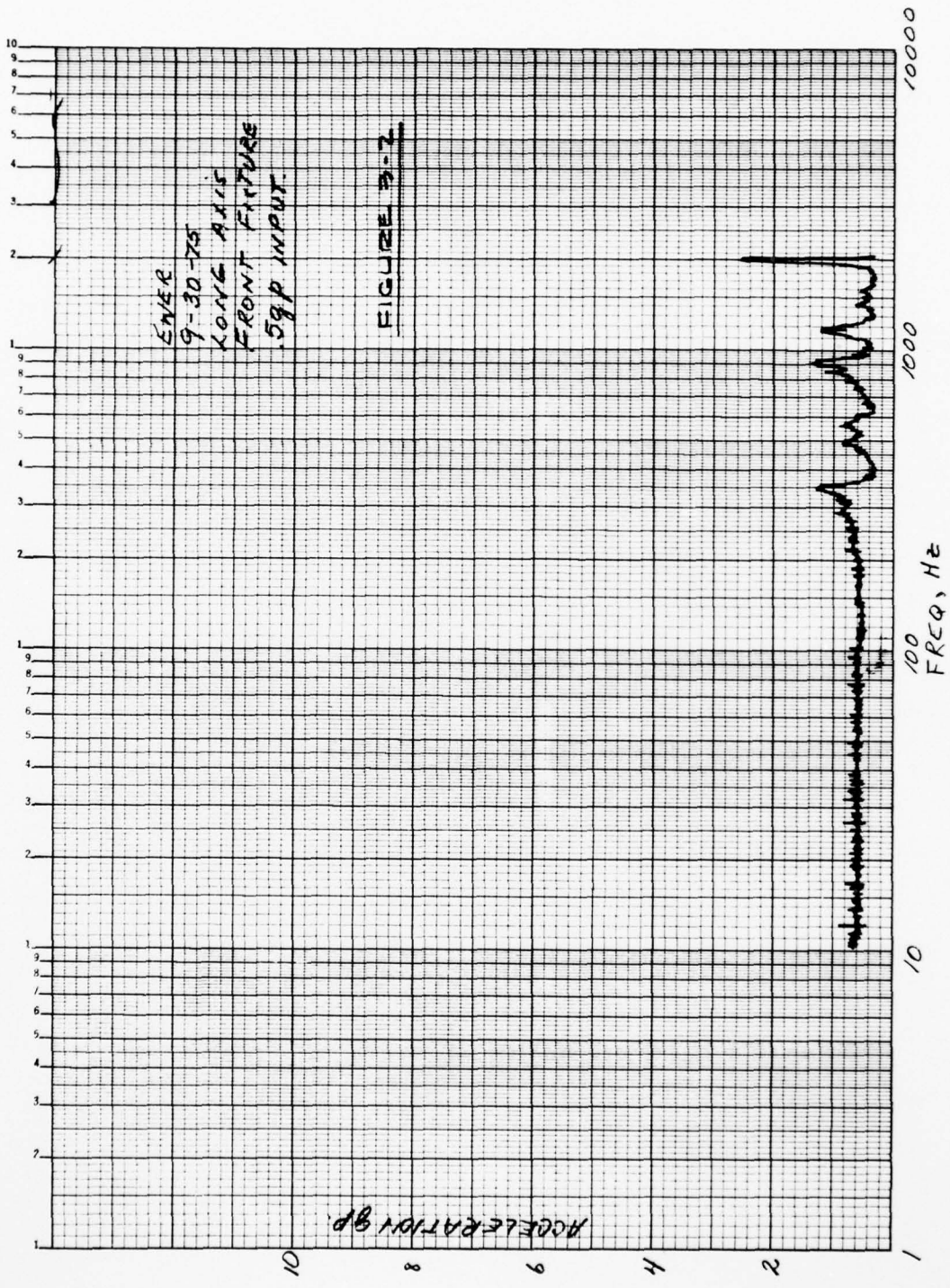
ENTER
9-30-75
KONIG AXIS
FRONT FIXTURE
.5gp INPUT
FIGURE B-2
ACCELERATION gp
FREQ, Hz
10000
1000
100
10
1
10
8
6
4
2

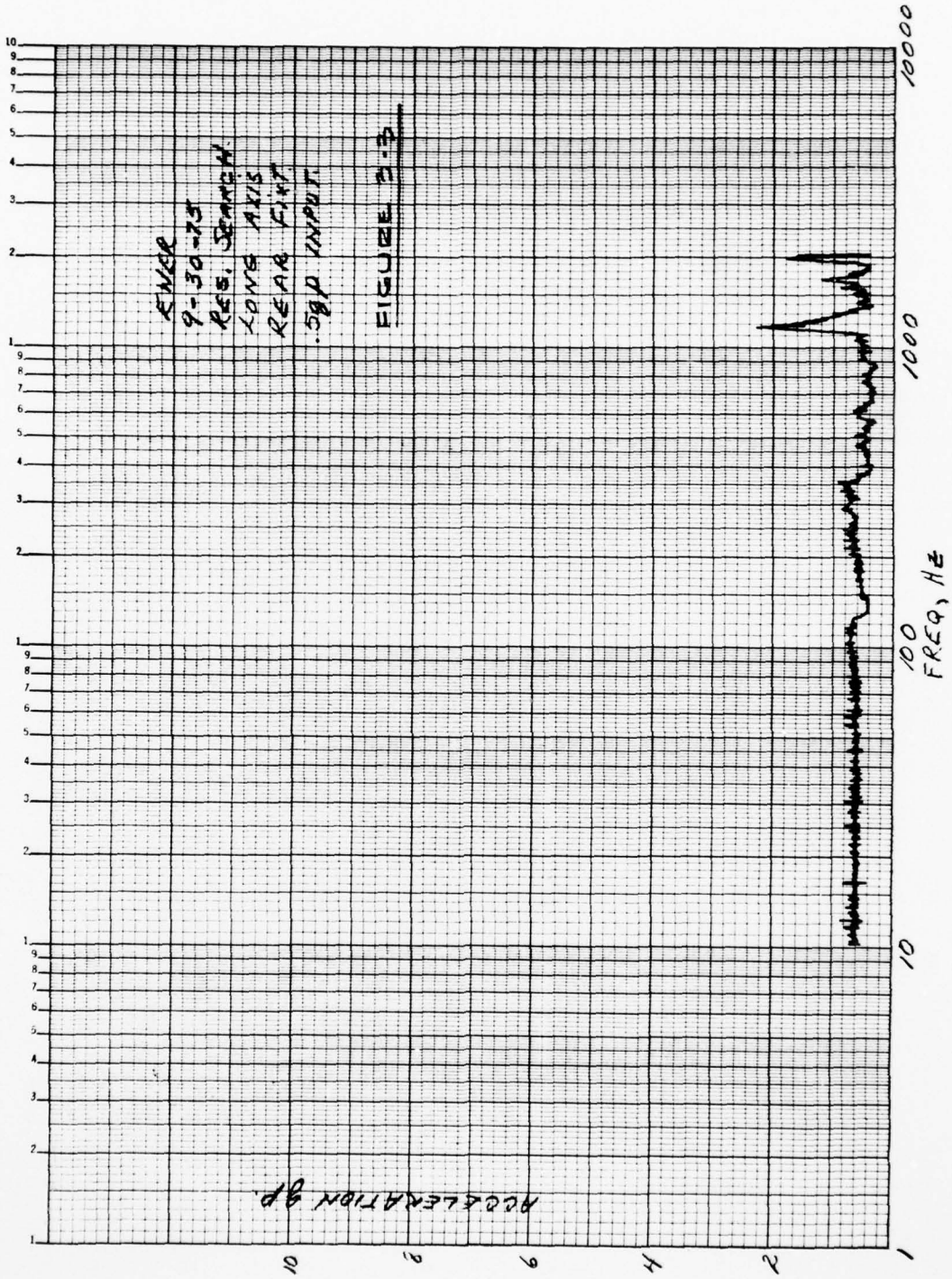
ACCELERATION gp
FREQ, Hz
10
9
8
7
6
5
4
3
2
1
10000
1000
100
10
1
FIGURE 3-3
RENEE
9-30-75
RES. SEAT CH.
LONG AXIS
REAR LIFT
.5gp INPUT

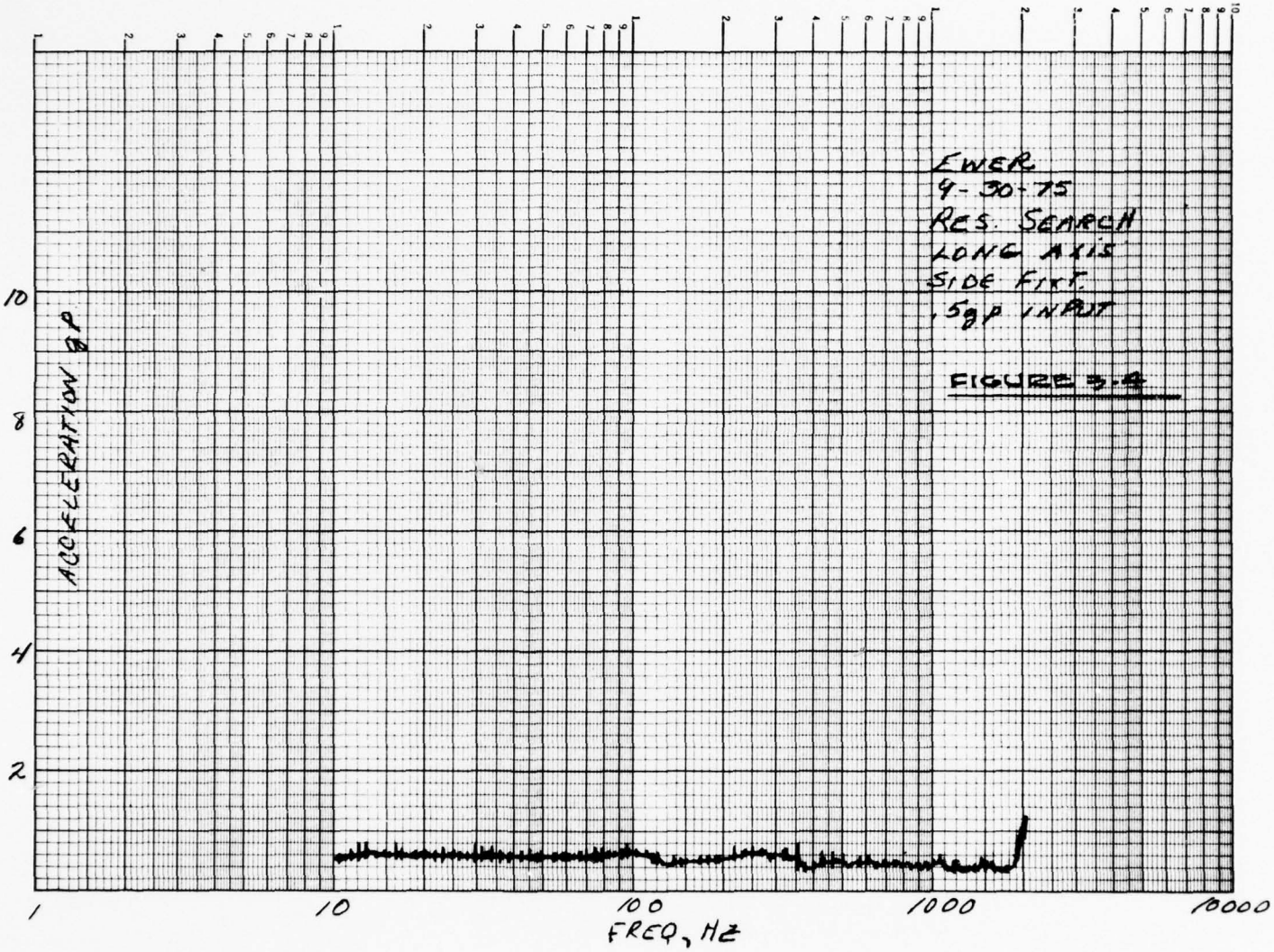
EWER
4-30-75
RES SEARCH
LONG AXIS
SIDE FIXT.
.5g P INPUT
FIGURE 5-4
ACCELERATION g P
10
8
6
4
2
1
10
100
1000
10000
FREQ, HZ

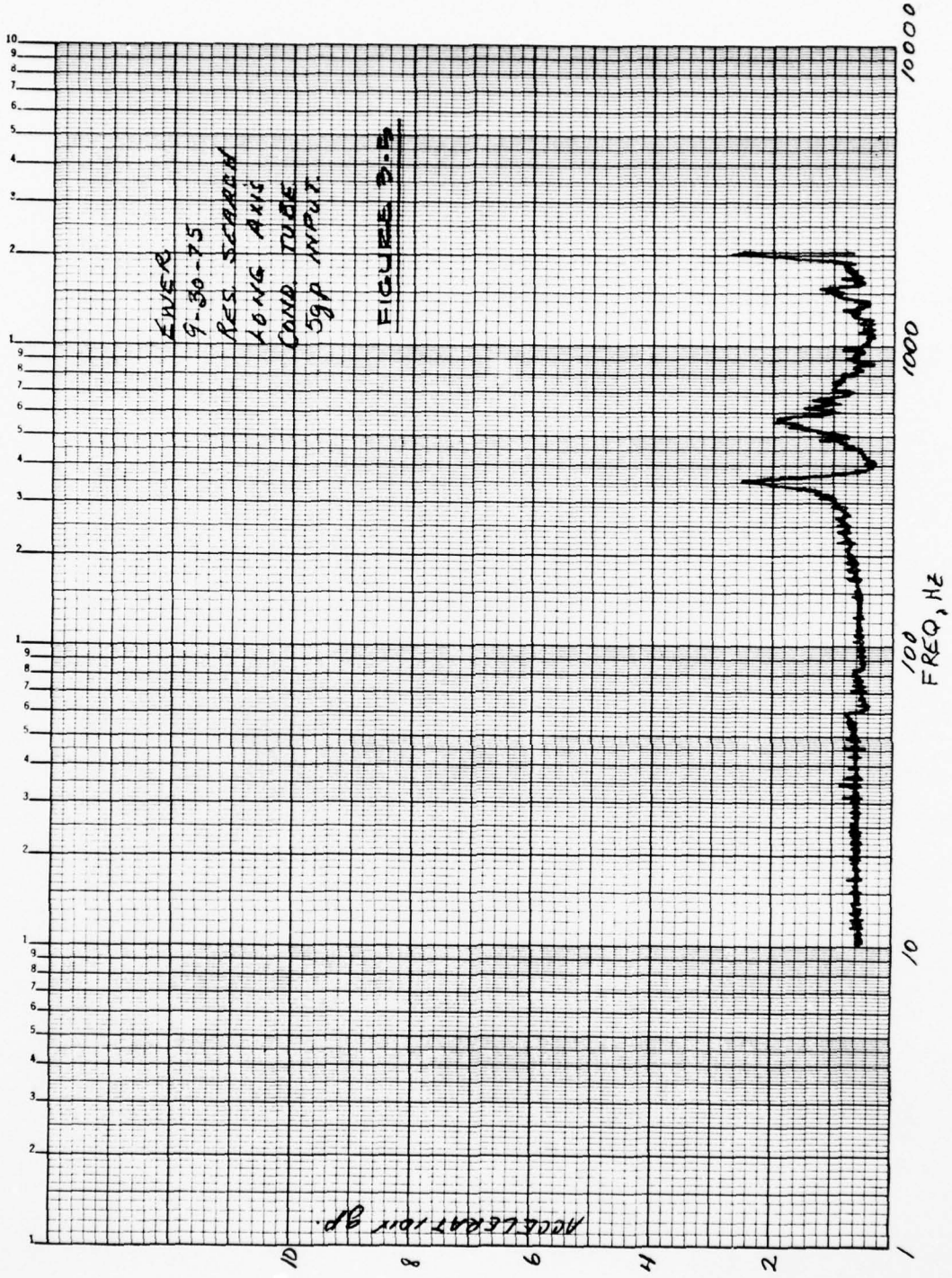
ENVER
9-30-75
RES. SCREEN
LONG AXIS
CONE TUBE
5gp INPUT.
FIGURE B-5
ACCELERATION gp
FREQ, Hz
10000
1000
100
10
1
10
8
6
4
2

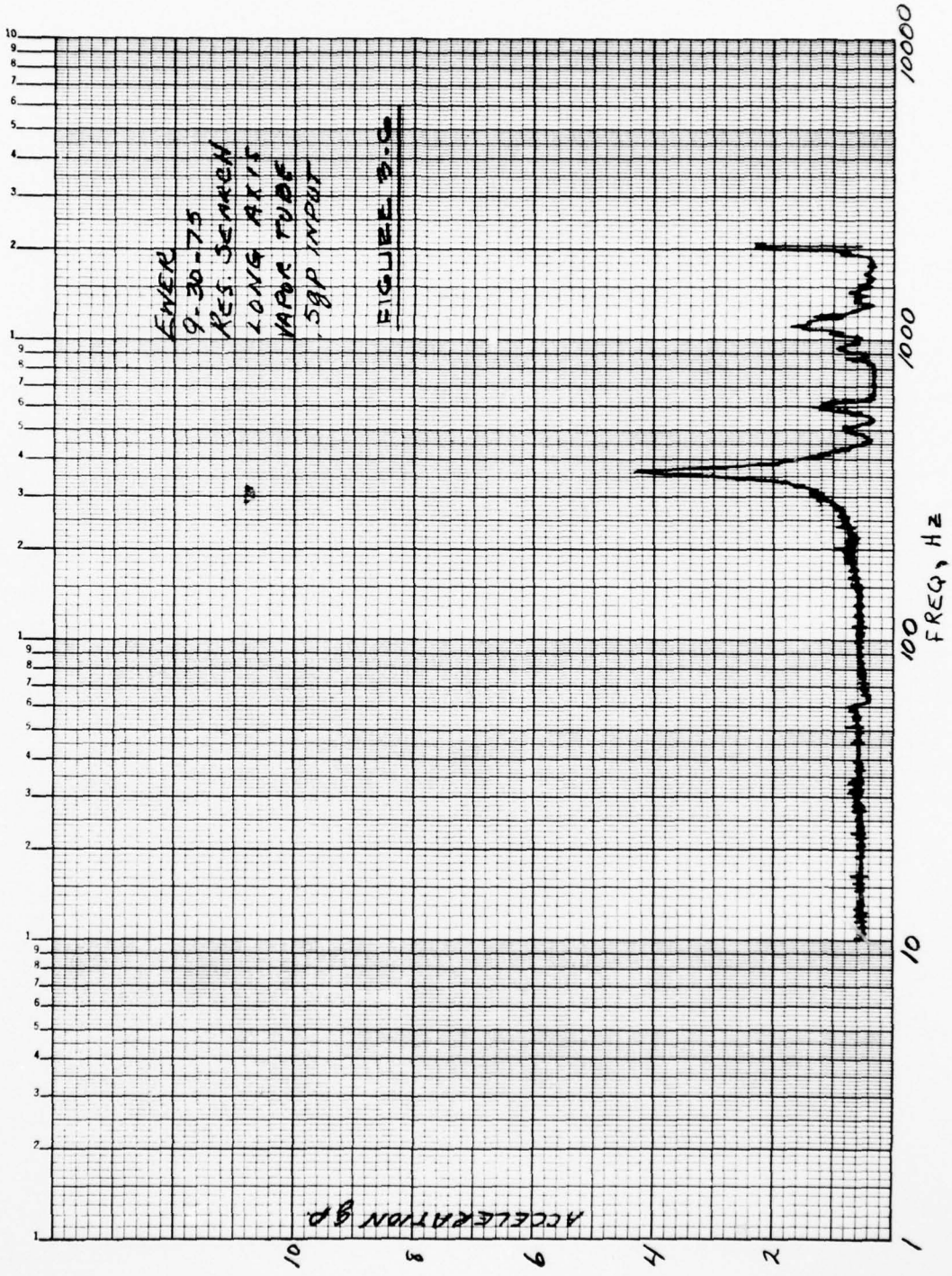
ENERG
9-30-75
RES. SCREEN
LONG AXIS
VAPOR TUBE
SGP INPUT
FIGURE 3-5
ACCELERATION g²
FREQ, Hz
10
8
6
4
2
1
10000
1000
100
10

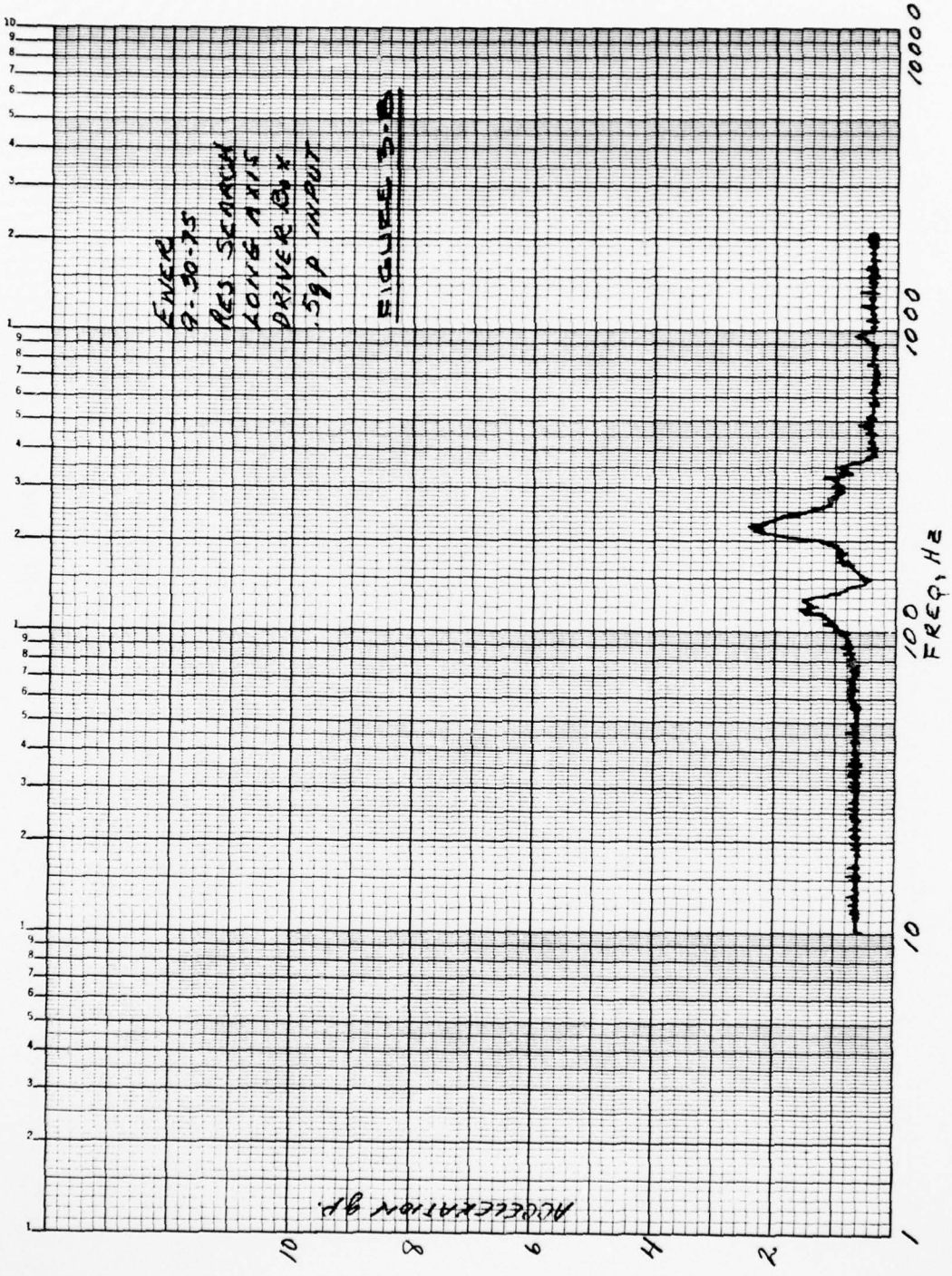
ENVEL
Q=30-35
RES SEARCH
LONG AXIS
DRIVER BOX
.5g p INPUT
FIGURE 5-8
ACCELERATION gp
FREQ, Hz
10000
1000
100
10
1
10
8
6
4
2

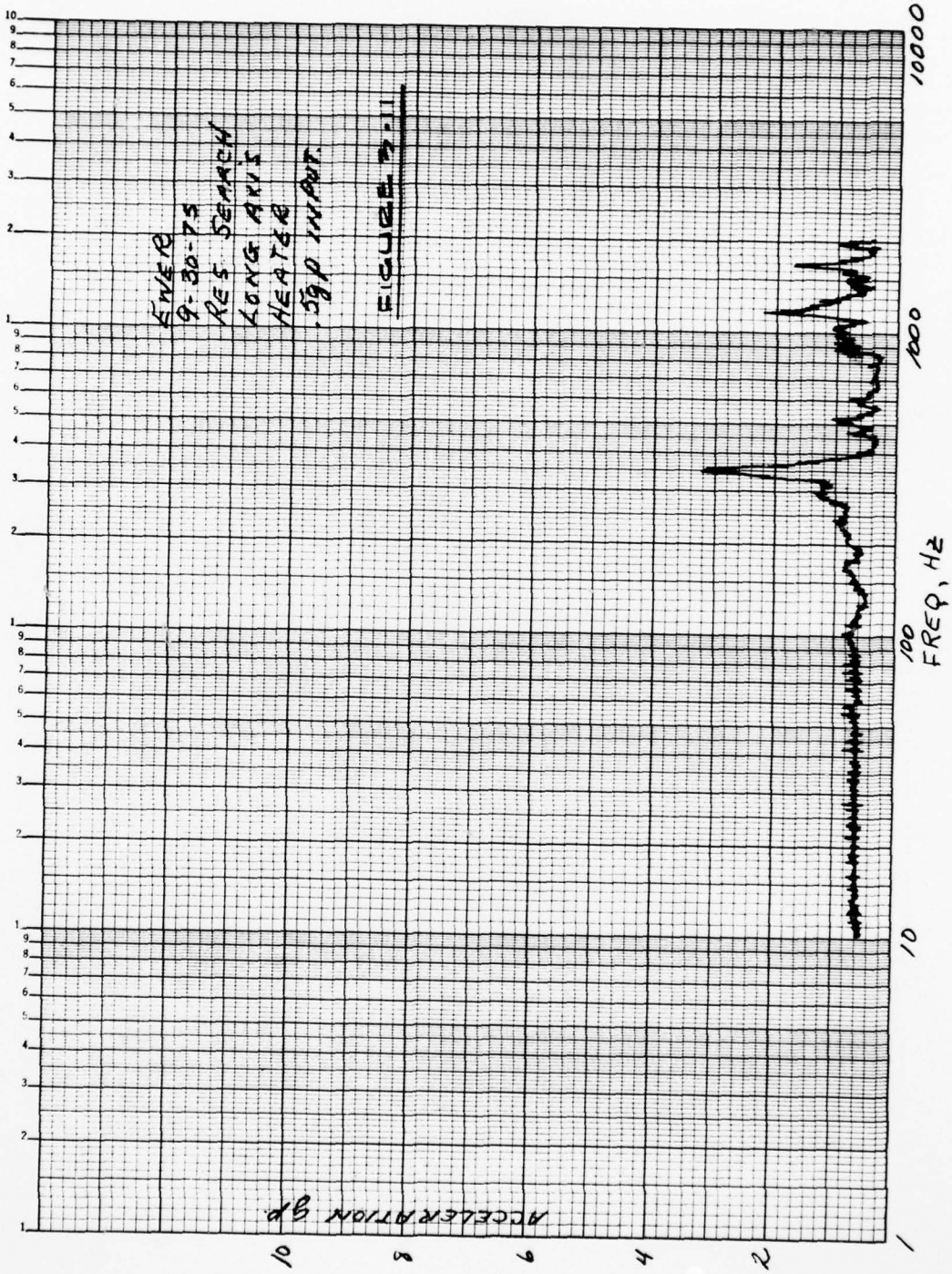
ENVIR
9-30-75
RES SEARCH
LONG AXIS
HEATER
SGP INPUT
FIGURE B-11
ACCELERATION g's
FREQ, Hz
10000
1000
100
10
1
10
8
6
4
2

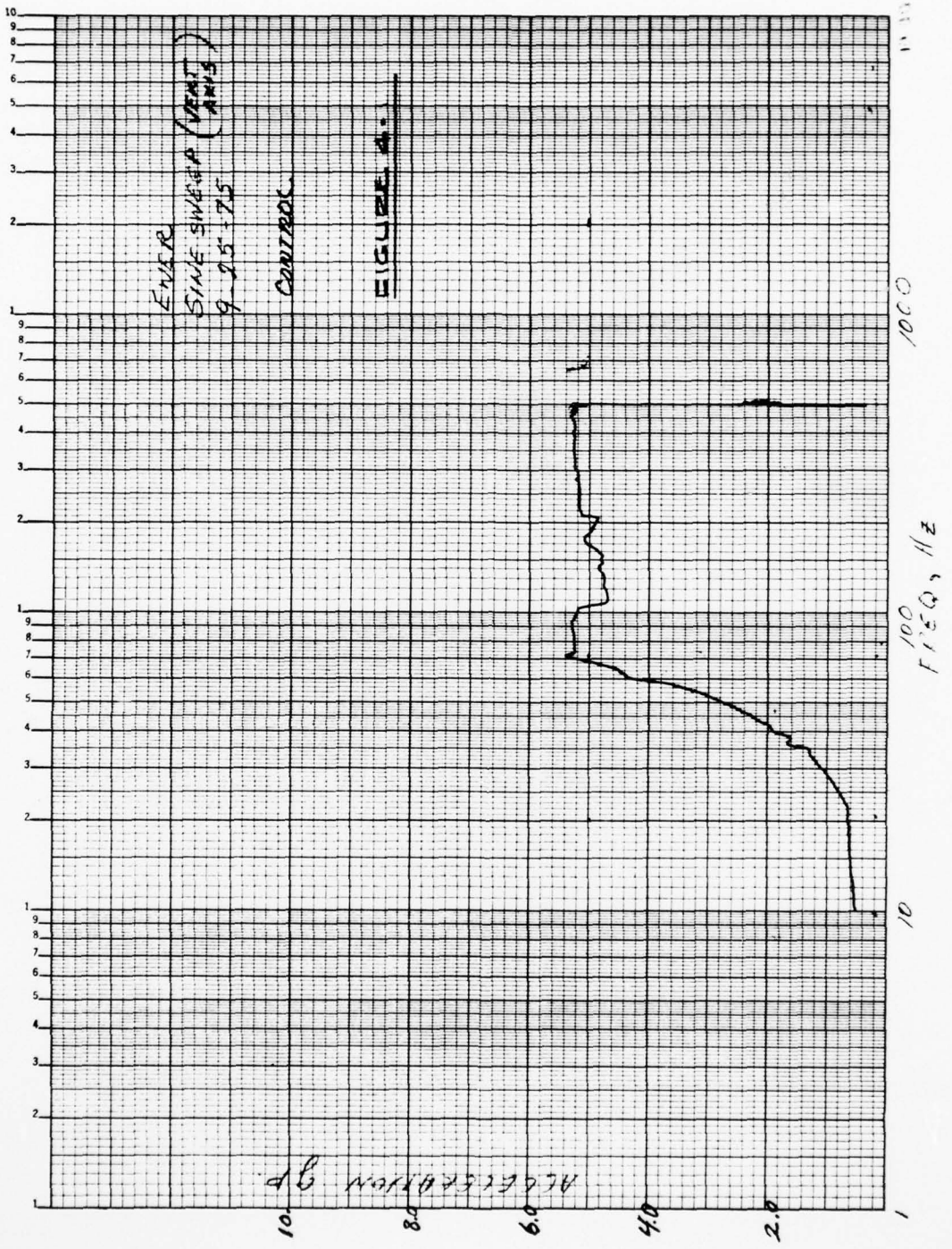
ENTER
SINE SWEEP (VERT AXIS)
q 2.5 + 2.5
CONTROL
FIGURE 4.
ACCELERATION g p
10.
8.0
6.0
4.0
2.0
1
10
100
1000
FREQ, Hz

ARD 8135
AUG 67

ACCELERATION SPECTRAL DENSITY PLOT

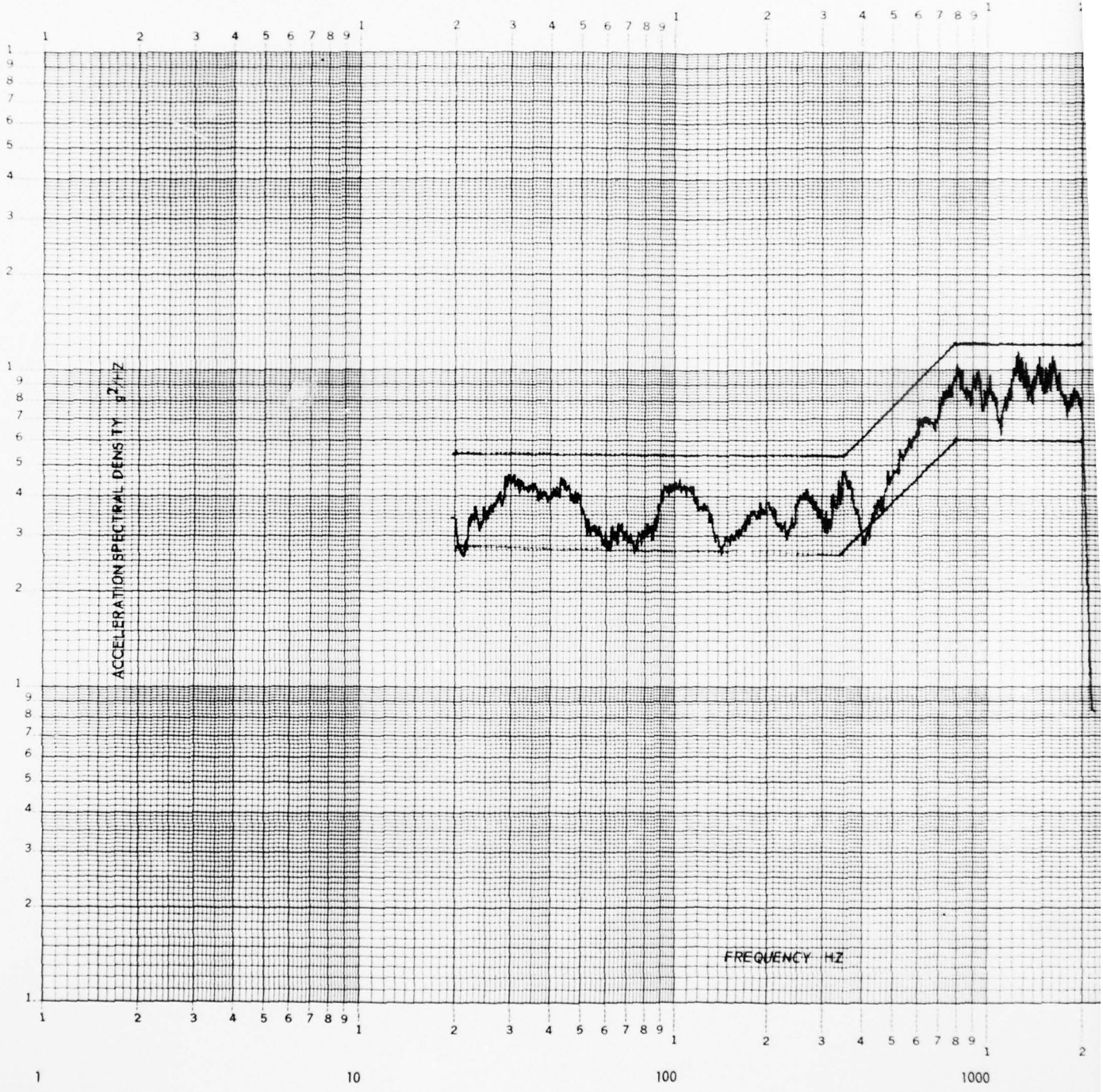

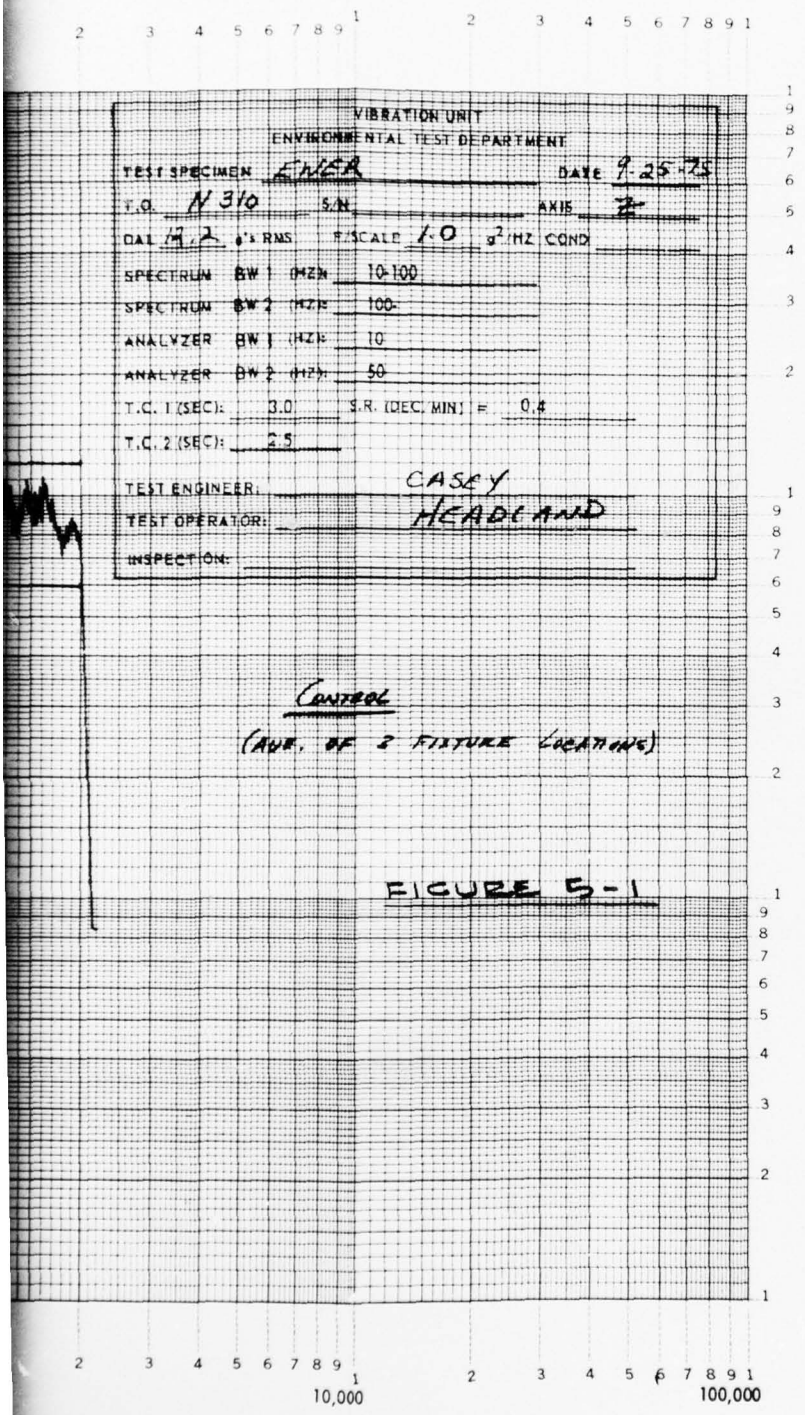
VIBRATION UNIT
ENVIRONMENTAL TEST DEPARTMENT
TEST SPECIMEN ENEA
DATE 9-25-75
T.O. N 310
S/N
AXIS Z
OAL 17.2 g's RMS
SCALE 1.0 g²/HZ COND
SPECTRUM BW 1 (HZ): 10-100
SPECTRUM BW 2 (HZ): 100
ANALYZER BW 1 (HZ): 10
ANALYZER BW 2 (HZ): 50
T.C. 1 (SEC): 3.0
S.R. (DEC/MIN) = 0.4
T.C. 2 (SEC): 2.5
TEST ENGINEER: CASEY
TEST OPERATOR: HEADLAND
INSPECTION:
CONTROL
(AVE. OF 2 FIXTURE LOCATIONS)
10,000
100,000

FIGURE 5-1

AD-A061 255 AEROSPACE CORP EL SEGUNDO CALIF F/G 4/1
DEVELOPMENT OF CLOUD WATER CONTENT METER, EWER.(U)
MAR 78 D A DURRAN, D H ROSS, W J SWARTWOOD F04701-77-C-0078
UNCLASSIFIED TR-0078(3550-38)-1 SAMSO-TR-78-113 NL

3 OF 3
AD
A061255

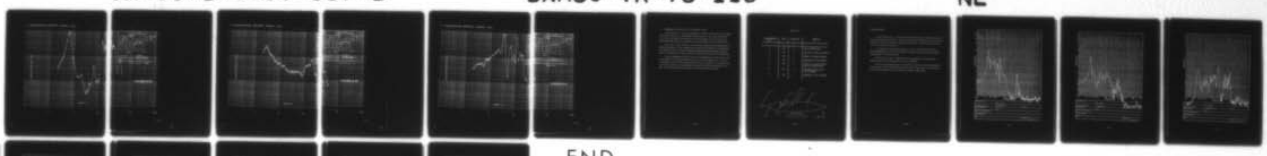

END
DATE
FILMED
2 - 79
DDC

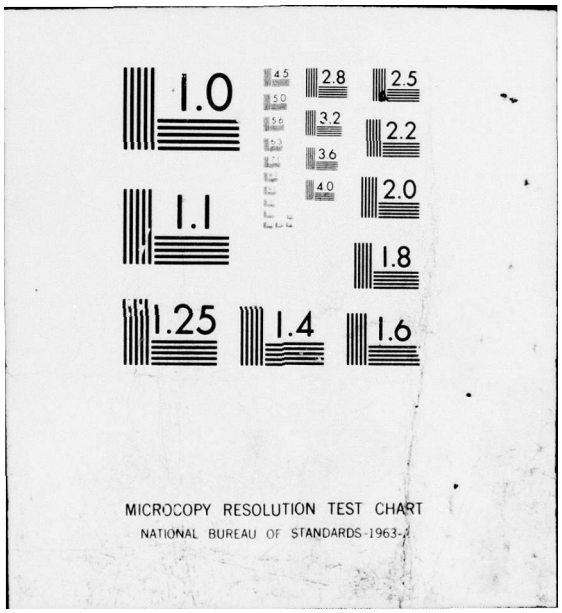
1.0
1.1
1.25
1.4
1.6
1.8
2.0
2.2
2.5
2.8
3.2
3.6
4.0
4.5
5.0
5.6
MICROCOPY RESOLUTION TEST CHART
NATIONAL BUREAU OF STANDARDS-1963-

ARD 8135
AUG '67

ACCELERATION SPECTRAL DENSITY PLOT

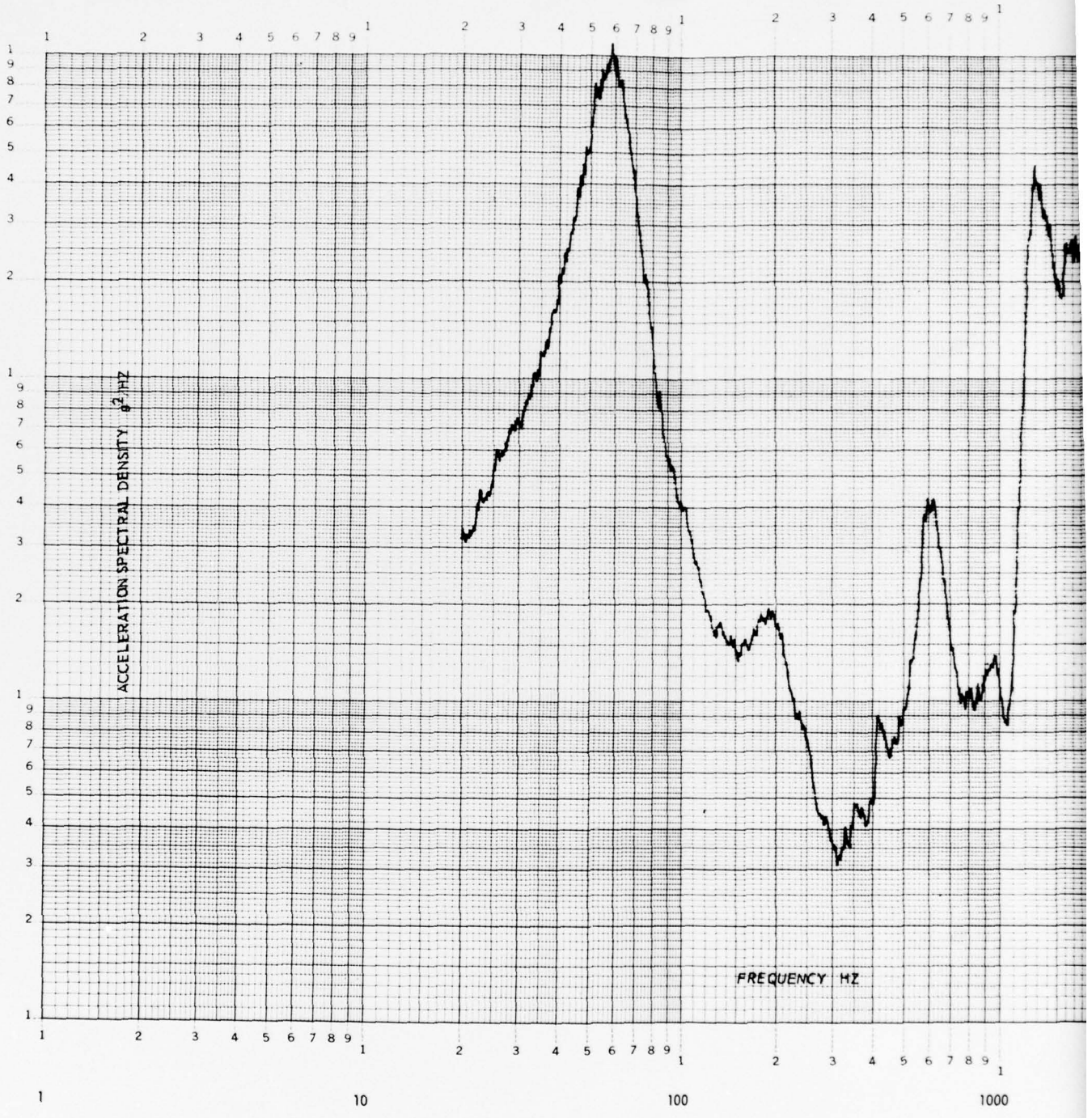

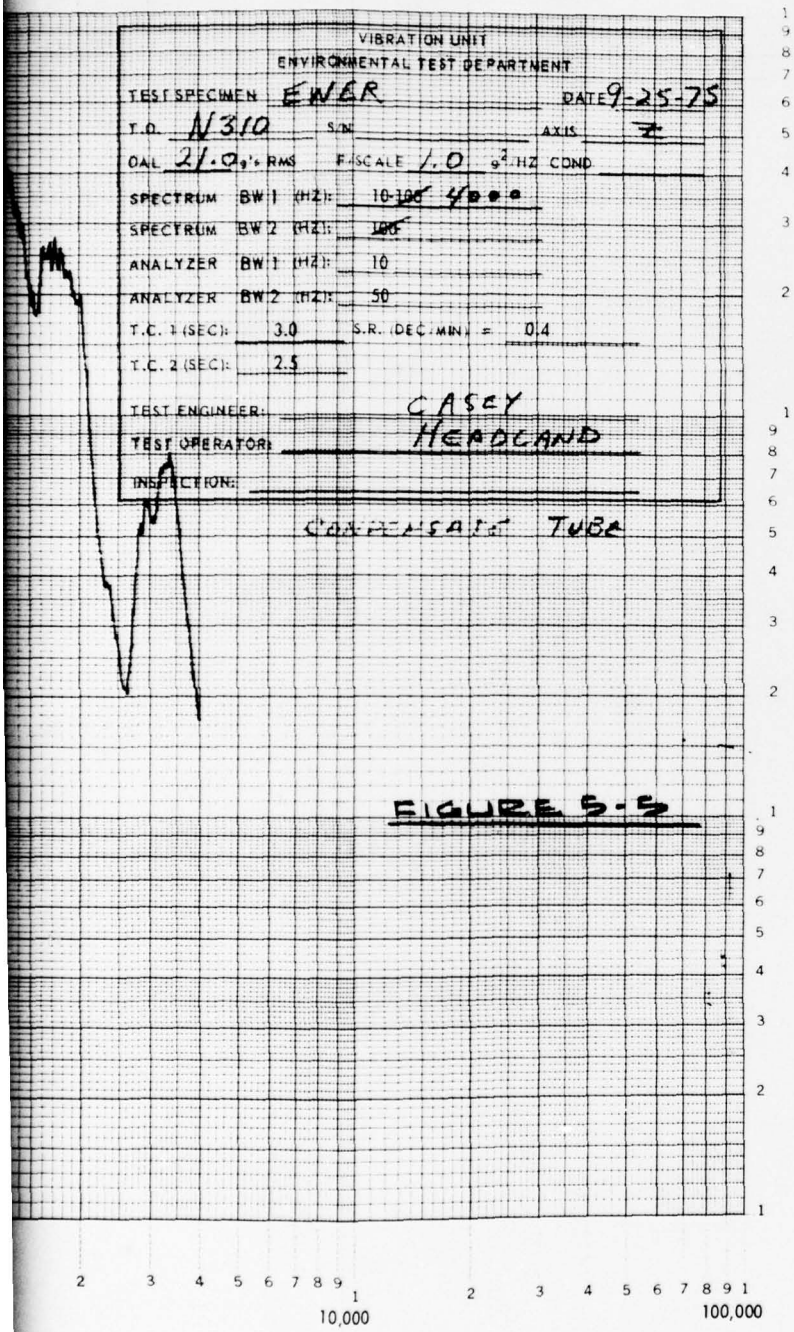
VIBRATION UNIT
ENVIRONMENTAL TEST DEPARTMENT
TEST SPECIMEN EWER
DATE 9-25-75
T.O. N310
S/N
AXIS Z
OAL 21.0 g's RMS
F-SCALE 1.0 g² HZ COND
SPECTRUM BW 1 (HZ): 10-1000
SPECTRUM BW 2 (HZ): 100
ANALYZER BW 1 (HZ): 10
ANALYZER BW 2 (HZ): 50
T.C. 1 (SEC): 3.0
S.R. (DEC/MIN) = 0.4
T.C. 2 (SEC): 2.5
TEST ENGINEER: CASEY
TEST OPERATOR: HEADLAND
INSPECTION:
CONDENSATE TUBE

FIGURE 5-5

2

ARD 8135
AUG '67

ACCELERATION SPECTRAL DENSITY PLOT

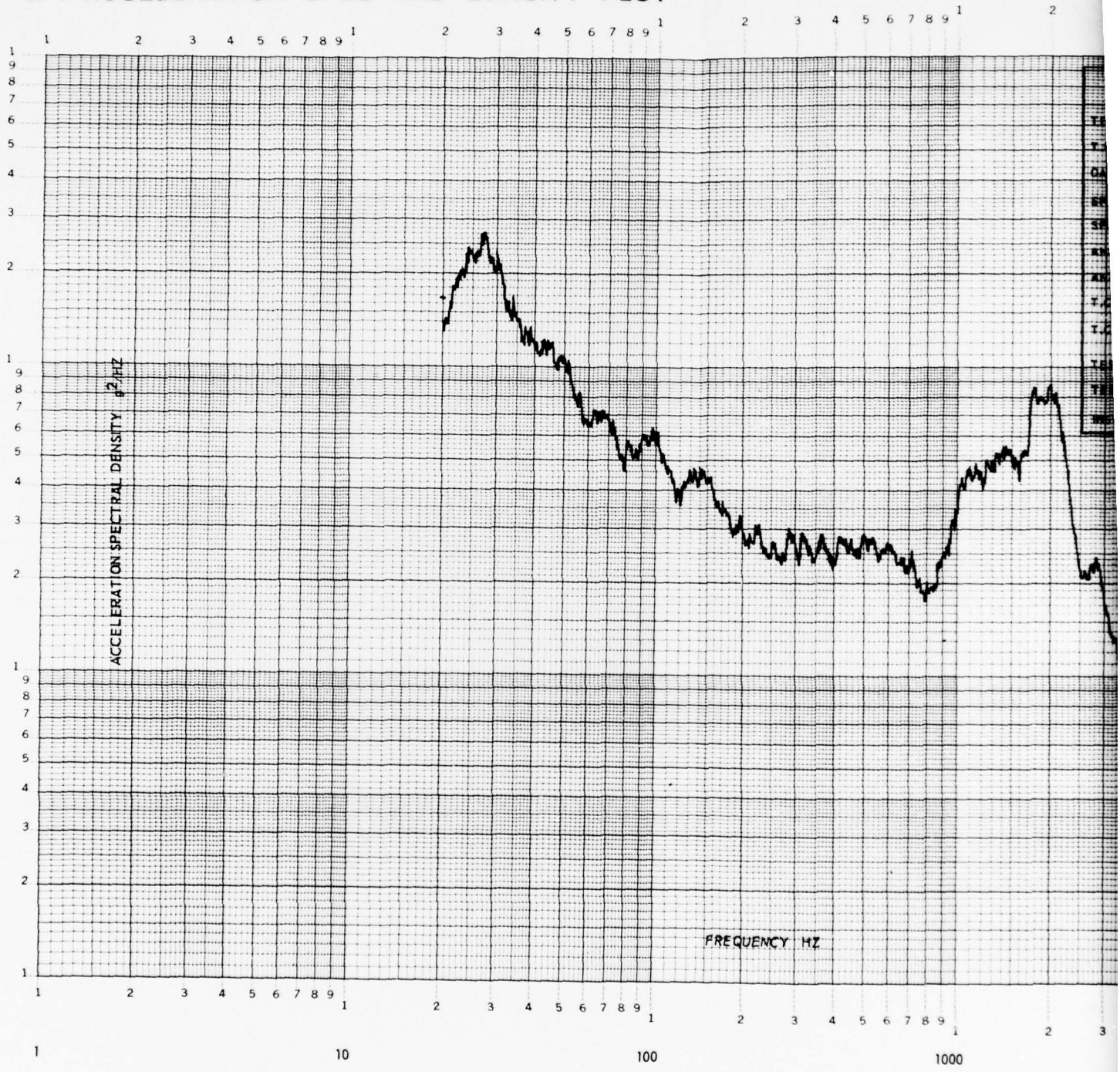

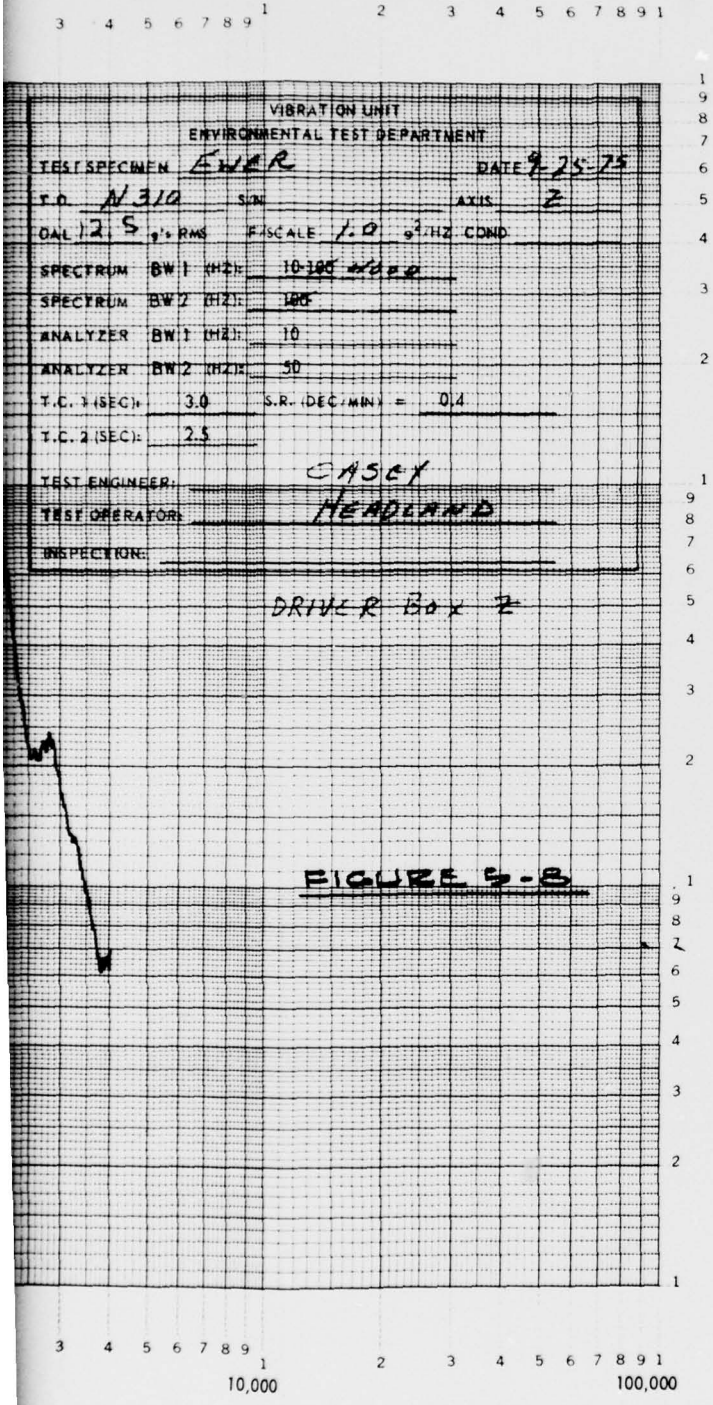
VIBRATION UNIT
ENVIRONMENTAL TEST DEPARTMENT
TEST SPECIMEN EWER
DATE 9-25-75
T.O. N310
S/N
AXIS Z
OAL 12.5 g's RMS
F/SCALE 1.0 g²/HZ COND
SPECTRUM BW 1 (HZ): 10-100 HPO
SPECTRUM BW 2 (HZ): 100
ANALYZER BW 1 (HZ): 10
ANALYZER BW 2 (HZ): 50
T.C. 1 (SEC): 3.0
S.R. (DEC/MIN) = 0.4
T.C. 2 (SEC): 2.5
TEST ENGINEER: CASEY
TEST OPERATOR: HEADLAND
INSPECTION:
DRIVER Box Z
10,000
100,000

FIGURE 5-8

ARO 8135
AUG 67

ACCELERATION SPECTRAL DENSITY PLOT

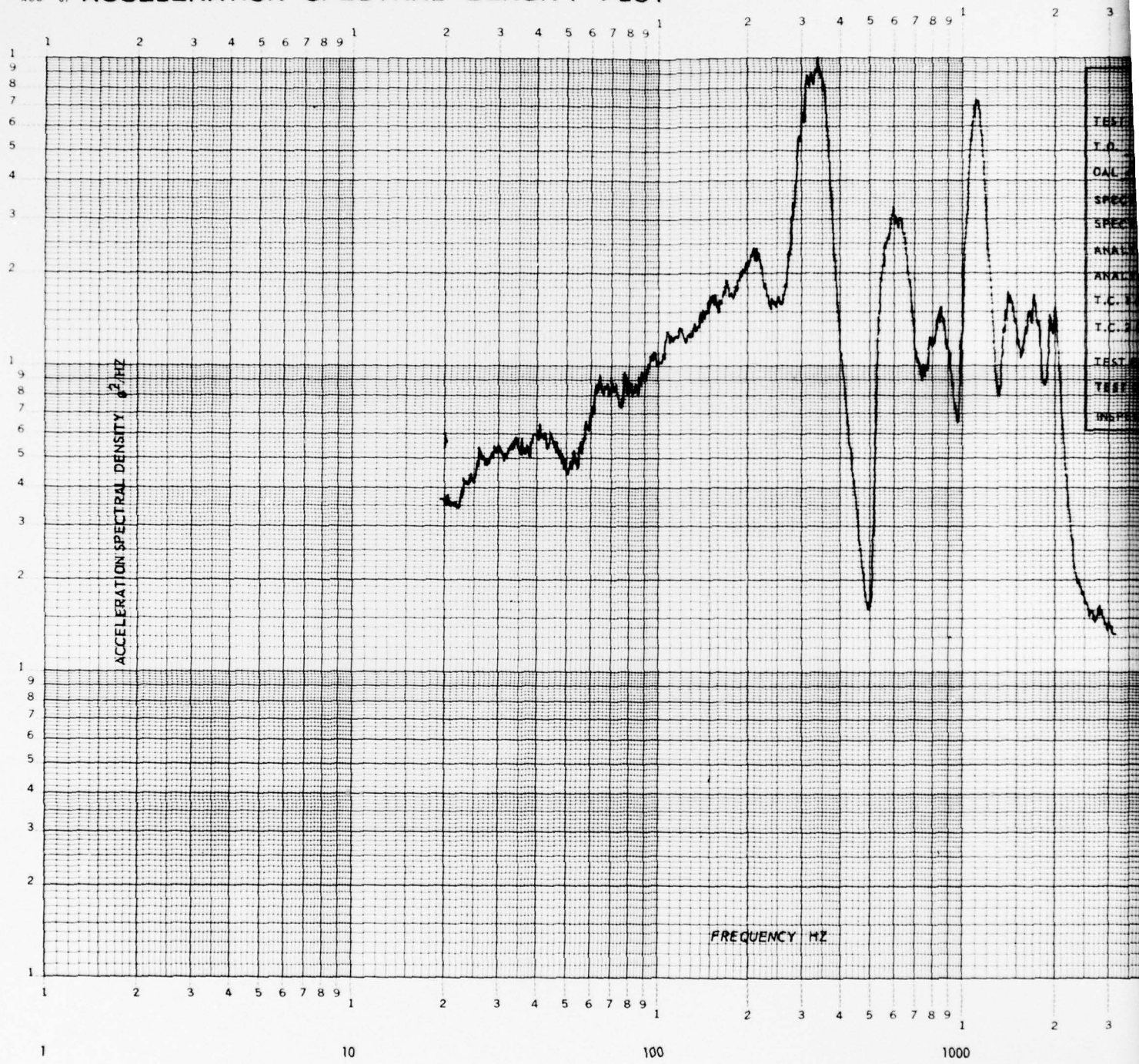

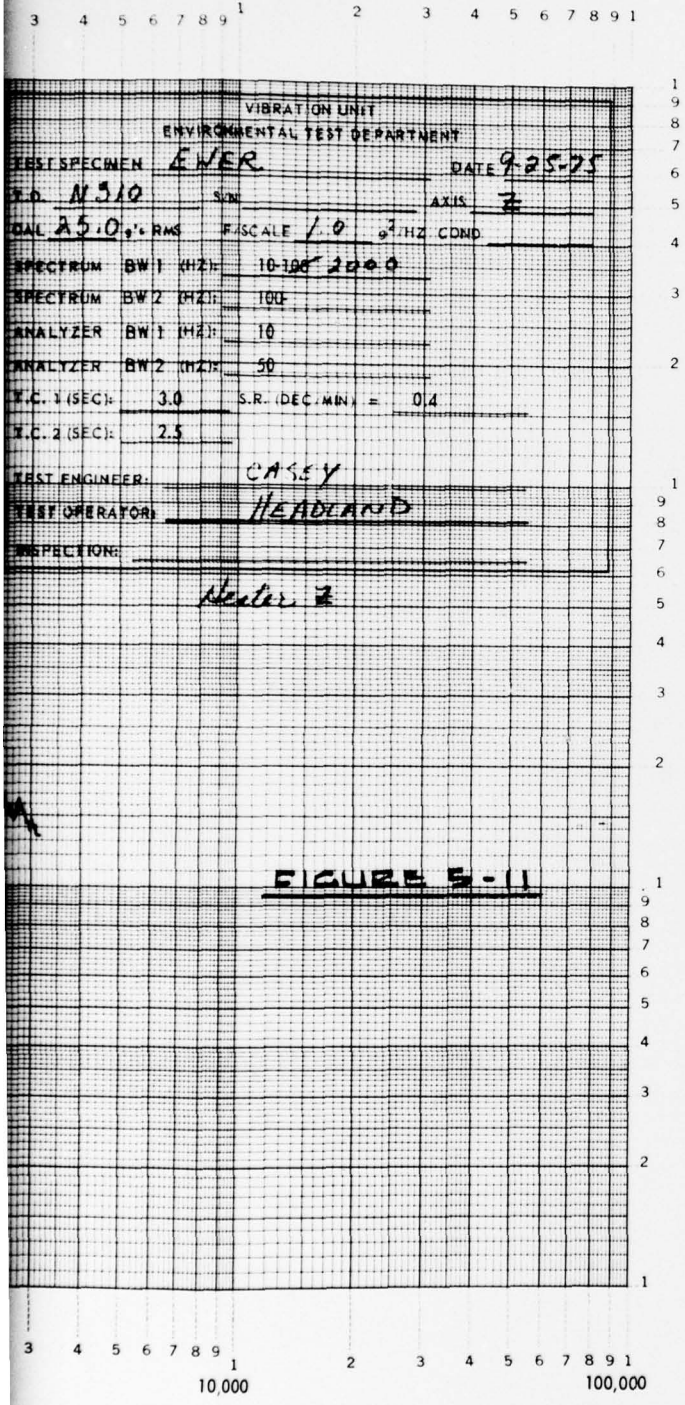
VIBRATION UNIT
ENVIRONMENTAL TEST DEPARTMENT
TEST SPECIMEN EWER
DATE 9-25-75
T.O. N310
S/N
AXIS Z
GAL 25.0 g's RMS
F SCALE 1.0 g²/HZ COND
SPECTRUM BW 1 (HZ): 10-1000 2000
SPECTRUM BW 2 (HZ): 100
ANALYZER BW 1 (HZ): 10
ANALYZER BW 2 (HZ): 50
T.C. 1 (SEC): 3.0
S.R. (DEC/MIN) = 0.4
T.C. 2 (SEC): 2.5
TEST ENGINEER: CASEY
TEST OPERATOR: HEADLAND
INSPECTION:
Shaker Z
3 4 5 6 7 8 9 1 2 3 4 5 6 7 8 9 1
1 2 3 4 5 6 7 8 9 1
10,000
100,000

FIGURE 5-11

2

2. PHASE 2 (Kirtland AFB, 13 November 1975)

On 11 June 1975, the left-hand pod on C-130E, S/N 64-0571, was shake tested to determine its vibrational characteristics. This data, along with the known vibrational characteristics of the airplane, were to be used as design guidelines for new equipment to be pod mounted on the 130 aircraft.

Since the 11 June 1975 test, the left-hand pod has been modified with a EWER installation. This modification consists of installing a new bulkhead just forward of the existing forward bulkhead and installing approximately 40 lb of equipment on a truss structure cantilevered off of the new bulkhead.

A post-modification shake test was accomplished on 13 November 1975 to determine the vibrational characteristics of the modified pod. The test consisted of a 60 sec sine-sweep printout on an x-y plotter, acceleration (g) vs frequency (Hz), of accelerometers mounted at selected locations in the pod. The pod was excited by input in the vertical direction only.

Table C-3

ACCELEROMETER NO.	INPUT	DIRECTION	LOCATION
	g	x-y	
1	.25	y	Tip of EWER probe
2	.25	y	Fwd end of truss structure
3	.25	x	Center of added bulkhead
4	.25	y	Centered on fwd-bulkhead
5	.25	y	End of 2-D precipitation particle spectrometer
6	.25	y	Centered between fwd & aft bulkheads
7	.25	y	Centered on aft bulkhead

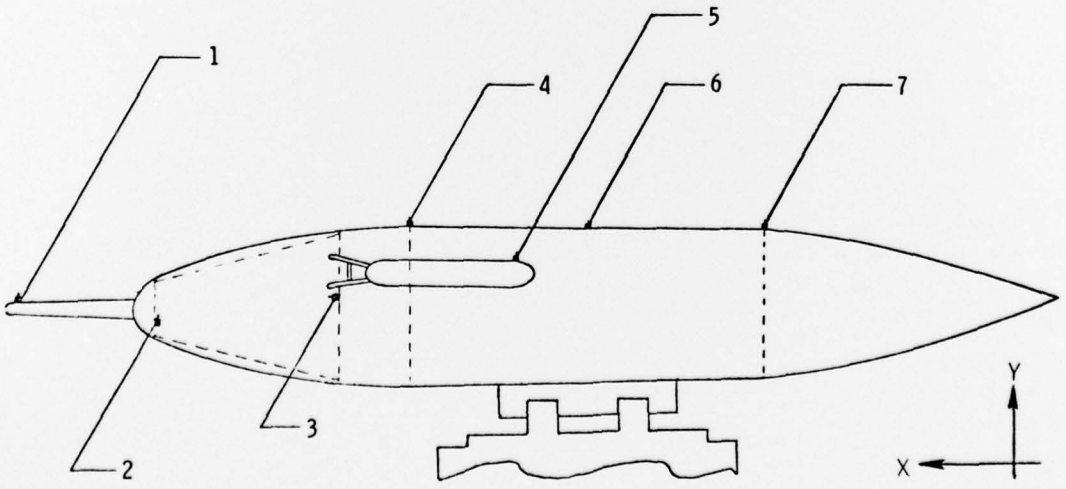

CONCLUSIONS

Accelerometer No. 2 was selected to determine the resonant frequencies of the forward end of the pod. The test results show that there is only one predominant resonant frequency, approximately 25 Hz. This 25 Hz shows up in every accelerometer location.

A comparison with the data taken on 11 June 1975 indicates that the forward bulkhead was the only location on primary structure which changed considerably, as was expected.

Accelerometer No. 3 indicates that no potentially hazardous plate bending modes were designed into the new bulkhead.

The 25 Hz resonance does not represent a potential structural problem because there are no vibrational sources in the 25 Hz range. We anticipate no structural problems as a result of the EWER modification.

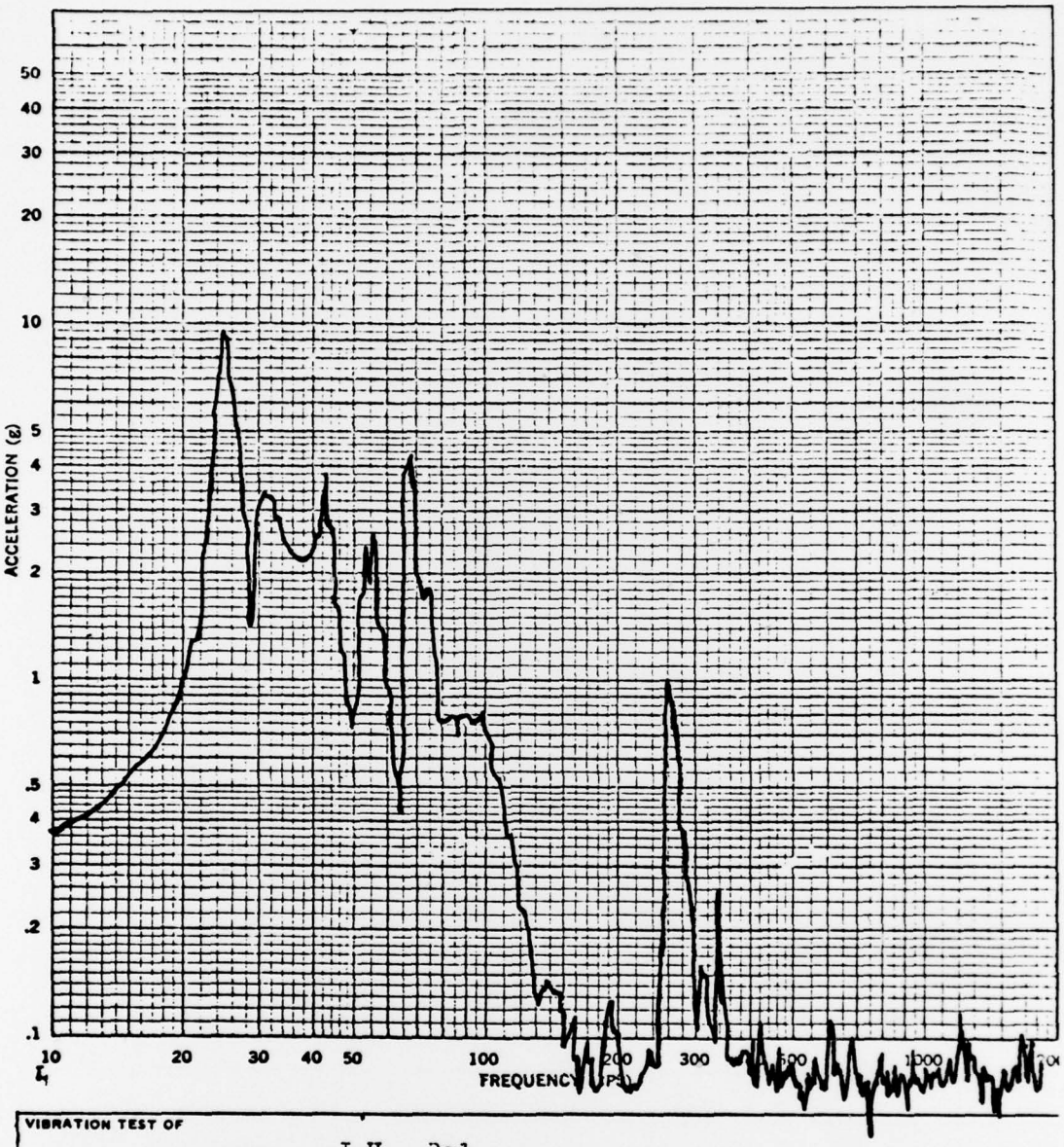

VIBRATION TEST OF	L.H. Pod
WITH IMPUT ALONG THE	Y Direction AXIS, AT °F
ACCEL LOCATION	No. 1
ACCEL TYPE AND SERIAL NO.	
FIGURE REFERENCE	
AXIS: Y	TEST DATE: 13 Nov 75

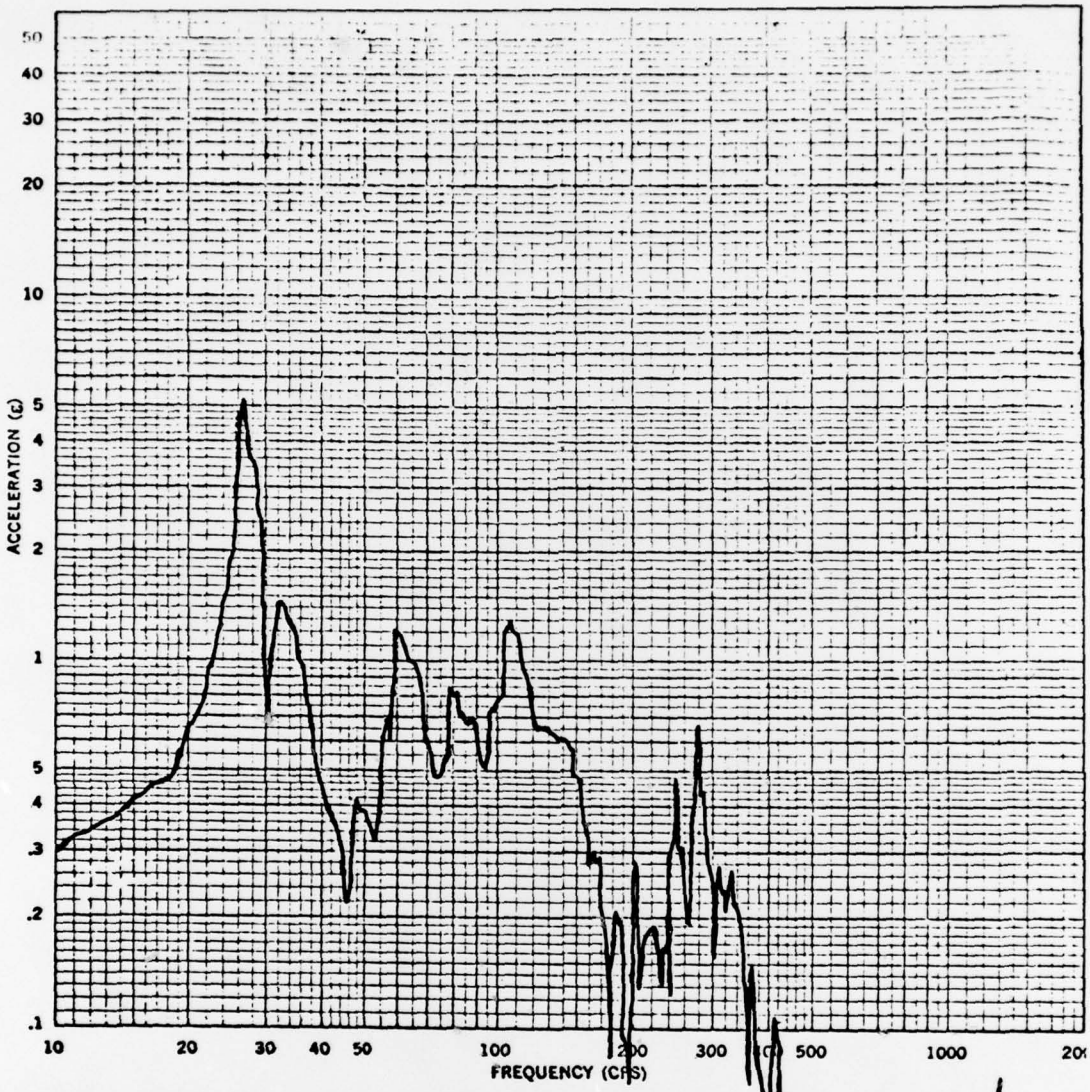

VIBRATION TEST OF	L.H. Pod
WITH IMPUT ALONG THE	Y Direction
ACCEL LOCATION	No. 2
ACCEL TYPE AND SERIAL NO.	
FIGURE REFERENCE	
AXIS: Y	TEST DATE: 13 Nov 75

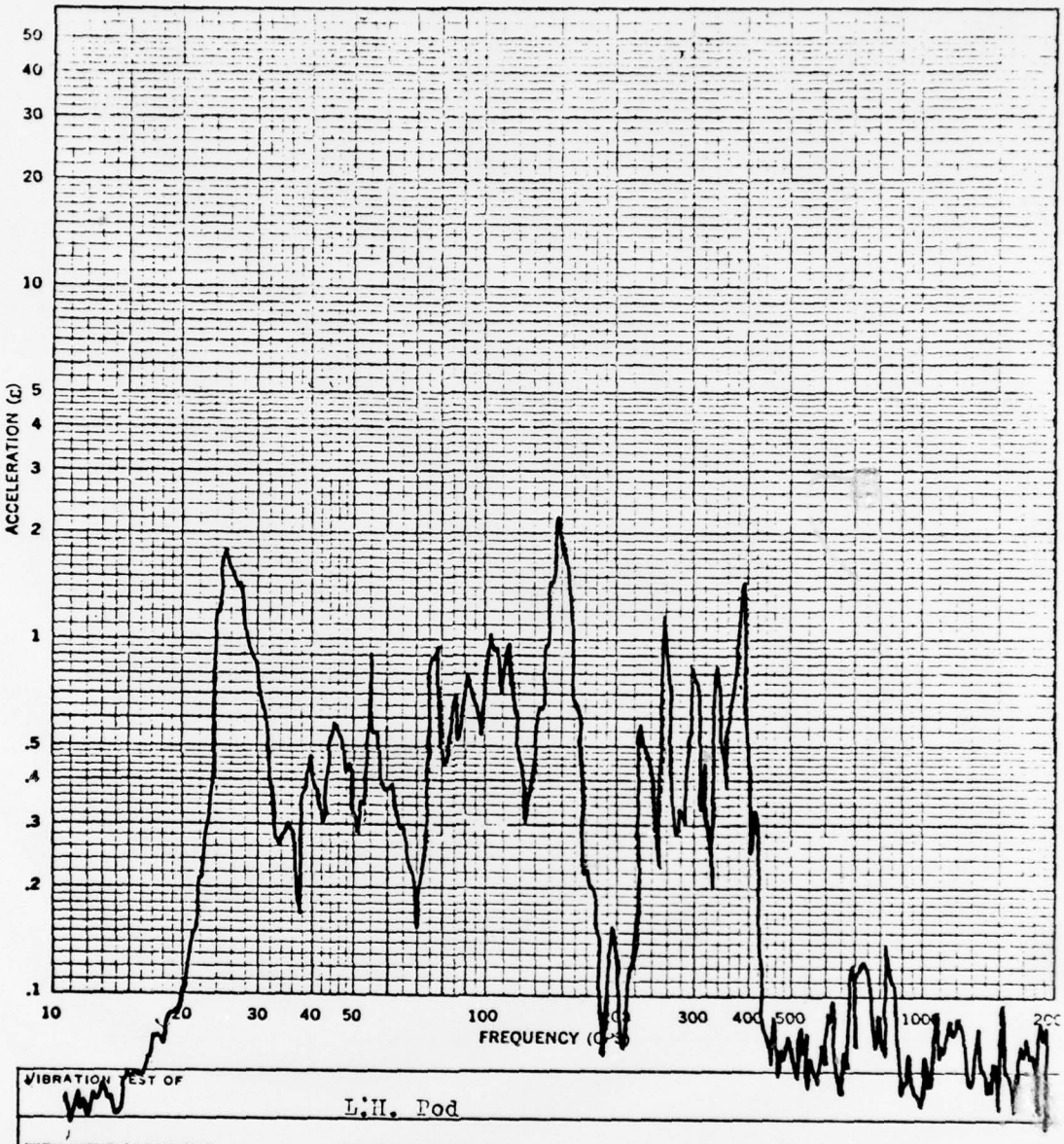

VIBRATION TEST OF	L.H. Pod
WITH IMPUT ALONG THE	Y Direction AXIS, AT °F
ACCEL LOCATION	No. 3
ACCEL TYPE AND SERIAL NO.	
FIGURE REFERENCE	
AXIS: X	TEST DATE: 13 Nov 75

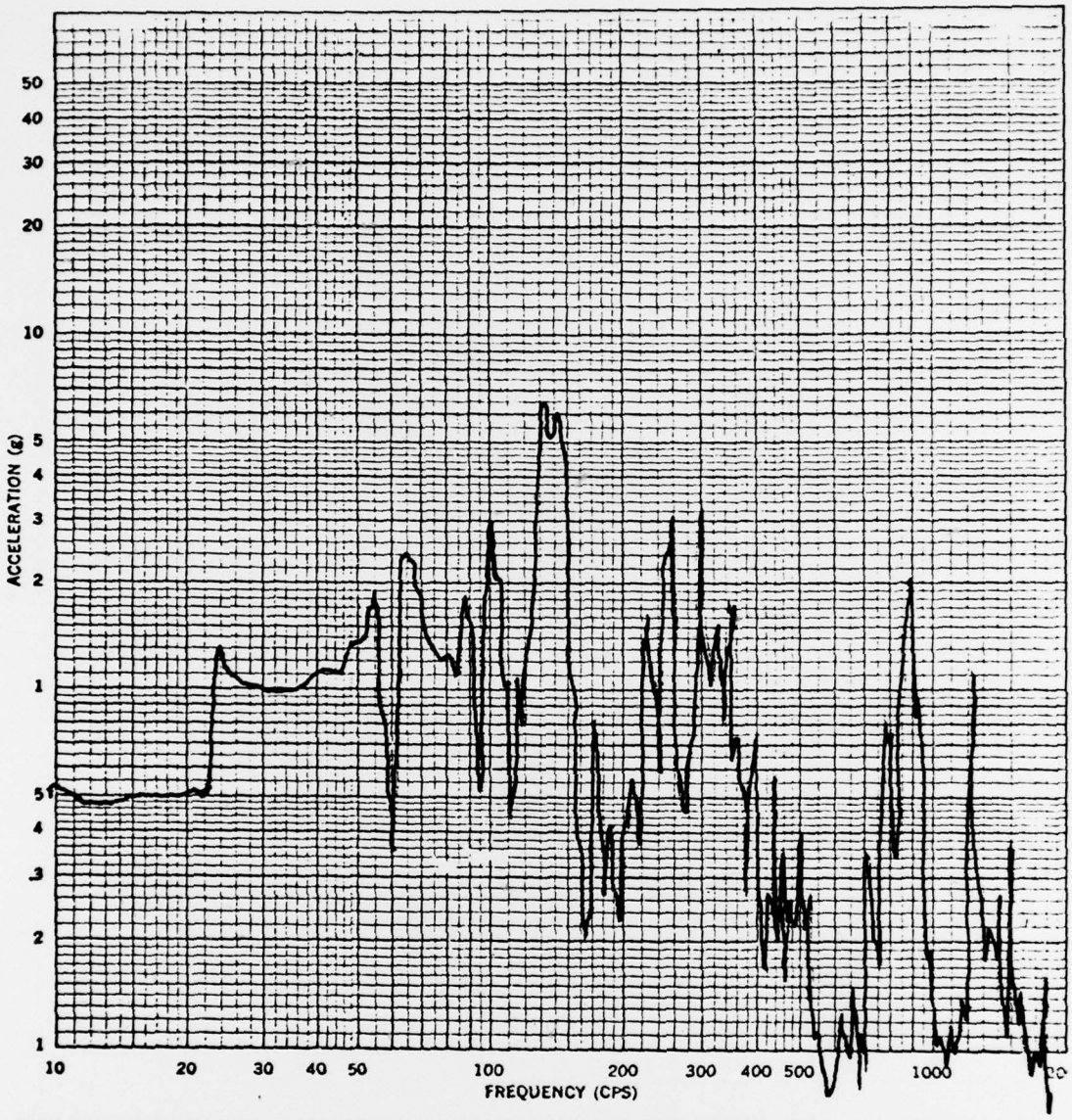

VIBRATION TEST OF	L.H. Pod
WITH IMPUT ALONG THE	Y Direction AXIS, AT ° F
ACCEL LOCATION	No. 4
ACCEL TYPE AND SERIAL NO.	
FIGURE REFERENCE	
AXIS: Y	TEST DATE: 11 June 73

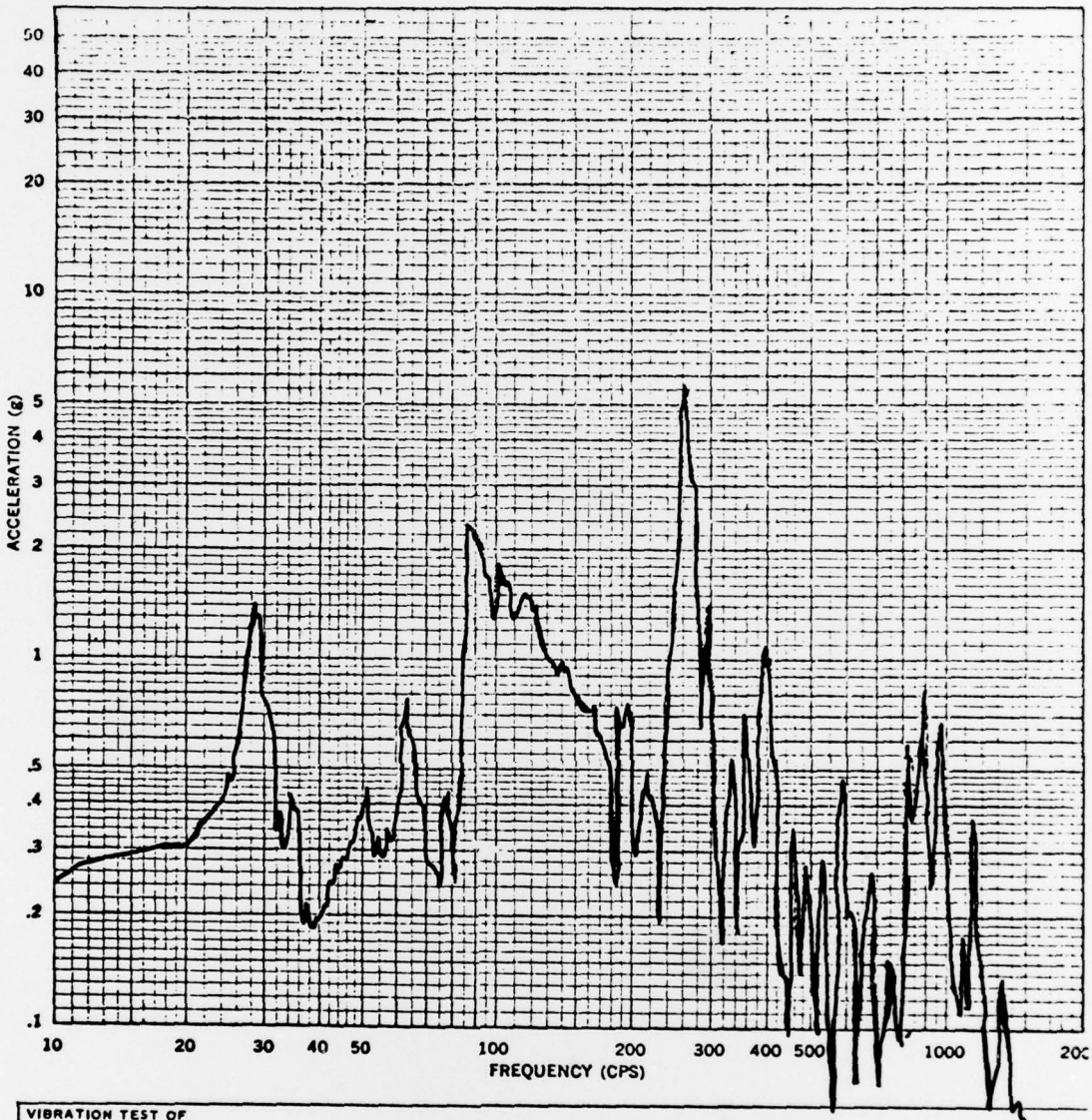

VIBRATION TEST OF	L.H. Pod
WITH IMPUT ALONG THE	Y Direction AXIS, AT °F
ACCEL LOCATION	No. 4
ACCEL TYPE AND SERIAL NO.	
FIGURE REFERENCE	
AXIS: Y	TEST DATE: 13 Nov 75

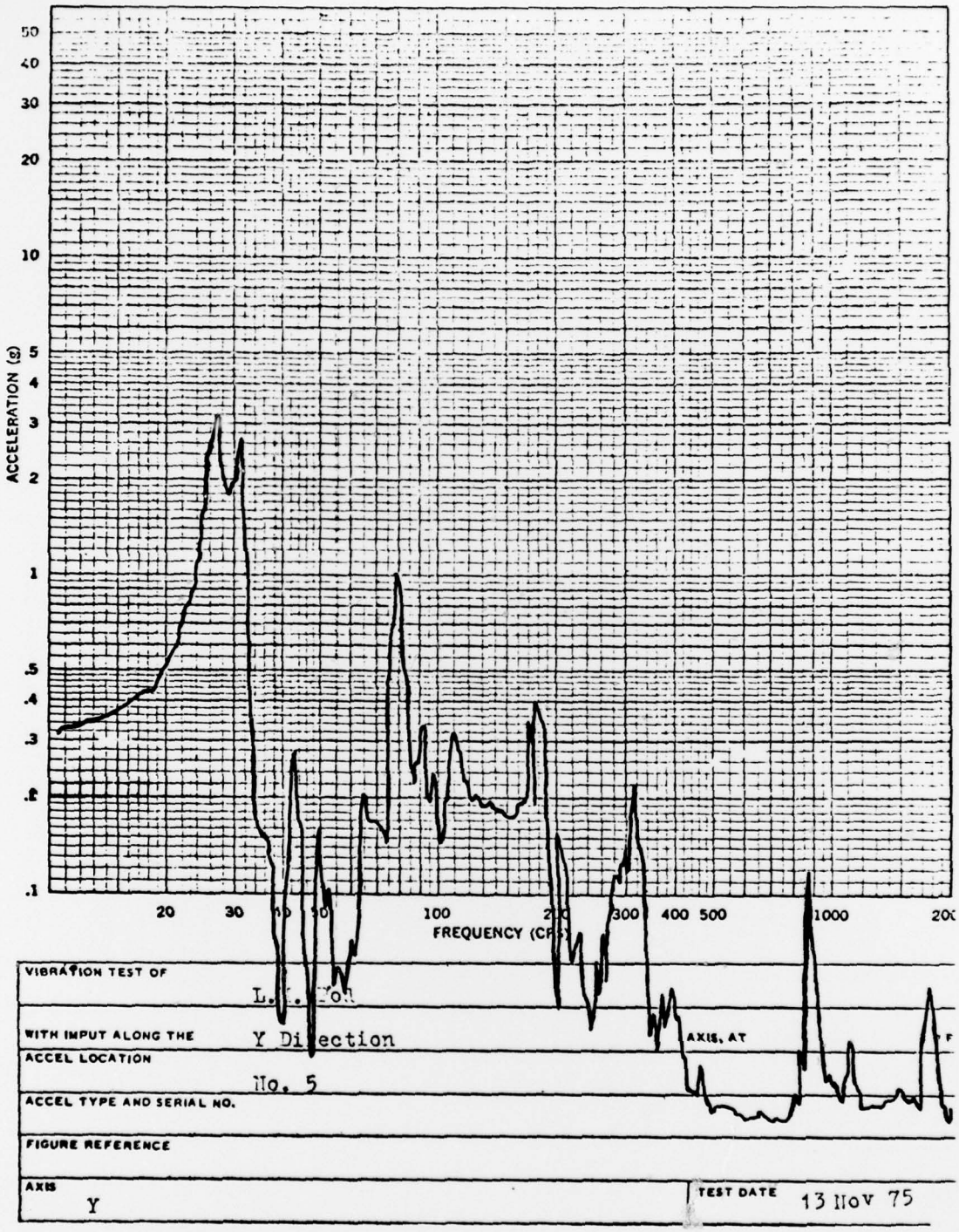
ACCELERATION (g)
50
40
30
20
10
5
4
3
2
1
.5
.4
.3
.2
.1
20
30
100
300
400
500
1000
FREQUENCY (CPS)
VIBRATION TEST OF
L. [illegible] Yoh
WITH IMPUT ALONG THE
Y Direction
AXIS, AT
ACCEL LOCATION
No. 5
ACCEL TYPE AND SERIAL NO.
FIGURE REFERENCE
AXIS
Y
TEST DATE
13 Nov 75

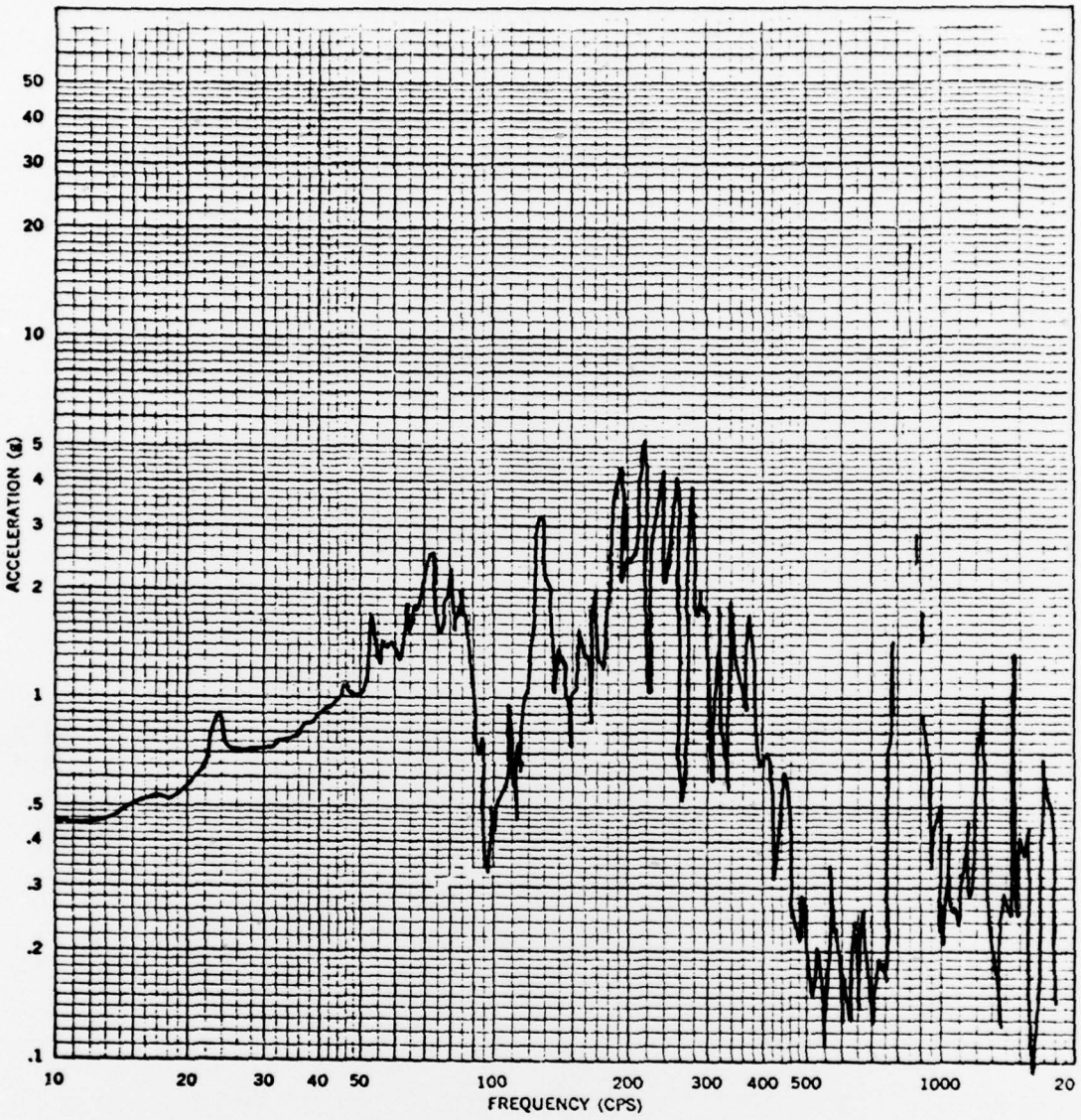

VIBRATION TEST OF	L,H. Pod
WITH INPUT ALONG THE	Y Direction AXIS, AT ° F
ACCEL LOCATION	No. 6
ACCEL TYPE AND SERIAL NO.	
FIGURE REFERENCE	
AXIS Y	TEST DATE 11 June 75

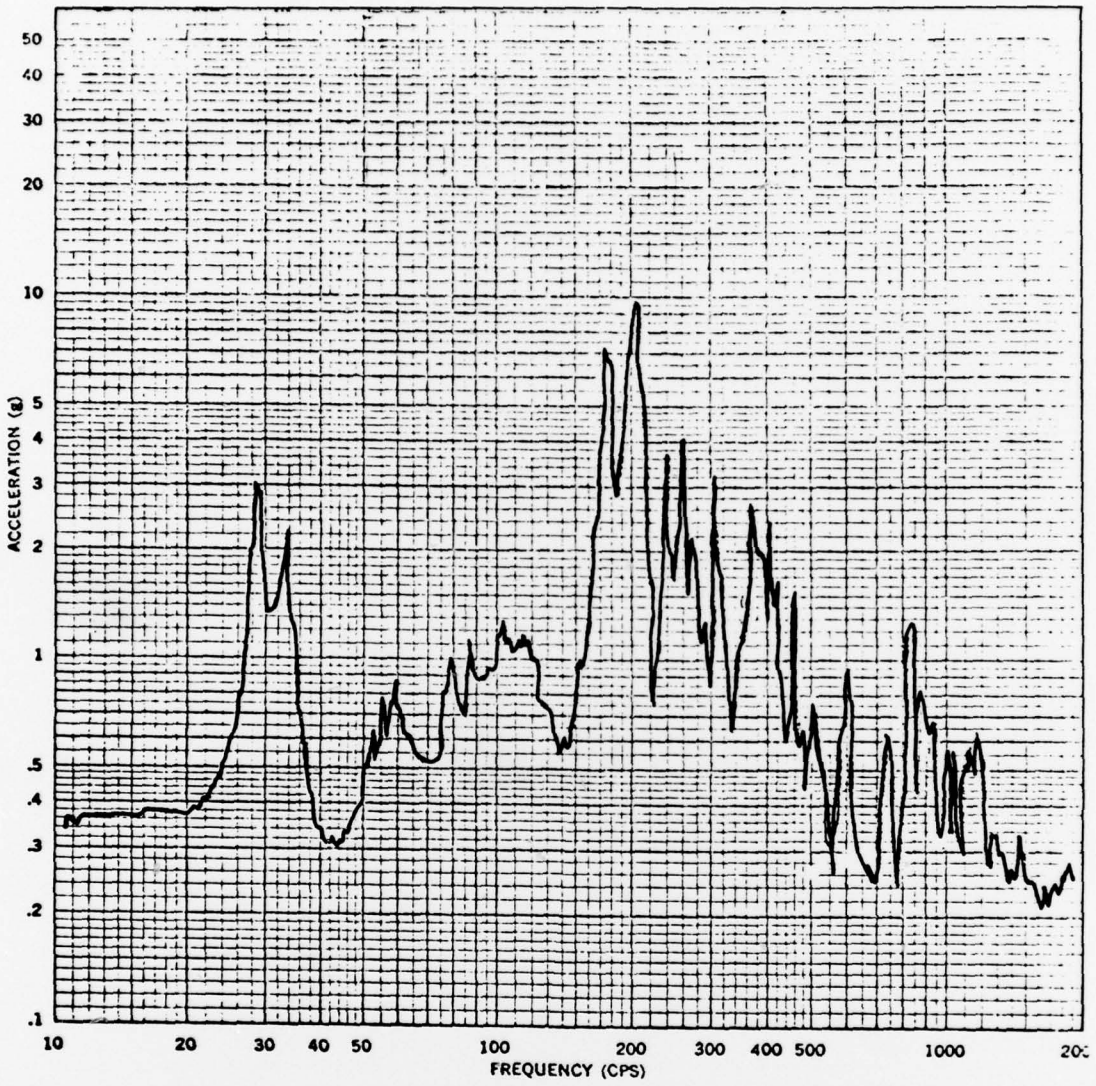

VIBRATION TEST OF	L.H. Pod
WITH IMPUT ALONG THE	Y Direction AXIS, AT ° F
ACCEL LOCATION	No. 6
ACCEL TYPE AND SERIAL NO.	
FIGURE REFERENCE	
AXIS: Y	TEST DATE: 13 Nov 75

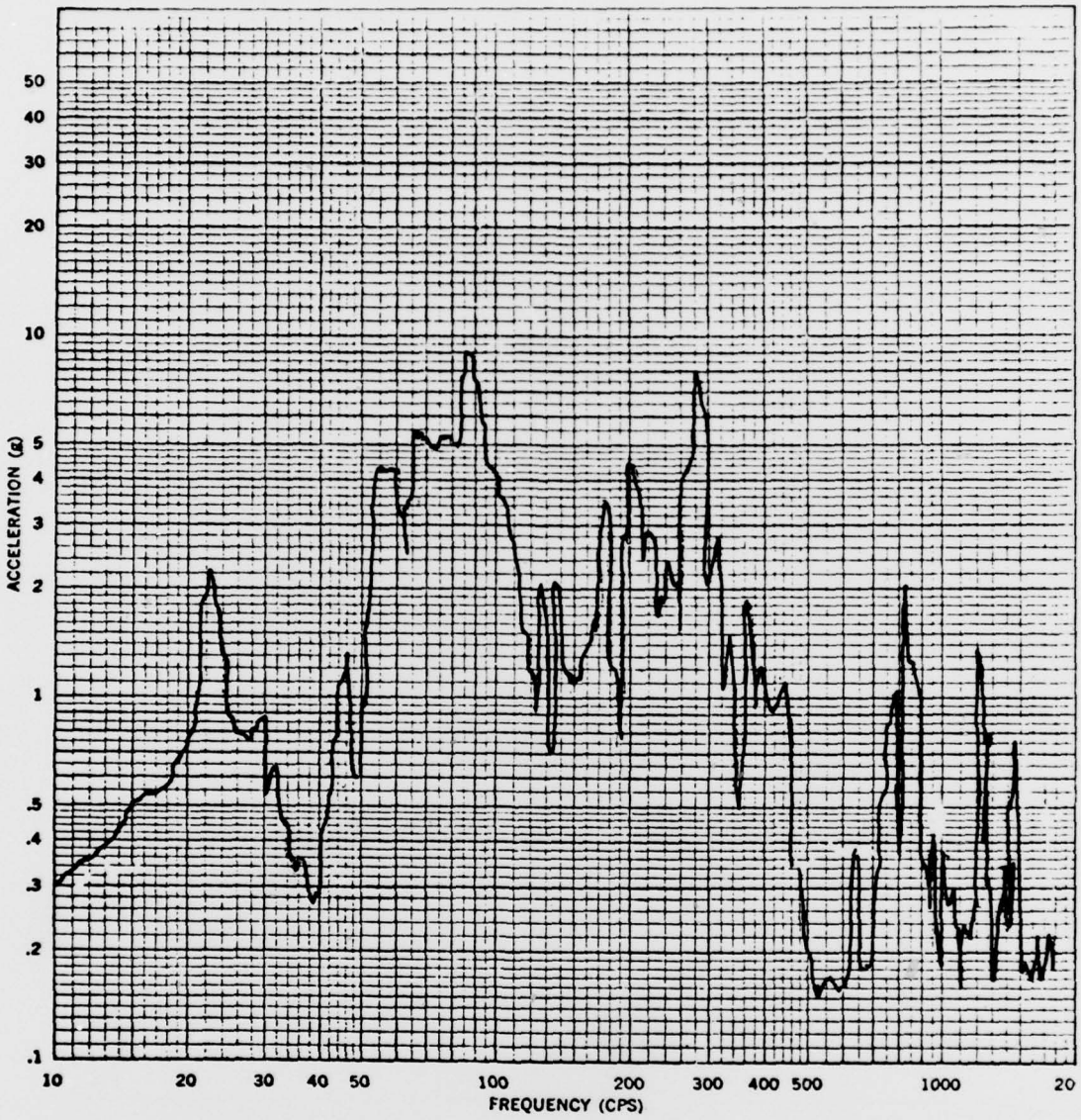

VIBRATION TEST OF	L.H. Pod
WITH INPUT ALONG THE	Y Direction AXIS, AT °F
ACCEL LOCATION	No. 7
ACCEL TYPE AND SERIAL NO.	
FIGURE REFERENCE	
AXIS Y	TEST DATE 11 June 75

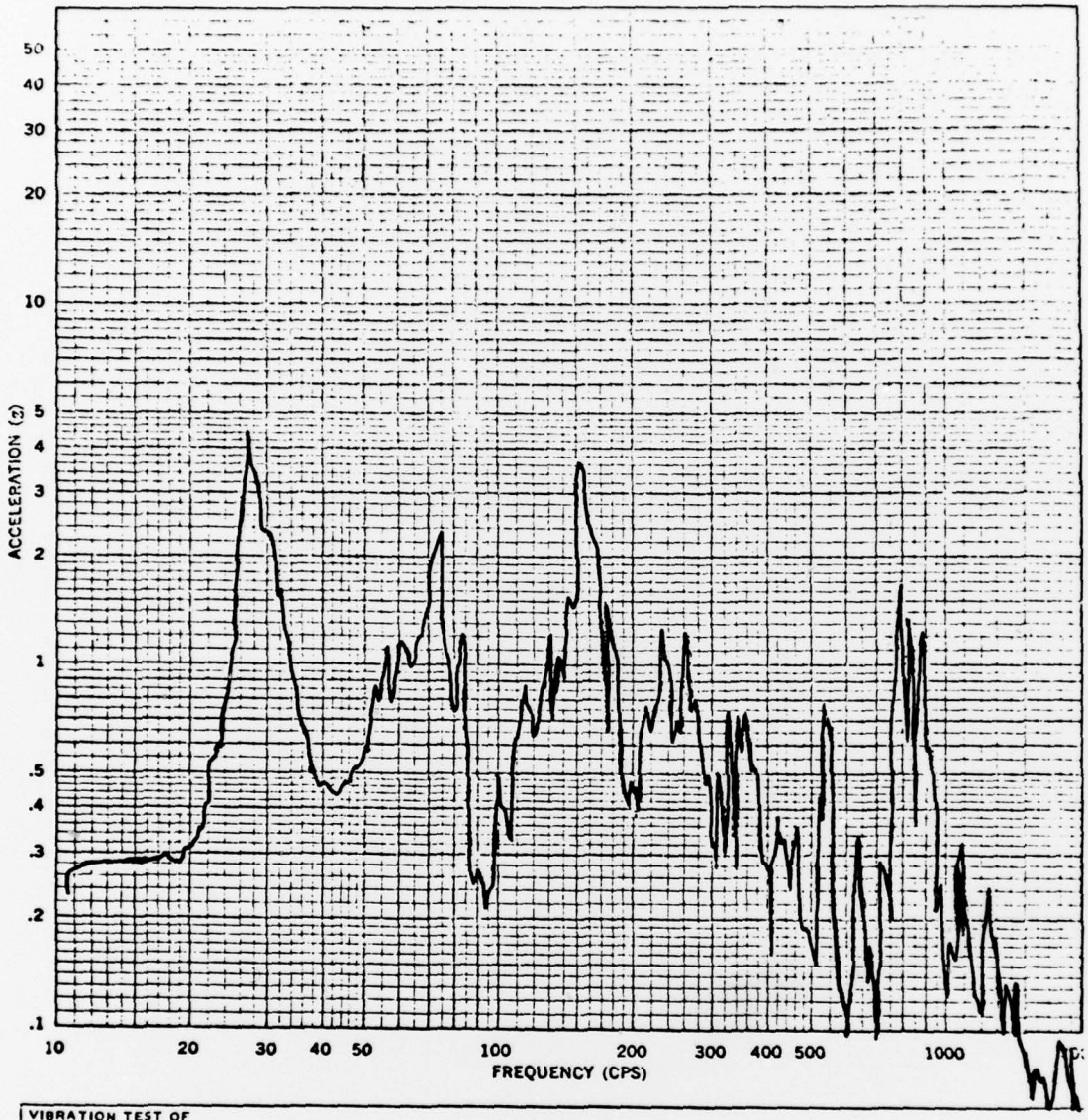

VIBRATION TEST OF	L.M. Pod
WITH IMPUT ALONG THE	Y Direction AXIS, AT °F
ACCEL LOCATION	No. 7
ACCEL TYPE AND SERIAL NO.	
FIGURE REFERENCE	
AXIS: Y	TEST DATE: 13 Nov 75